UNIVERSITY OF SOUTHAMPTON

Faculty of Environmental and Life Sciences
School of Biological Sciences

Defining the role of mesenchymal Factor Inhibiting HIF (FIH) in pulmonary fibrosis

by

Siyuan Wang

A thesis for the degree of
Doctor of Philosophy

April 2026

University of Southampton

Abstract

Faculty of Environmental and Life Sciences
School of Biological Sciences

Doctor of Philosophy

Defining the role of mesenchymal Factor Inhibiting HIF (FIH) in pulmonary fibrosis

by Siyuan Wang

Idiopathic pulmonary fibrosis (IPF) is the prototypic fibrotic lung disease in which progressive extracellular matrix deposition and remodelling impairs lung function and ultimately causes death. The cause of IPF remains unclear, and no approved treatment for IPF can halt disease progression. Injury to and/or dysfunction of alveolar epithelium are strongly implicated in IPF disease initiation, but what factors determine why fibrosis progresses rather than tissue repair occurs remain poorly understood. We have recently identified that the activity of factor inhibiting HIF (FIH) is reduced in IPF fibroblasts compared to normal healthy lung fibroblasts. Functionally, FIH regulates the expression of LOXL2 and PLOD2 via regulating hypoxia-inducible factor (HIF) activity. This study aims to investigate the hypothesis that in IPF loss of function of FIH is a key regulator of progressive fibrosis via both HIF-dependent and -independent pathways. Specifically, I will use IPF disease models in conjunction with transcriptomic analysis and molecular cell biology to determine (1) global transcriptomic alteration in FIH-depleted fibroblasts; (2) altered biological processes when FIH is depleted in human lung fibroblasts; (3) determine if the biological alteration is HIF-dependent or not.

Our results showed that FIH depletion in lung fibroblasts led to notable transcriptomic changes, including changes in cell cycle processes, pathways related to hypoxia, cellular metabolism and ECM deposition. Further experiments suggest that FIH depletion impaired mitochondrial function, reducing oxygen consumption rates and ATP production, a process reversed by co-depleting HIF1β, confirming FIH's impact on bioenergetics via HIF pathways. Meanwhile FIH-depletion downregulated glycolysis but induced cellular senescence in a HIF-independent manner. FIH also reduced TGFβ-induced α-SMA and collagen 1 expression in a HIF-independent manner, suggesting a role in fibroblast-to-myofibroblast transition through non-HIF mechanisms (Figure.1).

In conclusion, FIH plays a critical role in regulating fibroblast metabolism, senescence, and fibroblast-to-myofibroblast transition (FMT) through either HIF-dependent or HIF-independent pathways, offering potential new avenues for therapeutic targeting in fibrotic diseases.

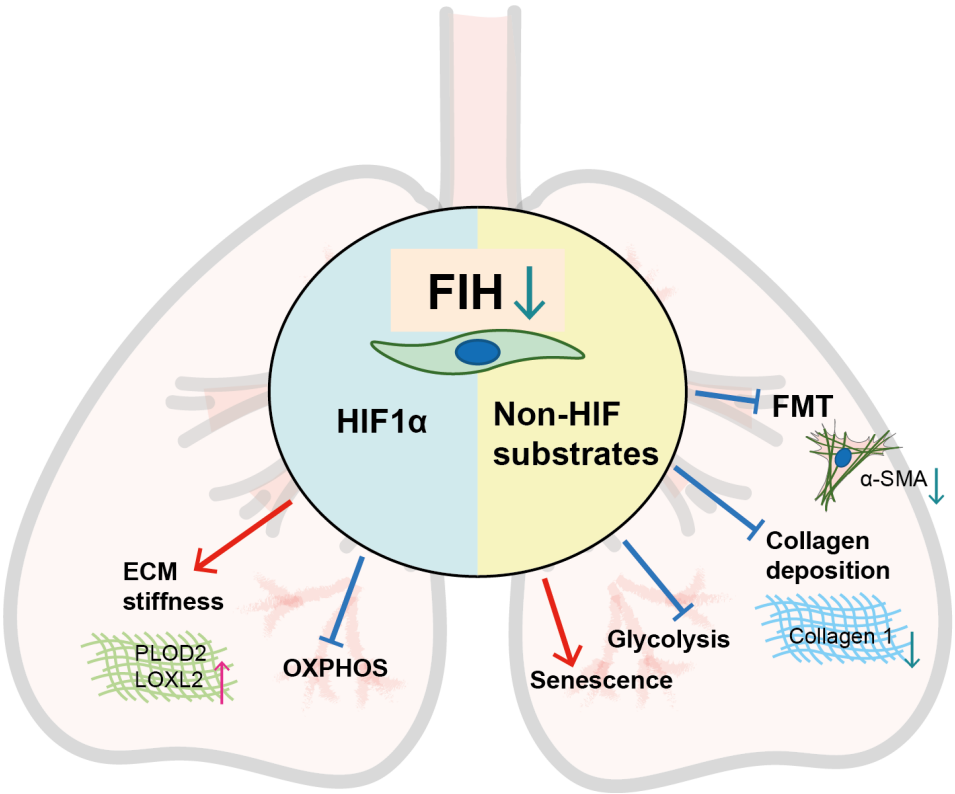

FIGURE 1: **The role of mesenchymal FIH in lung fibrosis**

Schematic representation illustrating the dual role of FIH in regulating fibroblast function through both HIF-dependent and HIF-independent mechanisms. Previous work from our lab demonstrated that FIH inhibition increases the expression of LOXL2 and PLOD2 via HIF-1α. In this thesis, FIH depletion was shown to impair OXPHOS in a HIF-dependent manner. In contrast, the results reveals that FIH depletion downregulates glycolysis and induces cellular senescence in the HIF-independent pathway. Additionally, FIH modulates fibroblast activation by reducing TGF-β-induced α-SMA and collagen1 expression, highlighting its role in the fibroblast-to-myofibroblast transition (FMT) through non-HIF mechanisms. ECM, extracellular matrix.

Contents

List of Figures

List of Tables

Declaration of Authorship

I declare that this thesis and the work presented in it is my own and has been generated by me as the result of my own original research.

I confirm that:

1. This work was done wholly or mainly while in candidature for a research degree at this University;
2. Where any part of this thesis has previously been submitted for a degree or any other qualification at this University or any other institution, this has been clearly stated;
3. Where I have consulted the published work of others, this is always clearly attributed;
4. Where I have quoted from the work of others, the source is always given. With the exception of such quotations, this thesis is entirely my own work;
5. I have acknowledged all main sources of help;
6. Where the thesis is based on work done by myself jointly with others, I have made clear exactly what was done by others and what I have contributed myself;
7. None of this work has been published before submission

Signed:..... Date:.....

Acknowledgements

If someone had told me a few years ago that I would one day write my PhD thesis in English, I would have found it hard to believe. Yet, here I am, having completed this journey—a testament to the whirlwind that has been the past four years.

First and foremost, I owe my deepest gratitude to my supervisor, Dr. Yihua Wang, for his unwavering guidance and trust over these years. His support and encouragement have been invaluable. When I began my PhD, I lacked confidence in my research abilities. While I may not claim extraordinary strength now, I have grown to have much more faith in myself.

I am also deeply thankful to my second supervisor, Dr. Mark Jones, for his insightful guidance on IPF-related knowledge and experiments, as well as for the additional support he has extended throughout. My heartfelt thanks go to Dr. Jonathan Swann and Dr. Charlie Birts, whose patient teaching in metabolism—both theoretical and practical—has been essential. I cannot express enough how grateful I am for their help. Special thanks to Prof. Donna Davies, Prof. Nullin Divecha, and Dr. Bav Sheth for their invaluable experimental guidance.

To the members of our lab: Liudi, who welcomed me warmly when I first arrived in the UK and guided me into the lab; Yilu, my first mentor in bioinformatics, whose patient teaching and detailed explanations helped me immensely; Hualong, for your assistance in the lab and in daily life; Zijian, for your advice and encouragement, especially the lesson to step out and explore what interests me—and for the gym memories we shared. I am also grateful to Beatriz, Yomna, Xi, Kun, Rong, Tao, and Zhe for their friendship and support. The hard work we did together in the lab and the moments of joy we shared are truly precious to me.

A special thank you goes to my family and friends. Yuting, Ying, Jiaoqi—our time together brought so much happiness, and I am grateful that you chose to spend it with someone as socially awkward as I am. You helped me feel less alone. To my parents and my grandfather, your endless support and trust gave me the strength to pursue my studies abroad. Despite the distance, you always managed to send me comfort, warmth, and the feeling of home.

I would also like to thank the Chinese Scholarship Council, Medical Research Council (MR/S025480/1), an Academy of Medical Sciences/the Wellcome Trust Springboard Award [SBF002/1,038] and AAIR for their financial support, which made my studies and research possible.

As this PhD journey draws to a close, a new chapter of my life is about to begin. I hope I have done justice to the hard work and perseverance of these four years. The

love and support from my supervisors, friends, and family will continue to be my motivation as I move forward.

Definitions and Abbreviations

2-DG	2-Deoxy-D-glucose
ABCA3	ATP Binding Cassette Subfamily A Member 3
ACTA2	Actin Alpha 2, Smooth Muscle
ACTB	Actin Beta
ADP	Adenosine Diphosphate
AEC	Alveolar Epithelial Cells
AKAP13	A-Kinase Anchoring Protein 13
AKT	Protein Kinase B
AMs	Alveolar Macrophages
ASB4	Ankyrin Repeat and SOCS Box Containing 4
ASPP2	Apoptosis-Stimulating Protein of P53 2
ATP	Adenosine Triphosphate
C-TAD	C-Terminal Transactivation Domain
CCL	C-C Motif Chemokine Ligand
CCN2	Cellular Communication Network Factor 2
CDKN1A	Cyclin Dependent Kinase Inhibitor 1A
CMV	Cytomegalovirus
COPD	Chronic Obstructive Pulmonary Disease
CTGF	Connective Tissue Growth Factor
CXCR	C-X-C Chemokine Receptor
DAMPs	Damage-Associated Molecular Patterns
DATPs	Deoxynucleoside Triphosphates
DEG	Differentially Expressed Gene
DKC1	Dyskerin Pseudouridine Synthase 1
DPP9	Dipeptidyl Peptidase 9
DSP	Desmoplakin
EBV	Epstein-Barr Virus
ECAR	Extracellular Acidification Rate
ECM	Extracellular Matrix
EGFR	Epidermal Growth Factor Receptor
EMT	Epithelial-Mesenchymal Transition
ERK	Extracellular Signal-Regulated Kinase

ETC	Electron Transport Chain
FADH	Flavin Adenine Dinucleotide (Hydrogen)
FAK	Focal Adhesion Kinase
FCCP	Carbonyl Cyanide-4-(trifluoromethoxy)phenylhydrazone
FGF	Fibroblast Growth Factor
FIH	Factor Inhibiting HIF
FMT	Fibroblast-to-Myofibroblast Transition
FPF	Familial Pulmonary Fibrosis
FVC	Forced Vital Capacity
GAPDH	Glyceraldehyde-3-Phosphate Dehydrogenase
GLUT	Glucose Transporter
GM-CSF	Granulocyte-Macrophage Colony-Stimulating Factor
GO	Gene Ontology
GSVA	Gene Set Variation Analysis
GWAS	Genome-Wide Association Study
HACE1	HECT Domain and Ankyrin Repeat Containing E3 Ubiquitin Protein Ligase 1
HHV	Human Herpesvirus
HIF	Hypoxia-Inducible Factor
HK	Hexokinase
IFN	Interferon
IGF	Insulin-Like Growth Factor
ILD	Interstitial Lung Disease
IPF	Idiopathic Pulmonary Fibrosis
JNK	c-Jun N-terminal Kinase
KIF15	Kinesin Family Member 15
KRT	Keratin
LAP	Latent Associated Peptide
LDH	Lactate Dehydrogenase
LOX	Lysyl Oxidase
LOXL	Lysyl Oxidase Like
LZIP	Leucine Zipper Protein
MAD1L1	Mitotic Arrest Deficient 1 Like 1
MAPK	Mitogen-Activated Protein Kinase
MIP	Major Intrinsic Protein
MLCP	Myosin Light Chain Phosphatase
MMP	Matrix Metalloproteinase
mTOR	Mechanistic Target of Rapamycin
MUC2	Mucin 2
MUC5B	Mucin 5B
N-TAD	N-Terminal Transactivation Domain
NADH	Nicotinamide Adenine Dinucleotide (Hydrogen)

NLRP3	NOD-like Receptor Pyrin Domain Containing 3
NMR	Nuclear Magnetic Resonance
NOX4	NADPH Oxidase 4
NSCLC	Non-Small Cell Lung Cancer
OCR	Oxygen Consumption Rate
OTUD7B	OTU Deubiquitinase 7B
OXPHOS	Oxidative Phosphorylation
PARN	Poly(A)-Specific Ribonuclease
PBS	Phosphate-Buffered Saline
PCA	Principal Component Analysis
PDGF	Platelet-Derived Growth Factor
PDGFR	Platelet-Derived Growth Factor Receptor
PFD	Pulmonary Fibrosis Disease
PFK	Phosphofructokinase
PFK1	Phosphofructokinase 1
PGAM	Phosphoglycerate Mutase
PHD	Prolyl Hydroxylase Domain
PI3K	Phosphoinositide 3-Kinase
PKB	Protein Kinase B
PKM	Pyruvate Kinase M
PLOD	Procollagen-Lysine, 2-Oxoglutarate 5-Dioxygenase
PPAR	Peroxisome Proliferator-Activated Receptor
PPP	Pentose Phosphate Pathway
ROS	Reactive Oxygen Species
RTEL1	Regulator of Telomere Elongation Helicase 1
SASP	Senescence-Associated Secretory Phenotype
SCLC	Small Cell Lung Cancer
SEMA	Semaphorin
SFTPA2	Surfactant Protein A2
SFTPC	Surfactant Protein C
SNAIL	Snail Family Transcriptional Repressor
SRF	Serum Response Factor
STN1	Suppressor of Telomere Elongation 1
TAZ	Transcriptional Coactivator with PDZ-Binding Motif
TCA	Tricarboxylic Acid Cycle
TERC	Telomerase RNA Component
TERT	Telomerase Reverse Transcriptase
TGFβ	Transforming Growth Factor Beta
TIMP	Tissue Inhibitor of Metalloproteinases
TINF21	Type I Interferon Gene Expression Factor 21
TLR	Toll-Like Receptor

TNKS2	Tankyrase 2
TOLLIP	Toll Interacting Protein
TP53	Tumor Protein P53
TRPA1	Transient Receptor Potential Ankyrin 1
TRPV3	Transient Receptor Potential Vanilloid 3
UIP	Usual Interstitial Pneumonia
VEGFR	Vascular Endothelial Growth Factor Receptor
VEGF	Vascular Endothelial Growth Factor
WHO	World Health Organisation
YAP	Yes-Associated Protein
ZEB	Zinc Finger E-Box Binding Homeobox

Chapter 1

Introduction

1.1 Idiopathic pulmonary fibrosis (IPF)

Idiopathic pulmonary fibrosis (IPF) is a chronic, fibrosing interstitial pneumonia of unknown cause that is associated with radiological and histologic features of usual interstitial pneumonia (UIP) (Martinez et al., 2017). It occurs primarily in older adults, is characterised by progressive worsening of dyspnea and lung function, and has a poor prognosis (Raghu et al., 2018, 2022).

1.1.1 Incidence and prevalence

The incidence and prevalence of IPF vary based on country/geographic region, case definition and population demographics. Both of them increase significantly with age. The estimated global incidence of IPF varies widely across regions, ranging from approximately 1 to 24 per 100,000 persons, with the highest incidence reported in South Korea, Italy, and the United States. Prevalence estimates similarly show significant regional variation, ranging from about 3 to 111 per 100,000 persons, with the highest prevalence rates observed in South Korea, Canada, and the USA (Table.1.1). More men have been reported with IPF than women, and most of patients have a history of smoking (Raghu et al., 2006; Behr et al., 2015).

The increasing incidence and prevalence of IPF present significant challenges that are not fully explained by demographic factors such as age. These trends may be partly attributed to evolving definitions of IPF, the more widespread use of CT scans, and improved diagnostic rates (Gribbin et al., 2006). As the global population continues to age with the mean age at diagnosis typically around 65–70 years (Raghu et al., 2018), the burden of IPF is expected to grow, fueled by greater awareness of its clinical manifestations and the rising prevalence of risk factors like air pollution.

The growing incidence of IPF has led to a significant increase in cumulative prevalence, to the point where it challenges the classification of IPF as a rare disease (Richeldi et al., 2017). This trend underscores the need for heightened awareness, early diagnosis, and improved management strategies to address the increasing burden of IPF worldwide.

TABLE 1.1: **Global incidence rate and prevalence of IPF**

Region	**Country/Area**	**Publication year**	**Incidence (/100,000)**	**Prevalence (/100,000)**	**Ref.**
Asia-Pacific	South Korea	2015	1.7		(Gjonbrataj et al., 2015)
		2016	12.9	38.9	(Lee et al., 2016)
		2021	2.5-3.8		(Song et al., 2021)
	Japan	2014	2.23	10	(Natsuizaka et al., 2014)
	Taiwan (China)	2012	3.1	4.9	(Lai et al., 2012)
		2020	0.7-1.3	3.1-6.4	(Yang et al., 2020)
Europe	Finland	2015	1.3	8.6	(Kaunisto et al., 2015)
	France	2017	2.8	8.2	(Duchemann et al., 2017)
	Greece	2009	0.9	3.4	(Karakatsani et al., 2009)
	Italy	2014	9.3	25.6	(Agabiti et al., 2014)
		2016	2.6	21.2	(Harari et al., 2016)
	United Kingdom	2018	1.2	11.6	(Strongman et al., 2018)
North America	Canada	2016	9.0	20.0	(Hopkins et al., 2016)
		2018	21.7	72.7	(Tarride et al., 2018)
	United States	2010	8.8	28.1	(Pérez et al., 2010)
		2014	24.2	111	(Raghu et al., 2014)
		2016	2.6	6.7	(Raimundo et al., 2016)
Oceania	Australia	2022	10.2	32.6	(Cox et al., 2022)

Information collected from (Maher et al., 2021; Cox et al., 2022; Yang et al., 2020; Song et al., 2021)

1.1.2 Morbidity and mortality

The median survival time for patients diagnosed with IPF has traditionally been reported as 3 to 5 years from the time of diagnosis (Podolanczuk et al., 2023). Specifically, in a cohort of United State adults aged over 65 years diagnosed with IPF between 2001 and 2011, the median survival was found to be 3.8 years (Raghu et al., 2014). A Canadian study conducted from 2007 to 2011 reported a 41% risk of death within four years of diagnosis (Hopkins et al., 2016). Survival rates tend to decrease with advancing age and are generally lower in males (Raghu et al., 2014). Notably, several studies have reported an improvement in survival over the past two decades, which is likely attributable to earlier diagnosis, decreased use of immunosuppressive medications, and advancements in treatment options (Raghu et al., 2014; Margaritopoulos et al., 2018; Guenther et al., 2018; Behr et al., 2020; Moon et al., 2021).

Globally, the number of deaths attributed to IPF continues to rise, despite evidence indicating that survival rates among those diagnosed are improving. Data from the World Health Organisation (WHO) mortality database showed that the median mortality rate due to IPF in Europe between 2011 and 2013 was 3.75 per 100,000 for men and 1.50 per 100,000 for women (Marshall et al., 2018). In the United States, using a broader definition of pulmonary fibrosis, the age-adjusted mortality rate in 2017 was reported at 26.7 per 100,000 for men and 16.3 per 100,000 for women, with significant variability observed across different racial and ethnic groups (Dove et al., 2019). Furthermore, death certificate data from 2010 revealed age-adjusted mortality rates ranging from 4.6 per 100,000 in Sweden to 9.9 per 100,000 in Japan, with similarly high rates observed in the United Kingdom (8.5 per 100,000 in England and Wales, and 9.7 per 100,000 in Scotland) and lower rates in Spain and New Zealand (5.3 and 5.6 per 100,000, respectively) (Hutchinson et al., 2014).

Between 2000 and 2012, there was an annual increase in IPF-related mortality of approximately 2–3% across all countries for which data were available (Hutchinson et al., 2014). In the United States, the age-adjusted mortality rate due to IPF increased by an average of 0.7% per year between 1999 and 2017 (Pérez et al., 2010). Recent estimates indicate that approximately 5,500 people in the United Kingdom and up to 17,000 people in the United States die from IPF each year (Navaratnam and Hubbard, 2019; Hutchinson et al., 2014). The most common cause of death among IPF patients is the progression of lung disease, frequently leading to acute exacerbations and acute respiratory failure, accounting for 60–70% of deaths (Olson et al., 2007; Kärkkäinen et al., 2018). Other notable causes of death include ischemic heart disease, lung cancer, pneumonia, pulmonary embolism, and chronic obstructive pulmonary disease (COPD) (Kärkkäinen et al., 2018).

1.1.3 Risk factors

1.1.3.1 Genetic factors

IPF can occur both sporadically and within families, pointing to a genetic predisposition. Familial Pulmonary Fibrosis (FPF), where two or more family members have idiopathic interstitial pneumonia, accounts for about 5-20% of IPF cases (Raghu et al., 2011; Cutting et al., 2021). The presence of pulmonary fibrosis in family clusters and certain rare genetic conditions suggests that genetics play a key role in IPF. Differences in the incidence and progression of IPF among patients with similar exposures also indicate that genetic background significantly influences the disease (Loyd, 2003; Borie et al., 2023).

The genetic risk factors for IPF can be categorized into several functional groups (Table.1.2). In the domain of host defense, the *MUC5B* mutation (rs35705950) significantly increases IPF risk by upregulating *MUC5B* expression in the lungs, with carriers exhibiting much higher expression levels and a strong association with disease presence (Fingerlin et al., 2013; Seibold et al., 2011). Mouse models show that overexpression of *Muc5b* disrupts mucociliary clearance, leading to a fibroproliferative response that may contribute to IPF pathology (Hancock et al., 2018). Conversely, mutations in the *TOLLIP* gene, particularly the rs5743890_G variant, are associated with a lower risk of developing IPF, suggesting a protective role, although individuals with this variant who develop IPF tend to have higher mortality rates. This indicates that *TOLLIP* influences both disease risk and severity by affecting immune responses and inflammatory pathways (Noth et al., 2013). Variants in telomere maintenance genes, including *TERT, TERC, PARN, RTEL1, DKC1, TINF2, OBFC1*, and *STN1*, are linked to both familial and sporadic IPF cases, leading to telomere shortening, accelerated cellular aging, and defective epithelial repair (Fingerlin et al., 2013; Noth et al., 2013; Armanios et al., 2007; Stuart et al., 2015; Kropski et al., 2014; Alder et al., 2015; Song et al., 2021). In the area of surfactant dysfunction, mutations in *SFTPC* have been linked to familial lung fibrosis, damaging type II lung cells and resulting in various lung diseases, suggesting a common genetic origin (Thomas et al., 2002). Similarly, mutations in *SFTPA2* disrupt the structure of surfactant protein A2, leading to its retention in the endoplasmic reticulum, interfering with protein trafficking and contributing to familial IPF and lung cancer (Wang et al., 2009). Additionally, rare mutations in cell cycle regulation genes such as *KIF15, MAD1L1, CDKN1A*, and *TP53* have been identified in IPF cases (Allen et al., 2020; Korthagen et al., 2012). Finally, a large genome-wide association study of non-Hispanic White subjects identified associations with variants in the *DSP* and *DPP9* genes, which are involved in cell adhesion and may lead to a loss of epithelial integrity (Fingerlin et al., 2013), further emphasizing the multifaceted genetic contributions to IPF.

TABLE 1.2: **Genetic risk factors for IPF**

Category	Gene	Ref.
Host defence	*MUC5B*	(Fingerlin et al., 2013; Seibold et al., 2011)
	MUC2	(Fingerlin et al., 2013)
	ATP11A	(Fingerlin et al., 2013)
	TOLLIP	(Noth et al., 2013)
Telomere maintenance	*TERT*	(Armanios et al., 2007)
	TERC	(Armanios et al., 2007)
	PARN	(Stuart et al., 2015)
	RTEL1	(Stuart et al., 2015; Cogan et al., 2015)
	DKC1	(Kropski et al., 2014)
	TINF2	(Alder et al., 2015)
	OBFC1	(Fingerlin et al., 2013)
	STN1	(Noth et al., 2013)
Cell-cycle regulation	*KIF15*	(Allen et al., 2020)
	MAD1L1	(Allen et al., 2020)
	CDKN1A	(Korthagen et al., 2012)
	TP53	(Korthagen et al., 2012)
Surfactant processing	*SFTPC*	(Thomas et al., 2002)
	SFTPA1	(Takezaki et al., 2019)
	SFTPA2	(Wang et al., 2009)
	ABCA3	(Campo et al., 2014)
Epithelial intergrity	*DSP*	(Fingerlin et al., 2013)
	DPP9	(Fingerlin et al., 2013)
Fibrotic signaling	*AKAP13*	(Allen et al., 2017)

Information collected from (Podolanczuk et al., 2023; Moss et al., 2022; Raghu et al., 2011)

1.1.3.2 Cigarette

Smoking is associated with an increased risk of developing IPF, with former smokers and those with higher cumulative smoking exposure showing significantly elevated odds. The study found that 72% of IPF cases had a history of smoking, compared to 63% of controls, with an odds ratio (OR) of 1.6 for ever smoking. Although no clear exposure-response pattern was observed with cumulative cigarette consumption, there was a trend indicating higher risk among those who had recently quit smoking (Baumgartner et al., 1997). Additionally, chronic cigarette smoke can induce time-dependent epigenetic alterations in bronchial epithelial cells, leading to a predisposition for oncogenic transformation, which may contribute to the pathogenesis of smoking-related lung diseases, including IPF (Vaz et al., 2017).

1.1.3.3 Microbial agents

Certain viral exposures, particularly to Epstein-Barr virus (EBV), cytomegalovirus (CMV), human herpesvirus 7 (HHV-7), and HHV-8, have been associated with an increased risk of IPF (Moore and Moore, 2015; Sheng et al., 2020). Research on the role of chronic viral infections in IPF has largely focused on EBV and hepatitis C. Studies have found higher viral loads of EBV and CMV in IPF patients, with EBV antigens specifically detected in alveolar epithelial cells (AECs). These antigens are linked to markers of endoplasmic reticulum (ER) stress, suggesting a potential connection between latent viral infections and the development of IPF (Kropski et al., 2015). EBV genome rearrangements, indicating active replication, were found in a significant number of EBV DNA-positive IPF biopsies (Kelly et al., 2002). Additionally, Tang *et al.* detected the presence of eight herpesviruses, including EBV, in lung specimens from 33 patients with IPF, and found that one or more herpesviruses were detected in almost all IPF lungs compared with one-third of the control lungs (Tang et al., 2003). The rise in incidence and prevalence of IPF predates the COVID-19 pandemic, but exploring potential links between the two diseases remains relevant as IPF cases continue to grow. The symptoms and clinical presentation of acute COVID-19 infection are similar to those of IPF (Upadhya et al., 2021), and one study has identified IPF as a potential risk factor for COVID-19 (George et al., 2020). Additionally, IPF has been reported as a complication of COVID-19, as well as a symptom of long COVID (Zhang et al., 2021).

1.1.3.4 Environmental exposure

Environmental exposures have been increasingly recognized as potential risk factors for IPF, although establishing a direct causal link remains challenging. Numerous studies have documented correlations between IPF and various occupational exposures, such as agricultural chemicals, livestock, wood dust, metal dust, stone, and sand, as well as broader environmental factors like cigarette smoke (CS) and air pollution (Sack and Raghu, 2019). The lung microbiome also represents a persistent environmental exposure, with animal models and patient studies suggesting an association between increased bacterial burden, loss of microbial diversity, and fibrosis in IPF (Lipinski et al., 2020; O'Dwyer and Garantziotis, 2021). However, the structural changes in the lungs of IPF patients likely alter the local microbial environment, complicating conclusions about causality. Further, increased risk of IPF has been linked to occupations such as farming, bird raising, hairdressing, and stone cutting, with higher exposure to dusts from metals (brass, lead, steel), wood (pine), livestock, and vegetables (Hubbard et al., 1996; Miyake et al., 2005; Hubbard et al., 2000; Abramson et al., 2020). Autopsy studies have detected elevated levels of inorganic particles in the lymph nodes of patients with pulmonary fibrosis, supporting an environmental etiology (Kitamura et al., 2007).

However, these observations must be interpreted with caution due to the biases and limitations inherent in epidemiological studies of environmental risk factors.

1.1.4 Pathogenesis

The adult lung consists of four major, biologically distinct components: the trachea, bronchi, bronchioles, and alveoli, each with its own specific stem or progenitor cell population (Hackett et al., 2008). The pathogenesis of IPF primarily involves the lung alveoli and is driven by a complex interplay of various cell types and signaling pathways. The prevailing paradigm suggests that IPF results from repetitive micro-injuries to an aging alveolar epithelium, coupled with aberrant epithelial-mesenchymal communication. This leads to excessive extracellular matrix deposition and lung remodeling, ultimately impairing the lung's gas exchange capacity (Richeldi et al., 2017). However, this model is continually being challenged by emerging studies on IPF.

Historically, medical experts have faced challenges in understanding the intricate pathophysiology of IPF. It was initially thought to be a chronic inflammatory disorder (Haschek and Witschi, 1979), later considered an immune disorder, and today is recognized as a multifactorial disease driven by a combination of genetic and environmental factors. Despite significant advances, the precise causes and molecular mechanisms of IPF remain incompletely understood. Given the lack of effective treatment options, further exploration of the underlying mechanisms in IPF pathogenesis is crucial for developing potential therapies.

1.1.4.1 Epithelial cell injury and dysfunction

Alveoli, the specialized terminal structures of the distal airways, are essential for gas exchange. The alveolar surface is lined by two main epithelial cell types: alveolar type 1 (AT1) and alveolar type 2 (AT2) cells. AT1 cells are broad, flat cells that cover approximately 95% of the alveolar surface, mediating gas exchange and providing the majority of the epithelial surface area (Desai et al., 2014). In contrast, AT2 cells are smaller, cuboidal cells responsible for secreting surfactant to prevent alveolar collapse (Herzog et al., 2008).

Injuries and dysfunction of the alveolar epithelium play a key role in the initiation of IPF (Wynn, 2011; Parimon et al., 2020). Most studies on AT1 cell turnover in the injured, mature rodent lung indicate that AT1 cells are derived from AT2 cells during alveolar repair to maintain the epithelial lining (Evans and Hackney, 1972; Fujino et al., 2011; Olajuyin et al., 2019). However, repetitive injury to the alveolar epithelium—whether due to environmental insults or antigen stimulation—leads to significant loss of AT1 cells and pathological alterations in AT2 cells, including increased apoptosis, cellular

senescence, abnormal differentiation, and reduced regenerative capacity (Zhu et al., 2022; Liu et al., 2022) .

The first factor is cellular senescence of AT2 cells. Normally, the alveolar epithelium is maintained by the proliferation of AT2 cells, which act as multi-functional stem cells and produce pulmonary surfactant when in a resting state (Barkauskas et al., 2013). However, under genetic or environmental stress, the ability of AT2 cells to proliferate is reduced, impairing epithelial maintenance. Xu *et al.* used single-cell RNA sequencing to show that fibrotic regions in IPF lung tissue are characterised by both a loss of AT2 cells and abnormal activation of pathways related to cellular senescence, such as p53 signaling (Xu et al., 2016). They also found that AT2 cells from IPF lungs have a reduced ability to form alveolospheres (Liang et al., 2016). *Sin3a* loss in AT2 cells induces senescence, leading to persistent lung fibrosis resembling human IPF, whereas simple depletion of AT2 cells causes only transient fibrosis in mice (Yao et al., 2021).

Moreover, in IPF, AT2 cells exhibit mitochondrial dysfunction and increased ER stress. Deletion of Grp78 in AT2 cells induces ER stress, apoptosis, senescence, and fibrosis resembling IPF, effects that are more pronounced in older and male mice. The reduction of Grp78 in AT2 cells is associated with aging and IPF progression (Borok et al., 2020).

In IPF lungs, most of the epithelial cells are abnormally activated and secrete virtually numerous fibrogenic growth factors and cytokines that contribute to the expansion of the fibroblast and myofibroblast populations and to the remodeling of the ECM, including TGF-β, PDGF, TNF, CTGF, several matrix metalloproteinases (MMP1, MMP2, MMP7, MMP19) and a numerous of chemokines (including CCL2 and CXCL12) (Zhu et al., 2022; Yanagihara et al., 2022; Prata et al., 2017; Liu, Liu, Wang, Liu and Min, 2023; Golan-Gerstl et al., 2012). Several recent transcriptomic studies have identified epithelial cells with a molecular profile indicating a transitional state between AT2 and AT1 cells, commonly referred to as "transitional cells," "damage-associated transitional progenitors" (DATPs), or "prealveolar type-1 transitional cells" (PATS) (Details described in Table.1.3). For instance, Strunz *et al.* used scRNA-seq to profile cellular dynamics during mouse lung regeneration and identified KRT8+ ADI cells as a transitional state between AT2 and AT1 cells. These cells facilitate lung repair by promoting tissue remodeling and differentiation into mature AT1 cells. However, in IPF, KRT8+ ADI cells persist abnormally, secreting pro-fibrotic factors like Ctgf and Edn1, and interacting with mesenchymal cells and macrophages, driving fibrosis (Strunz et al., 2020). Peng Jiang and colleagues, using scRNA-seq, found that AT2 cells differentiate into AT1 cells in two stages: an early stage with upregulation of KRT8/KRT18, driven by TGF-β signaling, and a late stage where TGF-β signaling decreases. In fibrosis, persistent TGF-β activation blocks this process, causing an accumulation of KRT8/KRT18^{hi} transitional cells, which hinders lung repair and may contribute to IPF (Jiang et al., 2020). Kobayashi *et al.* identified KRT17 and TP63 positive cells as a subset of transitional epithelial cells in fibrotic lungs, particularly in IPF, using organoid cultures and

scRNA-seq. These cells resemble PATS-like populations derived from AT2 cells that fail to fully differentiate into AT1 cells, contributing to fibrosis. Enriched in senescence, TP53 signaling, and TGF-β pathways, these cells exhibit aberrant repair and persistent stress responses, leading to impaired tissue regeneration. They are vulnerable to DNA damage, which may further drive fibrosis (Kobayashi et al., 2020). Choi and colleagues used scRNA-seq and lineage tracing to identify two important cell types, Il1r1+ AT2 cells and DATPs, essential for lung regeneration. Inflammatory signals, especially IL-1β, control the differentiation of these cells during repair. Persistent IL-1β signaling disrupts cell transitions, impairing regeneration and contributing to lung diseases (Choi, Park, Tsagkogeorga, Yanagita, Koo, Han and Lee, 2020). Auyeung *et al.* used genetic knockouts and a selective IRE1α inhibitor to investigate its role in lung regeneration and fibrosis. Persistent IRE1α signaling traps DATPs in a transitional state, hindering repair and promoting fibrosis. Inhibiting IRE1α reduced fibrosis and stimulated alveolar cell regeneration, making IRE1α a potential therapeutic target (Auyeung et al., 2022). Habermann and colleagues identified KRT5$-$/KRT17+ epithelial cells expressing both epithelial and mesenchymal markers, representing an intermediate state contributing to ECM production in fibrosis (Habermann et al., 2020).

These studies reveal that transitional cell types, such as KRT8+ ADI cells, KRT17+ TP63+ cells, and DATPs, play a central role in both lung regeneration and fibrosis. Under normal conditions, these cells facilitate tissue repair following injury by transitioning AT2 cells into AT1 cells. However, in diseases like IPF, persistent activation of stress pathways such as TGF-β, IL-1β, TP53, and IRE1α prevents these cells from fully differentiating, leading to fibrosis. Instead of promoting repair, they secrete pro-fibrotic factors, interact with fibroblasts, and contribute to ECM deposition, ultimately driving disease progression.

TABLE 1.3: **Summary of the role of transient epithelial cellsin lung injury repair and fibrosis**

Cellular marker	**Description**	**Ref.**
KRT8+	• Role in Cell-Cell Communication: Krt8+ ADI cells interact with mesenchymal cells and macrophages, mediating signaling through the secretion of pro-fibrotic factors like Ctgf, Itgb6, Areg, Hbegf, and Edn1. • Balance Between Repair and Fibrosis: Essential for lung repair but associated with fibrotic pathways when abnormally regulated, contributing to IPF and other lung diseases. • Comparison to EMT and Senescence: While sharing features with EMT and senescence, Krt8+ ADI cells do not convert into fibroblasts but overlap in gene expression with cells undergoing epithelial-mesenchymal transition.	(Strunz et al., 2020)
KRT8/KRT18^{hi}	• Initiation of AT2-to-AT1 Differentiation: KRT8/KRT18^{hi} cells initiate the early differentiation of AT2 to AT1, regulated by TGF-β signaling. • Support of Alveolar Regeneration: Serve as a transitional state in early lung repair, aiding full differentiation of AT1 cells. • Response to Injury: Upregulated in response to injury, representing an intermediate phase aiding alveolar repair. • Potential Contribution to Fibrosis in IPF: Persistent expression in fibrosis disrupts AT2-to-AT1 differentiation, contributing to fibrotic remodeling. • Regulation of Differentiation Dynamics: Critical for initiating AT2 differentiation in vitro, with expression patterns regulated by TGF-β.	(Jiang et al., 2020)

Continued on next page

TABLE 1.3: **Summary of the role of transient epithelial cellsin lung injury repair and fibrosis (continued)**

Cellular marker	Description	Ref.
SFN+, KRT17+, TP63+	• Contributing to Fibrosis and Aberrant Repair: KRT17+TP63+ cells, enriched in senescence and TGF-β pathways, impair AT2-to-AT1 differentiation and contribute to fibrosis. • Potential Origin and Heterogeneity: Likely derived from AT2 cells and are part of a heterogeneous alveolar and airway population. • Vulnerability to DNA Damage and Stress: Display increased DNA damage from cellular stretching and stress-induced pathways linked to fibrosis and cancer.	(Kobayashi et al., 2020)
IL1R1+	• Regeneration Initiation: Il1r1+ AT2 cells initiate repair by responding to IL-1β signaling, aiding AT2-to-AT1 differentiation. • Promoting Differentiation: Prime AT2 cells for differentiation into AT1 cells, acting as intermediaries in lung regeneration. • Generation of DATPs: Contribute to DATPs, which are necessary for AT1 cell production. • Facilitating Tissue Repair: Play a crucial role in alveolar regeneration and repair. • Response to Inflammatory Signals: Bridge inflammatory signals to cell differentiation in the repair process.	(Choi, Park, Tsagkogeorga, Yanagita, Koo, Han and Lee, 2020)

Continued on next page

TABLE 1.3: **Summary of the role of transient epithelial cellsin lung injury repair and fibrosis (continued)**

Cellular marker	**Description**	**Ref.**
KRT7+, KRT8+	• Transitional State During Lung Repair: DATPs are transitional cells that emerge after epithelial injury and facilitate repair with stress and fibrosis-related gene programs. • Dual Role in Regeneration and Fibrosis: Promote regeneration during normal repair, but failure to differentiate can lead to fibroblast activation and fibrosis. • IRE1α Signaling and Fibrosis: IRE1α signaling sustains DATP phenotype, reinforcing TGF-β pathways and preventing differentiation, with inhibition promoting regeneration.	(Auyeung et al., 2022)
KRT5−, KRT17+	• Intermediate State in Epithelial Remodeling: KRT5−/KRT17+ cells act as intermediates between AT2 and AT1 cells, possessing both epithelial and mesenchymal-like features. • Pathological Contribution to Fibrosis: Co-express mesenchymal genes alongside epithelial markers, contributing to ECM deposition and fibrosis. • TGF-β and Stress Response: Associated with upregulated lung injury and fibrosis pathways, maintaining a fibrotic niche. • Aberrant Differentiation and Senescence: Represent an aberrant differentiation state failing to transition to mature AT1 cells, contributing to dysregulated repair in fibrotic regions.	(Habermann et al., 2020)

ADI, alveolar-damaged intermediate; Ctgf, connective tissue growth factor; Itgb6, integrin beta-6; Areg, amphiregulin; Hbegf, heparin-binding EGF-like growth factor; Edn1, endothelin-1; IPF, idiopathic pulmonary fibrosis; EMT, epithelial-mesenchymal transition; AT2, alveolar type 2 cells; AT1, alveolar type 1 cells; TGF-β, transforming growth factor-beta; IL-1β, interleukin-1 beta; Il1r1, interleukin-1 receptor 1; DATPs, damage-associated transitional progenitors; IRE1α, inositol-requiring enzyme 1 alpha; ECM, extracellular matrix; KRT, keratin.

1.1.4.2 Inflammation and immune response

IPF was first characterised as an inflammation-driven disease. However, clinical trials with broad immunosuppression failed to show benefit and sometimes caused harm. Even so, inflammatory responses—both innate and adaptive—are central to wound healing and fibrosis in many tissues, including the lung (Moss et al., 2022). Here, I outline how innate immune triggers initiate and sustain fibroblast activation in IPF, how these cues connect to adaptive immunity, and how specific cell types (macrophages, monocytes, lymphocytes, fibrocytes) shape the fibrotic niche.

Injured or apoptotic alveolar epithelial cells release damage-associated molecular patterns (DAMPs) that activate Toll-like receptors (TLRs) and downstream inflammatory cascades. Genetic studies also implicate innate regulators: for example, TOLLIP variants affect TLR and TGF-β signalling (Noth et al., 2013). The innate system further engages cytosolic inflammasomes—multimeric complexes (e.g., NLRP3, AIM2) that process IL-1β/IL-18 via caspase-1 (Tweedell and Kanneganti, 2024; Martinon et al., 2002). The NLRP3 inflammasome recognises pathogen- and damage-associated signals and can promote fibrosis through TGF-β and EMT-linked pathways (Artlett, 2022; Lasithiotaki et al., 2016). In addition, TLR9 activation has been proposed to accelerate fibrotic progression by promoting myofibroblast differentiation (Hogaboam et al., 2012).

The healthy lung contains alveolar macrophages (AMs), interstitial macrophages, and—after injury—recruited monocyte-derived macrophages. Although the M1/M2 scheme is simplified, it is useful here: M2-like programmes support wound repair (ECM deposition, angiogenesis, tissue remodelling) but become profibrotic if sustained. In IPF, M2-skewed macrophages and monocytes are increased, and markers such as CD163 are elevated on lung macrophages (Gibbons et al., 2011). At baseline, resident AMs are essential for lung development, surfactant homeostasis, pathogen clearance, and immune balance (Lambrecht, 2006). Macrophages are also major sources of profibrotic mediators, including TGF-β (MacKinnon et al., 2012) and growth factors (FGF, PDGF, IGF1, VEGF) that support fibroblast activation and ECM accumulation (Heukels, Moor, Von der Thüsen, Wijsenbeek and Kool, 2019; Phan et al., 2021; Khalil et al., 1989).

Classically activated (M1-like) macrophages produce IL-1β and TNFα, which contribute to IPF pathogenesis (Wilson et al., 2010; Gasse et al., 2007; Krausgruber et al., 2011). Elevated IL-1β in BALF from IPF patients likely derives from alveolar/interstitial macrophages (Wilson et al., 2010). In the bleomycin model, deletion of the IL-1 receptor (Il1r1) reduces lung inflammation and fibrosis (Gasse et al., 2007). IL-1β effects are time- and dose-dependent: transient, low-level signalling supports AT1 differentiation and repair, whereas sustained production impairs regeneration and drives maladaptive remodelling (Choi, Park, Tsagkogeorga, Yanagita, Koo, Han and Lee, 2020). Consistent with a pathogenic role for inflammasomes, both NLRP3 and AIM2 are activated in AMs

in human and murine fibrotic lungs (Lasithiotaki et al., 2016), and Nlrp3 deficiency confers resistance to bleomycin-induced inflammation and fibrosis.

After lung injury, circulating monocytes are recruited and mature into macrophages within the fibrotic lung (Ginhoux and Jung, 2014). Higher levels of circulating classical/intermediate monocytes associate with disease progression, and intermediate monocytes can predict poorer outcomes in IPF (Moore et al., 2014). These cells release pro-inflammatory cytokines (e.g., IFN-α, CCL3/MIP-1α, CCL4/MIP-1β) that can promote myofibroblast differentiation (Landsman et al., 2007).

Innate sensing by AMs and dendritic cells (DCs) produces IL-1β, IL-6, GM-CSF and TGF-β and enhances antigen presentation. DCs then migrate to draining lymph nodes. Chemokines such as CCL19/21 and CXCL13 help recruit and organise T and B cells. These cues shape $CD4^+$ T-cell fates (Th1 vs Th2/Th17/Treg) and support B-cell activation and BALT formation. Thus, chronic innate activation provides the conditions for adaptive immune engagement in IPF.

$CD8^+$ cytotoxic T cells recognise MHC I, and $CD4^+$ Th cells recognise MHC II and coordinate immune responses. Th1 (T-bet$^+$ IFN-γ^+), Th2 (GATA3$^+$), and Th17 (RORγT$^+$) subsets have all been implicated in ILD (Ruterbusch et al., 2020). IL-17A promotes lung fibrosis by stimulating EMT, fibroblast recruitment/proliferation, and ECM production (Wilson et al., 2010; Mi et al., 2011; Zhang et al., 2019). In early inflammation, IL-23 drives IL-17A production by Th17 and $\gamma\delta$ T cells, thereby enhancing fibrotic responses in murine bleomycin models (Gasse et al., 2011). (While IL-23 can activate fibroblasts in some contexts, its adverse effects in vivo are thought to be mediated primarily through lymphoid cells.)

B-cell involvement is also evident in IPF. IgA^+ memory B cells are increased in blood and lung and co-localise with PD-1^+ Tfh cells (Heukels et al., 2019). Circulating plasmablasts ($CD19^+/CD38^+CD27^+$) are more abundant and correlate negatively with lung function (Xue et al., 2013). Lung biopsies frequently contain $CD20^+$ B-cell aggregates and plasma cells, and BALT with germinal centres can form. These structures correlate with cytokines that organise T–B interactions (CCL21, CXCL13, BAFF, ICOSL) (Kim et al., 2020; Rangel-Moreno et al., 2006).

Fibrocytes are bone-marrow–derived, circulating cells ($CD45^+$, intracellular collagen-1^+) that arise from monocytes and can differentiate toward myofibroblasts (Bucala et al., 1994). They produce matrix proteins (collagen I/III, vimentin, fibronectin) and secrete IL-8, IL-6, TGF-β, PDGF, GM-CSF, and VEGF, thereby promoting fibroblast activation, angiogenesis, and inflammatory cell recruitment (Andersson-Sjöland et al., 2008; Chesney et al., 1998). In co-culture, fibrocytes enhance fibroblast production of collagen I, MMP-1, and PDGF-β (García de Alba et al., 2015).

Together, these data support a model in which innate pathways (DAMP–TLR signalling, inflammasomes, macrophage/monocyte programmes) initiate and sustain a profibrotic niche, while adaptive axes (selected T- and B-cell responses, tertiary lymphoid structures) contribute in a context- and stage-dependent manner. This framework helps reconcile why broad immunosuppression is not beneficial in IPF, yet immune mechanisms still shape disease biology: targeted, phase-appropriate modulation of specific pathways may be required, whereas antifibrotic agents remain the standard of care.

1.1.4.3 Myofibroblast activation

Myofibroblasts are the main effector cells in the progression of IPF. Under normal condition, resident fibroblast generically describes a connective tissue cell with the ability to produce connective tissue substance like collagens. However, under tissue injury or stimulus from profibrotic signals, fibroblasts temporarily suspend their specialized functions and adopt repair mechanisms to rapidly contain tissue damage by producing a fibrous, collagen-rich ECM, which eventually contracts to form a mechanically stabilizing scar. This is called fibroblast-to-myofibroblast transition (FMT) or myofibroblast activation.

There are also many types of myofibroblast precursors reported in human lung except for fibroblasts, such as epithelial cells (through EMT), endothelial cells, fibrocytes and macrophages via various signaling pathways. Myofibroblast differentiation from these precursors and resistance to apoptosis is mediated by a host of factors, including TGF-β, integrin αVβ6, PDGF, CTGF, VEGF, overexpression of Wnt, decreased expression of BMP2, decreased AMP-activated protein kinase (AMPK) activation, and imbalance of oxidant-antioxidants. Many of these signaling pathways, including TGF-β, PDGF receptor, epidermal growth factor, FGF, and Wnt, specifically promote expression of mesenchymal genes and downregulation of epithelial genes and thus activation of fibroblasts.

Epithelial cells

Alveolar epithelial cells are very important cells during the development of lung fibrosis as introduced before. EMT is a biological process in which epithelial cells (mainly AT2 cells) lose cell-cell adhesion and apical-basal polarity, undergo significant cytoskeletal changes, and acquire mesenchymal features such as increased invasion, migration, and ECM production (Salton et al., 2019). Although EMT is a physiological and often reversible process necessary for normal embryonic development and wound healing, it also plays a role in the initiation of IPF. During fibrosis, TGF-β can induce EMT in human AT-II cells in a time- and concentration-dependent manner (Kasai et al., 2005). Key features of EMT include the downregulation of E-cadherin and the miRNA200 family, loss of epithelial cell apical-basal polarity, and increased expression of mesenchymal

markers such as fibroblast-specific protein 1 (FSP1), α-SMA, collagen type I, vimentin, and fibronectin (Kalluri et al., 2009; Rout-Pitt et al., 2018). Additionally, transcription factors that drive fibroblast proliferation and mesenchymal differentiation, including ZEB1, ZEB2, Twist, Slug, and Snail, are upregulated during EMT. However, the occurrance of EMT remain controversial.

Previous studies have provided different perspectives on the contribution of EMT to fibroblast populations in lung fibrosis. Tanjore *et al.* demonstrated that EMT accounts for approximately one-third of FSP+ fibroblasts derived from lung epithelial cells two weeks after bleomycin-induced fibrosis in a mouse model (Tanjore et al., 2009). Similarly, Kim *et al.* showed that AT-II cells act as progenitors capable of undergoing EMT and contributing to fibroblast-like cells during lung injury and fibrosis (Kim, Kugler, Wolters, Robillard, Galvez, Brumwell, Sheppard and Chapman, 2006). In contrast, a study by Rock and colleagues, using lineage tracing techniques, found no evidence that epithelial cells convert into myofibroblasts in vivo (Rock et al., 2011). Adding to the debate, scRNA-seq data from IPF lungs have been analysed to identify mesenchymal markers within aberrant transitional epithelial cells; however, these findings do not support an epithelial origin for fibroblast populations (Adams et al., 2020; Tsukui et al., 2020). The discrepancies between studies on EMT contribution to fibroblast and myofibroblast populations in IPF may reflect differences in experimental models, methodologies, and disease context. For example, lineage-tracing in mice often shows limited evidence for fully differentiated myofibroblasts arising from epithelial cells, whereas in vitro studies and human biopsy analyses report robust EMT-like signatures. This divergence may be due to variations in the stage of disease examined, the sensitivity of lineage-tracing techniques, or the fact that epithelial cells can undergo partial EMT, acquiring mesenchymal traits without fully transitioning. Furthermore, microenvironmental factors such as TGF-β signaling intensity, hypoxia, and extracellular matrix stiffness differ between experimental systems and may influence the degree to which EMT contributes to fibroblast pools. Thus, conflicting results may not be mutually exclusive, but rather highlight the context-dependent nature of EMT in fibrotic remodeling..

Pericytes

Pericytes, the mural cells of blood microvessels, play a crucial role in tissue fibrosis (Armulik et al., 2011). Genetic lineage tracing by Humphreys *et al.* has shown that pericytes expand and differentiate into myofibroblasts in response to kidney injury (Humphreys et al., 2010). Similarly, Hung *et al.* identified two distinct populations of lung mesenchymal cells with roles in fibrosis, one being Foxd1-derived pericytes. These cells originate from Foxd1-expressing progenitors that enter lung buds during embryonic development and mature into a microvascular network, expressing pericyte markers such as PDGFRβ, NG2, and CD146. When stimulated by TGF-β, primary Foxd1-lineage stromal cells isolated from transgenic mouse lungs upregulate α-SMA

expression. Importantly, Foxd1-derived pericytes constitute a significant source of myofibroblasts during lung injury, accounting for around 68% of α-SMA+ myofibroblasts in fibrosis (Hung et al., 2013). However, the precise characterization of pericyte markers remains a topic of ongoing debate since Rock and colleagues did not find significant contribution to myofibroblasts in the lung using NG2 as the genetic label for lung pericytes (Rock et al., 2011).

Resident fibroblasts

Resident fibroblasts populations are generally recognized as the primary sources of activated myofibroblasts. Significant efforts have been made to better characterise the heterogeneity of lung mesenchymal populations. However, the lack of a single, definitive marker complicates the ability to accurately quantify their relative contributions to myofibroblasts. Another population that Hung *et al.* identified in lung fibrosis consists of resident fibroblasts that produce collagen-Iα1 and express PDGFRα, showing both transcriptional and morphological differences from Foxd1-derived pericytes. These cells resemble typical fibroblasts and likely contribute to up to 55% of the myofibroblast population post-injury, highlighting their significance as another major source of fibrogenic cells in the lung (Hung et al., 2013). Other markers of resident fibroblasts include Thy-1 (Hagood et al., 2005), fibronectin, and desmin (Phan, 2002).

The activation of resident fibroblasts is induced by TGF-β produced from injured epithelium or AMs. The activation of PDGF and CTGF by TGF-β are also involved in the activcation of fibroblasts.

Myofibroblasts are not only abnormally activated but also resistant to apoptosis. TGF-β1 has been shown to promote α-SMA expression and myofibroblast differentiation while preventing IL-1β-induced apoptosis by inhibiting iNOS expression, thereby reducing NO-mediated apoptotic signals from fibroblasts (Zhang and Phan, 1999). Additionally, myofibroblasts in both healthy and IPF lungs express TRPA1 ion channels, but TGF-β1 significantly down-regulates their expression. This down-regulation shields myofibroblasts from oxidative stress-induced cell death, supporting their survival and contributing to the persistence of fibrosis (Virk et al., 2021).

1.1.4.4 ECM remodeling

Extensive reorganisation of the lung ECM is a pathological alteration that leads to functional changes in lung function for several chronic lung diseases including asthma, COPD and IPF. The remodeling of the ECM is regulated through diverse mechanisms, including ECM protein synthesis, post-translational modifications, deposition, and degradation.

Excessive ECM protein deposition

The lung ECM is generated and maintained by various cell types, including fibroblasts, smooth muscle cells, as well as epithelial, endothelial, and immune cells. Activated fibroblasts and myofibroblasts in fibroblastic foci are believed to be the major producers of the ECM.

The main components of the basement membrane consist of collagen IV, collagen V, and laminins (the most abundant non-collagenous component), along with chondroitin sulfate proteoglycans (perlecan, agrin, and dystroglycan), entactin, fibronectin, fibulin I, and fibulin II. In contrast, the interstitial matrix is primarily composed of a meshwork of elastin, fibronectin, vitronectin, tenascin, versican, decorin, and fibrillar collagen I and III (Halfter et al., 2015; LeBleu et al., 2007; Faffe and Zin, 2009). Several studies have shown that collagen III is predominately deposited in early IPF, whereas more collagen I deposition is present in late-stage IPF (Kuhn III et al., 2012; Kage and Borok, 2012). Hoffman *et al.* demonstrated the ECM composition in IPF lungs is significantly altered compared to normal lungs, with notable region-specific differences. While the total collagen content is reduced, there is a distinct increase in COL3A1 within the whole ECM (wECM) and vascular ECM (vECM), a feature associated with fibrotic processes in IPF. The alveolar ECM (aECM) and wECM in IPF show changes in protein composition, including an increased proportion of fibulins (FBLN2 and FBLN3), which are linked to ECM remodeling. Additionally, the ECM glycoprotein content is elevated in IPF wECM compared to normal lungs, potentially influencing disease progression through altered biochemical signaling. While the airways ECM (airECM) maintains an increased presence of cartilage-associated collagens and proteoglycans, contributing to airway stiffness and remodeling, the overall changes across different regions highlight the complex remodeling of ECM components in IPF pathology (Hoffman et al., 2023).

ECM crosslinking

The ECM in fibrotic lungs exhibits abnormal biochemical and biomechanical characteristics. Increased ECM content and altered post-translational modifications are thought to enhance matrix stiffness, which, in turn, may drive sustained mesenchymal cell activation and progressive fibrosis through a positive feedback loop.

Fibrillar collagens are a major component of lung ECM, providing a scaffold that supports tissue architecture and significantly influences tissue stiffness (White, 2015). Highly crosslinked collagens are more resistant to degradation by MMPs (Issa et al., 2004). During biosynthesis, collagen undergoes various post-translational modifications, such as lysine hydroxylation and oxidation, which are essential for its structure and function.

Enzymatic crosslinking is primarily mediated by the lysyl oxidase (LOX) enzyme family, which includes LOX and LOX-like proteins (LOXL1-4). These enzymes, which are copper-dependent amine oxidases, produce reactive aldehydes that form covalent intra- and intermolecular crosslinks by reacting with other aldehydes or specific lysine and hydroxylysine residues (Eekhoff et al., 2018). Previous studies have found

increased expression of LOX, LOXL1, and LOXL2 in IPF compared to non-IPF lung tissues (Aumiller et al., 2017; Barry-Hamilton et al., 2010; Tjin et al., 2017). A recent study by Ma *et al.* revealed that LOXL4 plays a crucial role in pathological collagen cross-linking in lung fibrosis and may serve as a promising therapeutic target, whereas LOXL2 appears to have a limited role (Ma et al., 2023). LOX inhibition has been shown to reduce fibrillar collagen crosslinking and ECM stiffening in decellularized matrix models (Chen, Li and Li, 2019). The formation of LOX/LOXL-mediated collagen cross-links is influenced by the hydroxylation of telopeptides, a process catalyzed by lysyl hydroxylase 2 (LH2) or procollagen lysine,2-oxoglutarate 5-dioxygenase 2 (PLOD2) (Brinckmann et al., 1999). PLODs hydroxylate lysine residues inside cells before collagen is secreted, and LOX then acts on hydroxylysine residues in the extracellular collagen fibers, promoting cross-link formation (Saito and Marumo, 2010). This enzyme-dependent collagen crosslinking stabilizes new collagen fibers and enhances matrix stiffness, which contributes to IPF progression. Emerging evidence suggests that HIFs may regulate enzymes such as PLOD2 and LOXL2 in this context, thereby linking hypoxic signaling to collagen crosslinking and tissue stiffening. The role of HIF signaling in fibrosis will be discussed in detail in a later section.

ECM feedback on myofibroblasts

Myofibroblast activation is a multi-step process involving biochemical and biomechanical signaling pathways. Fibroblasts secrete TGF-β1 in a latent form, complexed with its latency-associated peptide (LAP). This latent complex is stored in the ECM by binding to latent TGF-β1-binding protein 1 (LTBP1) (Rifkin et al., 2018). Within the stiff ECM of tissues undergoing repair, contractile forces transmitted through actomyosin bundles and αv integrins to RGD-binding domains in LAP lead to a conformational change that releases active TGF-β1 (Wipff et al., 2007; Henderson et al., 2013).

Active TGF-β1 then binds to TGF-β receptors, triggering SMAD signaling, which results in SMAD4-SMAD2-SMAD3 complexes entering the nucleus to regulate the transcription of pro-fibrotic genes, such as *ACTA2* (encoding α-SMA) (Lodyga and Hinz, 2020; Massagué and Sheppard, 2023; Frangogiannis, 2022). This is counteracted by the negative regulator SMAD7. Additionally, TGF-β1 induces non-canonical signaling through pathways like JNK, p38, ERK, MAPK, and Rho-ROCK (Zhang, 2017; Derynck and Budi, 2019).

In the presence of mechanical stress (such as a stiff ECM), integrins undergo conformational changes, which lead to recruitment of signaling and structural proteins to their cytoplasmic side, forming focal adhesion complexes. These complexes involve proteins like vinculin, kindlin, talin (Sun et al., 2019), and FAK (Thannickal et al., 2003), which connect to actin filaments (F-actin) and support the formation of stress fibers.

The activation of ROCK is a key downstream event in myofibroblast signaling. Following the activation of RhoA by factors like LPA and thrombin binding to GPCRs, ROCK

enhances fibroblast contraction by inhibiting myosin light chain phosphatase (MLCP) and activating myosin light chain kinase (MLCK) (Zhang et al., 2022; Sakai et al., 2017). Additionally, Rho GTPases regulate actin polymerization, which is crucial for controlling gene transcription through co-transcription factors like MRTFA (Bialik et al., 2019). When actin polymerizes, MRTFA is released from G-actin and moves into the nucleus, where it associates with serum response factor (SRF) to promote the transcription of pro-fibrotic genes like CCN2 and ACTA2 (Yamamura et al., 2023).

The activation of RhoA also leads to the regulation of YAP/TAZ signaling. When stress fibers form, LATS1 and LATS2 (components of the Hippo pathway) are inhibited, increasing the levels of unphosphorylated YAP and TAZ in the cytosol (Dey et al., 2020). Unlike their phosphorylated forms, which are degraded, unphosphorylated YAP and TAZ translocate to the nucleus. There, they interact with transcription factors such as TEAD, β-catenin, and TCF–LEF to drive the expression of pro-fibrotic genes like CCN2 and microRNA-21 (Luo, 2017).

Overall, myofibroblast activation is driven by the release of TGF-β1, the formation of stress fibers through ROCK and RhoA signaling, actin polymerization, and the nuclear translocation of co-transcription factors such as MRTFA, YAP, and TAZ, which collectively enhance the transcription of pro-fibrotic genes.

In conclusion, the pathogenesis of IPF is a complex interplay of epithelial injury, immune response, and fibroblast activation, all leading to excessive extracellular matrix deposition and progressive lung scarring. Alveolar epithelial cell dysfunction, particularly of AT2 cells, triggers aberrant repair processes that promote fibrosis rather than regeneration. Key signaling pathways involving TGF-β, RhoA/ROCK, and YAP/TAZ drive myofibroblast activation and resistance to apoptosis, perpetuating the fibrotic cycle. Understanding these mechanisms provides valuable insights into potential therapeutic targets aimed at halting or reversing fibrosis in IPF (Figure.1.1 and Figure.1.2).

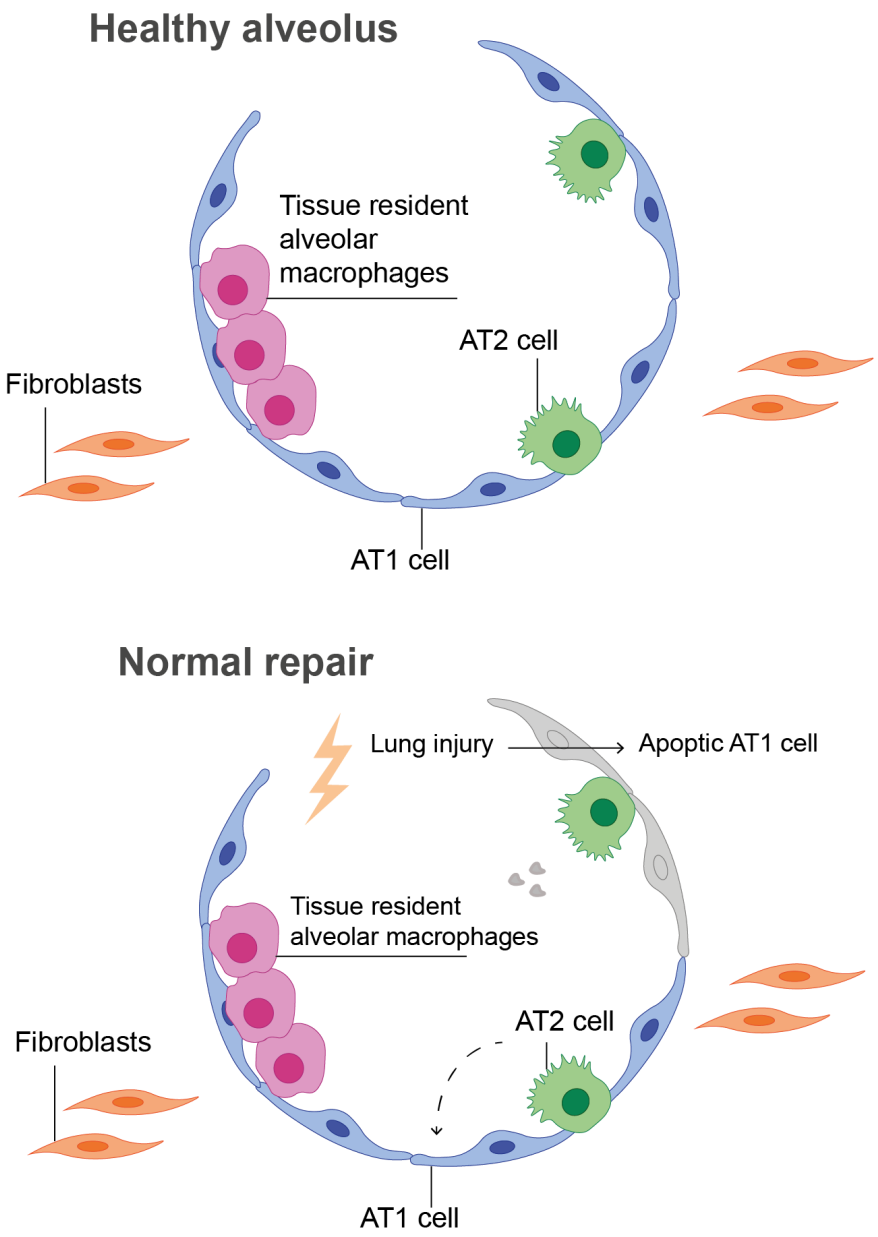

FIGURE 1.1: **Diagram of normal lung alveolar and normal repair after lung injury**
The diagram illustrates the key cell types within the human lung alveolus and the process of normal lung repair following injury. During this repair, AT1 cells undergo apoptosis and are subsequently cleared by lung-resident alveolar macrophages. Meanwhile, a portion of AT2 cells differentiate into new AT1 cells to restore the alveolar epithelium. Figure adapted from (Liu et al., 2022).

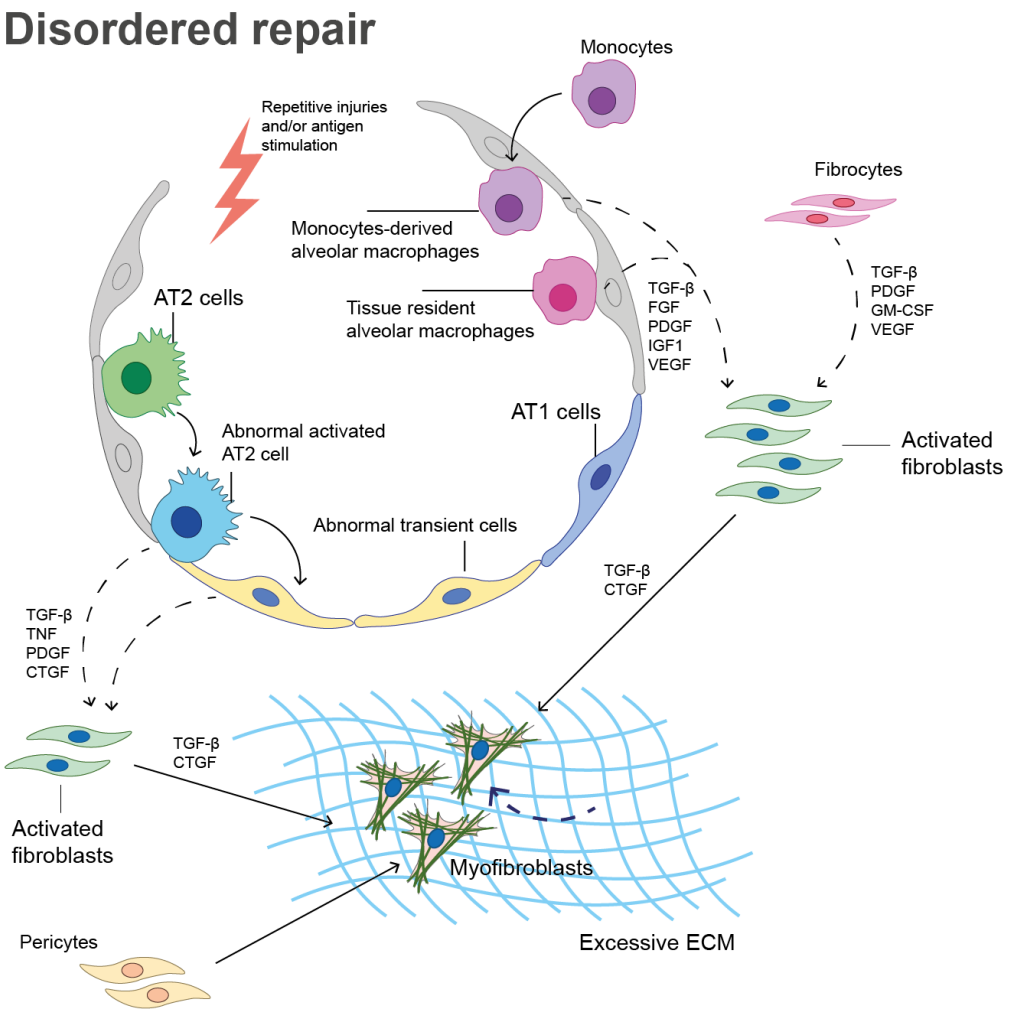

FIGURE 1.2: **Diagram of mechanisms invloved in the development of IPF**
The diagram illustrates the progression of IPF in the alveolar region, focusing on disordered repair mechanisms. Recurrent injuries to the alveolar epithelium, caused by environmental insults or antigen stimulation, lead to AT1 cell death and aberrant activation of AT2 cells. The process of AT2 cells differentiating into AT1 cells is impaired in fibrotic regions, resulting in the formation of transient cells that secrete large amounts of cytokines, promoting the differentiation of fibroblasts into myofibroblasts. Abnormally activated AT2 cells also contribute to fibroblast and myofibroblast proliferation through the production of PDGF, TGF-β, and CTGF. In response to failed epithelial repair, circulating monocytes are recruited to the alveolar space and differentiate into profibrotic alveolar macrophages. These monocyte-derived macrophages, along with resident alveolar macrophages, secrete PDGF and other growth factors, facilitating the activation, proliferation, and differentiation of fibroblasts into myofibroblasts. Pericytes further differentiate into myofibroblasts under TGF-β stimulation. The resulting myofibroblasts produce excess ECM proteins, leading to lung tissue stiffening. The stiff matrix inhibits fibroblast apoptosis, creating a positive feedback loop that sustains fibrosis.

1.1.5 Treatment

Since the pathogensis of IPF is complex and multiple molecular pathways involve in it, the treatment targeting IPF become a challenge. A variety of approaches have been utilised in the treatment of IPF, unfortunately the majority of these have been ineffective. Ninetdanib and pirefenidone, two FDA approved drugs for the treatment of IPF have been shown to reduce the rate of the fibrosis progression but can not stop it or reverse it. In the last two decades, amount of clinical trials on IPF failed but the development of treatment for IPF is still moving forward. This section will outline the pharmacotherapeutic and non-pharmacotherapeutic strategies for managing IPF.

1.1.5.1 Pharmacotherapy

Pirfenidone

Pirfenidone (PFD) is an oral antioxidant, antifibrotic, and anti-inflammatory drug approved by the US FDA for the treatment of IPF in October 2014. Its efficacy was demonstrated in three pivotal phase 3 trials: CAPACITY I, CAPACITY II, and ASCEND. In CAPACITY I and II, pirfenidone significantly slowed disease progression by reducing the decline in forced vital capacity (FVC) over 72 weeks compared to placebo (-8.5% vs. -11.0%; P = 0.005) (Noble et al., 2011). In the ASCEND trial, pirfenidone reduced the proportion of patients experiencing a 10% or greater decline in FVC or death after 52 weeks (16.5% vs. 31.8%; $P < 0.001$). Pooled analyses further showed lower all-cause and IPF-specific mortality, and a reduced risk of respiratory-related hospital admissions (P = 0.001) (King Jr et al., 2014; Ruwanpura et al., 2020).

One of the primary mechanisms by which PFD achieves its therapeutic benefits is through its antifibrotic activity. It inhibits the production of proteins (Ma et al., 2018; Hirano et al., 2006; Oku et al., 2008; Liu et al., 2005) or mRNA expression (Pourgholamhossein et al., 2018) of TGF-β1, a key mediator in fibrosis, thereby blocking pathways involved in fibroblast proliferation and myofibroblast differentiation (Conte et al., 2014; Ma et al., 2018; Qin et al., 2018; Molina-Molina et al., 2018). Vicens-Zygmunt *et al.* showed that PFD suppresses the production of ECM components, including collagen I, II, III, and fibronectin (Vicens-Zygmunt et al., 2015). It also inhibits heat shock protein 47 (HSP47), reducing collagen synthesis and ECM deposition, key drivers of fibrosis progression (Kakugawa et al., 2004; Nakayama et al., 2008; Torre et al., 2024). Beyond TGF-β1, PFD regulates other growth factors like PDGF and bFGF, both fibroblast mitogens (Gurujeyalakshmi et al., 1999), and inhibits the protein expression of PDGF-A and -B in bleomycin-induced lung fibrosis models (Yu et al., 2017). Kurita *et al.* reported that PFD reduces myofibroblast differentiation by inhibiting PDGFR-PI3K-Akt signaling (Kurita et al., 2017). PFD was also found to suppress bFGF expression in bleomycin-induced lung fibrosis (Oku et al., 2008). Fibrosis development, driven by

an imbalance of MMPs and TIMPs, leads to excess ECM production (Giannandrea and Parks, 2014; Tomos et al., 2023). PFD demonstrated therapeutic effects by reducing TIMP1 expression in bleomycin-induced lung fibrosis (Tian et al., 2006).

In addition to its antifibrotic effects, PFD has potent antioxidant properties. In a paraquat-induced lung injury and fibrosis mouse model, PFD significantly reduced the expression of reactive oxygen species(ROS)-related genes, such as *iNos*, *Nox1*, *Nox4*, and *Gpx1*. It also decreased lipid peroxidation and restored antioxidant enzymes, including superoxide dismutase and catalase. These actions mitigate oxidative stress, a major contributor to lung injury, protecting lung cells from further damage (van der Vliet et al., 2018).

PFD also shows substantial anti-inflammatory effects, contributing to its clinical efficacy. It reduces fibrosis by inhibiting macrophage-driven cytokines like IL-1, TNF-α, TGF-β1, PDGF (Gurujeyalakshmi et al., 1999; Iyer et al., 1999), HSP47 (Kakugawa et al., 2004), and MCP-1 (Rouhani et al., 2009), and by decreasing macrophage numbers (Trivedi et al., 2012; Xie et al., 2024). Additionally, PFD significantly suppresses TGF-β1 production induced by IL-4 and IL-13 in rat alveolar macrophages in vitro (Toda et al., 2018). It also inhibits NLRP3 inflammasome activation, reducing the secretion of cytokines like IL-1β (Li et al., 2018). These anti-inflammatory effects help alleviate chronic inflammation in IPF, supporting the long-term use of PFD in managing the disease.

PFD is approved for treating IPF in many countries and is recommended by current clinical guidelines for patients with mild-to-moderate IPF (Raghu et al., 2011). Studies have shown that it provides similar benefits for patients with advanced IPF (Chung et al., 2020) and for other interstitial lung diseases (ILDs) (Maher et al., 2020; Behr et al., 2021) with recent disease progression.

Nintedanib

Nintedanib (BIBF 1120) is a tyrosine kinase inhibitor (TKI) with anti-angiogenic properties, primarily by blocking the VEGF pathway (Wollin et al., 2014). It was also approved by the US FDA for the treatment of IPF in October 2014, based on results from two phase 2 INPULSIS trials (Richeldi et al., 2014). Both trials showed that nintedanib significantly reduced the annual decline in FVC at 52 weeks compared to placebo. In INPULSIS 1, the difference in FVC decline was 125.3 mL/year (95% confidence interval [CI], 77.7 to 172.8; P $<$0.001), while in INPULSIS 2, the difference was 93.7 mL/year (95% CI, 44.8 to 142.7; P $<$0.001). However, pooled analyses showed no significant difference between nintedanib and placebo regarding time to the first acute exacerbation, all-cause mortality, or respiratory-related death.

Nintedanib is a tyrosine kinase inhibitor originally developed as an anti-angiogenic cancer drug, designed to block PDGFR, FGFR-1, and VEGFR-2. Its inhibitory activity was confirmed in primary human lung fibroblasts from both IPF patients (IPLF) and

control donors (NHLF). Nintedanib effectively blocked PDGF-BB-stimulated PDGFR autophosphorylation and significantly reduced growth factor-induced cell proliferation in both IPF-HLF and N-HLF. It also reversed the pro-proliferative effects of PDGF-BB, FGF-2, and VEGF in IPF-HLF (Wollin et al., 2014). Additionally, nintedanib inhibited the migration of fibroblasts stimulated by PDGF and FGF in a concentration-dependent manner, demonstrating strong efficacy in reducing fibroblast motility in both cell types (Hostettler et al., 2014). Another study in primary lung fibroblasts derived from IPF patients showed that nintedanib exerts its antifibrotic effects by inhibiting ECM production, such as collagen and TIMP-2, and blocking TGF-β signaling. It also suppresses fibroblast-to-myofibroblast differentiation by inhibiting TGF-β signaling, and induces noncanonical autophagy, though this process does not directly contribute to its antifibrotic action (Rangarajan et al., 2016).

Moreover, nintedanib effectively inhibits angiogenesis and fibrosis by targeting endothelial cells, pericytes, and smooth muscle cells. It has demonstrated potent antiangiogenic and antifibrotic effects in preclinical models, where it suppresses tumor growth, cell proliferation, and fibrosis progression (Hilberg et al., 2008; Wollin et al., 2015). Although IPF is primarily a fibrotic disease, abnormal blood vessel growth also contributes to its progression. IPF lungs show uneven vascular changes, with excess capillaries in non-fibrotic regions and loss in fibrotic areas, while the new vessels that form are often abnormal. This imbalance promotes endothelial injury, hypoxia, and fibroblast activation. By blocking VEGFR, PDGFR, and FGFR pathways, nintedanib reduces both pro-fibrotic and pro-angiogenic signaling, helping to restore vascular balance and slow disease progression (Mondoni et al., 2024).

Novel treatment under clinical trials

The pathogenic mechanisms driving irreversible fibrosis remain incompletely understood. However, recent advances in basic and translational research have uncovered new potential therapeutic targets and several molecular pathways strongly linked to the disease, leading to numerous randomized controlled trials. A summary of ongoing or completed phase 2 and 3 trials is provided in Table.1.4. For instance, BMS-986278, an oral lysophosphatidic acid receptor 1 (LPA1) antagonist, is being developed for treating IPF and PPF. In a phase 2 trial (NCT04308681), 278 IPF patients were randomized to receive placebo or BMS-986278 (30 mg or 60 mg) twice daily for 26 weeks. The primary endpoint was the rate of change in percent predicted forced vital capacity (ppFVC). Patients receiving the 60 mg dose showed a 54% reduction in ppFVC decline compared to placebo, with a 62% reduction using the while-on-treatment strategy. A post hoc analysis also revealed that the 60 mg group had fewer progression events (23%) compared to placebo (39%). Adverse events, including diarrhea, cough, and orthostatic hypotension, were similar across groups, with serious AEs reported in 11% of the 60 mg group (Kreuter et al., 2024; Corte et al., 2023). Currently, BMS-986278 is under phase3 trial (NCT06003426). BI 1015550, an oral phosphodiesterase 4B (PDE4B) inhibitor, is being

developed for the treatment of IPF due to its anti-inflammatory and antifibrotic effects. In a phase 2, double-blind, placebo-controlled trial, BI 1015550 was shown to significantly reduce the decline in FVC over 12 weeks in IPF patients, both with and without background antifibrotic therapy. The trial enrolled 147 patients, and those treated with BI 1015550 had a median FVC decline significantly smaller than placebo, with a difference of 88.4 ml in those without antifibrotics and 62.4 ml in those on antifibrotics. These findings suggest that BI 1015550 effectively preserves lung function. The ongoing phase 3 trial is now evaluating the long-term tolerability of BI 1015550 and its ability to improve lung function and delay symptom progression, hospitalization, or death in patients with pulmonary fibrosis (Richeldi et al., 2022). Treprostinil, a prostacyclin analogue, is under phase 3 trial for IPF treatment. It improves mitochondrial function and reduces mitochondrial damage in lung fibroblasts from IPF patients, while also downregulating fibrosis-related proteins such as collagen and PAI-1. Its antifibrotic effects are mediated through the IP receptor in a cAMP-independent pathway, making it more effective than other cAMP-inducing agents (Waxman et al., 2020; Deeney et al., 2024; Fang et al., 2023). Additionally, several comprehensive reviews on IPF treatment have been published in recent years, following a surge in novel therapeutic approaches being tested for the condition (Antoniou et al., 2021; Bonella et al., 2023; Guo et al., 2023; R Lapthorn et al., 2024).

TABLE 1.4: **Clinical studies for IPF**

Target Category	NCT Number	Name	Machanism of action	Phase
Cytokines and Pathways	NCT05671835	TTI-101	STAT3 inhibitor	2
	NCT06097260	Bexotegrast (PLN-74809)	Dual $\alpha v\beta 1/\alpha v\beta 6$ integrin inhibitor	2
	NCT06132256	Axatilimab	Anti-CSF-1R mAb	2
	NCT05983471	ME-015 (Suplatast Tosilate)	Selective Th2 cytokine inhibitor	2
	NCT06588686	Buloxibutid	Angiotensin II Type 2 Receptor Agonist	2
	NCT06422884	ENV-101	Hh pathway inhibitor	2
	NCT05785624	Vixarelimab	Oncostatin M receptor β mAb	2
	NCT05060822	HEC585	TGF-βR1 inhibitor	2
	NCT05722964	SHR-1906	Anti-CTGF mAb	2
Kinases	NCT05975983	INS018_055	TNIK inhibitor	2
	NCT05570058	RXC-007	ROCK2 inhibitor	2
	NCT04598919	Saracatinib	Dual Src/ Bcr-Abl tyrosine-kinase inhibitor	2
	NCT05119972	ZSP-1603	Triple tyrosine kinase inhibitor	1/2
Phosphodiesterases	NCT04419506	BI-1015550	PDE4B inhibitor	2
	NCT06238622			3
Other compounds	NCT06567717	Nicotinamide Riboside (NR)	NAD+ precursors	2
	NCT06125327	Sufenidone (SC1011)	Pirfenidone analogue	2/3
	NCT06317285	GSK3915393	Irreversible tTG2 inhibitor	2
	NCT06003426	BMS-986278	LPA1 antagonist	3
	NCT04965298	Lansoprazole	Selective menbrane H+/K+ATPase inhibitor	3
	NCT06335303	BI 1819479	ATX inhibitor	2
	NCT05571059	Lfetroban	TxA2/PGH2 Receptor Antagonist	2
	NCT03865927	GKT137831	Nox1/4 dual inhibitor	2
	NCT05424887	GDC-3280 (AK 3280)	Pirfenidone derivative	2
	NCT06331624	GRI-0621	iNKT activation inhibitor	2
	NCT05951296	Leramistat	Mitochondrial complex 1 inhibitor	2
	NCT05389215	DWN12088	Prolyl-tRNA Synthetase Inhibitor	2
	NCT04708782	Treprostinil	Epoprostenol analog	3
	NCT02538536	PBI-4050	GPR-40 agonist and GPR-84 antagonist	2
	NCT02503657	Tipelukast	LT-R antagonist, PDE3/4 and 5-LO inhibitor	2

Information collected from ClinicalTrial.gov (https://www.clinicaltrials.gov/) and (Antoniou et al., 2021; Bonella et al., 2023; R Lapthorn et al., 2024) (STAT, signal transducer and activator of transcription; CSF, colony stimulating factor; TGF-βR, transforming growth factor beta receptor; TNIK, TRAF2 and NCK-interacting kinase; ROCK, Rho-associated protein kinase; PDE, phosphodiesterase; NAD, nicotinamide adenine dinucleotide; TG, transglutaminase; PGH, prostaglandin H; LPA, lysophosphatidic acid; ATX, autotaxin; iNKT, invariant natural killer T cells; GPR, G protein-coupled receptor).

1.1.5.2 Non-pharmacotherapy

In addition to pharmacological therapies, non-pharmacological interventions play a key role in managing IPF.

Pulmomary rehabilitaion (PR)

Pulmonary rehabilitation (PR) is a vital part of the non-pharmacological management of IPF. It involves a comprehensive approach that starts with a detailed patient assessment, followed by a personalized treatment plan aimed at improving the physical and

psychological well-being of individuals with chronic respiratory diseases. PR also encourages long-term commitment to health-promoting behaviors (Spruit et al., 2013). Research has demonstrated that PR significantly enhances the quality of life and functional capacity of IPF patients, and it remains the only intervention proven to improve exercise tolerance (Holland et al., 2008; Sharif, 2017).

The evidence for PR in IPF has grown significantly. The most recent Cochrane review included 21 RCTs on PR in ILD, nine of which focused on IPF, and found that PR improved the 6-minute walk distance (6MWD) by 37 m (95% CI 26–48 m), exceeding the minimal important difference of 30 m (Dowman et al., 2021; Holland et al., 2009). Although the impact on anxiety and depression is less clear, some subgroups with mood disorders saw improvements (Jarosch et al., 2016; Edwards et al., 2023). A review of 240 ILD patients, 45% with IPF, showed PR effectively improved dyspnea and exercise capacity regardless of diagnosis or severity (Brunetti et al., 2021). The long-term benefits of PR are uncertain. Kataoka *et al.* (Kataoka et al., 2023) conducted the first RCT evaluating a maintenance strategy for PR in IPF, demonstrating that adding a 40-week maintenance program with home exercise and monthly sessions improved cycle endurance time at 12, 16, and 52 weeks. Maintenance exercise programs may help preserve PR benefits, but more research is needed to determine the most effective approaches (Dowman and Holland, 2024).

Lung transplantation (LT)

Lung transplantation is the only treatment that significantly improves both quality of life and survival for patients with advanced IPF, particularly when other treatments have failed (Le Pavec et al., 2020). Early evaluation for transplantation is essential, especially for patients with limited treatment options and a predicted mortality risk exceeding 50% within two years (George et al., 2019). Current survival rates post-lung transplantation for IPF have steadily improved, with a 1-year survival rate of 88.8% and a 5-year survival rate of 50% to 56% (Valapour et al., 2021; Le Pavec et al., 2020). Studies suggest that IPF patients have favorable long-term survival compared to other conditions requiring transplantation (George et al., 2019; Anderson et al., 2024).

However, precise timing for transplantation remains unclear, with decisions typically based on disease progression and diffusion capacity. The choice between single-lung transplantation (SLT) and bilateral lung transplantation (BLT) is still debated, as the survival benefit of one approach over the other is uncertain. While SLT was previously preferred due to fewer cardiac complications, advancements in surgical techniques have led to an increasing trend toward BLT, which is now performed in over 50% of IPF cases and is associated with better long-term outcomes (Thabut et al., 2009; Kapnadak and Raghu, 2021).

Over the past decade, lung transplants for IPF have increased, accounting for 28% of all procedures in 2009, up from 16% in 2000, nearing rates seen in COPD (Valapour

et al., 2021). Given the complexities of lung transplantation, including donor scarcity and the increasing comorbidities of IPF patients, early referral for transplant evaluation is recommended to maximize outcomes according to ISHLT guidelines.

Oxygen therapy

Long-term supplemental oxygen is used for patients with advanced IPF to maintain adequate oxygen saturation and alleviate hypoxemia, improving both exercise tolerance and quality of life. The ATS/ERS/JRS/ALAT international evidence-based guideline strongly recommended to treatment long term oxygen therapy (LTOT) for IPF patients with hypoxemia (Raghu et al., 2011). Ishiwari *et al.* showed that the patients with connective tissue disease-related interstitial lung disease (CTD-ILD) had longer overall survival than those with IPF (36.0 vs 23.5 months, P =0.028), there was no significant difference in prognosis after the initiation of LTOT between the two groups (Ishiwari et al., 2024). Currently the studies of the impact of LTOT on IPF patients and the prognosis are still lacking.

It is crucial that IPF patients have access to both pharmacological and non-pharmacological therapies. Regular assessments are essential to ensure treatments are evaluated and adjusted as needed. Eligible patients should also be referred for participation in clinical trials.

1.2 TGF-β signaling pathway

1.2.1 Overview

As we introduced in the previous section, many studies have focused on the pathogenesis mechanisms, which mainly include the Smad, MAPK, and ERK signaling pathways (Zhou et al., 2024). Among these mechanisms, TGF-β1 holds significant importance. This section aim to summarize the role of TGF-β1 and relevant pathways in the development of IPF.

1.2.2 TGF-β subfamily

TGF-β is the prototype of a family of secreted polypeptide growth factors. Since its identification in 1981 (Roberts et al., 1981), when it was found to induce the transforming growth of cultured fibroblasts, more than 40 members of this superfamily have been discovered. The TGF-β family consists of three isoforms—TGF-β1, TGF-β2, and TGF-β3—each formed by interrelated dimeric polypeptide chains. These isoforms are encoded by genes located on different chromosomes: *TGFB1* is found on the long arm of chromosome 19 (19q13.1) for TGF-β1, *TGFB2* on chromosome 1 (1q41) for TGF-β2,

and *TGFB3* on chromosome 14 (14q24) for TGF-β3 (Fujii et al., 1986; Barton et al., 1988). TGF-β1 is the most prevalent isoform in human tissues, such as the lungs, liver, kidneys, and heart. When analysing their primary structure, polypeptides in the TGF-β family form a highly homologous group. TGF-β1 and TGF-β2 share 71.4% of their amino acid sequences, while TGF-β3 shares 76% of its sequence with TGF-β1 and 80% with TGF-β2 (Marquardt et al., 1987). Despite these differences, all three isoforms function through the same receptor signaling system.

1.2.3 Canonical TGF-β1/Smad signaling pathway

The Smad family is divided into three subfamilies: five receptor-activated Smads (R-Smads), one common mediator Smad (Co-Smad), and two inhibitory Smads (I-Smads). R-Smads are further classified into two groups: BMP-Smads and TGF-β/activin-Smads. Smad1, Smad5, and Smad8 are phosphorylated by BMP type I receptors (ALK-2, ALK-3, ALK-6) and ALK-1, while Smad2 and Smad3 are activated by TGF-β and activin type I receptors (ALK-5 and ALK-4) and the orphan receptor ALK-7. Smad6 and Smad7, known as inhibitory or anti-Smads, structurally differ from other family members and inhibit Smad signaling by blocking R-Smad activation (Werner et al., 2000). In mammals, a single Co-Smad, Smad4, has been identified (Itoh et al., 2000). Typically, TGF-β1 activates Smads via the transmembrane receptor serine/threonine kinase, sequentially regulating target gene transcription (Ye and Hu, 2021).

Following TGF-β1 activation of the TGF-β type I receptor - ALK5, Smad2 and Smad3 are phosphorylated which can be inhibited by Smad7 and form a complex with Smad4, which translocates to the nucleus to regulate gene expression (Figure.1.3).

1.2.4 The role of TGF-β1/Smad signaling pathway in IPF

The TGF-β1/Smad signaling pathway contributes to IPF through four key processes: myofibroblast differentiation, EMT, endothelial-to-mesenchymal transition (EndMT), and fibrogenesis.

1.2.4.1 Myofibroblast differentiation

TGF-β1 is crucial for regulating the differentiation of HLFs and promotes the expression of ECM proteins, along with the myofibroblast marker αSMA. The TGF-β1/Smad2/-Smad3 signaling pathway is the main mechanism driving fibroblast differentiation. However, the role of Smad2 in TGF-β1-induced FMT remains debated.

Gu *et al.* found that TGF-β1 induces αSMA transcription via a Smad3-dependent, but not Smad2-dependent, pathway, increasing αSMA expression in HFLFs (Gu et al.,

2007). Conversely, Deng *et al.* reported that TGF-β1 activation of Smad3 in HLFs does not affect collagen I or αSMA expression (Deng et al., 2015).

In contrast, Lim *et al.* demonstrated that Smad2 is essential for TGF-β1-induced fibroblast differentiation. Gal-1 interacts with Smad2, enhancing its phosphorylation and nuclear retention, both of which are crucial for differentiation. Knockdown of Gal-1 reduced Smad2 activity, preventing fibroblast differentiation (Lim et al., 2014). Ard *et al.* further suggested that sustained Smad2 phosphorylation, dependent on Smad3 activity, is required for myofibroblast differentiation (Ard et al., 2019).

MicroRNAs are also involved in regulating TGF-β-mediated fibrosis. TGF-β1 upregulates miR-424 through the Smad3-dependent pathway. miR-424 acts as a positive feedback regulator by inhibiting Slit2, which suppresses TGF-β1's profibrogenic effects. Inhibiting miR-424 reduces Smad3 phosphorylation, reinforcing its role in the TGF-β1/Smad3 feedback loop (Huang, Xie, Abel, Wei, Plowman, Toews, Strah, Siddique, Bailey and Tu, 2020). Additionally, miR-101 inhibits lung fibroblast activation by targeting ALK5, reducing Smad2/3 phosphorylation and suppressing fibroblast activation (Huang et al., 2017).

TGF-β1/Smad3 signaling also contributes to NOX4-mediated production of H_2O_2, which is essential for myofibroblast differentiation in lung mesenchymal cells, suggesting NOX4 as a potential therapeutic target in IPF. TGF-β1 further accelerates lung fibrosis by stimulating ROS production through NOX4, promoting the nuclear export of HDAC4 and the formation of αSMA fibers in NHLFs (Guo et al., 2017). ROS exposure also upregulates miR-9-5p, which inhibits the transformation of mesothelial cells into myofibroblasts and reduces fibrogenesis by targeting TGFBR2 and NOX4, suggesting a self-limiting mechanism in fibrosis regulation (Fierro-Fernandez et al., 2015).

Additionally, TGF-β1 upregulates SIRT6 in HFLFs. Overexpression of SIRT6 inhibits TGF-β1-induced myofibroblast differentiation by suppressing both TGF-β1/Smad2 and NF-κB signaling pathways (Zhang, Tu, Tian, Han, Wang, Chen and Zhou, 2019). Inhibition of TGF-β1/Smad signaling also downregulates Rock1, RhoC, and RhoA, indicating that Rho kinase is a key mediator of TGF-β1/Smad-induced myofibroblast differentiation (Ji et al., 2014; Mendoza and Jimenez, 2022).

1.2.4.2 EMT and EndMT

TGF-β is one of the most studied growth factors involved in EMT. The SMAD complex in nucleus represses the expression of E-cadherin through SNAIL1 and SNAIL2 transcription factors, which induce the expression of mesenchymal proteins such as N-cadherin, fibronectin and metalloproteinases. Furthermore, TGF-β1/Smad signaling drives the EMT transcription response indirectly through induced expression of

TWIST, ZEB1 and ZEB2, and overlaps with other EMT pathways such as Wnt (Willis and Borok, 2007; Chilosi et al., 2017; Salton et al., 2019).

TGF-β also serves as a key regulator of EndMT in pulmonary fibrosis. TGF-β1 upregulates CXCR7, a seven-transmembrane G protein-coupled receptor in endothelial cells, in a Smad2/3-dependent manner. Overexpression of CXCR7 inhibits TGF-β1-induced EndMT and lung fibrosis by suppressing the Jag1-Notch pathway (Guan and Zhou, 2017). Additionally, TGF-β1 significantly increases the expression of RELM-β via the Smad2/3/4 pathway, which has been shown to enhance TGF-β1-induced cell proliferation and EndMT (Jiang et al., 2018). Rho kinase signaling, activated by TGF-β1 during EMT, positively regulates PDE4, promoting EMT in AECs (Kolosionek et al., 2009). In a bleomycin-induced pulmonary fibrosis mouse model, combined treatment with active TGF-β and Ras induced the expression of Snail and Twist in endothelial cells (Hashimoto et al., 2010; Nataraj et al., 2010).

1.2.4.3 Fibrogenesis

TGF-β1 plays a central role in promoting fibrogenesis in pulmonary fibrosis, largely through its regulation of multiple signaling pathways. One key regulator of fibrosis is peroxisome proliferator-activated receptor γ (PPARγ), which negatively regulates TGF-β1-induced fibrosis. TGF-β1 downregulates PPARγ in a Smad3-dependent manner, as cells lacking Smad3 exhibit a weakened repression of PPARγ by TGF-β1 (Ramirez et al., 2012). Furthermore, a study using a bleomycin-induced pulmonary fibrosis mouse model showed that co-treatment with recombinant CTGF and TGF-β increased profibrotic markers in fibroblasts, confirming the synergistic effect of CTGF with TGF-β/Smad3 signaling in promoting pulmonary fibrosis (Yanagihara et al., 2022).

Follistatin-like protein 1 (Fstl1), another significant player in fibrogenesis, is upregulated at both the transcriptional and translational levels by TGF-β1 through the Smad3/c-Jun pathway in pulmonary fibroblasts. This suggests that the TGF-β1/Smad3/c-Jun/Fstl1 axis contributes to IPF (Zheng et al., 2017). Additionally, TGF-β1/Smad3 signaling suppresses the expression of the long noncoding RNA FENDRR, which normally acts to reduce fibrosis and inhibit pulmonary fibrogenesis (Huang, Liang, Zeng, Yang, Xu, Gou, Sathiaseelan, Senavirathna, Wang and Liu, 2020).

The TGF-β1/Smad3 pathway also promotes pulmonary fibrosis by enhancing ERK5 phosphorylation, leading to increased collagen contraction and migration in fibroblasts (Kadoya et al., 2019). Interestingly, TGF-β1 also activates Semaphorin 7A (SEMA7A) and its receptors through Smad3-independent mechanisms, further driving pulmonary fibrosis (Kang et al., 2007).

Moreover, TGF-β1/Smad3 signaling increases the expression of activating transcription factor 4 (ATF4), a crucial regulator of amino acid metabolism. This occurs through

the activation of mTORC1 and its downstream target 4E-BP1, promoting collagen biosynthesis. This pathway is a key mechanism by which TGF-β1 stimulates collagen production in human lung fibroblasts, contributing to the development of IPF (Mukherjee et al., 2020).

1.2.5 Non-canonical TGF-β1 relavent pathways

TGF-β1/Smad1/5/8 signaling pathway

Unlike the canonical ALK5-Smad2/3 pathway, the TGF-β type I receptor ALK1 forms a heterodimer with ALK5 under stimulation by active TGF-β, leading to activation of Smad1/5/8 and suppression of ALK5-Smad2/3 signaling (Finnson et al., 2008; Zhang et al., 2017). The activation of Smad1/5/8 can be inhibited by Smad7 (Katsuno et al., 2018). Pannu *et al.* showed that in a mouse model of scleroderma-like fibrosis due to forced expression of ALK5, activation of a fibrogenic transcriptional program was dependent on Smad1 and Erk1/2, and not on Smad2/3 (Pannu et al., 2007). A recent study demonstrated the efficacy of PFD in reversing EMT of A549 cells in vitro by differentially regulating the TGF-β1 mediated Smad1-7 signaling pathway and modulating both E-Cadherin and Vimentin expression (Kulshrestha et al., 2023).

PI3K signaling pathway

Numerous studies have shown that phosphatidylinositol-3-kinase (PI3K) plays a key role in the pathogenesis of pulmonary fibrosis (Margaria et al., 2022; Wang, Hu, Cai, Yang, He, Wang and Weng, 2022). PI3K has also been identified as a crucial factor in TGF-β1-associated IPF.

TGF-β1 significantly upregulates hAT1R mRNA and protein levels through Smad2/3 activation. The study also emphasizes that the PI3K, p38 MAPK, and JNK pathways are essential for TGF-β1-induced hAT1R expression, as inhibition of these pathways markedly reduces hAT1R levels, demonstrating their critical role alongside the Smad pathway (Martin et al., 2007). TGF-β1 has been shown to induce EMT and ECM synthesis in lung epithelial cells via the TGF-β1/PI3K/CTGF signaling pathway (Shi et al., 2016). Treatment with a PI3K inhibitor in human lung epithelial cells not only suppresses CTGF and type I collagen synthesis but also reverses TGF-β1-induced EMT and fibrogenesis. Furthermore, TGF-β1 activates PI3K and PKB/AKT through SEMA7A-dependent mechanisms (Kang et al., 2007), and it synergistically activates the PI3K/JNK/AKT and AP-1 pathways to induce tissue factor expression in HLF, promoting IPF progression (Wygrecka et al., 2012).

JNK signaling pathway

Coagulation factor XII (FXII), a serine protease involved in fibrinolysis, has been shown to be produced in HLFs in response to TGF-β1 through JNK/Smad3 signaling pathways (Jablonska et al., 2010). Stimulation with TGF-β1 also significantly increased the expression of phosphorylated p38, phosphorylated JNK, and interstitial markers such as desmin, vimentin, and αSMA (Kasai et al., 2005). TGF-β1 induces the differentiation of HLFs into myofibroblasts in a dose- and time-dependent manner. Although TGF-β1 activates c-JNK, p38 MAPK, and ERK, the phenotypic shift from HLF to myofibroblast is primarily regulated by c-JNK, suggesting that TGF-β1 promotes this transition via a c-JNK-mediated pathway (Hashimoto et al., 2001). Furthermore, TGF-β1 has been reported to contribute to pulmonary fibrosis by downregulating VEGF-D expression in HLFs through the JNK signaling pathway, offering a potential mechanism for tissue remodeling in IPF (Cui et al., 2014). Another study found that TGF-β induces the synthesis of endothelin-1 (ET-1), a potent pro-fibrotic factor, through a non-Smad pathway involving ALK5/JNK/AP1 in both normal and fibrotic lung fibroblasts. The study also noted that fibrotic lung fibroblasts exhibit constitutive JNK activation, which sustains the myofibroblast phenotype in pulmonary fibrosis (Shi-Wen et al., 2006).

p38 signaling pathway

TGF-β1 inhibits fibroblast apoptosis by inducing a p38-dependent growth factor, which activates the PI3K/AKT pathway (Kulasekaran et al., 2009). Interestingly, while TGF-β1-induced activation of p38 MAPK promotes the expression of α-SMA in HLFs, it does not induce collagen I expression (Deng et al., 2015). TIMP3, an effective angiogenesis inhibitor that blocks VEGF binding to VEGFR2, has been identified as a key mediator of TGF-β1-induced IPF (Garcia-Alvarez et al., 2006). TGF-β1 strongly upregulates TIMP3 expression in HLFs via the p38 pathway, independent of ERK signaling. Furthermore, p38-mediated downregulation of epithelial complement inhibitory proteins (CIPs) by TGF-β1 exacerbates epithelial damage in IPF, triggering complement activation. This, in turn, reduces CIP levels and induces a feedback loop that further increases TGF-β1 expression (Gu et al., 2014).

Wnt/β-catenin signaling pathway

Growing evidence suggests that Wnt/β-catenin signaling is involved in TGF-β1-related IPF. TGF-β1 initiates the Wnt/β-catenin cascade by upregulating β-catenin and GSK-3β, promoting fibrotic differentiation of lung mesenchymal stem cells (Lu et al., 2019). In addition, Wnt/β-catenin is necessary for the initiation of TGF-β1-induced Smad2/3 signaling, indicating potential crosstalk between these pathways in myofibroblast differentiation (Xu et al., 2017). TGF-β1 activates β-catenin signaling, increasing transcriptionally active and total β-catenin protein levels, along with the expression of collagen1α1, αSMA, and fibronectin—effects that are reduced by β-catenin-specific siRNA and pharmacological inhibition (Baarsma et al., 2011). Further research from the same

group showed that GSK-3 signaling reduces CREB phosphorylation, weakening its antagonistic effect on TGF-β/Smad signaling, thus promoting myofibroblast differentiation in HLFs (Baarsma et al., 2013). However, Liu *et al.* suggested that in human skin fibroblasts, Wnt/β-catenin acts as a negative regulator of TGF-β1-induced myofibroblast transition (Liu, Wang, Pan, Su, Zhang, Han, Zhu, Tang and Hu, 2012). In alveolar epithelial cells (AECs), TGF-β1 induces nuclear accumulation of β-catenin, facilitating EMT through a CBP-dependent mechanism, revealing a potential TGF-β1/β-catenin/CBP cascade (Zhou et al., 2012).

In conclusion, TGF-β1 plays a central role in the pathogenesis of IPF by regulating key signaling pathways, including Smad, PI3K, JNK, p38/MAPK, Wnt/β-catenin. These pathways collectively drive processes such as myofibroblast differentiation, EMT, EndMT, and fibrogenesis, contributing to the progression of fibrosis. Targeting these signaling mechanisms, particularly the PI3K and JNK pathways, presents promising opportunities for therapeutic intervention. Future research should focus on developing targeted therapies that inhibit these pathways to attenuate fibrosis and improve outcomes for patients with IPF.

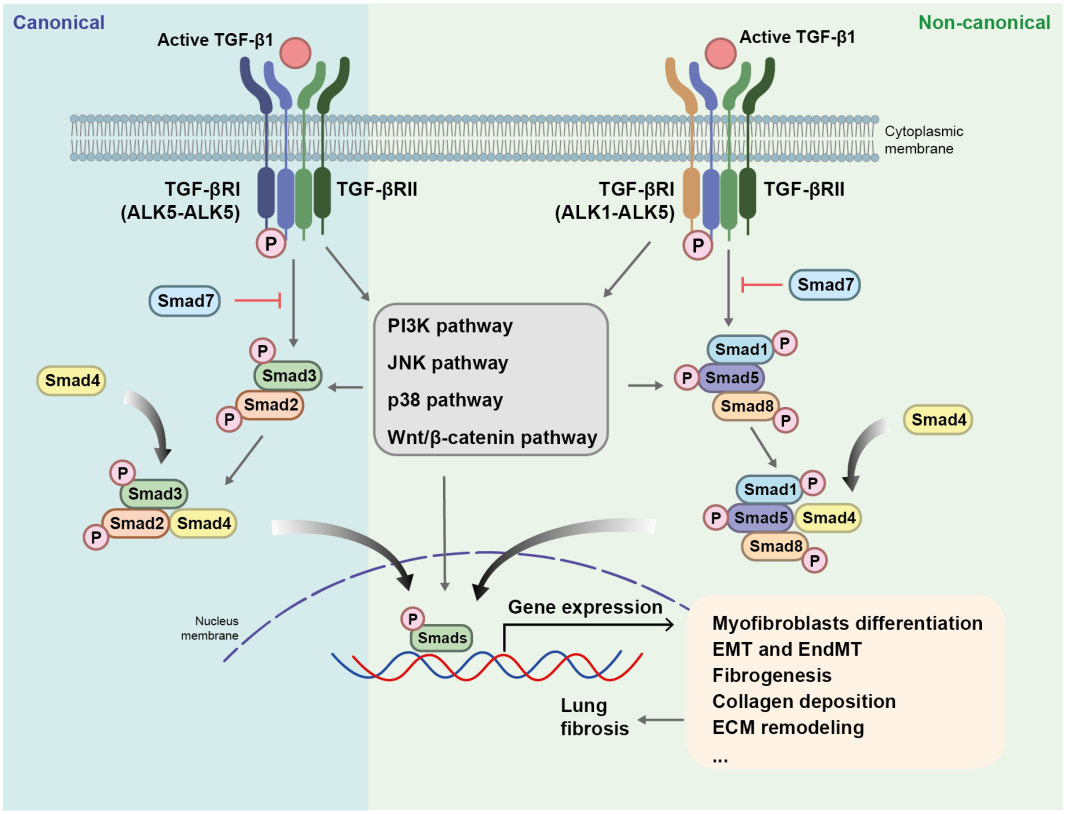

FIGURE 1.3: **Diagram of TGF-β1 relevant signaling pathways in lung fibrosis**
The diagram demonstrates the activation of TGF-β signaling through both Smad-dependent and non-Smad pathways, all converging to promote pulmonary fibrosis. Upon binding of TGF-β to its receptor complex (TGFBR), consisting of a type II receptor and type I receptors (ALK5 or ALK1), distinct signaling pathways are initiated. ALK5-ALK5 homodimer activates Smad2/3, while ALK1-ALK5 heterodimaer activates Smad1/5/8. The phosphorylated Smads form complexes with Smad4, translocate to the nucleus, and regulate gene expression, resulting in key fibrogenic processes such as myofibroblast differentiation, EMT, EndMT, fibrogenesis, and ECM remodeling. In parallel, TGF-β also triggers non-Smad pathways, including PI3K, JNK, p38/MAPK, and Wnt/β-catenin, which contribute to these same fibrotic outcomes. EMT, epithelial-to-mesenchymal transition; EndMT, endothelial-to-mesenchymal transition; PI3K, phosphatidylinositol-3-kinase; JNK, c-jun N-terminal kinase; MAPK, mitogen-activated protein kinase.

1.3 HIF-1α pathway

1.3.1 Overview

IPF is a chronic fibrosing lung disease with unclear pathogenesis and limited treatment. The hypoxic microenvironment is implicated in the IPF lung tissue due to the upregulation of hypoxia-inducible factor(HIF)-1α expression (Tzouvelekis et al., 2007) and HIF-related markers in IPF lung (Landi et al., 2014). The transcriptional complex HIF has emerged as a key regulator of the molecular hypoxic response, mediating a wide range of physiological and cellular mechanisms necessary to adapt to reduced oxygen. It's important to investigate the role of HIF in the progression of IPF (Semenza, 2000).

1.3.2 HIF proteins

Human HIF-α has three isoforms: HIF-1α, HIF-2α, and HIF-3α. Of these, HIF-1α and HIF-2α have been studied most extensively (Wang et al., 1995) (Figure.1.4).

HIF-1α is encoded by the *HIF1A* gene. It contains an N-terminal basic helix-loop-helix (bHLH) domain, followed by two Per-ARNT-Sim (PAS) domains, the oxygen-dependent degradation domain (ODDD), and two transactivation domains (TADs): the N-terminal TAD (N-TAD) and C-terminal TAD (C-TAD). Notably, the N-TAD partially overlaps with the ODDD (Weidemann and Johnson, 2008; Kaelin and Ratcliffe, 2008). The bHLH domain is responsible for DNA binding (Sadeghi et al., 2020), while the two PAS domains mediate heterodimerization with HIF-1β (Scheuermann et al., 2007; Ema et al., 1997). The ODDD contains two conserved proline residues (Pro402 and Pro564) that are hydroxylated by the prolyl hydroxylase domain (PHD) family, regulating the stability of HIF-1α. The C-TAD harbors a conserved asparagine (Asn803), which is hydroxylated by the factor inhibiting HIF (FIH) and regulates the transcriptional activity of HIF-1α (Schofield and Ratcliffe, 2004).

HIF-2α, encoded by the *EPAS1* gene, shares 48% amino acid identity with HIF-1α. Like HIF-1α, it is regulated by prolyl hydroxylation, forms heterodimers with HIF-1β, and binds to the same target DNA sequence as the HIF-1α β heterodimer (Befani and Liakos, 2018). HIF-2α and HIF-1α share 83% and 70% sequence identities in their DNA-binding and dimerization domains, respectively, with both the bHLH and PAS domains functioning similarly in the two isoforms. However, the N-TAD of HIF-2α confers target gene specificity, while the C-TAD drives the expression of genes shared by both HIF-1α and HIF-2α (Hu et al., 2007*a*). In this thesis, we will mainly discuss the regulation of HIF-1α.

HIF-3α differs significantly from the other two isoforms. It contains a leucine zipper (LZIP) domain, which facilitates protein-protein interactions. Additionally, it has a

transactivation domain at its N-terminus only, whereas both HIF-1α and HIF-2α have TADs at both the N- and C-termini. HIF-3α also exhibits substantial alternative splicing, with 10 known isoforms identified so far (Heikkilä et al., 2011; Gornostaeva et al., 2024). Interestingly, alternative splicing of HIF-3α generates an inhibitory PAS domain protein that is composed of the N-terminal basic helix-loop-helix and PAS domains but lacks TAD. It inhibits HIF response by forming transcriptionally inactive heterodimers with HIF-1α (Makino et al., 2001).

HIF-1β, a transcription factor belonging to the bHLH-PAS family, contains a bHLH domain for DNA binding, two PAS domains (PAS-A and PAS-B) essential for dimerization, and one transactivation domain (Rankin and Giaccia, 2008; Mandl and Depping, 2014).

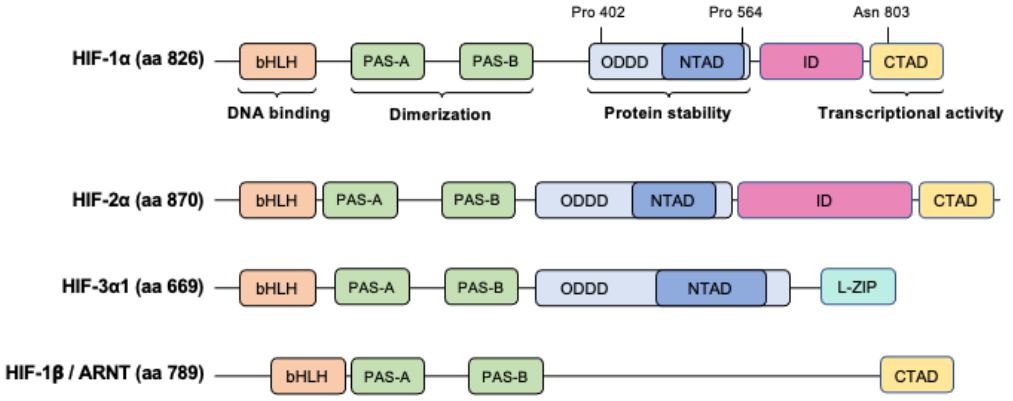

FIGURE 1.4: **The structure of hypoxia-inducible factors (HIFs)**
The structural domains of HIF-1α, HIF-2α, HIF-3α, and HIF-1β (or ARNT) proteins. The bHLH and PAS domains are involved in DNA binding and heterodimerization. The ODD domain is required for oxygen-dependent hydroxylation and degradation, containing two hydroxylation-sensitive proline residues. The N-TAD and C-TAD domains are essential for transcriptional activation, while the LZIP domain in HIF-3α facilitates protein binding. ARNT, aryl hydrocarbon nuclear receptor translocator; bHLH, basic helix-loop-helix; HIF, hypoxia-inducible factor; PAS, Per-ARNT-Sim; ODD, oxygen-dependent degradation domain; C-TAD, C-terminal activation domain; N-TAD, N-terminal activation domain; LZIP, leucine zipper.

1.3.3 HIF-1α and HIF-2α target genes

Although both HIF-1α and HIF-2α bind to the same hypoxia response element (HRE), they regulate overlapping yet distinct transcriptional programs due to differences in their transactivation domains and cofactor recruitment (Keith et al., 2012; Hu et al., 2007*b*). Broadly, HIF-1α preferentially drives the acute metabolic adaptation to hypoxia, while HIF-2α controls vascular, erythropoietic, and cell-fate programs more prominent

in chronic hypoxia. For example, HIF-1α strongly induces glycolytic enzymes such as *GLUT1/3, HK2, PFKP, ALDOA, ENO1, LDHA, PDK1* as well as pH regulators like *CA9* and mitophagy mediators *BNIP3/BNIP3L* (Semenza, 2013). In contrast, HIF-2α selectively activates *EPO* in kidney and liver, endothelial receptors such as *KDR/VEGFR2* and *TEK/TIE2*, and cell-fate genes such as *POU5F1/OCT4*, linking it to angiogenesis and stemness regulation (Haase, 2010; Covello et al., 2006). Some targets, including *VEGFA, ADM, SERPINE1*, and *NDRG1*, are regulated by both isoforms, though the relative contribution of HIF-1 versus HIF-2 is context-dependent (Branco-Price et al., 2012) (Table.1.5)

TABLE 1.5: Representative gene programs regulated by HIF-1α and HIF-2α

Program	HIF-1α-biased	HIF-2α-biased
Metabolism / pH control	GLUT1/3, HK2, PFKP, LDHA, PDK1, CA9	SOD2 (oxidative stress, context-dependent)
Cell survival / fate	BNIP3, BNIP3L	POU5F1/OCT4, TGF-α (context)
Vascular / erythropoietic	—	EPO, KDR/VEGFR2, TEK/TIE2
Shared (both isoforms)	VEGFA, ADM, SERPINE1/PAI-1, NDRG1, PGK1	

HIF-1α and HIF-2α show distinct patterns of tissue and cell distribution that help explain their different biological roles. HIF-1α is broadly expressed across most tissues and cell types and is considered the dominant isoform for acute hypoxic responses. It is particularly abundant in metabolically active cells such as epithelial cells, fibroblasts, and immune cells, where it rapidly induces glycolytic and stress-response programs. By contrast, HIF-2α has a more restricted distribution, being enriched in endothelial cells, type II alveolar epithelial cells, interstitial fibroblasts, kidney interstitial cells, and hepatocytes (Talks et al., 2000; Chandel and Simon, 2008). In the lung, HIF-2α is especially important for endothelial and epithelial regulation, linking it to angiogenesis, vascular remodeling, and erythropoietin production (Cowburn et al., 2016). These patterns support the view that HIF-1α primarily mediates rapid metabolic adaptation to hypoxia, whereas HIF-2α governs vascular, erythropoietic, and chronic hypoxic responses.

1.3.4 Regulation of HIF-1α

Under normoxic conditions, HIF-1α is rapidly degraded due to oxygen-dependent hydroxylation at two conserved proline residues (Pro402 and Pro564) on its α subunit (Figure.1.5). This results in a very short half-life of approximately 5–10 minutes (Jewell et al., 2001; Ivan et al., 2001). The hydroxylation is performed by the PHD family, which includes three major isoforms: PHD1, PHD2, and PHD3. Hydroxylation of HIF-1α by PHDs promotes its binding to the von Hippel-Lindau (VHL) protein, a component of the E3 ubiquitin ligase complex, leading to polyubiquitination and subsequent

degradation of the α subunit by the 26S proteasome (Maxwell et al., 1999; Ohh et al., 2000). VHL binding depends on the hydroxylation of Pro402 or Pro564 (or both) by PHD2, a dioxygenase that uses O_2 and α-ketoglutarate as substrates, generating CO_2 and succinate as by-products (Appelhoff et al., 2004). While PHD2 is ubiquitously expressed and well studied, the roles of PHD1 and PHD3 in regulating HIF-1α are less clear (Berra et al., 2003). Studies have shown that PHD2 and PHD3 are upregulated by HIF-1α under hypoxic conditions, promoting HIF-1α degradation and creating a negative feedback loop, while PHD1 expression remains unchanged (Marxsen et al., 2004; Stiehl et al., 2006). Additionally, PHD3 shows similar activity toward both HIF-1α and HIF-2α (Appelhoff et al., 2004).

HIF-1α is also regulated by hydroxylation at an asparagine residue (Asn803) in its C-terminal transactivation domain by FIH. This modification hinders the transcriptional activity of HIF-1α in normoxic conditions by preventing its interaction with coactivators such as CBP/p300 (Mahon et al., 2001; Lando et al., 2002). Therefore, oxygen-dependent hydroxylation represses HIF-1α under normal oxygen conditions.

However, under hypoxic conditions, PHD2 activity is reduced due to limited substrate availability, inhibition of its catalytic center, or both. As a result, HIF-1α degradation is blocked, allowing the protein to accumulate. It then dimerizes with HIF-1β, binds to HREs in target genes, and recruits coactivator proteins, leading to increased transcription. Notably, for FIH to directly affect HIF-α/β-mediated transcription, HIF-α must first accumulate to sufficient levels. This aligns with evidence suggesting that FIH is less sensitive to low oxygen levels than PHDs, making it less affected by hypoxia (Chan, Ilott, Schödel, Sims, Tumber, Lippl, Mole, Pugh, Ratcliffe, Ponting et al., 2016; Koivunen et al., 2004).

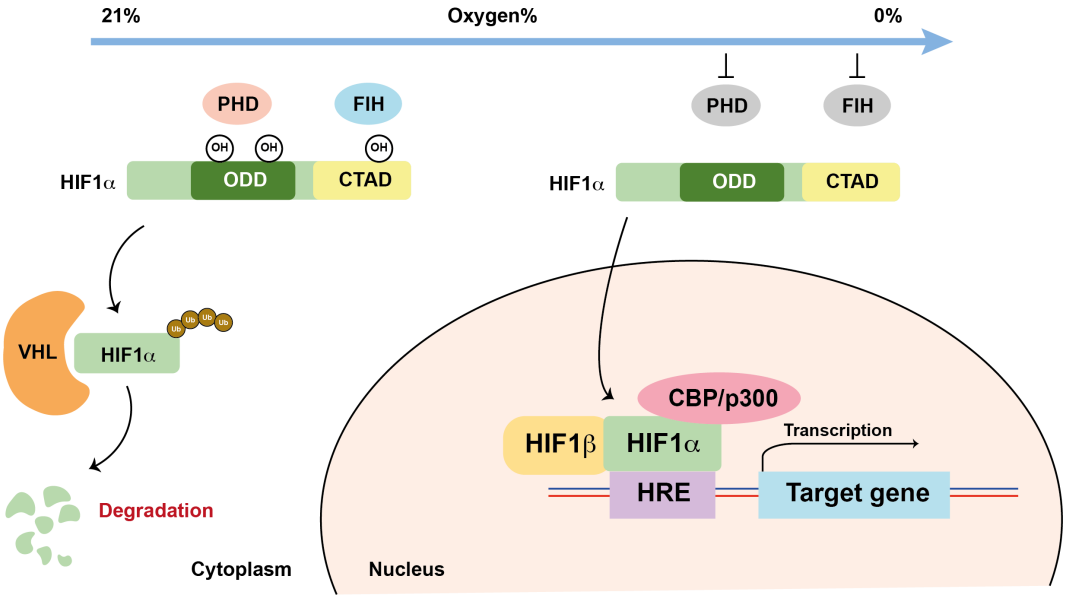

FIGURE 1.5: **Overview of the roles of FIH, and PHDs, in the dioxygen-dependent regulation of HIF-mediated transcription**

The diagram illustrates the regulation of HIF-1α under varying oxygen concentrations. Under normoxic conditions, HIF-1α is hydroxylated by PHDs, marking it for degradation via the 26S proteasome. Additionally, HIF-1α is hydroxylated by FIH, which suppresses its transcriptional activity. In hypoxic conditions, the activity of PHDs and FIH is inhibited, preventing the hydroxylation of HIF-1α. As a result, HIF-1α stabilizes, dimerizes with HIF-1β, and translocates to the nucleus, where it activates the transcription of target genes involved in the cellular response to hypoxia. CTAD, C-terminal activation domain of HIF-α; HRE, hypoxic response element sequence in the HIF target gene; ODD, oxygen-dependent degradation domain; VHL, von Hippel-Lindau protein-ubiquitin ligase complex; p300/CBP, histone acetyl transferases that promote transcription.

HIF stabilising agents

Pharmacological stabilisation of HIF is widely used to study oxygen-sensing pathways. The 2-oxoglutarate analogue dimethyloxalylglycine (DMOG) is a well-established and potent inhibitor of PHDs. It also acts on other 2-OG–dependent dioxygenases, which broadens its effects beyond HIF regulation but makes it a widely used and effective tool in both in vitro and in vivo studies (Jaakkola et al., 2001). Another commonly used compound is IOX2, which has greater selectivity for PHD2 and therefore allows more targeted stabilisation of HIF-α subunits with relatively little effect on FIH at standard concentrations (Rabinowitz, 2013). While IOX2 offers higher specificity, DMOG remains valuable in experimental models where broad HIF pathway activation is desired. Other approaches include cobalt chloride ($CoCl_2$), which stabilises HIF by substituting for Fe^{2+}, and deferoxamine (DFO), an iron chelator that reduces hydroxylase activity;

however, both influence a wide range of iron-dependent enzymes (Jaakkola et al., 2001). More recently, IOX4 has been developed as a brain-penetrant PHD inhibitor, and clinically approved compounds such as roxadustat, daprodustat, and molidustat provide selective PHD inhibition with pharmacokinetic control (Chan, Holt-Martyn, Schofield and Ratcliffe, 2016). In addition, VH298 stabilises HIF by blocking the VHL–HIF protein–protein interaction, thereby preventing degradation without hydroxylase inhibition (Frost et al., 2016). Together, these agents represent a versatile toolkit with differing specificities and translational relevance for dissecting HIF biology (Table .1.6).

TABLE 1.6: Commonly used HIF stabilising agents and their characteristics.

Agent	Primary target	Notes
DMOG	Pan-2OG dioxygenases (PHDs, FIH, others)	Potent and widely used; induces broad HIF stabilisation but also inhibits other 2-OG enzymes (Jaakkola et al., 2001).
IOX2	PHD2 > PHD1/3	More selective stabilisation of HIF-α; minimal FIH inhibition at standard doses (Rabinowitz, 2013).
IOX4	PHDs (brain-penetrant)	PHD-selective; useful in CNS models (Chan, Holt-Martyn, Schofield and Ratcliffe, 2016).
$CoCl_2$	Iron substitution	Inexpensive; affects multiple iron-dependent enzymes (Jaakkola et al., 2001).
DFO	Iron chelation	Stabilises HIF via Fe^{2+} depletion; off-target effects likely (Jaakkola et al., 2001).
Roxadustat and other clinical PHD inhibitors	PHDs	Clinically approved; selective, controlled pharmacokinetics (Chan, Holt-Martyn, Schofield and Ratcliffe, 2016).
VH298	VHL–HIF interaction	Prevents HIF degradation without hydroxylase inhibition (Frost et al., 2016).

Although HIF stability is primarily regulated by oxygen-dependent prolyl and asparaginyl hydroxylation, multiple mechanisms allow for hypoxia-independent control of HIF activity. Metabolic intermediates such as succinate and fumarate can accumulate in certain contexts (e.g., mitochondrial dysfunction, tumour metabolism) and inhibit PHD enzymes competitively, leading to HIF stabilisation even under normoxic conditions (Selak et al., 2005; Cramer-Morales et al., 2020). Similarly, depletion of essential cofactors such as ascorbate or Fe^{2+} impairs hydroxylase activity (Knowles et al., 2003). In addition, reactive oxygen and nitrogen species (ROS and RNS) can modify hydroxylase cofactors or cysteine residues, further reducing PHD activity (Jung et al., 2008). Beyond hydroxylase inhibition, several signalling pathways can promote HIF activation independently of oxygen tension. Growth factor and inflammatory cascades—including PI3K–AKT–mTOR, MAPK/ERK, and NF-κB—enhance HIF-α transcription, translation, or transactivation (Koh et al., 2011; Sang et al., 2003). Finally, proteins such as VHL,

HSP90, and Mint3/APBA3 can directly modulate HIF-α stability or co-activator recruitment (Isaacs et al., 2002; Sakamoto and Seiki, 2009). Collectively, these mechanisms demonstrate that HIF is not solely an oxygen sensor but is integrated into broader metabolic and signalling networks, enabling cells to fine-tune hypoxic responses in diverse physiological and pathological contexts(Kaelin and Ratcliffe, 2008; Semenza, 2012).

1.3.5 The role of HIF-1α pathway in IPF

HIF-1α is a central regulator of the cellular response to hypoxia, and its activation drives the expression of numerous target genes, such as *GLUT1*, *VEGF*, *ANGPT2*, and *IGF2*, which are involved in several key biological processes. Several studies have shown that HIF-1α target genes are implicated in pathological processes which contribute to the progressive fibrosis in IPF. Tzouvelekis and colleagues demonstrated that HIF-1α plays a crucial early role in the development of IPF, being overexpressed in alveolar epithelial cells before significant lung damage occurs. HIF-1α along with its target genes (such as *VEGF* and *p53*) contribute to key pathogenic processes, including metabolic reprogramming, angiogenesis, and ECM deposition, highlighting it as a potential therapeutic target for IPF (Tzouvelekis et al., 2007).

In metabolic programming, HIF-1α drives the expression of glycolysis-related genes like PDK1 and LDH5, which promote glycolytic reprogramming and lactate production, respectively, both of which enhance myofibroblast differentiation and fibrosis progression (Goodwin et al., 2018; Yan et al., 2023). HIF-1α also contributes to EMT, with genes such as Snail and LOX facilitating EMT in early fibrosis, particularly in injury-induced models (Zhu et al., 2016; Lu et al., 2018).

Additionally, HIF-1α supports pro-fibrotic signaling by regulating genes like ADORA2B, which modulates macrophage function, and CHOP, which induces AEC apoptosis (Philip et al., 2017; Delbrel et al., 2018). While the role of VEGFA remains unclear, other targets such as GPR81 promote fibrotic progression by enhancing MPC fibrogenicity (Barratt et al., 2018; Yang et al., 2023). In ECM remodeling, pseudohypoxia-mediated inhibition of FIH induces LOXL2 and PLOD2 expression, contributing to increased ECM stiffness and fibrosis. Through these pathways, HIF-1α exerts a multifaceted influence on the progression of IPF (Brereton et al., 2022). To provide a clearer view of the multifaceted role HIF-1α plays in the pathogenesis of IPF, the following table summarizes key HIF-1α target genes, categorizing them based on their associated biological processes and their contribution to the progression of fibrosis (Table.1.7).

TABLE 1.7: **Summary of HIF-1α target genes in IPF and their functional roles**

Category	Gene/Protein	Biological processes	Reference
Metabolic programming	*PDK1*	Hypoxia-induced PDK1 expression via HIF-1α enhances glycolytic reprogramming, leading to increased myofibroblast differentiation.	(Goodwin et al., 2018)
	LDH5	TGF-β-induced LDH5 via HIF-1α promoting lactate production and differentiation into myofibroblasts	(Yan et al., 2023)
EMT	Snail β-catenin	Induces EMT in PQ poisoning-induced early pulmonary fibrosis.	(Zhu et al., 2016)
	LOX	Induces EMT in PQ poisoning-induced early pulmonary fibrosis.	(Lu et al., 2018)
Pro-fibrotic	*ADORA2B*	With HIF-1α inhibitor, ADORA2B and profibrotic mediator expression reduce in lung macrophages	(Philip et al., 2017)
	CHOP	Induction of CHOP expression leads to AECs apoptosis	(Delbrel et al., 2018)
	VEGFA	Unclear	(Barratt et al., 2018)
	GPR81	Increasing the expression of GPR81, enhancing IPF MPC fibrogenicity driving fibrotic progression.	(Yang et al., 2023)
ECM remodeling	*LOXL2* *PLOD2*	peseudohypoxia-inhibited FIH induce expression of LOXL2 and PLOD2, resulting in increasing ECM stiffness.	(Brereton et al., 2022)

HIF-1α, hypoxia-inducible factor 1-alpha; PDK1, pyruvate dehydrogenase kinase 1; LDH5, lactate dehydrogenase 5; TGF-β, transforming growth factor beta; EMT, epithelial-mesenchymal transition; LOX, lysyl oxidase; ADORA2B, adenosine A2B receptor; CHOP, C/EBP homologous protein; VEGFA, vascular endothelial growth factor A; GPR81, G-protein-coupled receptor 81; MPC, mesenchymal progenitor cells; ECM, extracellular matrix; FIH, factor inhibiting HIF-1; PLOD2, procollagen-lysine, 2-oxoglutarate 5-dioxygenase 2; PQ, paraquat.

1.4 Factor Inhibiting HIF (FIH)

1.4.1 Overview

As discussed in the previous section, FIH is a key regulator of HIF-1α activity. However, beyond HIF-1α, FIH has numerous other substrates or potential binding partners whose functions remain unclear. Brereton and colleagues observed that FIH's catalytic activity on HIF-1α is reduced in IPF-derived primary lung fibroblasts compared to normal fibroblasts (Brereton et al., 2022). Furthermore, FIH inhibition leads to the upregulation of PLOD2 and LOXL2 in a HIF-dependent manner, resulting in increased ECM stiffness. These findings suggest that FIH may play an important role in the progression of IPF, warranting further investigation.

1.4.2 Structure

The FIH protein is encoded by the *HIF1AN* gene, located on human chromosome 10q24.31, and consists of 349 amino acids. The conserved double-stranded β-helix (DSBH) core of FIH consists of eight β-strands that support Fe(II) and 2OG binding. This core is located in the C-terminal half of FIH and forms two β-sheets. Additionally, six β-strands in the N-terminal region extend these β-sheets, which are surrounded by helical elements. At the C-terminus of the DSBH core, α-helices from each monomer form the dimer interface through strong hydrophobic helix-helix interactions (Elkins et al., 2003; Dann III et al., 2002).

1.4.3 Regulation of FIH activity

1.4.3.1 Hypoxic regulation of FIH activity

FIH-catalyzed asparagine hydroxylation requires Fe(II), O_2, and 2-oxoglutarate (2OG) as cofactors. Limiting access to these substrates, as occurs in hypoxia, directly inhibits its catalytic activity. Structural studies have identified His-199, Asp-201, and His-279 as key iron-binding residues, and substitution of His-199 or Asp-201 with alanine disrupts FIH activity in cells (McDonough et al., 2005; Hewitson et al., 2007; Lando et al., 2002). Crystal structure analyses revealed that FIH forms a homodimer dependent on its C-terminal α-helix, with a point mutation at L340R abolishing both dimer formation and catalytic activity (Elkins et al., 2003; Lancaster et al., 2004). Additional residues, including Tyr-145, Thr-196, Lys-214, and Asn-294, mediate 2OG binding, further defining the structural basis of hydroxylase function (Dann III et al., 2002). Under hypoxia, inhibition of asparagine hydroxylation of HIF-α enhances recruitment of transcriptional co-activators, thereby increasing HIF transcriptional activity.

1.4.3.2 Non-hypoxic regulation of FIH activity

Although FIH is best known as an oxygen sensor, several non-hypoxic mechanisms also regulate its function. As discussed in Section 1.4.3, several non-hypoxic mechanisms can regulate HIF stability, including the accumulation of metabolic intermediates such as succinate and fumarate, cofactor depletion (ascorbate, Fe^{2+}), reactive oxygen and nitrogen species, and activation of growth factor and inflammatory pathways. These mechanisms affect the activity of both PHDs and FIH, highlighting their shared dependence on oxygen, iron, and 2OG. However, FIH regulation extends beyond these general principles. FIH also displays greater sensitivity to oxidative stress compared to PHDs. Masson and colleagues showed that FIH-catalyzed asparagine hydroxylation is markedly inhibited by H_2O_2 at concentrations that have only modest effects on PHD

activity (Masson et al., 2012). Unlike PHD inhibition, which is largely reversible, FIH inhibition by peroxide is not rapidly restored, likely due to Fenton chemistry involving the Fe(II) cofactor and irreversible oxidative modifications. This difference suggests that under conditions of chronic oxidative stress, such as in IPF, FIH activity may be preferentially suppressed relative to PHDs, with consequences for both HIF-dependent and HIF-independent signalling. Furthermore, substrate competition from ARD-containing proteins, such as Notch and NF-κB, represents a unique mode of regulation not shared by PHDs (**??**). In addition, inflammatory and growth factor pathways influence FIH activity. NF-κB and PI3K–AKT–MAPK signalling can modulate FIH expression and activity, linking oxygen sensing with immune and growth control pathways (Cockman et al., 2006). These findings demonstrate that FIH activity is shaped by metabolic state, redox environment, signalling cues, and protein–protein interactions, making it a broader cellular regulator whose dysregulation may contribute to fibrotic disease.

1.4.4 Hydroxylation substrates

FIH-mediated hydroxylation often influences protein-protein interactions or modulates signaling pathways rather than causing degradation or major structural changes. As discussed in the regulation of the HIF pathway (Section 1.4.3), FIH hydroxylates HIF-1α at Asn-803, inhibiting its transcriptional activity. Similarly, FIH can hydroxylate HIF-2α at Asn-851, preventing the binding of the transcriptional co-activator p300/CBP and reducing the activity of the carboxy-terminal transactivation domain of HIF (Schofield and Ratcliffe, 2004).

Since 2006, many studies have shown that FIH can also hydroxylate a variety of ankyrin-repeat domain (ARD) proteins. ARDs are composed of a variable number of 33-residue ARs that individually fold into a helix-loop-helix hairpin loop conformation with pairs of α-helices arranged in antiparallel fashion connected by β-hairpin loops (Cockman et al., 2009). Among ARD proteins, FIH hydroxylates ASPP2 at Asn-986, enhancing its interaction with Par-3, crucial for cell polarity, without affecting its stability. Hydroxylation of IκBα at Asn-210 and Asn-244 is inconsequential, while FIH modifies IKKϵ at Asn-254, Asn-700, and Asn-701, suppressing its activation in IFN signaling by preventing TBK1 and TRAF3 binding, thus reducing antiviral responses and polyubiquitination (Cockman et al., 2006; Devries et al., 2010; Cai et al., 2024).

The Notch family proteins are significantly affected by FIH hydroxylation. For instance, FIH hydroxylates Notch1 at Asn-1945 and Asn-2012, potentially regulating HIF-1α activity, while hydroxylation of Notch2 at Asn-1902 and Asn-1969 impairs its transcriptional activity, affecting neurogenesis and myogenesis (Wilkins et al., 2009; Coleman et al., 2007; Zheng et al., 2008).

Other substrates include MYPT1, hydroxylated by FIH at Asn-67, Asn-100, and Asn-226, resembling the effect on Notch1, and p105, which is hydroxylated at Asn-678, inhibiting its processing into p50 and reducing NFκB pathway activation and inflammation (Webb et al., 2009). For proteins like TNKS2 (hydroxylated at Asn-586, Asn-706, and Asn-739) and TRPA1 (Asn-336), the functional consequences remain unclear, while hydroxylation of TRPV3 at Asn-242 inhibits its channel activity. Interestingly, in TNKS2 protein, FIH has been found to hydroxylate not only multiple asparagine residues but also two histidine residues to varying extents (Yang et al., 2011; Karttunen et al., 2015; Saward et al., 2023).

Non-ARD proteins like ASB4 (hydroxylated at Asn-246) and HACE1 (modified at Asn-191) are also FIH targets (Ferguson III et al., 2007; Kim et al., 2019). Although hydroxylation does not affect their stability, it alters their functions—FIH-mediated hydroxylation of HACE1 inhibits Rac1 ubiquitination, decreasing breast cancer cell migration and invasion. Peptide-based studies suggest that FIH may have a broader range of substrates than currently identified, potentially including dihydroxylation, oxidation of D-residues, and oxidation of hydrophobic residues (Yang et al., 2013; Choi, Hardy, Leissing, Chowdhury, Nakashima, Ge, Markoulides, Scotti, Gerken, Thorbjornsrud et al., 2020) (Details showed in Table.1.8).

TABLE 1.8: **Non-HIF substrates of FIH**

Category	Protein	Hydroxylated residue	Description	Ref.
ARD proteins	ASPP2	Asn-986	Does not affect ASPP2 stability or total cellular protein levels but enhances its interaction with partitioning defective 3 homologue (Par-3), a protein involved in cell polarity.	(Janke et al., 2013)
	IκBα	Asn-210, Asn-244	Inconsequential.	(Cockman et al., 2006; Devries et al., 2010)

Continued on next page

TABLE 1.8: **Non-HIF substrates of FIH (continued)**

Category	Protein	Hydroxylated residue	Description	Ref.
	IKKϵ	Asn-254, Asn-700, Asn-701	Suppresses its activation for IFN signaling and antiviral immune responses by preventing IKKϵ from binding to TBK1 and TRAF3. Reduces K63-linked polyubiquitination of IKKϵ at Lys-416, catalyzed by the cIAP1/cIAP2/TRAF2 E3 ubiquitin ligase complex.	(Cai et al., 2024)
	MYPT1	Asn-67, Asn-100, Asn-226	May be similar to Notch1.	(Webb et al., 2009)
	Notch1	Asn-1945, Asn-2012	Notch1 has a higher affinity for FIH, which may compete with HIF-1α for binding to FIH, regulating HIF-1α activity.	(Wilkins et al., 2009; Coleman et al., 2007; Zheng et al., 2008)
	Notch2	Asn-1902, Asn-1969	Significantly reduces transcriptional activity and impairs Notch-mediated control of neurogenesis and myogenesis.	(Wilkins et al., 2009)
	Notch3	Asn-1867, Asn-1934		(Wilkins et al., 2009)
	OTUD7B (Cezanne)	Asn-35	Greatly reduces the interaction of UBA^{Cez} with ubiquitin.	(Mader et al., 2020)
	p105	Asn-678	Inhibits processing of p105 into p50, reducing activation via the NFκB pathway and downstream inflammatory signaling.	(Scholz et al., 2013; Volkova et al., 2024)

Continued on next page

TABLE 1.8: **Non-HIF substrates of FIH (continued)**

Category	Protein	Hydroxylated residue	Description	Ref.
	TNKS2	Asn-586, Asn-706, Asn-739	Unclear.	(Yang et al., 2011)
	TRPA1	Asn-336	Unclear.	(Saward et al., 2023)
	TRPV3	Asn-242	The interaction of TRPV3 with FIH inhibits channel activity.	(Karttunen et al., 2015)
Other proteins	ASB4	Asn-246	Does not affect the stability or function of ASB4 in cells.	(Ferguson III et al., 2007)
	HACE1	Asn-191	Does not affect cellular levels but inhibits the ability to ubiquitinate active Rac1, reducing cell migration and invasion in breast cancer.	(Kim et al., 2019)
	OTUB1	Asn-22	Does not affect the stability or deubiquitinase activity of OTUB1 but alters interactions with proteins involved in oxidative metabolism.	(Pickel et al., 2019; Scholz et al., 2016)

ARD, ankyrin repeat domain; ASPP2, apoptosis-stimulating protein of p53 2; IκBα, inhibitor of nuclear factor kappa B alpha; IKKε, IκB kinase epsilon; TBK1, TANK-binding kinase 1; TRAF3, TNF receptor-associated factor 3; cIAP1/cIAP2, cellular inhibitor of apoptosis protein 1/2; TRAF2, TNF receptor-associated factor 2; MYPT1, myosin phosphatase target subunit 1; HIF-1α, hypoxia-inducible factor 1-alpha; FIH, factor inhibiting HIF-1; Notch1/2/3, members of the Notch receptor family (Notch homolog 1, 2, 3); OTUD7B (Cezanne), ovarian tumor domain-containing protein 7B; UBA, ubiquitin-associated domain; p105, precursor of nuclear factor NF-κB p50 subunit; NFκB, nuclear factor kappa-light-chain-enhancer of activated B cells; TNKS2, tankyrase 2; TRPA1, transient receptor potential ankyrin 1; TRPV3, transient receptor potential vanilloid 3; ASB4, ankyrin repeat and SOCS box protein 4; HACE1, HECT domain and ankyrin repeat-containing E3 ubiquitin-protein ligase 1; OTUB1, OTU deubiquitinase, ubiquitin aldehyde-binding 1.

1.4.5 The role of FIH in human diseases

Building on the understanding of FIH substrates, it is evident that FIH plays diverse and context-dependent roles in various human diseases by modulating key substrates and cellular pathways through its regulation of both HIF and non-HIF targets. In this

section, we summarize how FIH contributes to disease pathogenesis via its diverse substrates, focusing on both HIF-related and non-HIF-related pathways.

A detailed overview of the role of HIF-1α in IPF is provided in Section 1.4.4 (Table 1.7). However, few studies have directly examined the role of FIH in IPF. Brereton et al. demonstrated that FIH inhibition under pseudohypoxic conditions upregulates LOXL2 and PLOD2, contributing to ECM remodeling and fibrosis progression in a HIF-dependent manner. Whether FIH also influences IPF through the hydroxylation of non-HIF substrates remains unclear. In renal cell carcinoma, FIH inhibition increases HIF target expression and induces apoptosis in CCRCC cells (Khan et al., 2011). Acting as a tumor suppressor, FIH limits tumor invasion and metastasis in colon cancer by inhibiting HIF-1α activity, while paradoxically promoting tumor growth in other contexts through in vivo mechanisms (Chen et al., 2015; Pelletier et al., 2012). FIH's involvement in breast cancer is notable for its regulation of the FIH-HACE1-Rac1 axis, which affects cell migration and invasion, particularly in hypoxic conditions, and its hydroxylation of ASPP2, enhancing tumor suppressor activity by altering cell polarity (Kim et al., 2019; Hyseni et al., 2011; Janke et al., 2013). Tumor growth in osteosarcoma is facilitated by FIH through enhanced vessel maturation, while in pancreatic endocrine tumors, high FIH expression correlates with aggressive behavior and poor prognosis (Kuzmanov et al., 2012). Loss of FIH in glioblastoma multiforme leads to heightened HIF-mediated transcription of pro-tumorigenic genes like GLUT-1 and VEGF-A, a similar outcome seen in hepatocellular carcinoma (Ma et al., 2017), where reduced FIH expression is linked to more aggressive tumor phenotypes. In non-small cell lung cancer, FIH supports tumor proliferation, survival, and metabolism by regulating HIF-1α and other pathways, such as p53/p21 and YAP/TAZ. A deficiency in FIH results in reduced tumor growth and increased immune infiltration in these lung cancers (Giatromanolaki et al., 2008; García-del Río et al., 2023). Finally, in chronic kidney disease, FIH forms a hypoxia-sensitive complex with IκBβ, promoting NF-κB-mediated pro-inflammatory gene expression, contributing to CKD-related inflammation (Volkova et al., 2024).

Currently, only a few studies have reported global transcriptome alterations in human cells following FIH depletion. Given the important role of FIH in the progression of multiple diseases, understanding its function is crucial. As an asparaginyl hydroxylase, FIH has the potential to modify various substrates beyond HIF-α, indicating a broader scope of biological activity. Additionally, while FIH activity is regulated by hypoxia, emerging evidence suggests that it is also influenced by other cellular signals and environmental factors, underscoring the complexity of its regulation. These non-hypoxic mechanisms and alternative substrates imply that the role of FIH extends beyond the canonical HIF pathway, potentially impacting diverse cellular processes. Thus, a deeper investigation into the HIF-independent functions of FIH may reveal novel mechanisms underlying disease pathogenesis. This exploration could provide critical insights into FIH as a therapeutic target in human diseases.

TABLE 1.9: **The role of FIH in human diseases**

Disease	Related substrate	Description	Ref
Breast cancer	HACE1	FIH-1 hydroxylates HACE1, regulating its interaction with Rac1 and influencing tumor-suppressive functions, particularly in hypoxic breast cancer. The FIH-HACE1-Rac1 pathway modulates cell migration, invasion, and ubiquitin processes.	(Kim et al., 2019)
	HIF-1α	FIH-1 is widely expressed in invasive breast carcinomas, with subcellular localization correlating to tumor grade and HIF-1α overexpression. However, its expression does not explain the differences between diffuse and perinecrotic HIF-1α patterns.	(Hyseni et al., 2011)
	ASPP2	FIH-1 hydroxylates ASPP2, enhancing its interaction with Par-3, altering cell polarity and enhancing tumor suppressor function.	(Janke et al., 2013)
Chronic kidney disease	IκBβ	FIH forms a hypoxia-sensitive oxomer with IκBβ, preventing IκBβ from binding to NF-κB dimers and promoting pro-inflammatory gene expression, potentially contributing to inflammation in CKD.	(Volkova et al., 2024)
Colon cancer	HIF-1α	FIH-1 acts as a tumor suppressor in colorectal cancer (CRC) by inhibiting cell proliferation, migration, invasion, and tumor growth. Its reduced expression is associated with deeper tumor invasion, lymph node involvement, and metastasis, potentially due to the loss of FIH-1's ability to inhibit HIF-1α-mediated transcription of key target genes like GLUT1 and VEGF.	(Chen et al., 2015)

Continued on next page

TABLE 1.9: **The role of FIH in human diseases (continued)**

Disease	Related substrate	Description	Ref
	HIF-1α	FIH promotes tumor growth in vivo in both colon adenocarcinoma and melanoma cells. Silencing of FIH severely decreased the size of mice xenografts originating from two different cell lines (LS174 and A375), whereas overexpression of FIH increased tumor growth.	(Pelletier et al., 2012)
	Not identified	Reduced FIH-1 protein expression was linked to advanced tumor stage and grade, suggesting its potential role in CRC progression.	(Vakil et al., 2016)
Glioblastoma multiforme	HIF-1α	Loss of FIH-1 promotes GBM progression by enhancing HIF-mediated transcription of genes like GLUT-1 and VEGF-A, even under hypoxic conditions.	(Wang et al., 2014)
Hepatocellular carcinoma	HIF-1α	Reduced expression of PHD3 and FIH is associated with more aggressive tumor behavior, higher TNM stage, and poorer prognosis, with their combined low levels enhancing HIF-1α activity and serving as strong indicators of unfavorable outcomes.	(Ma et al., 2017)
IPF	HIF-1α	Under pseudohypoxic conditions, FIH inhibition induces the expression of LOXL2 and PLOD2, further promoting the stiffening of the ECM, which plays a significant role in the fibrotic process.	(Brereton et al., 2022)

Continued on next page

TABLE 1.9: **The role of FIH in human diseases (continued)**

Disease	Related substrate	Description	Ref
NSCLC	HIF-1α	PHDs and FIH are co-expressed in NSCLC, with their expression correlating with HIF levels to reveal distinct tumor subgroups characterized by upregulated, standard, or defective hypoxia regulation.	(Giatromanolaki et al., 2008)
	HIF-1α	FIH promotes lung cancer cell proliferation, survival, and metabolism by regulating HIF activity and other key pathways, such as p53/p21 and YAP/TAZ signaling. FIH deficiency leads to reduced tumor growth and increased immune infiltration.	(García-del Río et al., 2023)
Osteosarcoma	Not identified	Overexpression of FIH in osteosarcoma cells promotes tumor growth by enhancing vessel maturation, facilitated through increased recruitment of α-SMA-positive pericytes and upregulation of PDGF-C.	(Kuzmanov et al., 2012)
Pancreatic endocrine tumors	HIF-1α	FIH and PHDs are highly expressed in PETs, with their cytoplasmic localization correlating with aggressive tumor behavior and poor prognosis. FIH plays a key role in targeting HIF-1α for regulation within the cytoplasm.	(Couvelard et al., 2008)
Renal cell carcinoma	HIF-1α	FIH-1 inhibition in CCRCC cells can increase expression of HIF targets, and inhibiting FIH-1 can increase apoptosis in these cells.	(Khan et al., 2011)

Continued on next page

TABLE 1.9: **The role of FIH in human diseases (continued)**

Disease	Related substrate	Description	Ref

CCRCC, clear cell renal cell carcinoma; CKD, chronic kidney disease; CRC, colorectal cancer; GBM, glioblastoma multiforme; GLUT1, glucose transporter type 1; HACE1, HECT domain and ankyrin repeat-containing E3 ubiquitin-protein ligase 1; IPF, idiopathic pulmonary fibrosis; LOXL2, lysyl oxidase-like 2; NF-κB, nuclear factor kappa-light-chain-enhancer of activated B cells; NSCLC, non-small cell lung cancer; Par-3, partitioning defective 3 homolog; PDGF-C, platelet-derived growth factor-C; PETs, pancreatic endocrine tumors; PHD, prolyl hydroxylase domain; PLOD2, procollagen-lysine, 2-oxoglutarate 5-dioxygenase 2; Rac1, Ras-related C3 botulinum toxin substrate 1; VEGF, vascular endothelial growth factor; YAP/TAZ, Yes-associated protein/transcriptional coactivator with PDZ-binding motif; α-SMA, alpha-smooth muscle actin; ASPP2, apoptosis-stimulating protein of p53 2; p53/p21, tumor protein p53/cyclin-dependent kinase inhibitor 1.

1.5 Summary and aims of thesis

Following the introduction, several key factors have led to the development of this project. This section outlines the current understanding and challenges in IPF, the role of HIF in fibrosis, and the significance of FIH. In addition, the limitations of existing studies on FIH are discussed, providing the rationale for the investigations conducted in this thesis.

Idiopathic pulmonary fibrosis: overview and current challenges

IPF is a chronic, progressive interstitial lung disease that primarily affects older adults, characterised by scarring of the lung tissue (fibrosis) and a pattern of UIP. The disease results in worsening lung function, leading to respiratory failure and death, with a median survival time of 3 to 5 years post-diagnosis. Though the exact cause of IPF is unknown, it is believed to arise from a combination of genetic predisposition and environmental factors, such as smoking, leading to repeated alveolar epithelial cell injury and aberrant wound healing responses. This excessive tissue remodeling and fibrosis compromise gas exchange, resulting in severe respiratory impairment. The global incidence of IPF is on the rise, particularly in countries like the USA, Italy, and South Korea, posing significant healthcare challenges, with more men affected than women.

Despite advancements in understanding the disease, the pathogenesis of IPF remains poorly understood. The persistence of activated fibroblasts and myofibroblasts, coupled with excessive deposition of the extracellular matrix, perpetuates fibrosis and lung dysfunction. Current treatment options, including pirfenidone and nintedanib, only slow the progression of the disease, and lung transplantation remains the only viable option for significantly improving survival in advanced cases, though it is not suitable for all patients. The disease mechanisms, involving mitochondrial dysfunction, immune activation, and abnormal epithelial-mesenchymal interactions, remain areas of active research. These challenges highlight the urgent need for novel therapeutic strategies to halt or reverse the fibrotic process in IPF, as current treatments are insufficient to fully address the disease burden.

The role of HIF-1α in IPF

HIF, particularly HIF-1α, is a key transcriptional regulator in response to hypoxic conditions. In IPF, the hypoxic lung microenvironment leads to the upregulation of HIF-1α, which drives several pathogenic processes contributing to fibrosis. HIF-1α is overexpressed in alveolar epithelial cells early in IPF development, before significant lung damage occurs. Through its downstream target genes, including VEGF, p53, and PDK1, HIF-1α mediates metabolic reprogramming, promotes angiogenesis, and regulates ECM remodeling—all central to the fibrotic response. Specifically, it induces EMT and myofibroblast differentiation, which are crucial events in fibrosis progression. Additionally,

the hypoxia-induced activation of HIF pathways in IPF promotes collagen cross-linking and ECM stiffening, further exacerbating the disease. Collectively, HIF-1α plays a pivotal role in the molecular mechanisms driving fibrosis, making it a potential therapeutic target for IPF.

FIH and its underexplored role in Disease

FIH is a dioxygenase enzyme that plays a crucial role in regulating HIFs by hydroxylating specific asparagine residues. This hydroxylation prevents the recruitment of transcriptional coactivators, thus inhibiting HIF-mediated transcription under normoxic conditions. FIH primarily targets HIF-1α and HIF-2α, but it has also been found to hydroxylate non-HIF substrates, such as ankyrin repeat domain proteins, indicating its broader regulatory potential.

In diseases like IPF, FIH may act as a key regulator of fibroblast metabolism, particularly influencing mitochondrial function and energy production, both of which are crucial for fibroblast activation and extracellular matrix remodeling. Despite the emerging evidence that links FIH to fibrotic diseases, much of its role remains underexplored. One major limitation of current studies is the focus on FIH's classical function in hypoxia regulation, often overlooking its potential hypoxia-independent roles and interactions with non-HIF substrates. This limited scope hampers a comprehensive understanding of FIH's involvement in broader disease mechanisms, such as metabolic reprogramming in fibroblasts. A deeper investigation into these areas may uncover novel therapeutic targets for diseases like IPF.

1.5.1 Hypothesis

Based on current understanding of IPF pathogenesis, the hypothesis is that FIH regulates fibrosis progression by modulating fibroblast behavior through both HIF-related and non-HIF-related pathways, affecting key processes like metabolism, senescence, and fibroblast activation.

1.5.2 Aim and objectives

The overall aim of this project is to investigate the functional role of FIH in fibrosis, specifically focusing on its influence on fibroblast behavior and the modulation of fibrotic pathways. This study will explore both HIF-related and non-HIF-related mechanisms in order to elucidate the broader impact of FIH in fibrotic processes.

The specific objectives of this thesis are:

1. **To determine the global transcriptomic changes resulting from FIH depletion in human lung mesenchymal cells:** This objective involves analysing multiple bulk RNA sequencing datasets using FIH-depleted fibroblasts to assess transcriptomic alterations. Comparisons will be made between siRNA and CRISPR-Cas9 methods of FIH depletion, as well as between human lung fibroblasts and mouse embryonic fibroblasts (MEFs).

2. **To investigate the role of FIH in modulating fibroblast phenotypes:** This objective focuses on exploring how FIH influences key fibroblast characteristics, including metabolism, cellular senescence, and fibroblast activation, to better understand its regulatory functions.

3. **To determine if FIH-mediated biological changes is HIF-related or not:** Using transcriptomic data and targeted experiments, this objective aims to distinguish pathways that are directly linked to HIF regulation from those arising through alternative FIH substrates, broadening understanding of its contribution to fibrotic disease.

Chapter 2

Materials and methods

2.1 Global transcriptomic processing

This study analysed three bulk RNA sequencing datasets and one microarray dataset to explore the role of FIH in fibroblasts. The microarray dataset (GSE20335) was obtained from the Gene Expression Omnibus (GEO) database. The first RNA-seq dataset focused on FIH wild-type (WT) and knockout (KO) MRC5 fibroblasts, with or without TGF-β treatment. FIH was knocked out using CRISPR-Cas9, and cells were treated with TGF-β (5 ng/ml) for 24 hours, resulting in four experimental groups with three biological replicates per group. This dataset was processed by the author and Dr. Zijian Xu.

The second RNA-seq dataset involved MRC5 fibroblasts transfected with FIH siRNA targeting FIH (siFIH), comprising two groups with triplicates. The third dataset contained siFIH-treated normal human lung fibroblasts (NHLFs), with two groups and duplicates. RNA samples for the microarray and siFIH MRC5 datasets were prepared by Dr. Liudi Yao, while the siFIH datasets were processed by Dr. Yilu Zhou using the same tools and protocols as the first RNA-seq dataset.

2.1.1 Bulk RNA sequencing data processing

2.1.1.1 RNA-seq library preparation and sequencing

For each RNA-seq sample, total RNA was extracted, and sequencing libraries were constructed using the RNeasy Mini Kits (QIAGEN, Germany) following the manufacturer's instructions. Libraries were pooled and sequenced as paired-end reads (2×150 bp) on the Illumina NovaSeq 6000 platform (Novogene, Cambridge, UK). Each dataset was processed to ensure sufficient biological replicates and comprehensive gene coverage.

2.1.1.2 Quality control, alignment, and quantification

Quality control of the raw RNA-seq data was performed using FastQC (http://www.bioinformatics.babraham.ac.uk/projects/fastqc). Adapter trimming and filtering of low-quality reads (Phred score > 30) and short reads (< 50 bp) were conducted using Trim Galore (https://github.com/FelixKrueger/TrimGalore). Filtered reads were aligned to the human genome (Ensembl GRCh38) using Hisat2, and the resulting SAM files were converted to BAM files using Samtools. Read counts for each gene were summarized with featureCounts for subsequent differential expression analysis.

2.1.1.3 Data processing environment and analysis

All computational steps were performed on the Iridis5 High Performance Computing (HPC) system at the University of Southampton under a Linux environment. The bioinformatics tools utilized, including FastQC, Trim Galore, Hisat2, Samtools, and featureCounts, were managed through Conda environments, ensuring standardization and reproducibility. The read count data from all RNA-seq datasets were analysed using the DESeq2 R package (version 1.26.0) within RStudio for normalization and differential gene expression analysis.

2.1.1.4 Differentially expressed genes (DEGs) analysis

The raw read counts were processed in RStudio for gene expression analysis. To account for sample variability, the data were normalized using the variance stabilization normalization (VSN) method, implemented with the `justvsn` function from the VSN package in R. Following normalization, the data were Log_2-transformed to stabilize variance across samples. DEGs were identified using the DESeq2 package (version 1.26.0) in R, applying a significance threshold of adjusted P-value < 0.05 and a $|\log_2$ fold change$| \geq 0.5$(may be changed in specific condition). Transcripts with low abundance (fewer than 10 counts across all samples) were excluded from further analysis.

2.1.2 Microarray data processing

2.1.2.1 Raw data download and processing

The microarray dataset (GSE20335) was processed and analysed to identify DEGs. The CEL files containing raw microarray data were downloaded from the Gene Expression Omnibus (GEO) database. Data processing was conducted in RStudio using the 'GEOquery', 'oligo', and 'affy' packages. CEL files were read and loaded using the

'read.celfiles' function from the 'oligo' package and the 'ReadAffy' function from the 'affy' package.

The robust multi-array average (RMA) algorithm was employed for background correction, normalization, and summarization of the microarray data using the 'rma' function. Boxplots of raw and normalized data were generated to assess the quality and distribution of the expression data. Following normalization, the expression values were extracted and transformed for downstream analysis. Gene symbols were annotated by downloading the soft file from the GEO database and extracting relevant information, including probe IDs and corresponding gene symbols.

To remove duplicate gene symbols, only the first gene name was retained when multiple symbols were present, and median expression values were calculated for genes with multiple probes. The data were then subset into specific groups for WT and FIH knockout (KO) analyses.

2.1.2.2 Differential expression analysis and annotation

Differential expression analysis was conducted using the 'limma' package in R. A linear model was designed for each comparison (e.g., FIH KO vs. WT). The model matrix was constructed using the 'model.matrix' function, and contrasts between conditions were created using the 'makeContrasts' function.

DEGs were identified by fitting the linear model to the expression data using the 'lmFit' function, followed by contrast fitting with 'contrasts.fit'. The empirical Bayes method was then applied using 'eBayes' to calculate the false discovery rate (FDR). DEGs were filtered based on an adjusted P-value threshold (< 0.05). Results for the differentially expressed genes were obtained using the 'topTable' function, which lists genes with significant expression changes in each comparison.

2.2 Cell culture

2.2.1 Cell lines

All cell lines and their complete media used in this thesis were listed in Table 2.1. Cells were usually cultured in Corning T75 flasks or 100mm dishes (both from Fisher Scientific, UK) at 37°C with 5% CO_2 in a humidified incubator. Unless otherwise stated, all reagents were obtained from Life Technologies (UK).

TABLE 2.1: **Preparation of cell culture media**

Cell Line	Originated from	Media composition
HEK293-FT	Highly transfectable clonal isolate derived from human embryonal kidney cells transformed with the SV40 large T antigen	DMEM with 10% heat-inactivated FBS, 50U/ml Penicillin, 50μg/ml Streptomycin
MRC5	Lung fibroblasts isolated from a male fetus	DMEM with 10% heat-inactivated FBS, 50U/ml Penicillin, 50μg/ml Streptomycin, 1mM sodium pyruvate, and 1mM non-essential amino acids
Normal human lung fibeoblasts (NHLFs)	Primary fibroblasts isolated from healthy people	

Primary human lung fibroblasts were kindly provided by the Brooke Lab at the Clinical and Experimental Sciences department of the University of Southampton (University Southampton Hospital, UK). Dr. Mark Jones and Franco Conforti, from the same lab, established primary lung fibroblast cultures from control and IPF lungs, following the methods outlined in their earlier work (Jones et al., 2018; Conforti et al., 2017). All human lung studies were approved by the local research ethics committees (Southampton and South West Hampshire, and Mid and South Buckinghamshire) under reference number 07/H0607/73. All participants provided written informed consent. The IPF samples were from patients later diagnosed with IPF according to international consensus guidelines (Jones et al., 2018). FIH KO MRC5 cells were used at passages 35–40. This passage range reflects the requirement for long-term selection of knockout clones and the limited availability of reserved cell stocks. Despite the higher passage number, cells at this stage retained stable growth and reproducible experimental responses.

2.2.2 Cell trypsinasation and passaging

When cells reached over 90% but not full confluency, they were passaged for experimental use or routine maintenance. To remove residual FBS that could inhibit trypsin activity, 1x room-tempratured phosphate-buffered saline (PBS) (Life Technologies, UK) was added to the cells. Then, 0.05% trypsin (Life Technologies, UK) was applied to the washed cell mono layer (the volume of trypsin was adjusted according to the different

culture dish). Cells were incubated at 37°C for about 5 minutes until the monolayer detached. Trypsinisation was halted by adding complete media, and the cell suspension was then centrifuged at 300 g for 5 minutes. The resulting cell pellet was resuspended in fresh complete media for routine maintenance or further plating.

2.2.3 Cell counting

After trypsinisation (Section 2.2.2), the cell were resuspend using complete medium. Then 10μL cell suspension was mixed with the same volume of 0.4%trypan blue (Life Technologies, UK) and 10 μL mixture was added to a Marienfeld Superior with Neubauer improved Hemocytometer (depth 0.1mm) (Fisher Scientific, Milton Keynes, UK), ensuring that the chamber was not overfilled. The chamber was then placed under a 10$\times$ objective on a light EVOS XL core microscope (Life Technologies, UK), using phase-contrast to distinguish the cells. The cells were counted within the large, central gridded square (1 mm^2). The count was multiplied by 2×10^4 to estimate the number of cells per mL.

2.2.4 Cell cryopreservation and thawing

Following trypsinisation (Section 2.2.2), the cells were resuspended in complete growth medium, and the viable cell count was determined (Section 2.2.3). After centrifugation, the supernatant was carefully removed using a pipette, leaving only a minimal volume without disturbing the cell pellet. The cells were then resuspended in freezing medium at a concentration of 1×10^6 to 2×10^6 cells/mL. The cell suspension was aliquoted into labeled 2ml cryogenic storage vials (SRATLAB, UK). The cryogenic vials were then transferred into a Mr. Frosty freezing container and placed in a -80°C freezer, before being transferred into liquid nitrogen the next day.

To begin the thawing process, the cryovial containing the frozen cells is promptly retrieved from liquid nitrogen storage or -80°C freezer and defrosted in a 37°C water bath as soon as possible. The vial is gently swirled to facilitate rapid thawing, typically within one minute, until only a small amount of ice remains. The thawed vial is then transferred to the biological safety cabinet (BSC). Pre-warmed complete growth medium is gradually added dropwise to the centrifuge tube containing the thawed cells. The cell suspension is subsequently centrifuged at 300g for 5 minutes. Following centrifugation, the supernatant is inspected for clarity, and the presence of a distinct cell pellet is confirmed. The supernatant is carefully decanted to avoid disturbing the pellet, after which the cells are gently resuspended in fresh complete growth medium. Finally, the resuspended cells are transferred to an appropriate culture vessel and placed at 37°C with 5% CO_2 in a humidified incubator. Change the medium to remove residual DMSO if necessary.

2.3 CRISPR-Cas9

The construction of CRISPR-Cas9 cell line was done under the supervision of Prof. Nullin Divecha and Dr. Bhav Sheth.

2.3.1 CRISPR-Cas9 plasmid design and construction

The lentiviral plasmids were constructed by Prof. Nullin Divecha. The first step in utilizing CRISPR-Cas9 technology involves designing the guide RNA (gRNA) sequences specific to the target gene of interest. The sgRNAs stargeting HIF1AN (gene encodes FIH) was designed on CRISPick (https://portals.broadinstitute.org/gppx/crispick/public). Once designed, the gRNA sequence is cloned into lentiCRISPR V1.0 (Figure.2.1) . This plasmid serves as the backbone for CRISPR-Cas9-mediated genome editing. The plasmid is then amplified and purified for subsequent use in transfection. We picked 5 sgRNA oligos for the following plasmids construction and finally chose two oligos (Table.2.2) whose knockout efficiency were best.

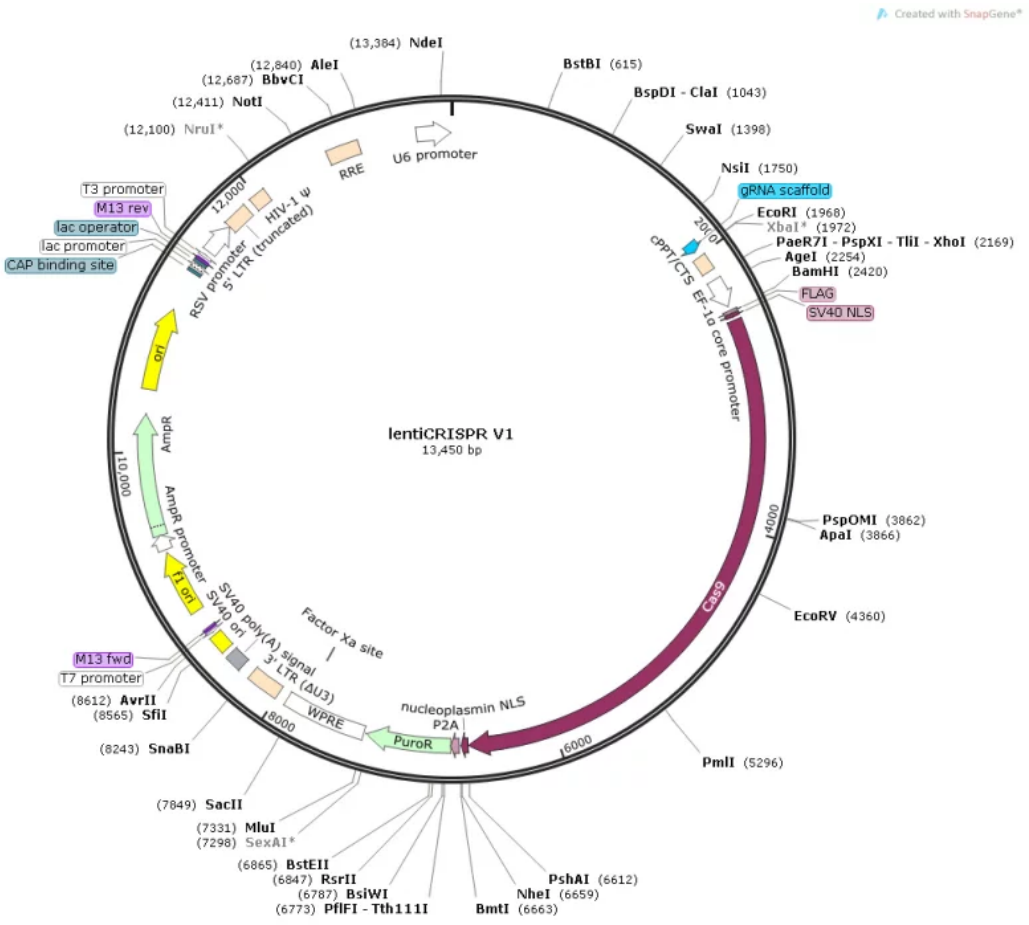

FIGURE 2.1: **LentiCRISPR V1.0 plasmid map**

TABLE 2.2: **List of sgRNA oligos targeting HIF1AN**

Oligo number	Sequence
*HIF1AN*_sgRNA_1	GAAGCTATAACTGCGCAACT
*HIF1AN*_sgRNA_2	GTCTGAGTCAGAGCGACCCC

2.3.2 Preparation of lentiviral particles

To facilitate the delivery of the CRISPR-Cas9 plasmids into target cells, lentiviral particles are produced using HEK 293FT cells.

Day 1: Cell plating 1×10^6 HEK293-FT cells were plated into each well of a 6-well plate with complete DMEM(10% FBS with Pen/Strep). The cells should be allowed to adhere and grow overnight in an incubater at 37°C with 5% CO_2.

Day 2: Transfection Approximately one hour before transfection, refresh the medium in each well to ensure a better transfect efficiency. Prepare the transfection mixture in a sterile Eppendorf tube as indicated in Table.2.3 for each well. After adding all components, the mixture was incubated for 15-20 minutes without disturbing. Once ready, the DNA/PEI (TOCRIS, UK) solution was added to the cells in each well in a dropwise manner. The cells should be incubated overnight under standard conditions.

TABLE 2.3: **Transfection mixture for generation of lenti virus**

Component	Volume or Amount
Opti-MEM	100 μL
Experimental plasmid	1.14 μg
GAG pol plasmid	0.57 μg
VSVG plasmid	0.28 μg
PEI (Polyethylenimine, 1mg/ml)	6 μL

Day 3: Media Change After overnight incubation, the medium in each well was carefully replaced with 4 mL of fresh complete medium, taking care not to disturb the cells. The cells were then incubated for an additional 48 hours to produce a higher yield of virus with improved efficiency.

Day 4: Target cell plating One day prior to virus transduction, 200,000 to 250,000 target cells were plated in a 6-well plate, ensuring that one well was reserved as a ”no virus” control.

Day 5: Virus Collection and filteration Collect 4 mL of the 48-hour viral production media into a 15 mL Falcon tube, then filter the medium through a 0.45 μm filter (Millipore, UK) to remove any cell debris. After collecting the supernatant, discard the remaining cells. Aliquot the filtered viral solution into 1 mL portions in cryovials, snap-freeze the aliquots, and store them in a -80°C freezer. Retain 1 mL of the viral suspension for immediate transduction experiments, while the remaining aliquots are stored for future use.

2.3.3 Lentiviral transduction of target cells

The target cells are prepared in six-well plates. The stored lentiviral particles are thawed and diluted in complete growth medium, with the addition of polybrene to enhance infection efficiency. The viral mixture is then added to the target cells, and the cells are incubated overnight. The following day, the medium is replaced with fresh growth medium. After an additional day of incubation, the cells are subjected to puromycin (Sigma Aldrich, UK) selection to isolate successfully transduced cells. Non-transduced cells, identified by the lack of survival under antibiotic pressure, are removed, ensuring a pure population of CRISPR-Cas9 modified cells.

2.3.4 Validation and expansion of CRISPR-Cas9 edited cells

After transduction and selection, the surviving cells are expanded and subjected to validation assays to confirm successful gene editing. This may include Western blot analysis to assess protein expression levels (Figure.2.2). Once validated, the edited cell population can be expanded further for downstream experiments or cryopreserved for future use.

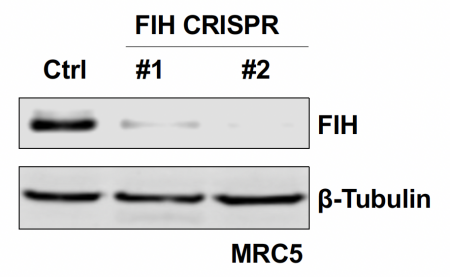

FIGURE 2.2: **Validation of FIH KO in MRC5 cells**
Protein expression of FIH in MRC5 after puromycin selection in MRC5. β-Tubulin was used as a loading control.

2.4 siRNA reverse transfection

Reverse transfection was used in the study. For reverse transfection, 25 pmol of siRNA and 3.75 μL of Lipofectamine RNAiMAX reagent (Invitrogen, UK) were used per well in a 6-well plate. siRNA oligos target interested genes were purchased from Dharmacon (USA) (Table. 2.4).

The siRNA-Lipofectamine RNAiMAX complexes were prepared directly in the wells. First, 25 pmol of siRNA was diluted in 150 μL of Opti-MEM medium and added to each well of the tissue culture plate. Lipofectamine RNAiMAX reagent was gently mixed before use, and 3.75 μL was added to each well containing the diluted siRNA. The mixture was gently mixed and incubated at room temperature for 10–20 minutes to allow complex formation.

MRC5 cells or NHLFs were diluted in complete growth medium so that 850 μL contained the desired number of cells, aiming for 60-70% confluence 24 hours after plating. After incubation, 850 μL of the diluted cells was added to each well, resulting in a final volume of 1000 μL per well. The cells were gently mixed with the siRNA-lipid complexes by rocking the plate back and forth. The plate was incubated at 37°C in a CO_2 incubator for at least 48 hours before validation for gene knockdown (Figure 2.3).

TABLE 2.4: **List of small interfering RNA (siRNA)**

siRNA	Catalog Number	Company
HIF1AN (FIH)	MU-005035-02-0010	Dharmacon
ARNT (HIF1β)	MU-010230-00-0002	Dharmacon
Control (siGENOME-RISCfree)	D-001220-01-20	Dharmacon

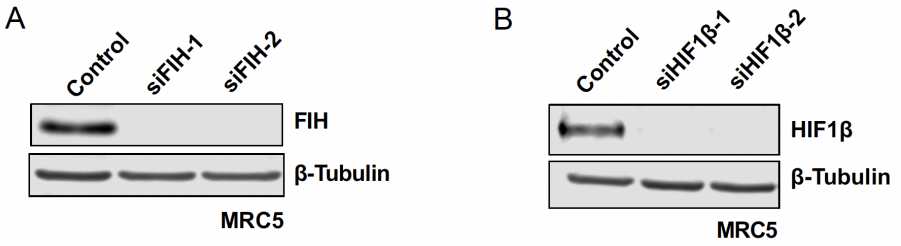

FIGURE 2.3: **Validation of siRNA targeting FIH and HIF1β in MRC5 cells**
Protein expression of FIH and HIF1β in MRC5 at 48 hours after reverse transfection. β-Tubulin was used as a loading control.

2.5 Quantitative real-time PCR (q-RT-PCR)

2.5.1 RNA quantification and extraction

To quantify the mRNA expression, RNA was extracted using RNeasy mini kits (QIAGEN, Germany) following the manufacturer's instructions. In a 6-well plate, cells were lysed using 350 μL buffer RLT. After homogenizing the lysate by pipeting, the lysate was mixed with an equal volume of 70% ethanol (Sigma Aldrich, UK) and the mixture was transferred to an RNeasy spin column placed in a 2 mL collection tube. The column was washed by 700 μL Buffer RW1 once and 500 μL Buffer RPE twice sequentially with centrifugation (8,000g, $>$ 30s) after each washing. Finally, the column was transferred into a brand new 1.5 mL tube and 50 μL RNAse-free water was used to elute the RNA by centrifuging at 8,000g for 1 min. RNA concentration was quantified on the Nanodrop Spectrophotometer 2000c (ThermoFisher Scientific) and stored in -80$Cuntilfurtherq PCRanalysis$.

2.5.2 Quantitative real-time PCR (q-RT-PCR)

The final concentration of RNA samples for qPCR is 20ng/μL diluted by RNase free water. Real-time PCR was performed using QuantiNova SYBR Green RT-PCR kit (QIAGEN, Germany) according to the manufacturer's instruction. The reaction setup (Table.2.5), the QuantiTect gene-specific primers (QIAGEN, Germany) (Table.2.6) and the thermocycling condition were listed (Table.2.7).

Triplicates were performed for each sample in a 96-well plate on StepOnePlus^{TM} Real-Time PCR System (ThermoFisher Scientific, UK). During the running, the fluorescent signal increases as the DNA amplifies. The Ct value is the cycle number at which the fluorescent signal crosses the threshold. The $\Delta\Delta$Ct method was used to calculate the relative expression level of a gene between two samples as following steps show:

1. ΔCt: Calculate the difference between the Ct value of the target gene and ACTB gene in each sample. ΔCt here is the average of the triplicates.

$$\Delta\text{Ct} = \text{Ct}_{Target} - \text{Ct}_{ACTB}$$

2. $\Delta\Delta$Ct: Calculate the difference between the ΔCt values of the two samples.

$$\Delta\Delta\text{Ct} = \Delta\text{Ct}_{\text{sample1}} - \Delta\text{Ct}_{\text{sample2}}$$

3. Fold Change: Calculate the relative expression level as a fold change.

$$\text{Fold Change} = 2^{-\Delta\Delta\text{Ct}}$$

Finally, the foldchange was demonstrated in barplot with P value generated by Graphpad Prism (V10.0.2).

TABLE 2.5: **qRT-PCR reaction setup**

Component	**Volume (μL)**
2× QuantiNova SYBR Green RT-PCR Master Mix	10
QN ROX Reference Dye	1
QN SYBR Green RT-Mix	0.2
10× primer mix	2
RNA (20 ng/μL)	2
RNase-Free Water	4.8
Total reaction volume	**20 μL**

TABLE 2.6: **List of qPCR QuantiTect primers (QIAGEN, Germany)**

Gene Name	**Reference Code**
GAPDH	QT01192646
ACTA2	QT00088102
COL1A1	QT00037793
COL3A1	QT00058233
FN1	QT00038024
ACTB	QT01680476

TABLE 2.7: **Thermocycling condition for qRT-PCR (StepOnePlus, Thermofisher)**

Step	**Time**	**Temperature**
Reverse transcription	10 min	50 *C*
PCR initial activation step	2 min	95 *C*
Two-step cycling		
Denaturation	5 s	95 *C*
Combined annealing/extension	10 s	60 *C*
Number of cycles	35-40	
Melting Curve		
Denaturation	15 s	95 *C*
Annealing	1 min	60 *C*
High resolution melting	15 s	95 *C*

2.6 SDS-PAGE and western blotting

2.6.1 Protein extraction and quantification

Cells were lysed using 100-200μL urea buffer (Table.A.1) with protease inhibitors(Roche, UK), added after washing the cell monolayer with ice-cold PBS. The lysate is collected using a cell scraper and left on ice for 30 minutes, then transferred to tubes for freezing or immediate use.

Samples are sonicated on ice for 5 minutes to break down cell structures and then centrifuged at high speed at 4C. $The supernatant is used for protein quantification via the Bradford assay using the Bio-Rad, UK), where samples and standards are mixed with Bradford reagent and absorbance is measured at 595 nm using Pol$ LDS loading buffer (Invitrogen, UK) and β-mercaptoethanol (ThermoFisher, UK). This mixture is boiled at $100C for 5 minutes to denature the proteins, centrifuged, and either loaded on to gels or stored at -$ 20C for future use.

2.6.2 Sodium dodecyl sulphate-polyacrylamide gel electrophoresis (SDS-PAGE) gel preparation

Before running the gel, the SDS-PAGE gel was prepared. SDS-PAGE plates (Bio-Rad, UK)were cleaned with ethanol or distilled water (ddH_2O) to ensure they were clean and dry. The front and spacer plates were assembled in the green casting frame, secured with clips, and placed in the casting stand.

For the separation gel, a solution of the required percentage was prepared according to standard protocols (detail listed in Table.A.2). This solution was poured into the cassette and overlaid with isopropanol to exclude oxygen, facilitating gel polymerization. After 20-30 minutes, the polymerized gel was rinsed with distilled water, and any excess water was blotted away.

A 5% stacking gel solution was then prepared and poured on top of the separation gel (detail listed in Table.A.3). A 10 or 15 well comb was inserted, ensuring no air bubbles were trapped. The stacking gel was left to set for 20-30 minutes. Once set, the gel cassette was removed from the casting stand and placed into the electrode assembly with the short plate facing inward.

2.6.3 SDS-PAGE gel electrophoresis

The chamber between the gels was filled with 1x running buffer (Table.A.4). Protein molecular weight markers (Lonza, UK) was used to reference and estimate the protein sizes. The remainder of the tank was filled with running buffer to the indicated level.

The assembly was connected to a PowerPac Basic power pack (Bio-Rad, UK), and electrophoresis was performed at 80V for sample concentration (20-30 minutes) and then at 120V for sample separation. The process continued until the bromophenol blue dye front reached the bottom of the separation gel. Gels were then carefully removed for subsequent steps.

2.6.4 Protein transferring

The stacking gel and the bromophenol blue dye at the bottom of the separating gel were cut off. The gel was placed in cold transfer buffer (Table.A.5) for several minutes to remove salts and preshrink. A nitrocellulose (NC) membrane was cut to match the gel size. The transfer cassette was assembled with presoaked layers in transfer buffer, ensuring no air bubbles. Electrophoretic transfer was performed at 80V for 3 hours in a TE22 mini tank transfer unit (GE Health Life Science, UK) in the cold room. Optionally, a transfer at 25V for 16 hours could be performed.

2.6.5 Ponceau S staining

After transfer, the membrane was briefly rinsed with TBST (Table.A.6) to remove residual gel fragments. Ponceau S solution (SigmaAldrich, UK) was used to stain the membrane for 1-2 minutes to check for protein transfer. The membrane was then destained with several changes of TBST until visible bands remained.

2.6.6 Blocking and antibody incubations

Non-specific binding sites on the membrane were blocked by incubating in 5% milk in TBST for 60 minutes on a shaker at room temprature. After washing by TBST for three times, the membrane was incubated in the primary antibody (Table.2.8) diluted in blocking buffer overnight at 4°C on a roller.

After primary antibody incubation, the membrane was equilibrated to room temperature for 15 minutes and washed with TBST (initial rinse followed by three 5-minute washes). The secondary antibody (LI-COR Bioscience, Lincoln, NE, USA) (Table.2.9) was diluted in blocking buffer and incubated with the membrane for 1 hours at room temperature on a roller. Unbound secondary antibody was removed with an initial rinse followed by three 5-minute washes in TBST.

2.6.7 Imaging and analysis

Protein bands were visualised by Odyssey Imaging System (LI-COR Bioscience). Protein band was quantified using FIJI software with β-Tubulin as the loading control.

TABLE 2.8: **List of primary antibodies**

Antibody	Supplier	Cat-No
α-SMA	Cell Signalling Technology	14968
β-tubulin	Cell Signalling Technology	86298
Phospho-Smad2/Smad3	Cell Signalling Technology	8828
FIH	Oxford, UK	Mouse monoclonal 162 C
Total-Smad2	Cell Signalling Technology	3122
Collagen 1	Abcam	ab34710
HIF1β	Cell Signalling Technology	5537

TABLE 2.9: **List of secondary antibodies**

Antibody	Supplier	Cat-No
IRDye 800CW Goat anti-Rabbit	LI-COR Biosciences	926-32211
IRDye 800CW Donkey anti-Goat	LI-COR Biosciences	926-32214
IRDye 680CW Goat anti-Mouse	LI-COR Biosciences	926-68020

2.7 Seahorse real-time assay

The mitochondrial stress test and glycolytic stress test were conducted by Dr. Charlie Birts, with me observing and assisting.

2.7.1 Mitochondrial stress test

Under the supervision of Dr. Charlie Birts, the Seahorse assay was performed to measure bioenergetic profiles both at basal levels and during a mitochondrial stress test. This test involved: (1) inhibiting ATP synthase with oligomycin to assess mitochondrial ATP production, (2) using the OXPHOS uncoupler FCCP to disrupt the mitochondrial membrane potential and evaluate maximal mitochondrial activity independently of ATP production, and (3) blocking residual mitochondrial activity with antimycin to measure non-mitochondrial oxygen consumption (Figure. 2.4).

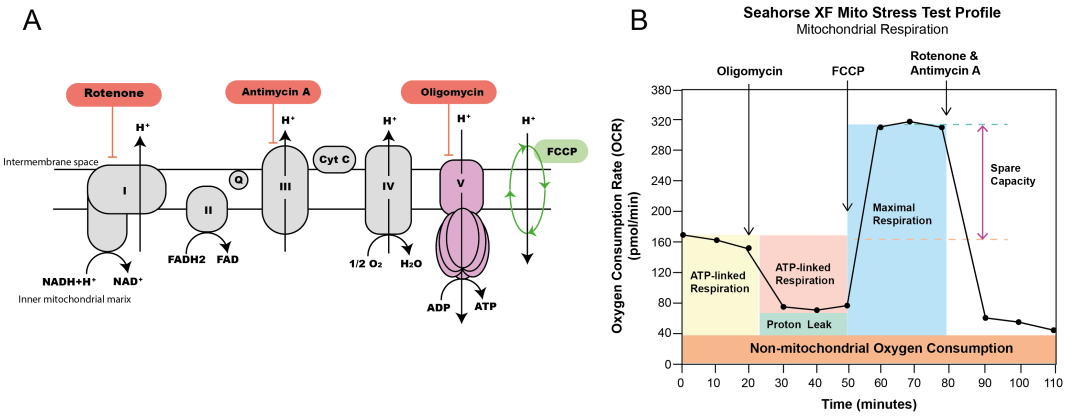

FIGURE 2.4: **Seahorse XF mito stress test overview**

The diagram illustrates the Seahorse XF Mito Stress Test used to assess mitochondrial respiration by measuring the OCR. (A) Diagram shows a schematic of the ETC within the inner mitochondrial membrane, highlighting the inhibition points for each chemical: Rotenone inhibits Complex I, blocking electron flow from NADH; Antimycin A inhibits Complex III, preventing electron transfer from ubiquinol to cytochrome c; Oligomycin inhibits ATP synthase (Complex V), stopping ATP production; and FCCP uncouples the proton gradient, driving maximal respiration. (B) Seahorse Mito-Stress test profile displays the fundamental parameters of mitochondrial function: basal respiration, ATP turnover, proton leak, maximal respiration and spare respiratory capacity.

Day 1: Cells were plated at a density of 7500 cells per well in a Seahorse XF96 plate (Agilent, UK) 48 hours prior to the assay. The sensor cartridge was prepared by immersing it in 200 μL of Seahorse calibrant per well and stored overnight at 37°C in a non-CO_2 incubator. Seahorse running media was prepared by mixing DMEM powder with water and penicillin/streptomycin, adjusting the pH to 7.4, filtering it, and storing at 4°C as per manufacturers' instructions (Sigma).

Day 2: After taking images of the cells, Seahorse running media for the mitochondrial stress test (RMmiG) was prepared by adding 1 mM pyruvate and 5 mM glucose to the basic Seahorse DMEM media with 2 mM glutamine. The working concentrations of the reagents for the mitochondrial stress test were as follows: 10 μM glucose, 1 μM oligomycin, 1 μM FCCP (Carbonyl cyanide-p-trifluoromethoxyphenylhydrazone), and a mixture of 1 μM antimycin and 1 μM rotenone (The manufacturer details of chemical components are listed in Table.2.10). The sensor cartridge was calibrated to eliminate any bubbles.

Cells were washed with Seahorse running media by aspirating the medium, leaving approximately 5 μL in each well, followed by washing with RMmiG. After the Seahorse calibration was complete, 150 μL of pre-warmed RMmiG with the relevant inhibitors was added to the wells, and the plate was placed back into the non-CO_2 incubator for 5

minutes. The cell plate was then loaded into the Seahorse machine, and the mitochondrial stress test was run. The oxygen consumption rate (OCR) was calculated according to the manufacturer's guidelines. After the run, cell attachment was checked, and Bradford protein normalization was performed to normalize the results to the total protein per well.

2.7.2 Glycolytic stress test

Similar to the Seahorse real-time mito-stress assay, the glycolytic assay involves sequentially injecting specific reagents into the cell culture. Briefly, bioenergetics profiles were measured at the basal state, followed by a glycolytic stress test. This test involved sequentially: (1) adding glucose to initiate glycolysis, which increases ECAR; (2) adding oligomycin, an inhibitor of mitochondrial ATP synthase, which forces cells to rely solely on glycolysis for ATP production, further elevating ECAR; and (3) injecting 2-DG, a glucose analog, to inhibit glycolysis by blocking hexokinase, resulting in a decrease in ECAR. These reagent-induced changes in ECAR allow for the assessment of glycolytic rate, capacity, and reserve, providing a comprehensive evaluation of the cells' glycolytic function (Figure. 2.5).

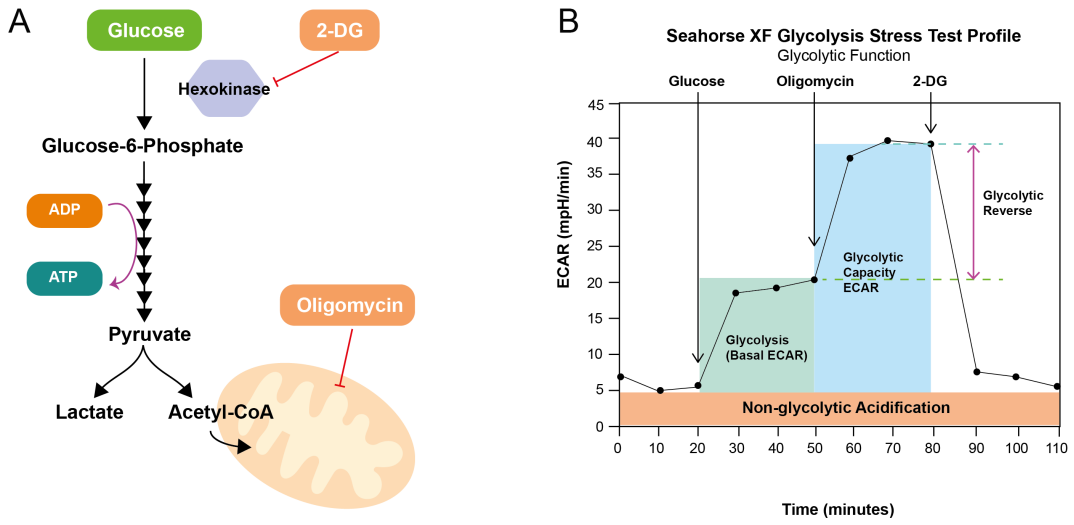

FIGURE 2.5: **Seahorse XF glycolytic test overview**

The diagram illustrates the Seahorse XF Glycolysis stress test, which measures glycolytic function by assessing ECAR. (A) An overview of glycolytic pathway, where glucose is converted to pyruvate, highlighting the inhibition points by 2-DG, which blocks hexokinase, and oligomycin, which inhibits ATP synthase. (B) The Seahorse Glycolytic stress assay profile: glucose addition initiates glycolysis, increasing ECAR (basal glycolysis); oligomycin further increases ECAR by inhibiting mitochondrial ATP production, thus revealing glycolytic capacity; and 2-DG addition sharply reduces ECAR, indicating non-glycolytic acidification.

Day 1: The procedure for the first day was the same as the mitochondrial stress test, with cells plated at 7500 cells per well in the XF96 plate and the sensor cartridge prepared and stored overnight.

Day 2: For the glycolytic stress test, Seahorse running media (RMgl) was prepared by adding 2 mM glutamine to Seahorse DMEM media. The working concentrations of the reagents for the glycolytic stress test were: 5 mM glucose, 1 μM oligomycin, and 50 mM 2-deoxyglucose (2-DG).

Cells were washed with RMgl in the same manner as the mitochondrial test. Once the Seahorse calibration was complete, 150 μL of pre-warmed RMgl with the relevant inhibitors was added to the wells. The plate was incubated for 5 minutes before loading onto the Seahorse machine to run the glycolytic stress test. The extracellular acidification rate (ECAR) was calculated according to the manufacturer's guidelines. As with the mitochondrial test, cell attachment was checked, and protein normalization was carried out afterward.

TABLE 2.10: **Seahorse reagent information**

Reagent	Manufacture	Cat. No.
DMEM powder	Sigma	D5030-10L
45% glucose solution	Fisher Scientific (Corning Media Tech)	15363581
2-deoxy-glucose	Fisher Scientific (Acros Organics)	111980050
Oligomycin	Sigma	O4876-5MG
FCCP	Sigma	C2920-10MG
Antimycin A	Sigma	A8674-25MG
Rotenone	Sigma	R8875-1G
Sodium Pyruvate	Sigma	S8636-100ml
Seahorse XFe96 FluxPaks	Agilent	102416-100
Seahorse XFe96 FluxPaks	Agilent	102601-100

2.7.3 Protein quantification after Seahorse assay

Following the Seahorse assay, protein quantification for normalization was performed using a modified Bradford assay. After aspirating the growth media, cells were lysed with 20 μL of lysis buffer (250 mM Tris, pH 7.4, and 0.1% Triton X-100) and incubated for 15 minutes at room temperature. To reduce detergent interference, 130 μL of dilution buffer (250 mM Tris, pH 7.4) was added to the lysates. The lysates were mixed with 150 μL of 2X Bradford reagent (diluted from 5×), and 200 μL of this mixture was transferred to a new 96-well plate for absorbance measurement at 595 nm using a microplate reader. Absorbance readings were taken within 1 hour to ensure accuracy.

The protein content in each well was determined by comparing the absorbance values to the standard curve, enabling accurate normalization of Seahorse assay data.

2.8 ^{1}H NMR based metabolite screening

2.8.1 NMR sample preparation

In this study, the volumes and vessel sizes used were suitable for a 6-well plate format. Bench surfaces and items to be used, including internal surfaces of the biological safety cabinet (BSC), were sprayed with 70:30 ethanol:water (EtOH:H_2O) and fully wiped down. Following the designed experiment treatment to the cells, the cultured media in the vessel were transferred into a sterilized tube within the BSC. The media were then centrifuged at 1500 rpm for 5 minutes at 4 °C to pellet dead cells, after which the supernatant was transferred to a fresh 1.5mL tube, leaving the pellet behind. Aliquots of the supernatant (typically 1 mL) were stored at -80 °C for subsequent NMR and MS analyses. The cells adhered to the culture vessel surface were washed twice with 1 mL of cold (4 °C) PBS to remove residual media. After each wash, the PBS was discarded. The cells were then quenched by adding 1 mL of cold filtered methanol (kept on dry ice) to the culture vessel and allowed to lyse at room temperature for 2 minutes in the BSC. The lysed cellular material was detached from the culture vessel using a cell scraper or cell lifter and transferred into a fresh tube. Steps involving methanol quenching and cell scraping were repeated to maximize metabolite recovery. The resulting suspensions were dried down using a Centrifugal Vacuum Concentrator (Eppendorf, UK) without a heat lamp, sealed, and stored at -80 °C.

2.8.2 NMR experiments and data processing

The methanol-quenched cell samples were obtained from the -80 °C freezer and placed on ice. While keeping the samples on ice, 80 μL of phosphate buffer (kindly offer by Joshua Green Jenkinson) was added to each sample. The samples were then vortexed for 30 seconds at full speed to ensure thorough mixing. Subsequently, the samples were centrifuged at 14,000 rpm (approximately 13,000 g) for 10 minutes. After centrifugation, 50 μL of the supernatant was carefully transferred into 1.7 mm NMR capillary tubes, which were then capped and labeled for subsequent NMR analysis. The NMR analysis was done and monitored by Dr Johnathan Swann.

2.8.3 Data processing

The data processing of NMR was done under the supervison of Dr. Johnathan Swann and Micheal Harvey. NMR spectral data were processed in Matlab (MATLAB R2018a). Initially, the spectral data were imported using the `spec_preproc` function, with options set for phase correction, baseline correction, and referencing to TSP, depending on the sample type. Uninformative spectral regions, such as those corresponding to water and other unwanted signals, were removed. The data were then normalized using the probabilistic quotient normalization (PQN) method to reduce variability due to sample concentration differences.

To correct for peak shifts across samples, the recursive segment-wise peak alignment (RSPA) algorithm was applied. This alignment process was further refined manually using the `uiAlignment` graphical interface for regions that exhibited significant peak shifting. Once aligned, the spectral data were plotted and visually inspected to ensure consistency across all samples.

Subsequent data analysis was carried out using Principal Component Analysis (PCA) and Orthogonal Signal Correction Partial Least Squares Discriminant Analysis (OPLS-DA) in MATLAB. Cross-validated PCA (`JTPcrossvalidatedPCA.m`) was used to examine data trends and identify potential outliers. For discriminant analysis, OPLS-DA was performed using `mjrMainO2pls.m`, and the number of components was selected based on model validation criteria such as explained variance (R^2) and predictive ability (Q^2). Loadings were back-scaled onto the original spectral data to identify key metabolic markers. Metabolites identification was done according to Chenomx NMR Suite.

2.9 CellTiter-Glo assay

The CellTiter-Glo Luminescent Cell Viability Assay (Promega, UK) was used to assess ATP production. NHLFs and MRC5 cells were seeded in a 96-well plate at a suitable density, aiming for 80-90% confluence at measurement. Control wells containing only DMEM medium were included to determine background luminescence.

Prior to the assay, the CellTiter-Glo reagent was prepared by reconstituting the lyophilized CellTiter-Glo® Substrate with the appropriate volume of CellTiter-Glo® Buffer, according to the manufacturer's instructions. The reagent was mixed by gentle inversion to ensure homogeneity.

At the day of measurement, the plate was equilibrated to room temperature for 30 minutes. Then, an equal volume of CellTiter-Glo Reagent (100μL) was added to each well, including experimental and control wells. The plate was gently shaken for 2 minutes to induce cell lysis and to allow the development of luminescence. Following lysis, the

plate was incubated at room temperature for 10 minutes to stabilize the luminescent signal.

Luminescence was measured using a microplate luminometer. The ATP levels, proportional to the number of viable cells, were calculated after subtracting the background luminescence from the control wells. The data were normalized to protein content in parallel wells to accurately quantify ATP production in each experimental condition. The method for protein quantification is adapted from the method for protein quantification after Seahorse assay (see section 2.7.3).

2.10 Lactate-Glo assay

The intracellualr and extracellualr lactate was measured using Lactate Glo^{TM} Assay kit (Promega, UK). 10,000 cells per well were plated in a 96-well plate, with control wells containing only the medium.

For measuring changes in extracellular lactate, at designated experimental time points, 5μL of medium was collected and diluted into 95μL PBS. Samples were either immediately processed or frozen at –20°C in a well-sealed 96-well plate with an adhesive plate sealer and plastic lid.

To assess intracellular lactate levels, the cells were washed with cold PBS to avoid contamination from extracellular lactate after collecting cultured medium. All steps were performed rapidly to minimize alterations in lactate metabolism. Following the PBS wash, Inactivation Solution (0.6N HCl) was directly added to the wells to lyse the cells, halt metabolic processes, and inhibit endogenous protein activity, eliminating the need for centrifugation or deproteinization. This step also destroys reduced NAD(P)H dinucleotides, ensuring accurate intracellular lactate measurement. Afterward, Neutralization Solution (1M Tris base) was added to each well to neutralize the sample. Samples were either assayed immediately using the Lactate-Glo Assay or stored at –20°C for future analysis.

On the day of the assay, frozen samples were thawed, and 50μL was transferred to a new 96-well assay plate. An equal volume (50μL) of Lactate Detection Reagent (details showed in Table.2.11) was added to each well, followed by shaking the plate for 30–60 seconds to ensure proper mixing. After incubating for 60 minutes at room temperature, luminescence was recorded to assess lactate levels. The final luminance signal was normalized to the protein amount from the parallele well.

TABLE 2.11: **Preparation of Lactate Detection Reagent)**

Component	Per reaction
Luciferin Detection Solution	50 μL
Reductase	0.25 μL
Reductase Substrate	0.25 μL
Lactate Dehydrogenase	0.25 μL
NAD	0.25 μL

2.11 β-galactosidase staining assay

2.11.1 β-galactosidase staining

For β-galactosidase staining, cells were cultured in 35 mm wells of a 6-well plate. All volumes described below are for a 35 mm well. Prior to staining, cells were washed with 2 mL of cold 1× PBS to remove residual growth media. 1 mL of freshly prepared 1X Fixative Solution (diluted from a 10× stock) was added to each well, and cells were incubated at room temperature for 10–15 minutes to fix. Following fixation, cells were rinsed twice with 2 mL of cold 1× PBS. At this point, plates could be stored in PBS at 4°C overnight, if necessary.

For staining, a β-galactosidase Staining Solution was prepared by combining 930 μL of 1× Staining Solution, 10 μL of 100× Solution A, 10 μL of 100× Solution B, and 50 μL of 20 mg/ml X-gal stock solution. The final pH of the staining solution was adjusted to 6.0 (acceptable range: 5.9–6.1) using HCl or NaOH if necessary. The staining solution was applied to each well (1 mL per well), and the plate was sealed with parafilm to prevent evaporation. The plates were incubated at 37°C in a dry incubator (without CO_2) overnight (around 14 hours).

The next day, the development of blue staining indicative of β-galactosidase activity was monitored using a microscope at 200X magnification. After staining, the β-galactosidase staining solution was removed, and the cells were overlaid with 70% glycerol for long-term storage at 4°C.

2.11.2 Quantification of β-galactosidase staining positive cells

For the quantification of β-galactosidase staining, each experimental group was performed in triplicate. In each well, 6 representative images were captured using a EVOS XL core microscope. Each image contained at least 100 cells. The number of positively

stained cells (blue cells) was manually counted in each image in FIJI, and the ratio of positive cells to the total number of cells was calculated for each image.

The ratio of β-galactosidase positive cells was determined by the following equation:

$$\text{Ratio of Positive Cells} = \frac{\text{Number of Positive Cells}}{\text{Total Number of Cells}} \times 100$$

The ratios were averaged across the 6 images for each well, and the mean ratio of positive cells was reported for each group of triplicates. This provided an accurate measurement of the percentage of cells expressing β-galactosidase activity in each experimental condition.

2.12 Statistical analysis

Experiments were validated with at least two independent repeats. Data are presented as mean ± SD (standard deviation). Statistical analyses were only performed when at least three independent biological repeats were available. For comparisons between two independent groups, a Student's t-test was applied for parametric data, and for multiple group comparisons, one-way ANOVA followed by Tukey's multiple comparisons test was used. Statistical significance was defined as $P < 0.05$, with * indicating $P < 0.05$, ** indicating $P < 0.01$, and *** indicating $P < 0.001$. In cases where only two repeats were performed, results are shown descriptively without statistical testing, as indicated in the corresponding figure legends. Unless otherwise stated, all data analysis and graph generation were performed using GraphPad Prism (version 9.0–10.0, GraphPad Software Inc).

Chapter 3

Comprehensive global transcriptomic analysis in FIH-depleted human lung fibroblasts

3.1 Introduction and rationales

IPF is a chronic, progressive fibrotic lung disease marked by excessive extracellular matrix deposition, leading to impaired lung function and poor prognosis (Martinez et al., 2017). Its incidence and prevalence vary globally, increasing with age, and is more commonly diagnosed in men than women. Smoking history is a significant risk factor. The global incidence of IPF ranges from 1 to 24 per 100,000 individuals, with prevalence estimates spanning from 3 to 111 per 100,000. The highest rates are reported in South Korea, Canada, and the United States (Raghu et al., 2006; Behr et al., 2015).

IPF progression is associated with high morbidity and mortality, with a median survival of 3 to 5 years post-diagnosis. The increasing incidence presents a substantial health burden, partly due to better diagnostic practices and an aging population. Despite advancements in early diagnosis and treatment, current pharmacotherapies such as nintedanib (Wollin et al., 2014) and pirfenidone (Noble et al., 2011; Raghu et al., 2011; Chung et al., 2020) can only slow disease progression and are not curative, emphasizing the need for more effective management strategies.

Recent studies suggest that loss of FIH activity in IPF fibroblasts promotes collagen post-translational modification and increases tissue stiffness through upregulation of PLOD2 and LOXL2, indicating that FIH may play a significant role in IPF progression (Brereton et al., 2022).

FIH is a critical regulator of HIF-1α, modulating its transcriptional activity through hydroxylation (Lando et al., 2002). Beyond HIF-1α, FIH targets various other substrates, particularly ARD proteins involved in pathways such as NFκB and Notch (Janke et al., 2013; Cockman et al., 2006; Devries et al., 2010; Cai et al., 2024; Wilkins et al., 2009). These hydroxylation activities impact numerous biological processes, including gene expression, cell signaling, metabolism, and cell polarity.

The FIH protein structure contains a DSBH core that binds Fe(II) and 2OG, essential for catalytic function (McDonough et al., 2005; Hewitson et al., 2007). FIH forms a homodimer stabilized by C-terminal α-helices, and its activity can be inhibited by hypoxia and ROS. Specific residues in FIH are responsible for binding iron, 2OG, and substrates, thereby influencing catalytic efficiency and specificity (Elkins et al., 2003; Lancaster et al., 2004; Mansfield et al., 2005).

FIH has been implicated in various diseases through its regulation of HIF and non-HIF pathways. In cancer (e.g., colon, breast, renal cell carcinoma), FIH activity influences tumor growth, cell proliferation, apoptosis, and hypoxia pathway regulation (Table.1.3).

Bulk RNA sequencing is a preferred method for transcriptomic analysis of pooled cell populations, tissue sections, or biopsies. Following raw data interpretation and normalization, analyses such as GSVA (Hänzelmann et al., 2013) and GO analysis (Consortium, 2019) provide insights into transcriptomic alterations after treatment.

Currently, there is limited data on the transcriptomic profile of FIH-depleted lung fibroblasts. Given FIH's broad range of substrates and multifaceted regulatory roles in both health and disease, further investigation is needed to understand its function and therapeutic potential. This chapter analyses bulk RNA sequencing data from human lung fibroblasts with FIH loss induced by either CRISPR-Cas9 or siRNA.

3.2 Aim and objectives

3.2.1 Aim

The aim of this study is to investigate the role of FIH in the regulation of cellular processes related to pulmonary fibrosis, by performing a comprehensive transcriptomic analysis on FIH-depleted human lung fibroblasts (MRC5 cells) and mouse embryonic fibroblasts (MEFs). Through the comparison of FIH KO via CRISPR-Cas9 and KD via siRNA, this study seeks to uncover the impact of FIH loss on gene expression profiles and the associated biological pathways involved in fibrosis progression.

3.2.2 Objectives

1. **characterise transcriptional changes in FIH-Depleted MRC5 Cells:**
    - Perform bulk RNA sequencing on FIH KO and siFIH KD MRC5 cells to identify DEGs and characterise transcriptional changes through PCA, heatmaps, and volcano plots.
2. **Identify Enriched Biological Processes Affected by FIH Depletion:**
    - Use GO analysis, hallmark pathway enrichment, and GSVA to determine enriched biological processes affected by FIH loss in fibroblasts.
3. **Compare the Effects of FIH KO vs. KD in MRC5 Cells:**
    - Assess the differences between FIH KO via CRISPR-Cas9 and FIH KD via siRNA to determine the specific impact of each method on the transcriptional landscape and the associated biological processes in human lung fibroblasts.
4. **Examine the Cross-Species Transcriptomic Changes in FIH-Depleted Cells:**
    - Conduct comparative GO analysis between FIH KO MRC5 cells and FIH KO MEFs to explore how FIH depletion differentially affects human lung fibroblasts and mouse fibroblasts, highlighting any conserved or species-specific pathways involved in cellular function and fibrosis.

By achieving these objectives, this study aims to provide a deeper understanding of the molecular mechanisms through which FIH influences fibrosis, potentially offering new perspectives on therapeutic interventions for fibrotic diseases.

3.3 Results

3.3.1 Global transcriptomic changes in FIH knocked-out MRC5 cells

We utilized CRISPR-Cas9 to knock out (KO) *HIF1AN* (FIH) in MRC5 cells.

After confirming the knockout efficiency, we selected the second strain of the cell line, along with control cells, for further experimentation. RNA samples from both FIH wildtype and FIH KO MRC5 cells were subjected to bulk RNA sequencing. Principal component analysis (PCA), a dimensionality reduction method, was applied to the RNA sequencing data to visualize the overall data structure and identify patterns of variation among the samples. This analysis revealed that lung fibroblast samples clustered into two distinct groups (Figure.3.1 A). Following normalization of the raw expression data, we identified 4,749 differentially expressed genes (DEGs) with significant differential expression (Adjusted P-value < 0.05), including 2,300 upregulated and 2,449 downregulated genes, as depicted in the volcano plot (Figure.3.1 B).

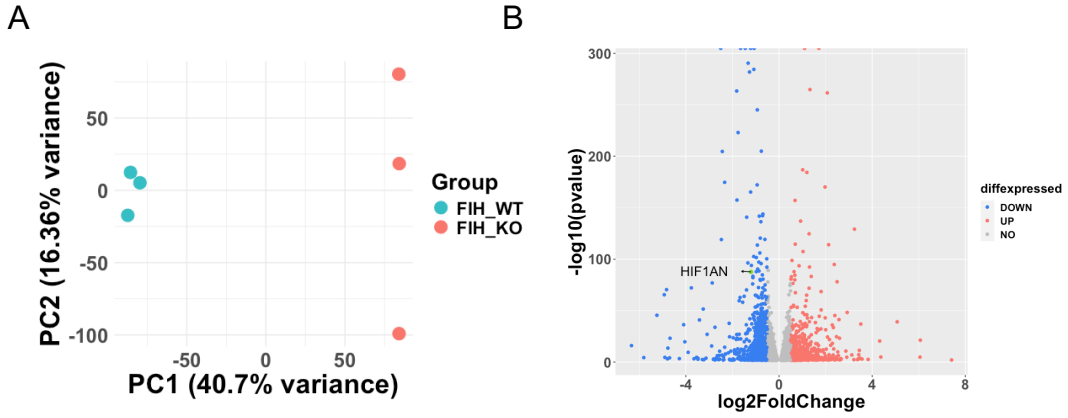

FIGURE 3.1: **Gene expression changes in FIH KO MRC5 cells**
(A) PCA plot of gene expression data obtained via RNA-seq data for three biological replicates corresponding to the samples from FIH WT and KO MRC5 cells. (B) Volcano plot showing up and down-regulated DEGs in FIH KO MRC5 cells. Red dots represent up-regulated DEGs (Log2Foldchange > 0.5) , blue dots represent down-regulated DEGs (Log2Foldchange $<$ -0.5) and grey dots represent no significant changed DEGs.

To further investigate the impact of FIH depletion in MRC5 cells, we utilized Metascape (Zhou et al., 2019) to perform GO term enrichment analysis on the upregulated and downregulated DEGs. The analysis was conducted using a threshold of adjusted P value < 0.05 and $|\text{Log2Foldchange}| > 0.5$. For the upregulated DEGs, the analysis identified 1,163 GO terms with a Log P value $<$ -2, which were categorized into Biological Process (823 items), Cellular Component (200 items), and Molecular Function

(140 items). The top 10 enriched GO terms in each category are presented in a bubble plot (Figure. 3.2 A). The enriched GO terms suggest that FIH depletion primarily upregulates the synthesis and transportation of intracellular proteins within the Biological Process category, with most of these proteins localized to organelle membranes as indicated by the Cellular Component category, and involved in protein kinase binding or activity according to the Molecular Function category. Additionally, a Treemap analysis of the top 50 Biological Process GO terms indicates that they are predominantly associated with metabolic processes and cellular localization (Figure. 3.3 A). These findings suggest that FIH depletion plays a significant role in the upregulation of protein degradation, localization, and activity within the cell, processes largely associated with post-translational modifications.

For the downregulated DEGs, the analysis identified 2,094 GO terms, categorized into Biological Process (1,612 items), Cellular Component (233 items), and Molecular Function (249 items). The top 10 enriched GO terms in each category are presented in a bubble plot (Figure. 3.2 B). The results indicate that FIH depletion predominantly downregulates biological processes involved in cell division and proliferation. According to the Cellular Component GO terms, most of the affected DEGs are localized to the cell chromosome, while the Molecular Function category highlights chromatin/transcription factor binding and ATP-dependent catalytic activity. The Treemap analysis of the top 50 Biological Process GO terms for downregulated DEGs primarily focuses on cellular processes and metabolic processes (Figure. 3.3 B). These results suggest that FIH depletion can significantly downregulate biological processes related to cell proliferation.

GSVA is an unsupervised Gene Set Enrichment (GSE) method that assesses variations in pathway activity across a sample population (Hänzelmann et al., 2013). The Hallmark collection, comprising fifty gene sets, succinctly represents distinct biological states or processes with coherent expression profiles (Liberzon et al., 2015). This collection was chosen to further analyse our RNA-seq data. We calculated the average GSVA scores for each group and presented the results in a heatmap (Figure.3.4). The heatmap demonstrates that in FIH KO MRC5 cells, gene sets linked to proliferation—such as *E2F Targets* (P = 1.02 $\times 10^{-6}$, Difference (FIH KO - FIH WT) = -0.998) , *G2M Checkpoint* (P = 1.34 $\times 10^{-5}$, Difference = -0.924) *MYC Targets V1* (P = 2.76 $\times 10^{-2}$, Difference = -0.516), *MYC Targets V2* (P = 4.73 $\times 10^{-3}$, Difference = -0.695), and *Mitotic Spindle* (P = 4.18 $\times 10^{-3}$, Difference = -0.462) (Liberzon et al., 2015)—were markedly downregulated. These findings align with the GO term enrichment analysis of downregulated DEGs. Additionally, the downregulation of *TGF-β Signaling* (P = 2.36 $\times 10^{-2}$, Difference = -0.427) and *Epithelial-Mesenchymal Transition* (P = 1.01 $\times 10^{-3}$, Difference = -0.327), both critical in lung fibrosis, was observed. Conversely, gene sets associated with metabolic processes were upregulated after FIH depletion, corroborating the results from our GO term enrichment analysis.

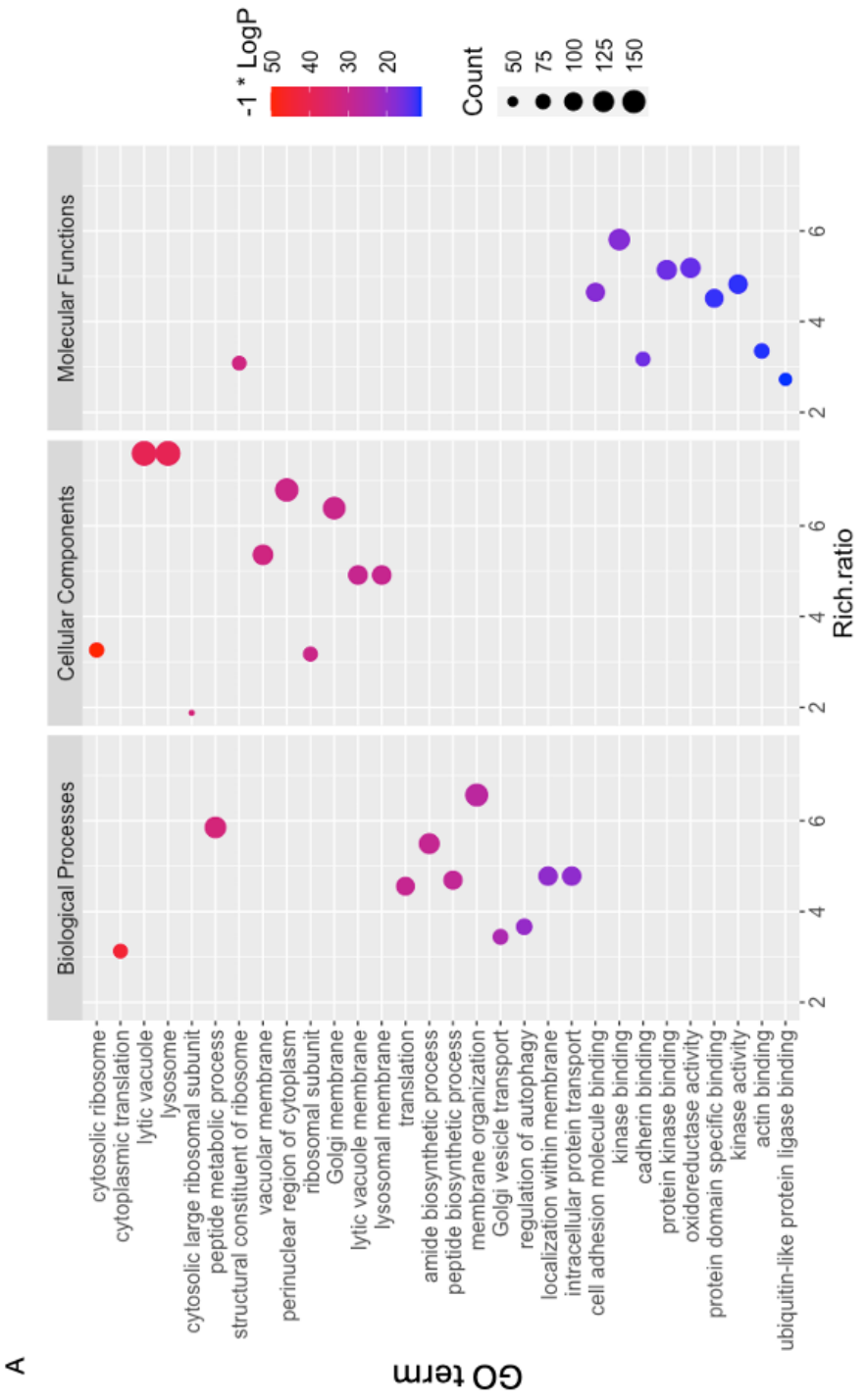
A
GO term
Biological Processes
Cellular Components
Molecular Functions
cytosolic ribosome
cytoplasmic translation
lytic vacuole
lysosome
cytosolic large ribosomal subunit
peptide metabolic process
structural constituent of ribosome
vacuolar membrane
perinuclear region of cytoplasm
ribosomal subunit
Golgi membrane
lytic vacuole membrane
lysosomal membrane
translation
amide biosynthetic process
peptide biosynthetic process
membrane organization
Golgi vesicle transport
regulation of autophagy
localization within membrane
intracellular protein transport
cell adhesion molecule binding
kinase binding
cadherin binding
protein kinase binding
oxidoreductase activity
protein domain specific binding
kinase activity
actin binding
ubiquitin-like protein ligase binding
2
4
6
Rich.ratio
-1 * LogP
50
40
30
20
Count
50
75
100
125
150

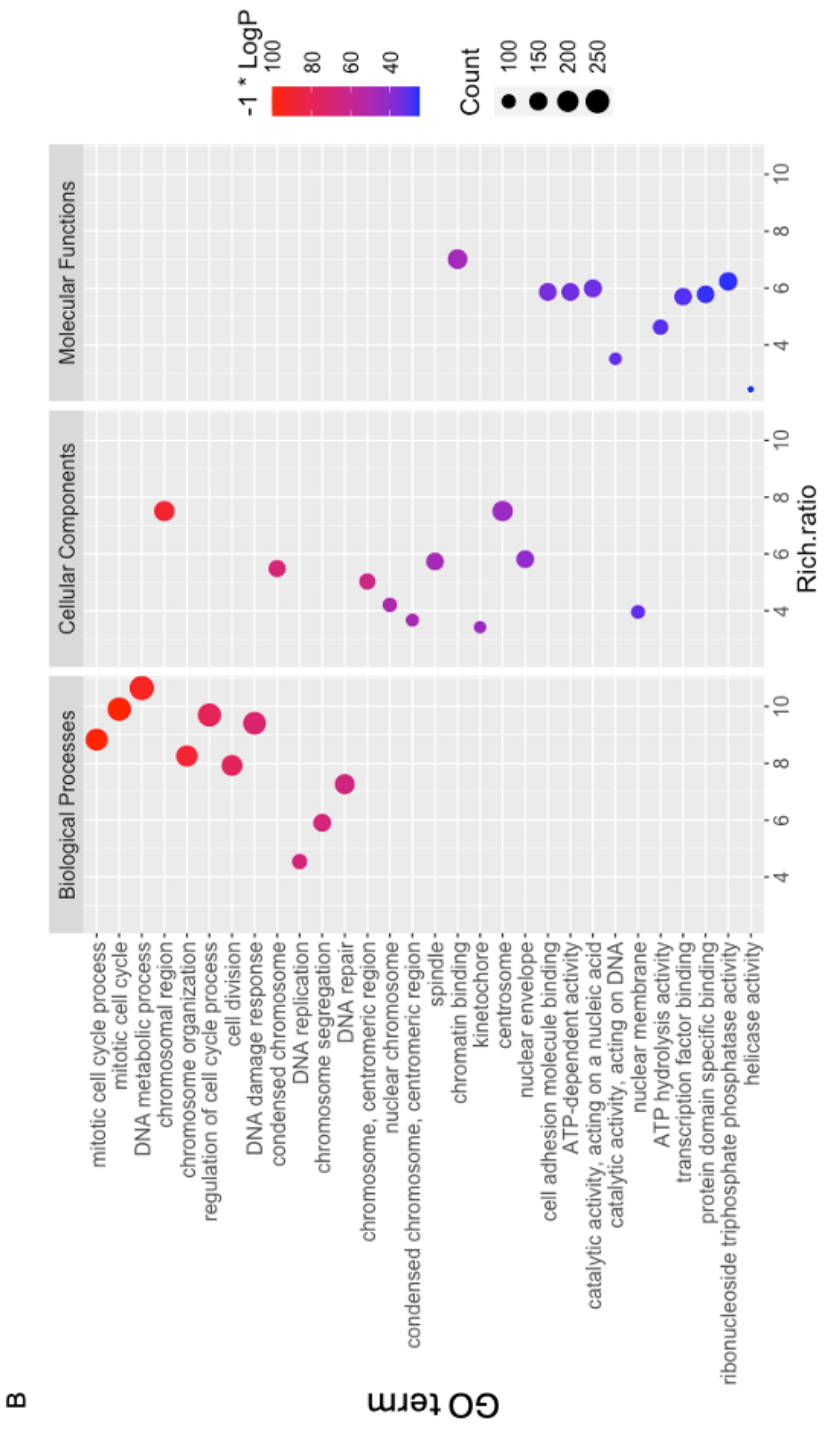

FIGURE 3.2: **GO enrichment analysis of DEGs in FIH KO MRC5 cells**
Scatter plot showing enriched Gene Ontology (GO) terms from three categories (BP, biological process; CC, cellular component; and MF, molecular function) of upregulated DEGs (A) and downregulated DEGs (B) in FIH KO MRC5 cells. DEGs are the genes with adjust p value < 0.05 and $|\text{Log2Foldchange}| > 0.5$. The sizes of circles represent gene counts, and the colours of circles represent the -Log10 of the P-value. GO enrichment analysis was conducted in Metascape(https://metascape.org/).

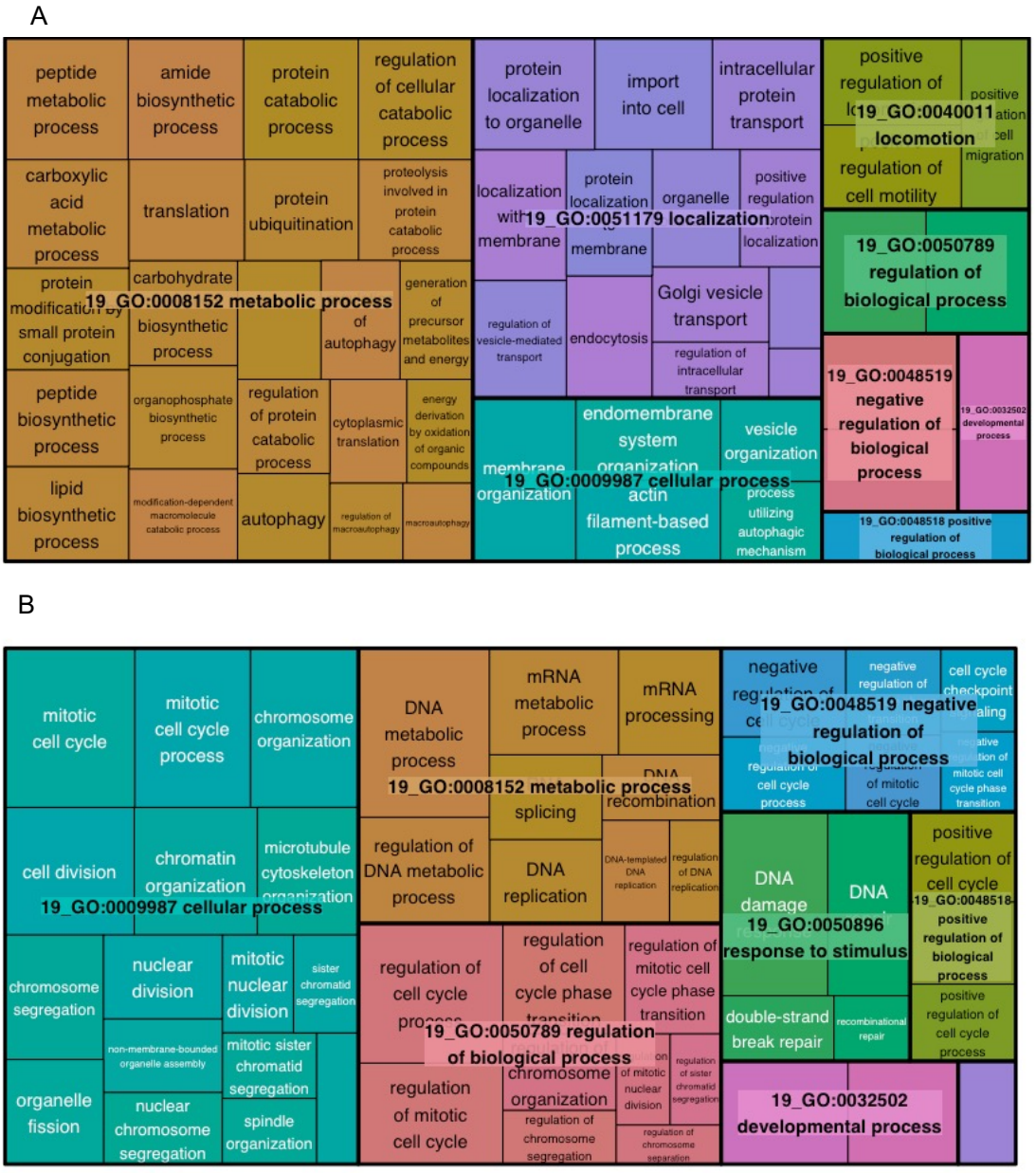

FIGURE 3.3: **Treemap of top 50 biological process GO terms for DEGs in FIH knock-out MRC5 cells**

The treemap shows the Top50 Biological Process GO)terms enriched in upregulated DEGs (A) and downregulated DEGs (B) in FIH-depleted MRC5 cells. Each rectangle corresponds to a specific GO term and is nested under its parent GO term. The size of the rectangles is determined by the number of genes (Rich.ratio) associated with each GO term, while the color represents the LogP, with darker colors indicating greater statistical significance.

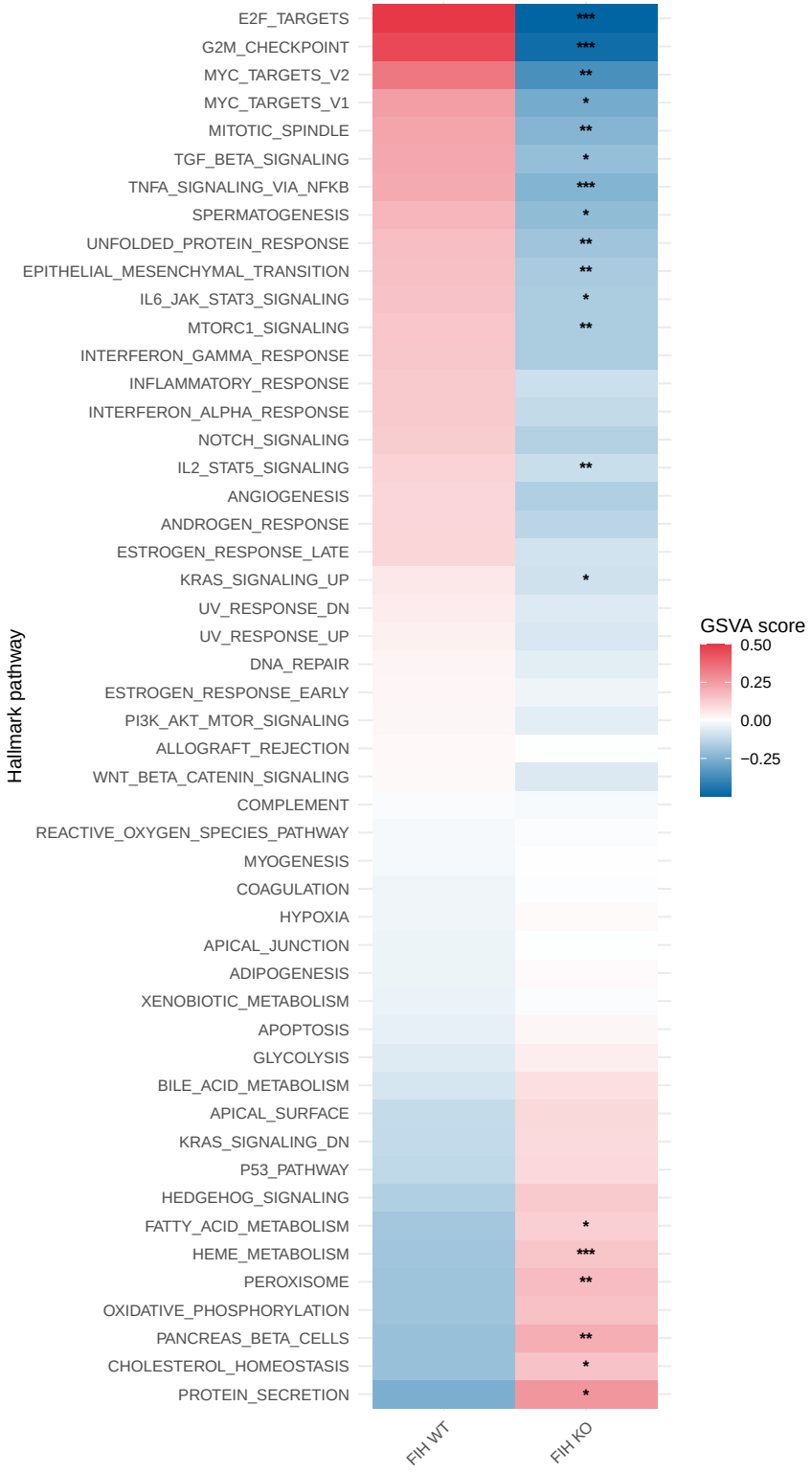

FIGURE 3.4: **Hallmark pathway GSVA score in WT and FIH KO MRC5 cells**
Heatmap showing the average hallmark GSVA score in WT and FIH KO MRC5 cells. GSVA, gene set variation analysis. * $P < 0.05$, ** $P < 0.01$, *** $P < 0.001$ by Student's t-test.

3.3.2 Global transcriptomic changes in siRNA-mediated FIH knocked-down (siFIH) MRC5 cells

To further confirm our observations in FIH KO MRC5 cells, we transfected MRC5 cells with siRNA targeting *HIF1AN* for 48 hours, followed by RNA extraction and sequencing (Sample preparation courtesy of Dr. Liudi Yao). PCA plot revealed that the lung fibroblast samples segregated into two distinct clusters (Figure. 3.5 A). Upon normalizing the raw expression data, we identified 7,452 DEGs exhibiting significant differential expression (adjusted P value < 0.05), with 3,707 genes upregulated and 3,745 genes downregulated, as depicted in the volcano plot (Figure. 3.5 B).

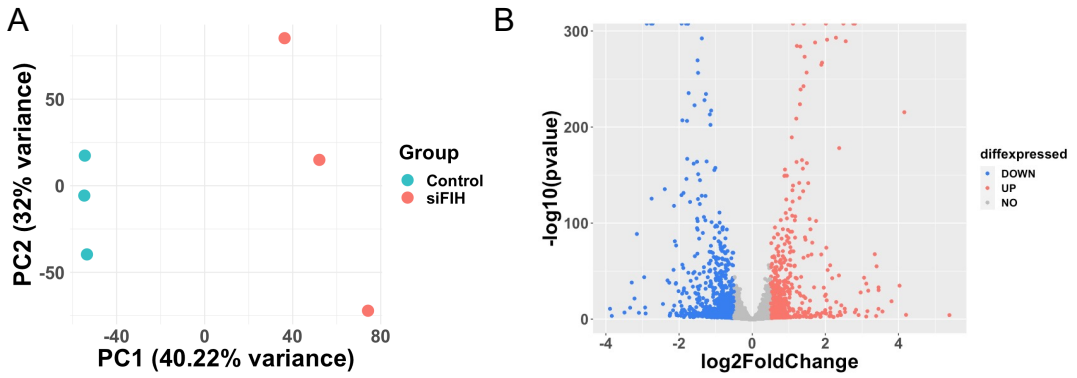

FIGURE 3.5: **Gene expression changes in siFIH MRC5 cells**
(A) PCA plot of gene expression data obtained via RNA-seq data for three biological replicates corresponding to the samples from control and siFIH MRC5 cells. (B) Volcano plot showing up and down-regulated DEGs in siFIH MRC5 cells. Red dots represent up-regulated DEGs (Log2Foldchange > 0.5), blue dots represent down-regulated DEGs (Log2Foldchange $<$ -0.5) and grey dots represent no significant changed DEGs.

As in the previous analysis, we employed Metascape to conduct GO term enrichment analysis for both upregulated and downregulated DEGs. For the upregulated DEGs, 759 GO terms were identified. These terms were categorized into Biological Process (640 items), Cellular Component (37 items), and Molecular Function (82 items). The top 10 enriched GO terms in each category are presented in a bubble plot (Figure. 3.6 A) and detailed in the accompanying table. The enrichment analysis revealed that FIH knockdown predominantly induced responses to oxygen levels and cell locomotion within the Biological Process category, with most genes localized to cell-cell junctions in the Cellular Component category and involved in signaling receptor binding or activity in the Molecular Function category. The Treemap analysis further demonstrated that the parental GO terms of the top 50 Biological Process GO terms were associated with responses to stimuli and locomotion (Figure. 3.7 A). These findings suggest that FIH knockdown induces cellular responses to oxygen levels, likely due to FIH's role as an enzyme that inhibits HIF activity, and promotes cellular locomotion.

For the downregulated DEGs, 783 GO terms were identified, categorized into Biological Process (597 items), Cellular Component (108 items), and Molecular Function (78 items). The top 10 enriched GO terms in each category are depicted in a bubble plot (Figure. 3.6 B) and detailed in the table. The analysis indicated that FIH depletion primarily downregulates biological processes related to the cell cycle and metabolism, with most DEGs localized to the extracellular matrix according to Cellular Component GO terms and associated with protein kinase activity in the Molecular Function category. The Treemap analysis of the top 50 Biological Process GO terms for downregulated DEGs highlighted a focus on metabolic processes, regulation of biological processes, and localization (Figure. 3.7 B). These results suggest that FIH knockdown mitigates cell cycle progression and cellular metabolism.

The Hallmark GSVA score indicates that in siFIH MRC5 cells, several gene sets associated with proliferation were significantly decreased, including *E2F Targets* (P = 1.65 $\times 10^{-2}$, Difference = -0.34) and *G2M Checkpoint* (P = 5.37 $\times 10^{-2}$, Difference = -0.332) (Figure. 3.8). This finding is consistent with the GO term enrichment results for downregulated DEGs. Additionally, some gene sets related to metabolism, such as *Cholesterol Homeostasis* (P = 1.34 $\times 10^{-4}$, Difference = -0.642), *Fatty Acid Metabolism* (P = 0.386 , Difference = 7.78 $\times 10^{-2}$), *Bile Acid Metabolism* (P = 6.64 $\times 10^{-2}$, Difference = -0.214), and *Xenobiotic Metabolism* (P = 0.669, Difference = 2.11 $\times 10^{-2}$), were also decreased, although these changes were not statistically significant. Conversely, gene sets related to signaling pathways, including *Hypoxia* (P = 7.96 $\times 10^{-2}$, Difference = 0.284), *Notch Signaling* (P = 0.107, Difference = 0.245), and *TNFα Signaling via NFκB* (P = 1.18 $\times 10^{-3}$, Difference = 0.532), were increased following FIH knockdown in MRC5 cells.

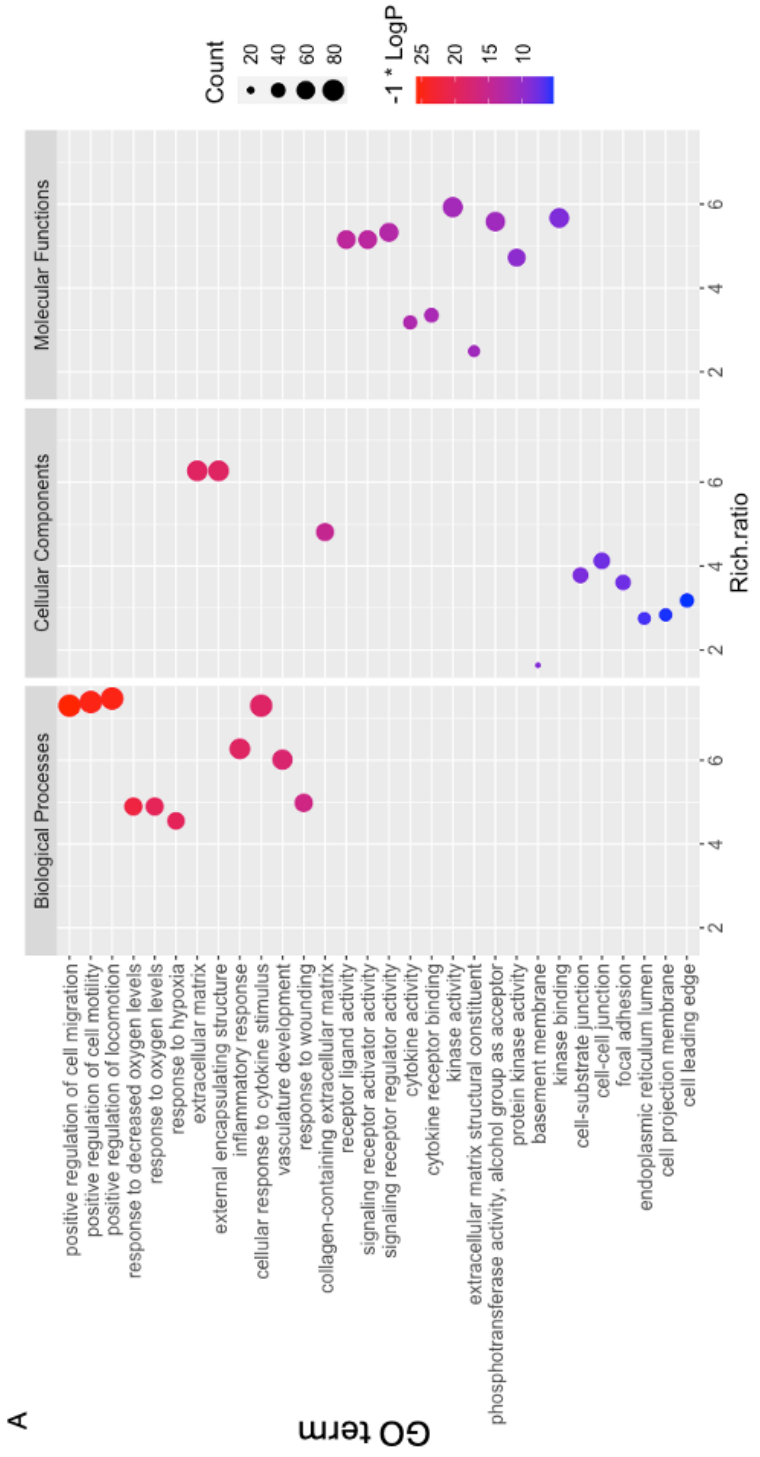
A
GO term
Biological Processes
Cellular Components
Molecular Functions
positive regulation of cell migration
positive regulation of cell motility
positive regulation of locomotion
response to decreased oxygen levels
response to oxygen levels
response to hypoxia
extracellular matrix
external encapsulating structure
inflammatory response
cellular response to cytokine stimulus
vasculature development
response to wounding
collagen-containing extracellular matrix
receptor ligand activity
signaling receptor activator activity
signaling receptor regulator activity
cytokine activity
cytokine receptor binding
kinase activity
extracellular matrix structural constituent
phosphotransferase activity, alcohol group as acceptor
protein kinase activity
basement membrane
kinase binding
cell-substrate junction
cell-cell junction
focal adhesion
endoplasmic reticulum lumen
cell projection membrane
cell leading edge
2
4
6
Rich.ratio
Count
20
40
60
80
-1 * LogP
25
20
15
10

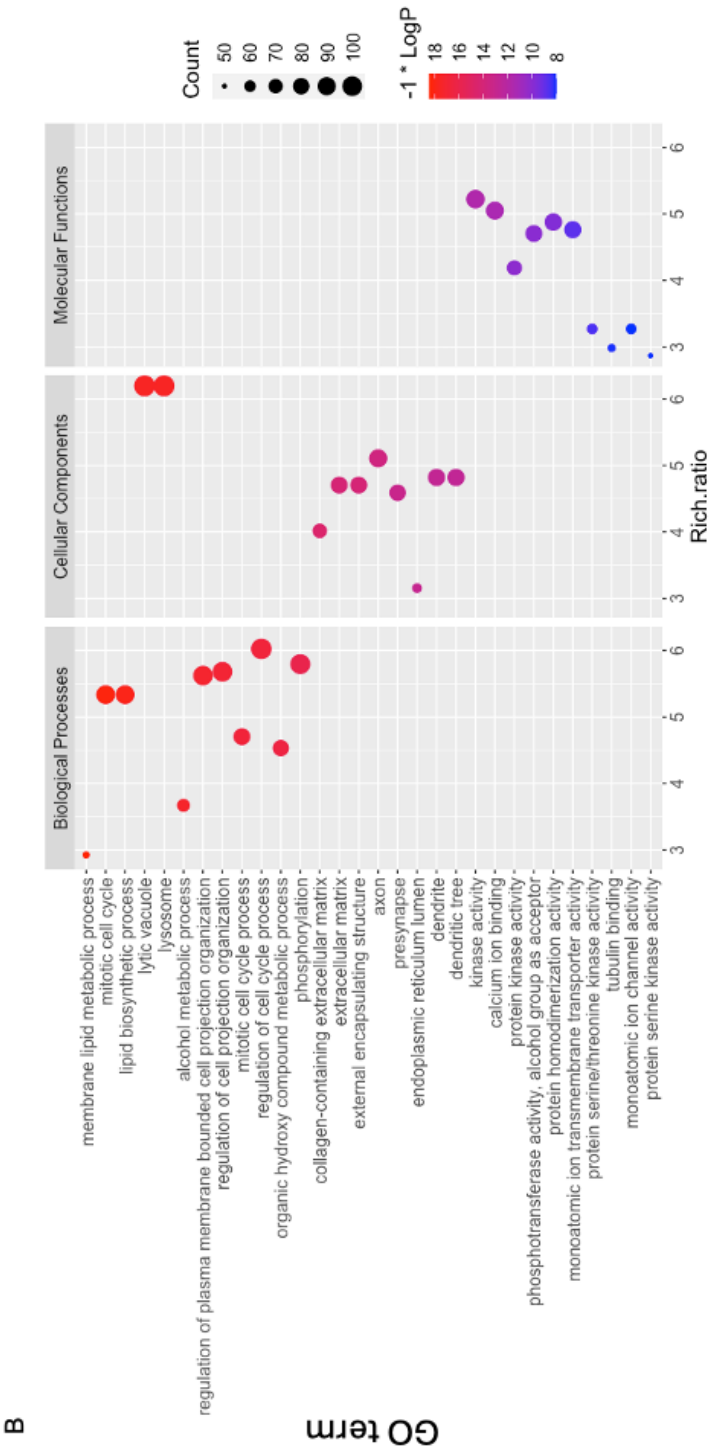

FIGURE 3.6: **GO enrichment analysis of DEGs in siFIH MRC5 cells**
Scatter plot showing enriched GO terms from three categories (BP, biological process; CC, cellular component; and MF, molecular function) of upregulated DEGs (A) and downregulated DEGs (B) in siFIH MRC5 cells. DEGs are the genes with adjust p value < 0.05 and $|\text{Log2Foldchange}| > 0.5$. The sizes of circles represent gene counts, and the colours of circles represent the -Log10 of the P-value. GO enrichment analysis was conducted in Metascape(https://metascape.org/).

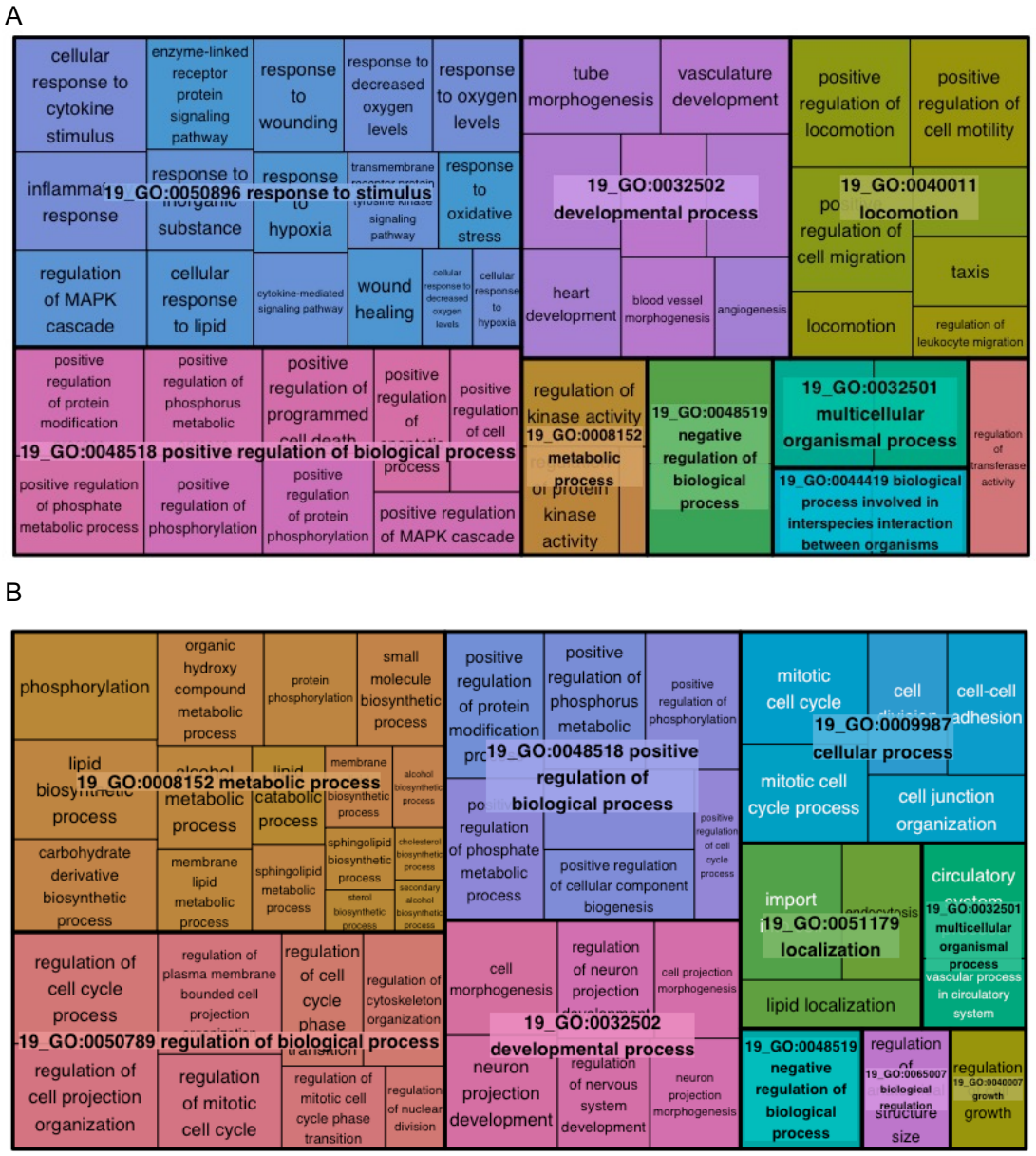

FIGURE 3.7: **Treemap of top 50 biological process GO terms for DEGs in siFIH MRC5 cells**

The treemap shows the Top50 Biological Process GO terms enriched in upregulated DEGs (A) and downregulated DEGs (B) in siFIH MRC5 cells. Each rectangle corresponds to a specific GO term and is nested under its parent GO term. The size of the rectangles is determined by the number of genes (Rich.ratio) associated with each GO term, while the color represents the LogP, with darker colors indicating greater statistical significance.

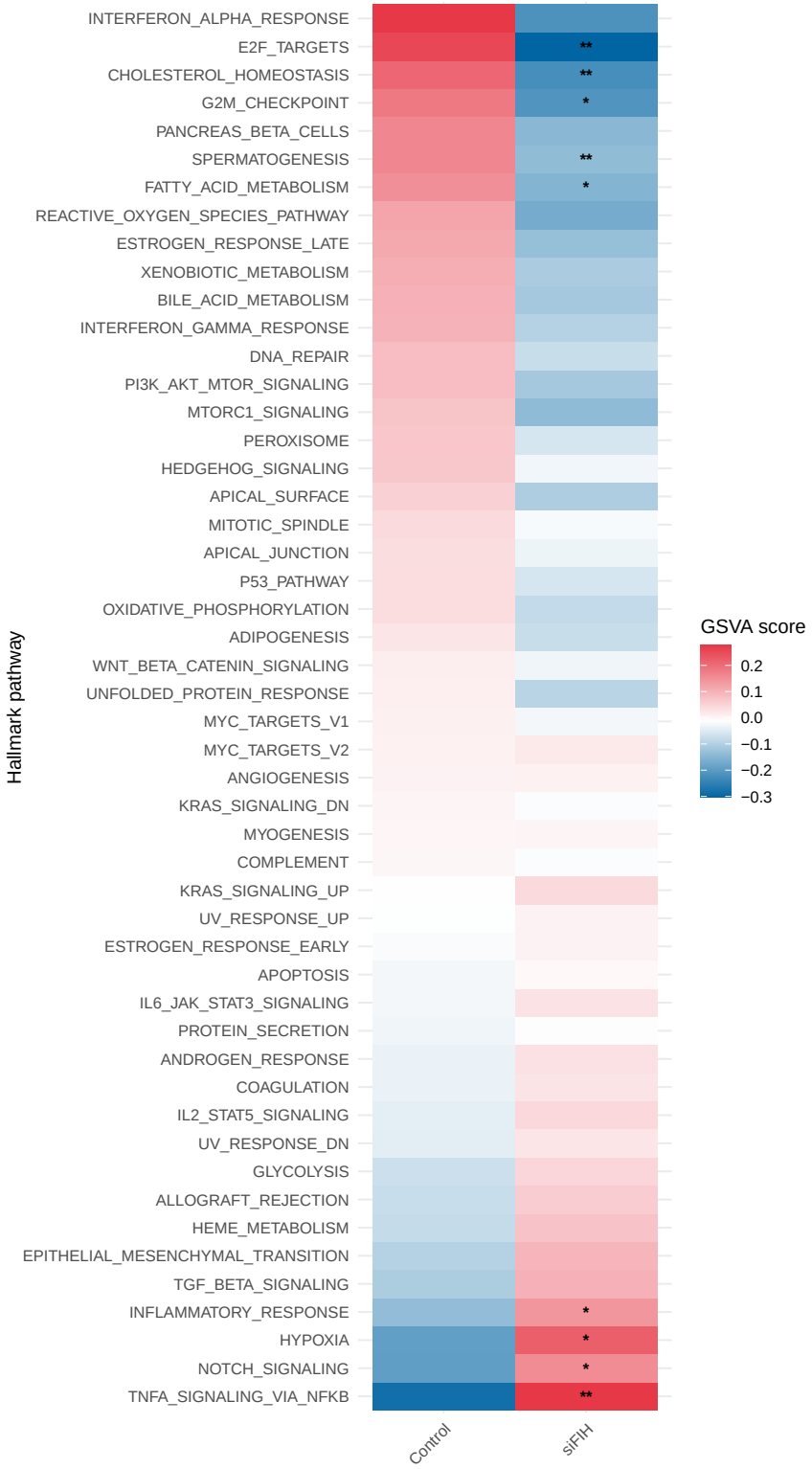

FIGURE 3.8: **Hallmark pathway GSVA score in control and siFIH MRC5 cells**
Heatmap showing the average hallmark GSVA score in control and siFIH MRC5 cells. GSVA, gene set variation analysis. *P $<$ 0.05, $**$ P $<$ 0.01, $***$ P $<$ 0.001 by Student's t-test.

3.3.3 Global transcriptomic changes in siRNA-mediated FIH knocked-down (siFIH) normal human lung fibroblasts (NHLFs)

Although MRC5 cell line is widely used in the lung fibrosis studies, primary human lung fibroblasts may be a more physiologically accurate model of lung fibroblast behaviour. So we transfected siRNA targeting HIF1AN into human normal lung fibroblasts and extracted RNA samples foe bulk RNA sequencing (sample preparation was done by Dr. Liudi Yao). Due to some technical issues, there were only 2 repeats in each group. PCA plot reveals that lung fibroblast samples clustered in 2 different groups (Figure. 3.9 A). After normalizing the raw expression data, we identified 6046 DEGs with a significant differential expression (Adjust P value < 0.05), of which 3084 genes were upregulated and 2962 genes were downregulated as the volcano plot shows (Figure. 3.9 B).

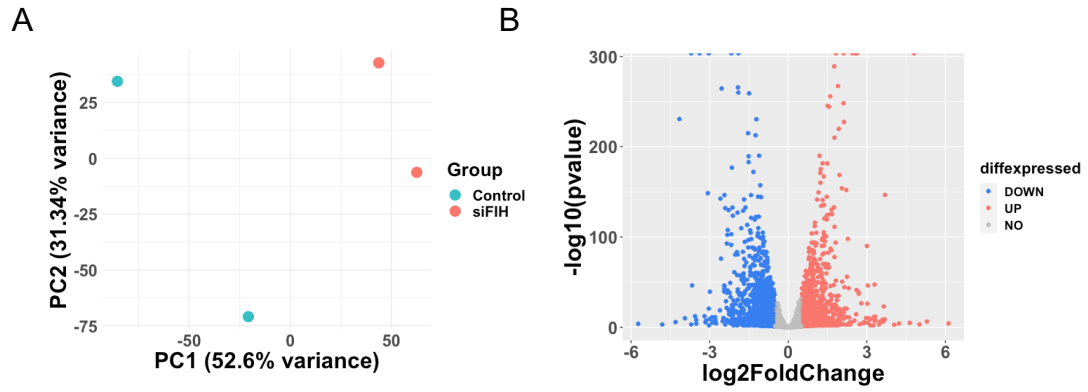

FIGURE 3.9: **Gene expression changes in NHLFs after FIH depletion**
(A) PCA plot of gene expression data obtained via RNA-seq data for biological duplicates corresponding to the samples from control and siFIH NHLFs cells. (B) Volcano plot showing up and down-regulated DEGs in siFIH NHLFs cells. Red dots represent up-regulated DEGs (Log2Foldchange > 0.5), blue dots represent down-regulated DEGs (Log2Foldchange $<$ -0.5) and grey dots represent no significant changed DEGs.

We also used Metascape to perform GO term enrichment analysis for upregulated DEGs and downregulated DEGs with a threshold of an adjusted P value less than 0.05 and $|$Log2Foldchange$| > 0.5$. From upregulated DEGs, the results retrieved 723 GO terms. The GO terms were further grouped into Biological Process (589 items), Cellular Component (53 items) and Molecular Function (81 items). Top 10 enriched GO terms of each category were displayed in the bubble plot (Figure. 3.10 A) and the table. Similar with the GO term enrichment result in MRC5 cells with knocked-down FIH, the enriched result shows that knocking down of FIH mainly induced the response to oxygen levels and cell locomotion in Biological Process, most of them located on cell-cell junction and cell membrane in Cellular Component, signaling receptor/ protein kinase binding or activity in Molecular Function. Also, the Treemap clearly showed that the

parental GO terms of top50 Biological Process GO terms were related to the response to stimulus and regulation of biological process (Figure. 3.11 A). These results indicate knockdown of FIH can induce cellular response to oxygen level and cellular locomotion in human primary lung fibroblasts.

From downregulated DEGs, the results retrieved 873 GO terms. The GO terms were further grouped into Biological Process (688 items), Cellular Component (102 items) and Molecular Function (83 items). Top 10 enriched GO terms of each category were displayed in the bubble plot (Figure. 3.10 B) and the table. The results showed that FIH depletion can mainly downregulate the biological process involved in extracellular matrix regulation and cell cycle, most of the DEGs are located at the cellular organelle membrane according to the Cellular Component GO terms, protein kinase binding/activity in Molecular Function. The Treemap demonstrate Top 50 BP GO terms for downregulated DEGs mainly focus on metabolic process and regulation of biological process (Figure. 3.11 B). These results indicate knockingdown of FIH in primary human lung fibroblasts can mitigate cell cycle, cellular metabolism and extracellular matrix organisation.

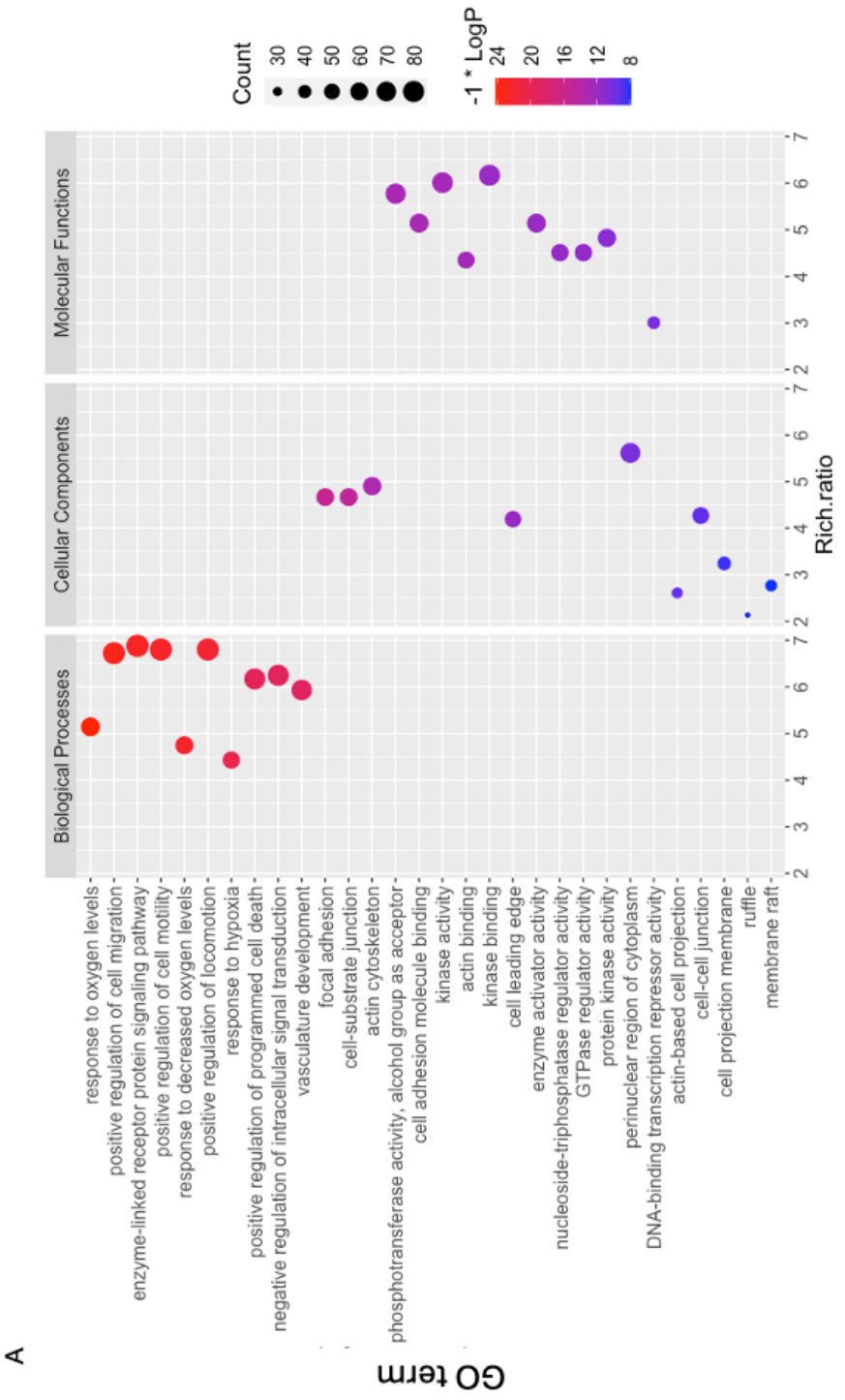
A
Count
30
40
50
60
70
80
-1 * LogP
24
20
16
12
8
Biological Processes
Cellular Components
Molecular Functions
GO term
response to oxygen levels
positive regulation of cell migration
enzyme-linked receptor protein signaling pathway
positive regulation of cell motility
response to decreased oxygen levels
positive regulation of locomotion
response to hypoxia
positive regulation of programmed cell death
negative regulation of intracellular signal transduction
vasculature development
focal adhesion
cell-substrate junction
actin cytoskeleton
phosphotransferase activity, alcohol group as acceptor
cell adhesion molecule binding
kinase activity
actin binding
kinase binding
cell leading edge
enzyme activator activity
nucleoside-triphosphatase regulator activity
GTPase regulator activity
protein kinase activity
perinuclear region of cytoplasm
DNA-binding transcription repressor activity
actin-based cell projection
cell-cell junction
cell projection membrane
ruffle
membrane raft
2
3
4
5
6
7
Rich.ratio

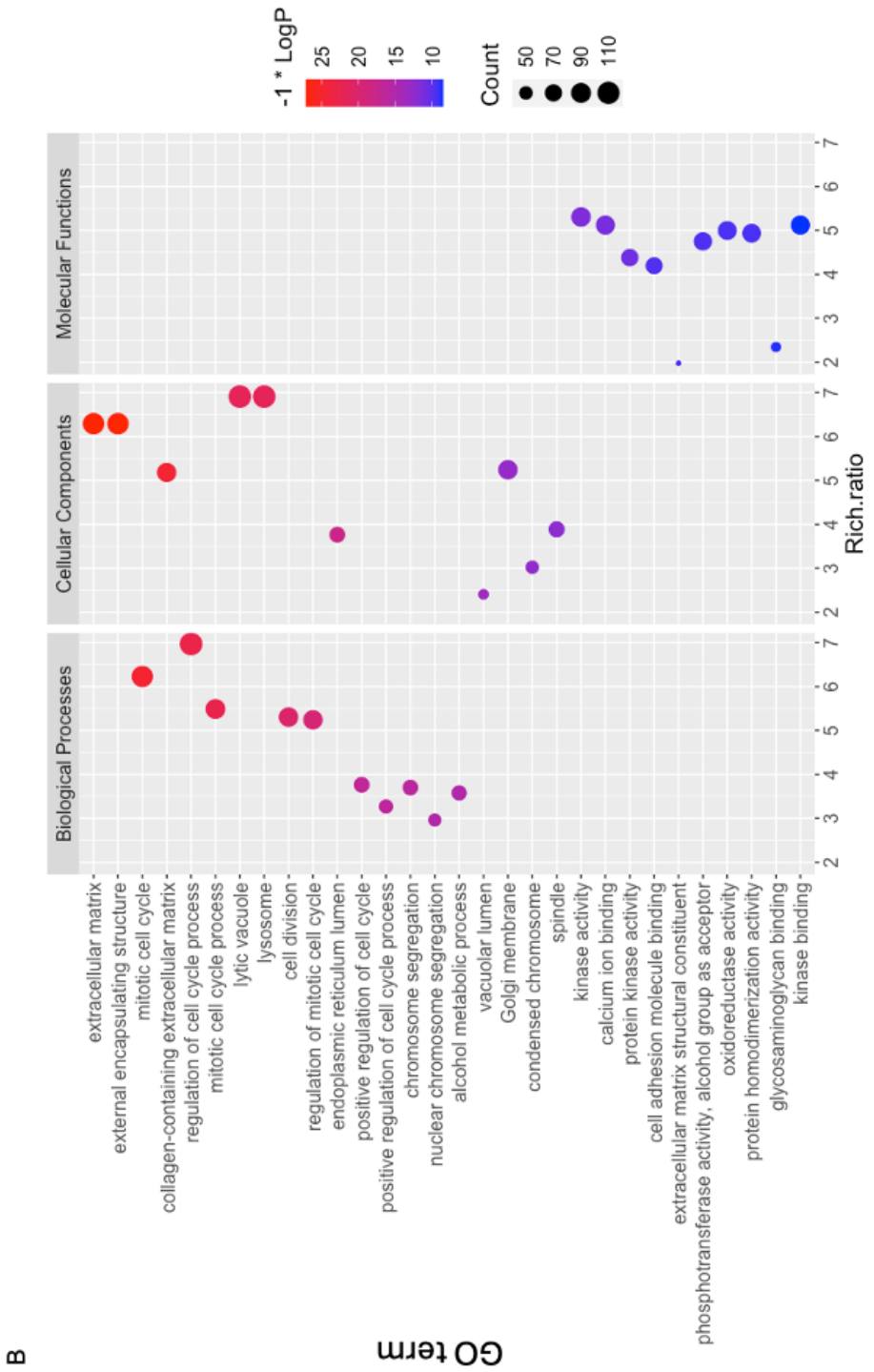

FIGURE 3.10: **GO enrichment analysis of DEGs in siFIH NHLFs**
Scatter plot showing enriched GO terms from three categories (BP, biological process; CC, cellular component; and MF, molecular function) of upregulated DEGs (A) and downregulated DEGs (B) in siFIH NHLFs. DEGs are the genes with adjust p value < 0.05 and $|\text{Log2Foldchange}| > 0.5$. The sizes of circles represent gene counts, and the colours of circles represent the -Log10 of the P-value. GO enrichment analysis was conducted in Metascape(https://metascape.org/).

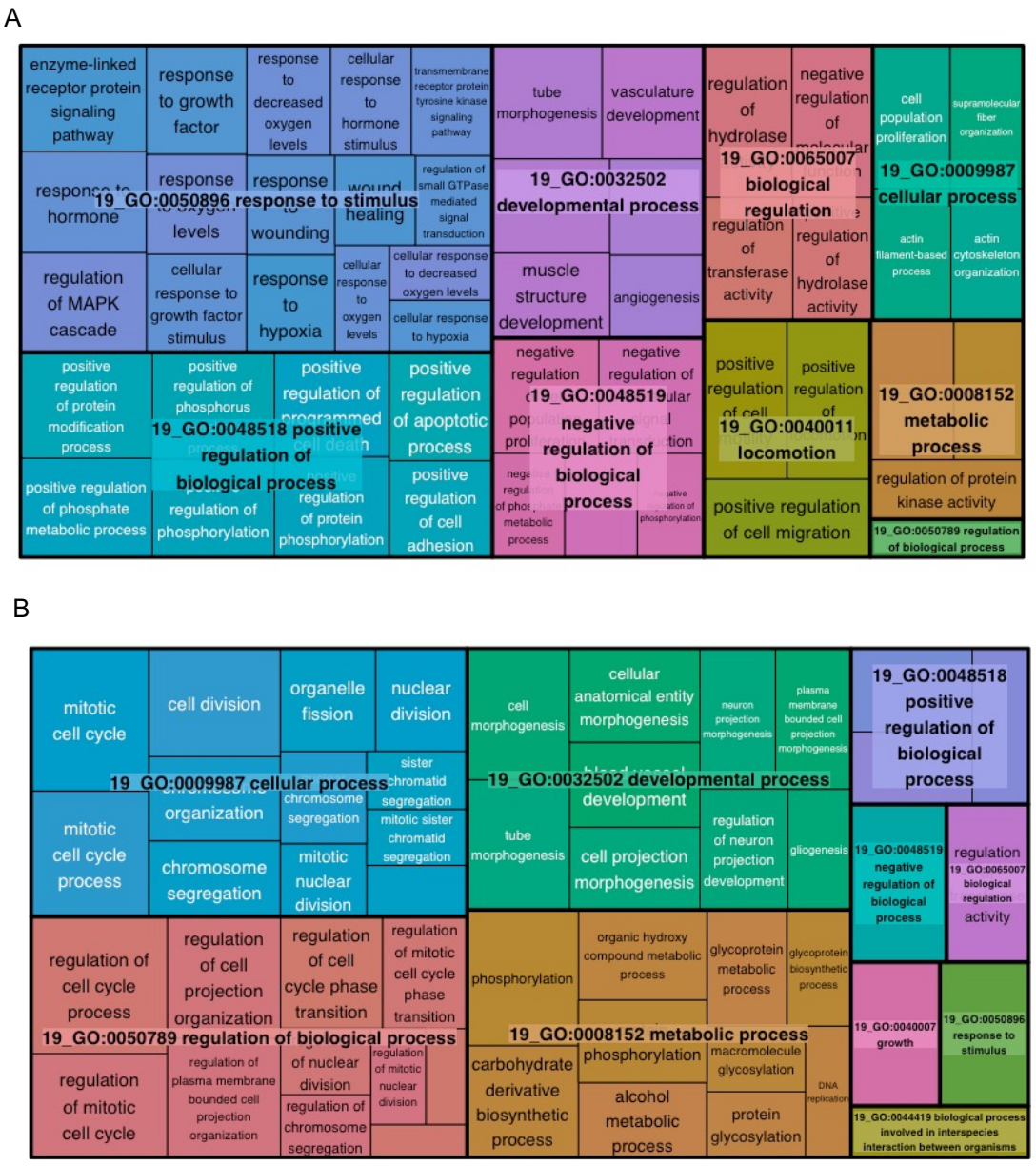

FIGURE 3.11: **Treemap of top 50 biological process GO terms for DEGs in siFIH NHLFs**

The treemap shows the Top50 Biological Process GO terms enriched in upregulated DEGs (A) and downregulated DEGs (B) in siFIH NHLFs. Each rectangle corresponds to a specific GO term and is nested under its parent GO term. The size of the rectangles is determined by the number of genes (Rich.ratio) associated with each GO term, while the color represents the LogP, with darker colors indicating greater statistical significance.

After analysing RNA sequencing data from MRC5 cells and NHLFs, we observed that the results from these two cell lines were remarkably similar. To further explore this similarity, we performed a Venn diagram analysis using Biological Process (BP) GO terms enriched in upregulated DEGs from both datasets (Figure. 3.12A). The Venn plot revealed 367 common BP GO terms between siFIH MRC5 cells and siFIH NHLFs. The top 10 ranked GO terms were primarily associated with cell migration/locomotion and response to stimuli, as illustrated in the bubble plot (Figure. 3.12B). Additionally, in the BP GO terms enriched in downregulated DEGs, we identified 420 common BP GO terms, with the top 10 ranked GO terms related to the regulation of the cell cycle.

These findings suggest that FIH knockdown regulates cell migration and response to hypoxia while simultaneously mitigating cell cycle regulation in both MRC5 cells and NHLFs. For a comprehensive comparison, we will proceed with further analysis using data from MRC5 cells and use data from NHLFs for confirmation purposes.

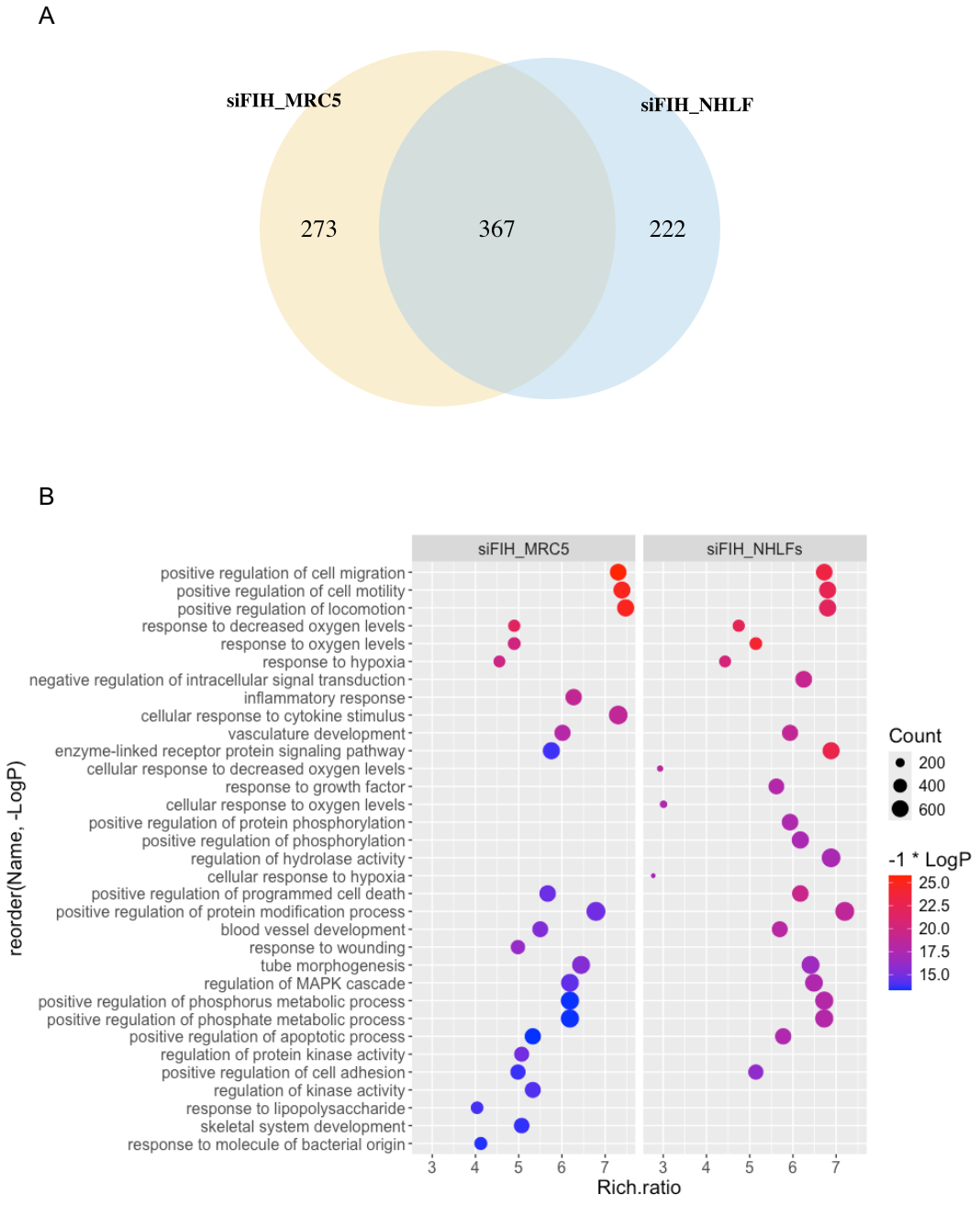

FIGURE 3.12: **Common enriched biological process GO terms in upregulated DEGs of siFIH MRC5 cells and NHLFs**

(A) Venn diagram showing 367 common BP GO terms enriched in upregulated DEGs in the two datasets; (B) Bubble plot depicting the top 25 BP GO terms from the common GO terms in the two datasets. GO BP terms are ranked according to their -Log10 P-value. The sizes of the circles represent gene counts, while the colors of the circles indicate the -Log10 P-value. GO enrichment analysis was performed using Metascape (https://metascape.org/).

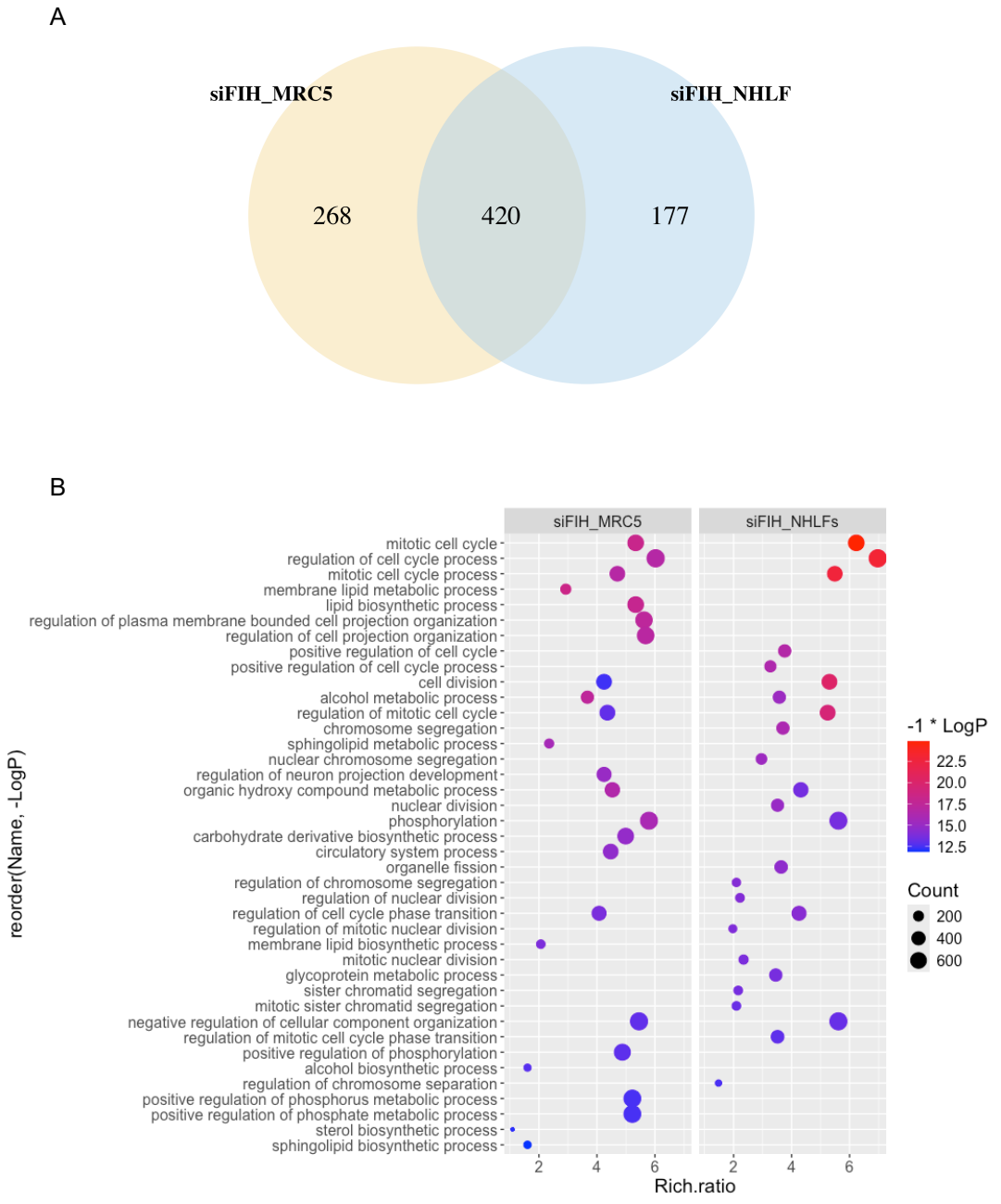

FIGURE 3.13: **Common enirched biological process GO terms in downregulated DEGs of siFIH MRC5 cells and NHLFs**

(A) Venn diagram showing 420 common BP GO terms enriched in downregulated DEGs in the two datasets; (B) Bubble plot depicting the top 25 BP GO terms from the common GO terms in the two datasets. GO BP terms are ranked according to their -Log10 P-value. The sizes of the circles represent gene counts, while the colors of the circles indicate the -Log10 P-value. GO enrichment analysis was performed using Metascape (https://metascape.org/).

3.3.4 Global transcriptomic changes in FIH knocked-out MEFs

To validate our findings in FIH KO MRC5 cells, we searched for other studies which use FIH KO cell lines and finally we found a microarray data set GSE20335 (Zhang et al., 2010). Zhang and colleagues conditionally knocked out in Mouse Embryonic Fibroblasts (MEFs) and extracted RNA samples for microarray analysis. PCA revealed that MEF samples clustered in 2 different groups (Figure. 3.14 A). After gene expression matrix analysis, we identified 648 DEGs with a significant differential expression (Adjust P value < 0.05), of which 198 genes were upregulated and 450 genes were downregulated as the volcano plot shows (Figure. 3.14 B).

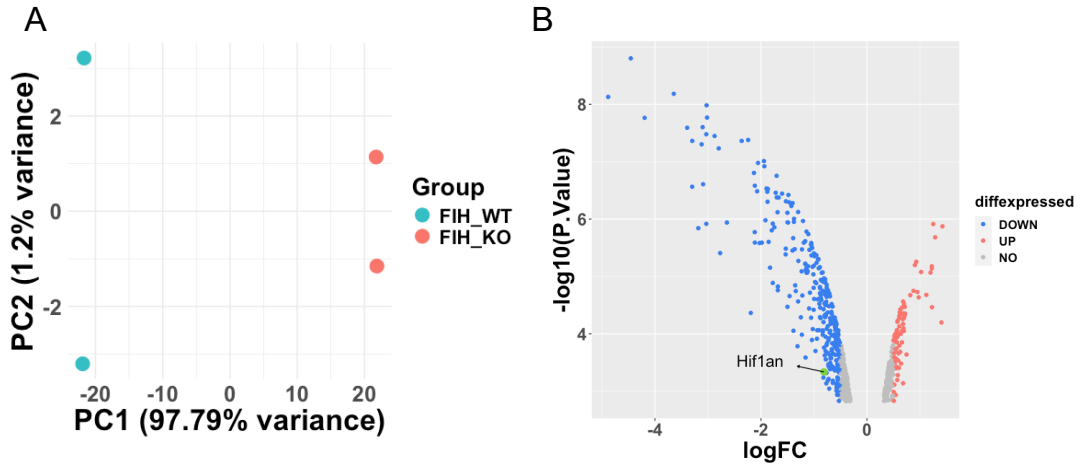

FIGURE 3.14: **Gene expression changes in FIH KO MEFs**
(A) PCA plot of gene expression data obtained via RNA-seq data for three biological replicates corresponding to the samples from FIH WT and KO MEFs (GSE20335). (B) Volcano plot showing up and down-regulated DEGs in FIH KO MEFs. Red dots represent up-regulated DEGs (Log2Foldchange > 0.5), blue dots represent down-regulated DEGs (Log2Foldchange $<$ -0.5) and grey dots represent no significant changed DEGs.

In the GO term enrichment analysis, Metascape identified 28 GO terms from the up-regulated DEGs with a Logq value threshold of $<$ -2. These GO terms were further classified into Biological Process (24 items), Cellular Component (3 items), and Molecular Function (1 item). The top-ranked enriched GO terms from each category are displayed in the bubble plot (Figure. 3.15 A) and detailed in the accompanying table. The enrichment analysis revealed that FIH depletion primarily upregulated processes related to morphogenesis within the Biological Process category, extracellular matrix in the Cellular Component category, and extracellular matrix structural constituent in the Molecular Function category. Additionally, the Treemap analysis clearly showed that

the parental GO terms for all Biological Process GO terms were associated with developmental processes and locomotion (Figure. 3.16 A). These findings suggest that FIH depletion primarily induces the regulation of morphogenesis in MEFs.

From the downregulated DEGs, 301 GO terms were identified. These were grouped into Biological Process (275 items), Cellular Component (4 items), and Molecular Function (22 items). The top 10 enriched GO terms from each category are presented in the bubble plot (Figure. 3.15 B) and summarized in the table. The results indicated that FIH depletion mainly downregulates processes related to skeletal system development and ECM organisation in the Biological Process category. Most of the DEGs were located in the ECM according to the Cellular Component GO terms, while the Molecular Function category primarily involved signaling receptor regulator or activator activity. The Treemap analysis of the top 50 BP GO terms for downregulated DEGs further demonstrated that the majority of these terms belonged to the developmental process category (Figure. 3.16 B). These findings suggest that FIH depletion downregulates biological processes related to cell proliferation.

These results indicate that FIH depletion consistently downregulates pathways involved in proliferation and key signaling processes, while upregulating pathways related to morphogenesis, extracellular matrix organisation, and apoptosis, revealing FIH's crucial role in cellular development and regulatory mechanisms.

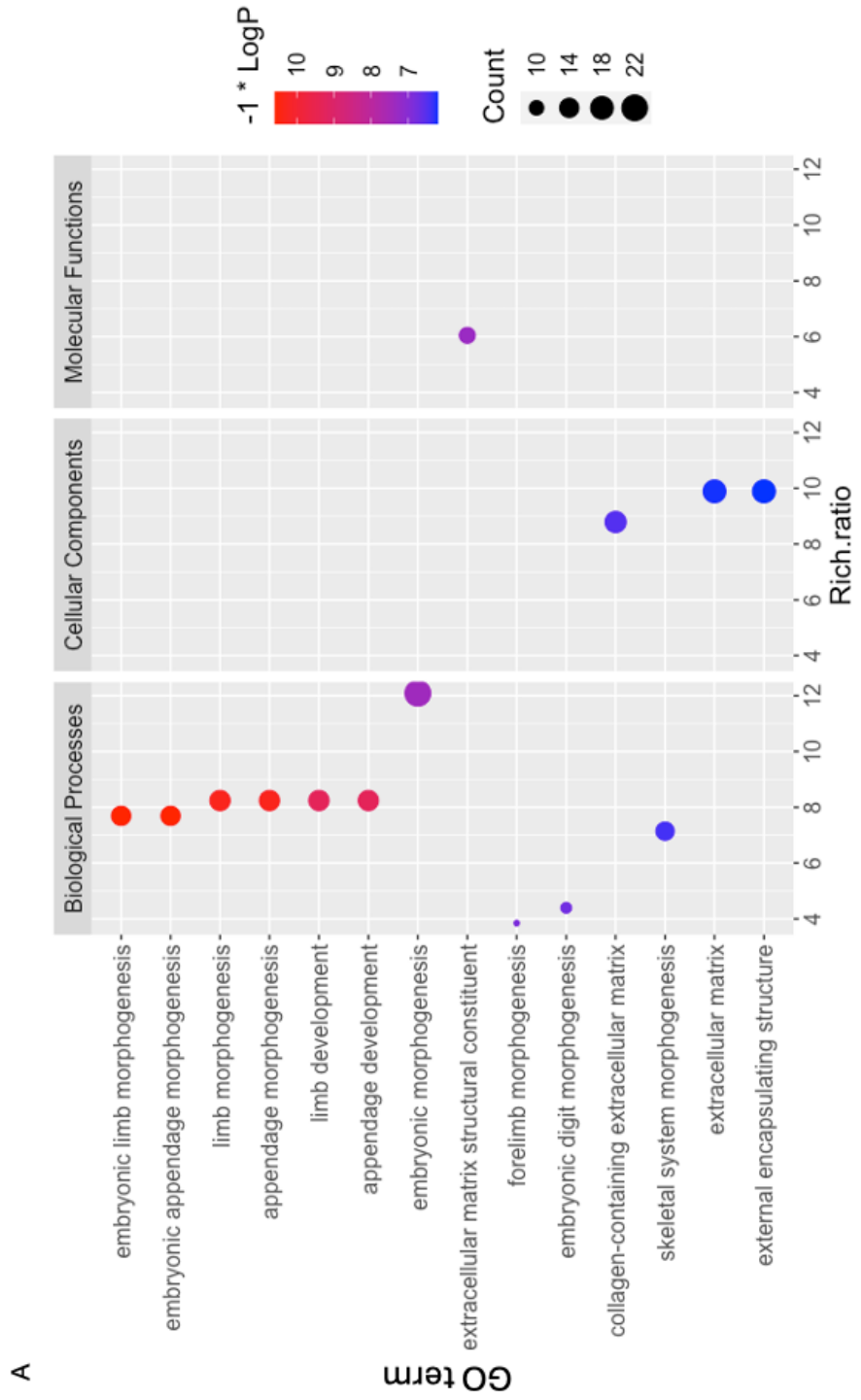
A
GO term
embryonic limb morphogenesis
embryonic appendage morphogenesis
limb morphogenesis
appendage morphogenesis
limb development
appendage development
embryonic morphogenesis
extracellular matrix structural constituent
forelimb morphogenesis
embryonic digit morphogenesis
collagen-containing extracellular matrix
skeletal system morphogenesis
extracellular matrix
external encapsulating structure
Biological Processes
Cellular Components
Molecular Functions
4
6
8
10
12
Rich.ratio
-1 * LogP
10
9
8
7
Count
10
14
18
22

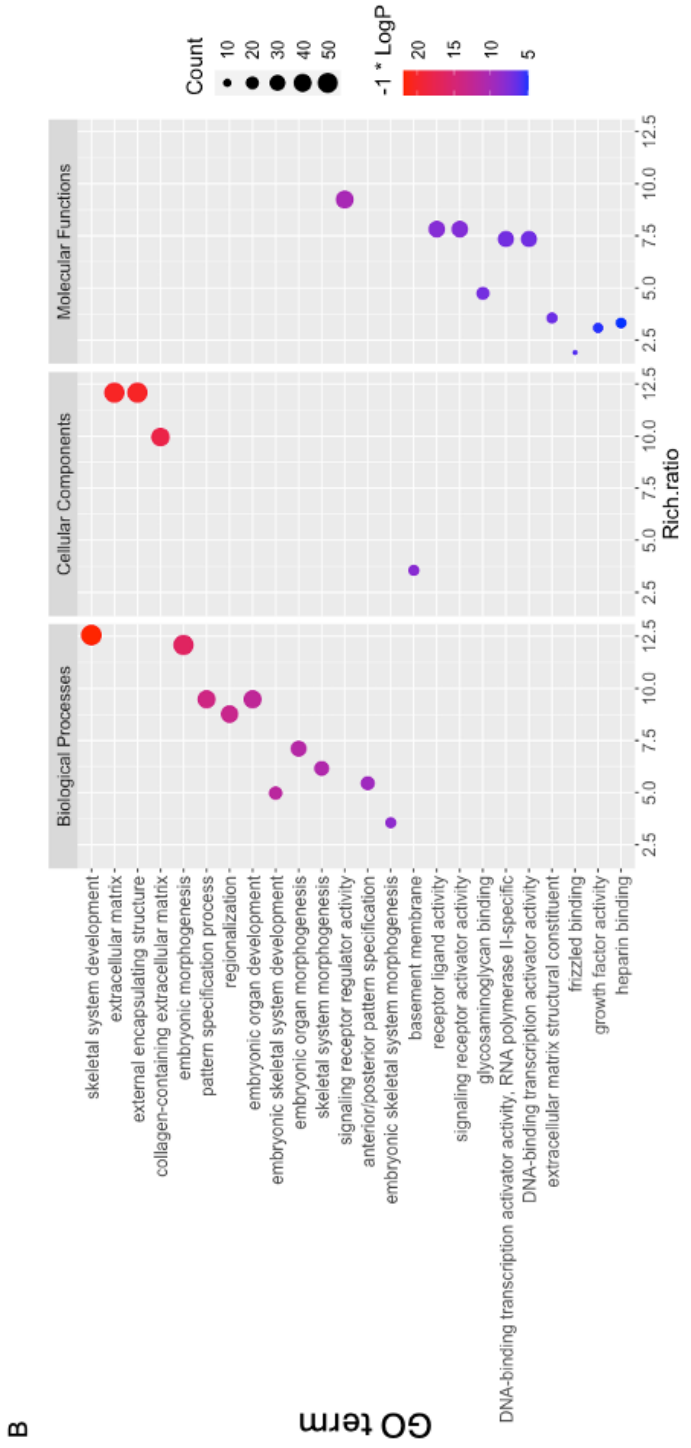

FIGURE 3.15: **GO enrichment analysis of DEGs in FIH KO MEFs**
Scatter plot showing enriched GO terms from three categories (BP, biological process; CC, cellular component; and MF, molecular function) of upregulated DEGs (A) and downregulated DEGs (B) in FIH KO MRC5 cells. DEGs are the genes with adjust P value < 0.05 and $|\text{Log2Foldchange}| > 0.5$. The sizes of circles represent gene counts, and the colours of circles represent the -Log10 of the P-value. GO enrichment analysis was conducted in Metascape (https://metascape.org/).

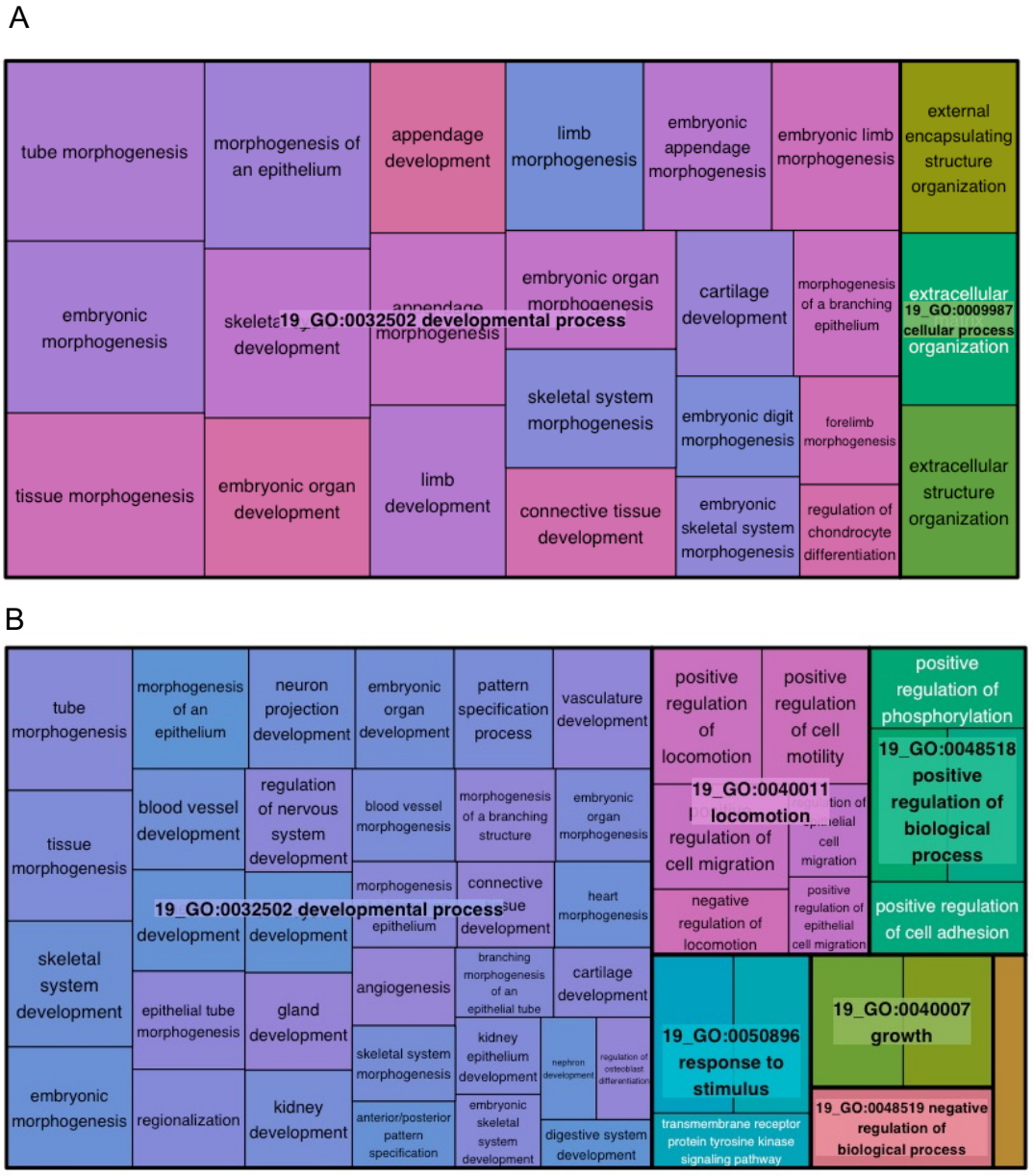

FIGURE 3.16: **Treemap of biological process GO terms for DEGs in FIH knockout MEFs**

The treemap shows the Biological Process GO terms enriched in upregulated DEGs (A) and downregulated DEGs (B) in FIH-depleted MEFs. Each rectangle corresponds to a specific GO term and is nested under its parent GO term. The size of the rectangles is determined by the number of genes (Rich.ratio) associated with each GO term, while the color represents the LogP, with darker colors indicating greater statistical significance.

3.3.5 Comparison and analysis among different datasets

After analysing three bulk RNA sequencing datasets and one microarray dataset, we observed both common and distinct effects of FIH depletion. We want to do comparison of hallmark pathway enrichment among these four datasets, as well as comparison between different genetic depletion methods (siRNA and CRISPR-cas9) and comparison between human and mice transcriptome after loss of FIH.

Comparative effects of FIH depletion in MRC5 fibroblasts via RNAi and CRISPR-Cas9

To quantify these effects, we calculated the GSVA score difference (average GSVA score of the FIH-depleted group minus the average score of the WT or control group) and indicated statistical significance with an asterisk (*), as shown in the heatmap (Figure. 3.17).

Loss of function for a gene can be achieved through RNA interference or CRISPR-Cas9 knockout, each with specific advantages and limitations. In MRC5 fibroblasts, we observed both common and divergent effects of FIH depletion using these approaches. Both RNAi and CRISPR-Cas9 reduced pathways related to the cell cycle and proliferation, including *E2F Targets*, *G2M Checkpoint*, *Mitotic Spindle*, and *MYC Targets V1* and *V2*.

By contrast, several metabolic pathways displayed opposing regulation between the two approaches. Pathways such as *Protein Secretion*, *Peroxisome*, and *Oxidative Phosphorylation* showed a trend toward upregulation in CRISPR-Cas9 knockout cells but were suppressed following RNAi-mediated knockdown, while others (e.g., *Heme Metabolism*, *Fatty Acid Metabolism*) showed less consistent changes. These differences suggest context-dependent effects of acute versus stable FIH loss on metabolic programs. This suggests that stable FIH knockout may enhance metabolic activity, whereas transient knockdown suppresses it. The lack of significant changes in glycolysis and the contrasting effects on other metabolic pathways warrant further investigation.

Additionally, signalling pathways such as *Hypoxia*, *TGF-β Signaling*, and *TNFα Signaling via NFκB* were downregulated in CRISPR-Cas9 knockout cells but upregulated in RNAi-treated fibroblasts. Finally, several pathways were consistently downregulated across both methods, including *Estrogen Response Early*, *Estrogen Response Late*, *MYC Targets V1* and *V2*, *IL6-JAK-STAT3 Signaling*, and *IL2-STAT5 Signaling*.

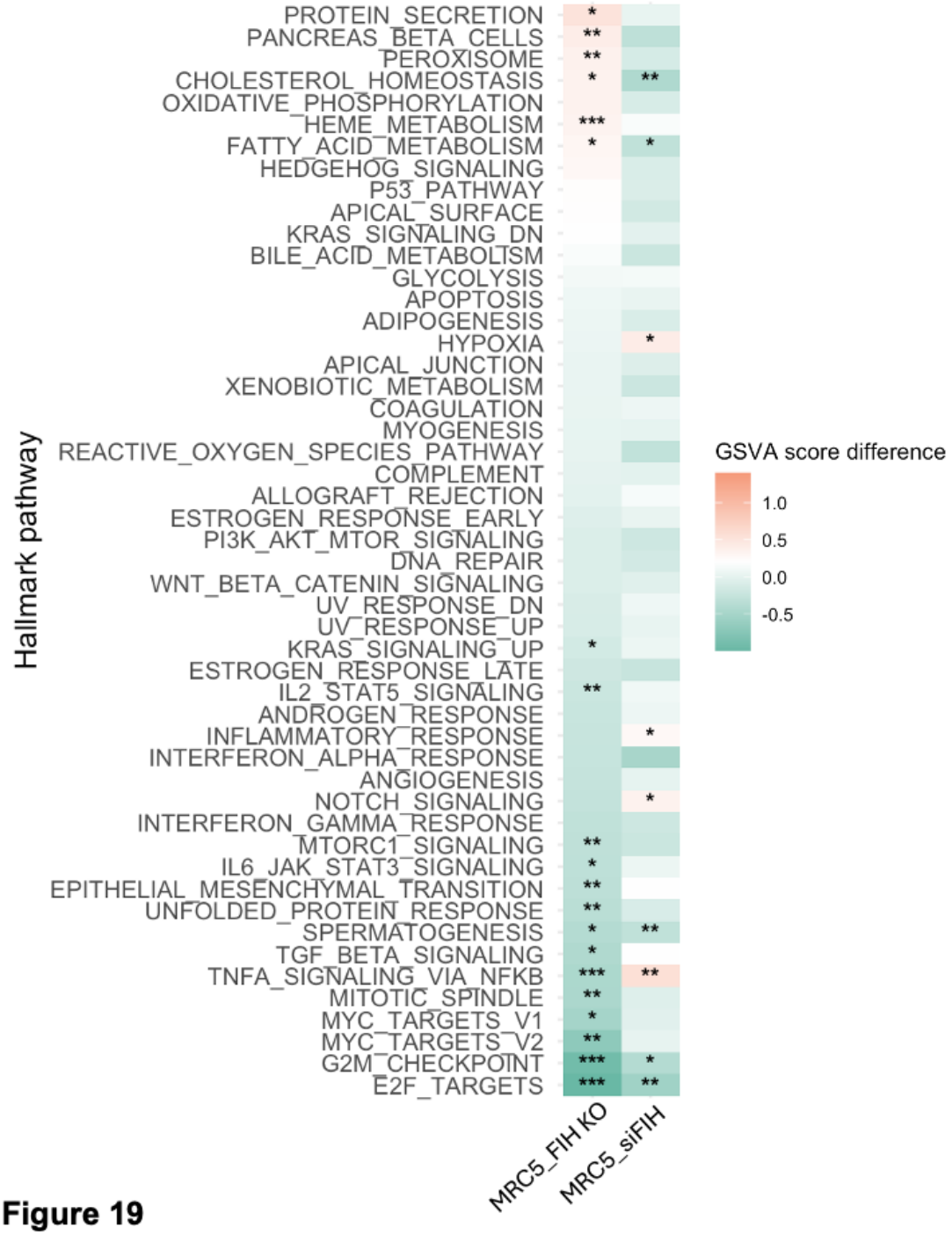

FIGURE 3.17: **Hallmark pathway enrichment score comparison among four different RNA sequencing datasets**

Heatmap showing the average hallmark GSVA average score difference (Average GSVA score of FIH KO/siFIH group – average GSVA score of WT/control group) between two different datasets analysed in previous subsections. GSVA, gene set variation analysis. *P $<$ 0.05, ***P $<$ 0.01, ***P $<$ 0.001 by Student's t-test.

We sought to identify common transcriptional changes resulting from two different methods of FIH depletion in MRC5 cells: gene knockout using CRISPR-Cas9 and gene knockdown via siRNA transfection. To achieve this, we compared the enriched biological process GO terms associated with upregulated DEGs in each dataset. The Venn plot shows that 256 BP GO terms are shared between the two datasets (Figure. 3.18 A). The bubble plot displays the top 25 biological process (BP) GO terms from the common GO terms identified in both datasets (Figure. 3.18 B). Notably, *Response to decreased oxygen levels*, *Response to hypoxia*, and several GO terms related to cellular response to stimuli were among the most enriched in the siFIH_MRC5 dataset. These terms also appeared in the FIHKO_MRC5 dataset, though they did not rank within the top 25 BP GO terms. This suggests that both FIH knockdown and knockout can activate the HIF pathway even under normoxic conditions, with a noticeably stronger response observed in siFIH_MRC5 cells. BP GO terms related to cellular migration, such as *positive regulation of cell migration*, *positive regulation of locomotion*, and *positive regulation of cell motility*, were prominently featured in both datasets. Overall, the common GO terms in the FIH KO and siFIH datasets are involved in various biological processes, including cellular migration/localization and cellular metabolism, though the significance of most GO terms differs considerably between the two datasets.

In FIH KO MRC5 cells, among the 25 distinct upregulated GO terms identified, the most prominently enriched include cytoplasmic translation, peptide metabolic process, translation, amide biosynthetic process, peptide biosynthesis, membrane organisation, Golgi vesicle transport, regulation of autophagy, and localization within membranes. These top GO terms suggest a strong activation of pathways related to protein synthesis, membrane dynamics, and cellular transport. Such enrichment highlights that FIH knockout has a significant impact on processes driving protein production, autophagy regulation, and membrane organisation within the cells (Figure.3.19 A). While in siFIH MRC5 cells, the upregulation of GO terms such as inflammatory response, cellular response to cytokine stimulus, response to lipopolysaccharide, cytokine-mediated signaling pathway, chemotaxis, taxis, cellular response to lipid, locomotion, and regulation of leukocyte migration indicates a heightened inflammatory and immune response in the cells. This suggests that pathways involved in responding to cytokines, lipids, and other inflammatory stimuli are significantly activated. Additionally, the increase in processes related to cell movement, such as chemotaxis and leukocyte migration, points to enhanced cellular motility and immune cell recruitment, highlighting a potential role in mediating immune responses and inflammation within the affected cells (Figure.3.19 B).

After analysing the upregulated GO terms, we also examined the downregulated GO terms across both datasets. A total of 387 commonly enriched downregulated GO terms were identified in both FIH KO and siFIH MRC5 cells (Figure.3.20 A). Among the top

common terms were processes such as the mitotic cell cycle, cell division, and regulation of the cell cycle, indicating that the loss of FIH significantly suppresses pathways related to cell cycle progression and mitosis (Figure. 3.20 B).

The downregulation of these pathways suggests that FIH is crucial for promoting cell cycle activity and division, and its depletion impairs cell proliferation, potentially hindering cell growth and renewal. This decrease in mitotic activity could affect cellular responses to stress, tissue regeneration, or development in FIH-dependent tissues.

To explore differences in downregulated pathways between the two datasets, we further analysed unique GO terms. In FIH KO MRC5 cells, processes maintaining genome stability, gene expression regulation, and chromatin structure—such as DNA metabolic regulation, chromatin organisation, mRNA processing, DNA recombination, and RNA localization—were among the most affected (Figure.3.21 A). This suggests that FIH KO impairs DNA repair, reduces gene transcription activity, disrupts chromatin remodeling, and potentially decreases cellular proliferation and genomic integrity.

In contrast, siFIH MRC5 cells showed downregulation of processes linked to lipid metabolism and homeostasis, including membrane lipid metabolism, alcohol metabolism, and lipid biosynthesis and transport (Figure.3.21 B). These alterations may disrupt lipid biosynthesis and catabolism, impair lipid signaling, reduce energy production from lipids, and compromise membrane structure and function—all of which are vital for maintaining cellular integrity and proper signaling.

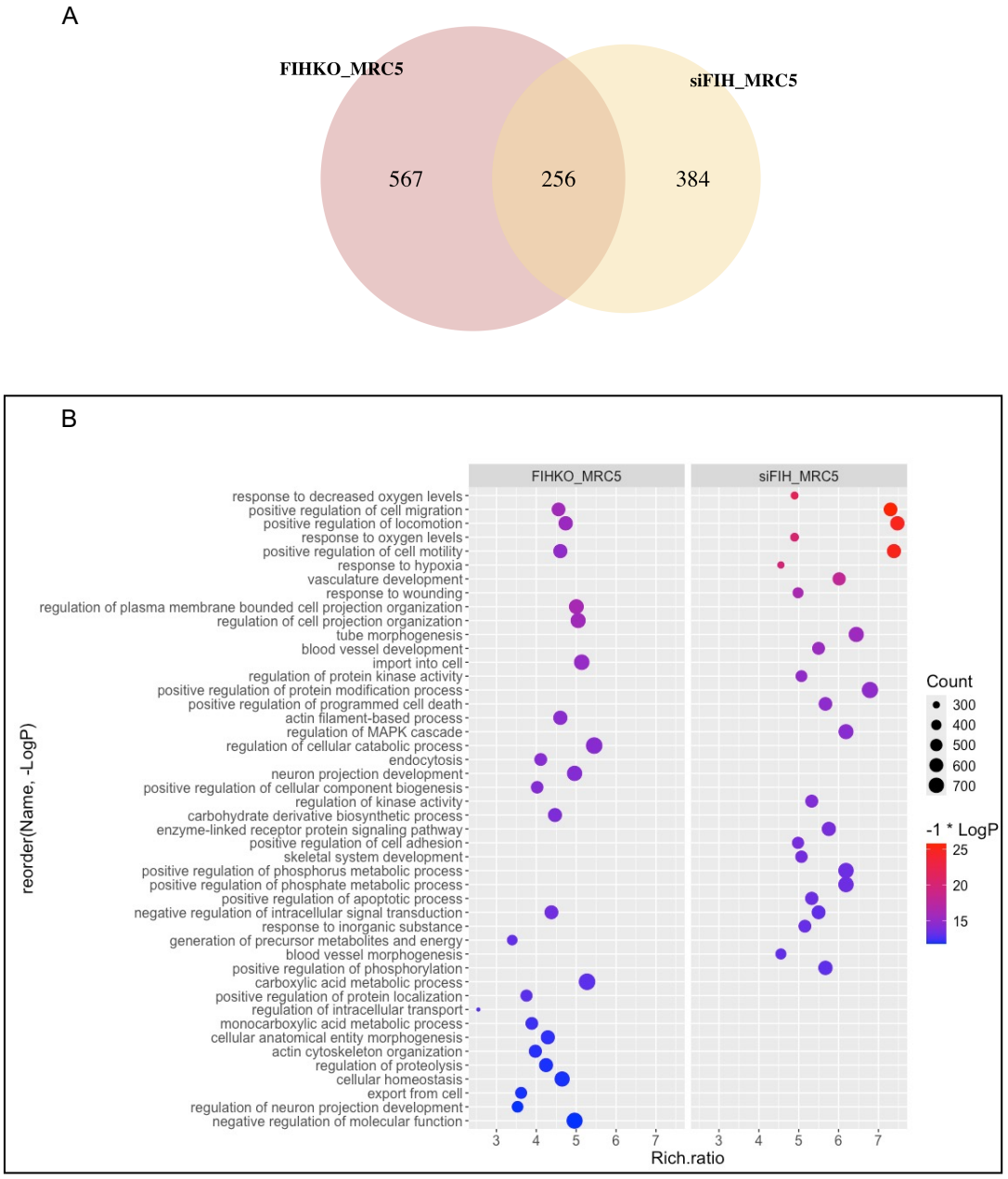

FIGURE 3.18: **Comparison of upregulated biological process GO term between FIH knocked out MRC5 cells and knocked down MRC5 cells**

(A) Venn diagram showing 256 common upregulated BP GO terms enriched in the two datasets; (B) Bubble plot depicting the top 25 BP GO terms from the common GO terms in the two datasets. GO BP terms are ranked according to their -Log10 P-value. The sizes of the circles represent gene counts, while the colors of the circles indicate the -Log10 P-value. GO enrichment analysis was performed using Metascape (https://metascape.org/).

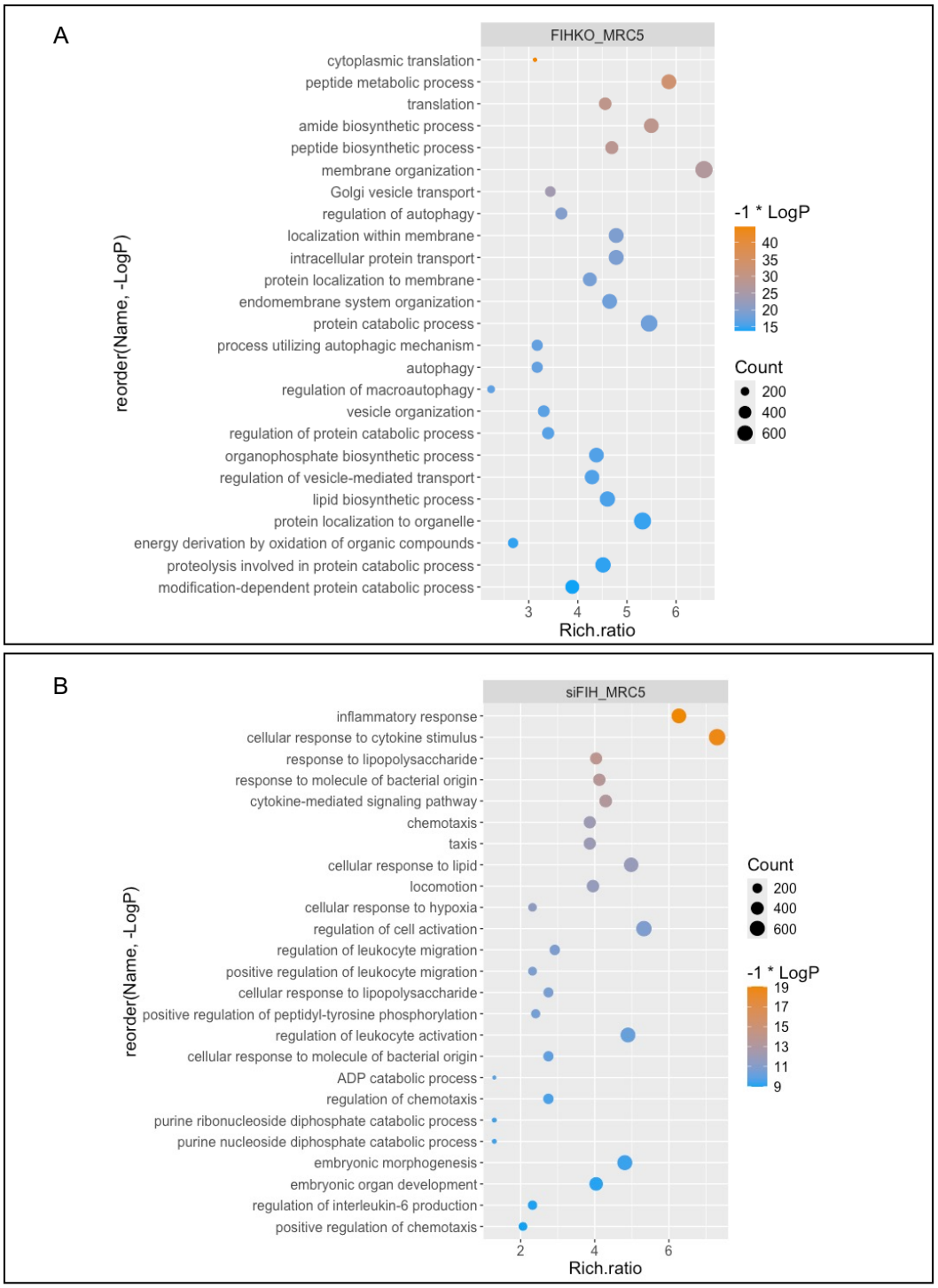

FIGURE 3.19: **Top 25 upregulated biological process GO terms unique to FIH KO and siFIH MRC5 cells**

Bubble plot showing top 25 BP GO terms enriched in upregulated DEGs unique to FIH KO MRC5 cells (A) and siFIH MRC5 cells (B). GO BP terms are ranked according to their -Log10 P-value. The sizes of the circles represent gene counts, while the colors of the circles indicate the -Log10 P-value. GO enrichment analysis was performed using Metascape (https://metascape.org/).

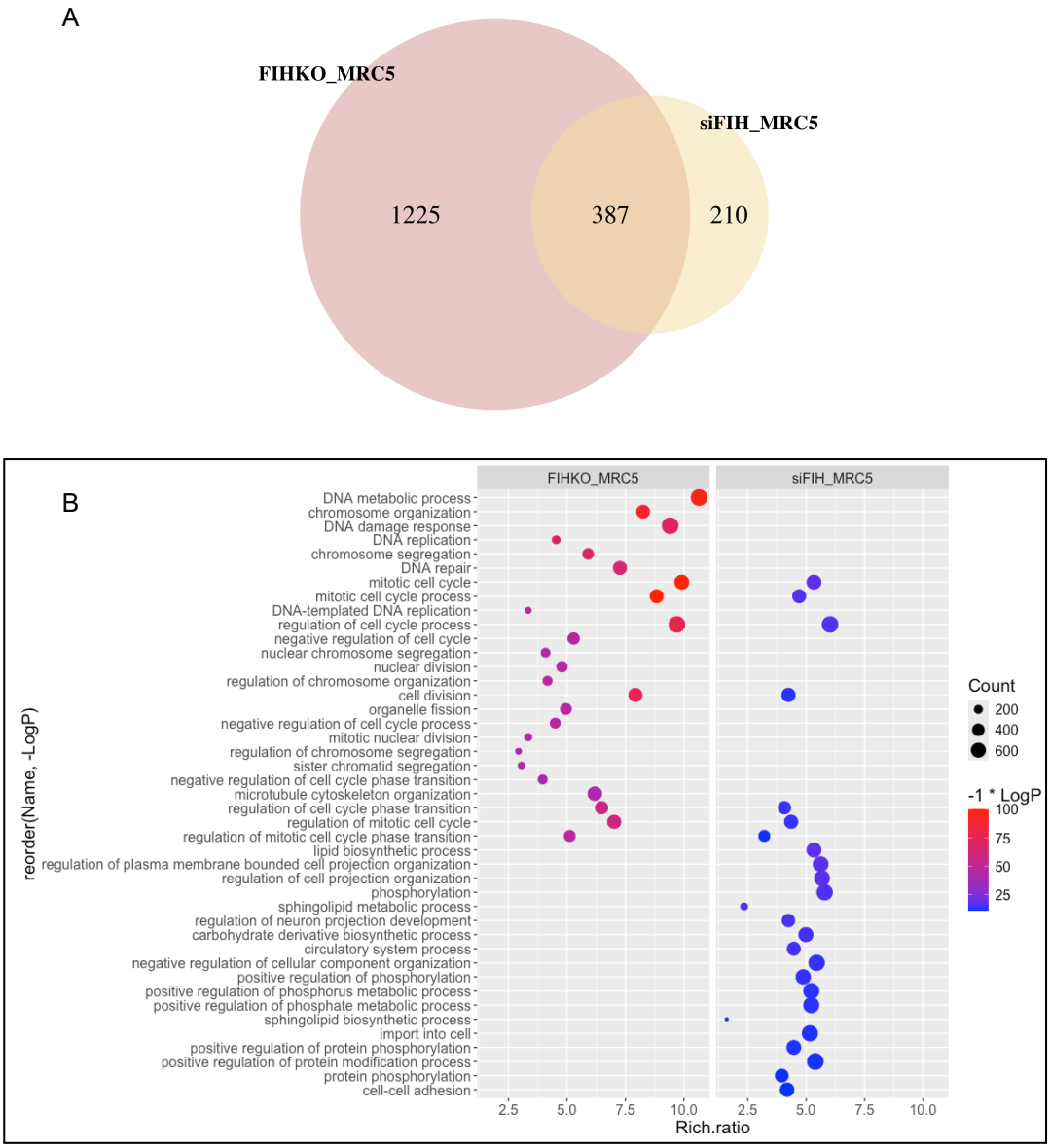

FIGURE 3.20: **Comparison of downregulated biology process GO term between FIH knocked out MRC5 cells and FIH knocked down MRC5 cells**

(A) Venn diagram showing 387 common downregulated BP GO terms enriched in the two datasets; (B) Bubble plot depicting the top 25 BP GO terms from the common GO terms in the two datasets. GO BP terms are ranked according to their -Log10 P-value. The sizes of the circles represent gene counts, while the colors of the circles indicate the -Log10 P-value. GO enrichment analysis was performed using Metascape (https://metascape.org/).

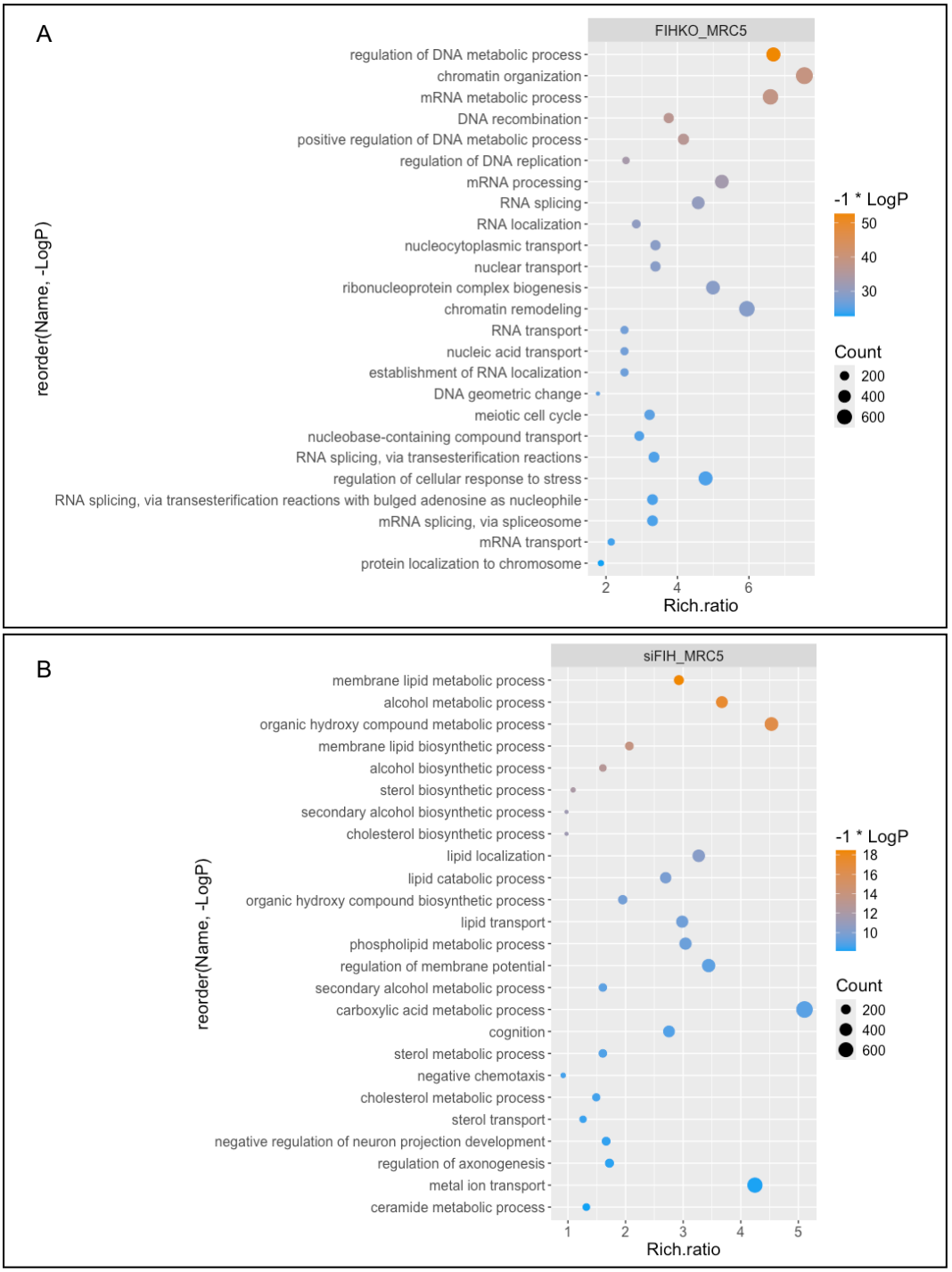

FIGURE 3.21: **Top 25 downregulated biological process GO terms unique to FIH KO and siFIH MRC5 cells**

Bubble plot showing top 25 BP GO terms unique enriched in downregulated DEGs unique to FIH KO MRC5 cells (A) and siFIH MRC5 cells (B). GO BP terms are ranked according to their -Log10 P-value. The sizes of the circles represent gene counts, while the colors of the circles indicate the -Log10 P-value. GO enrichment analysis was performed using Metascape (https://metascape.org/).

After comparing the effects of FIH depletion via CRISPR-Cas9 and siRNA, we also examined the similarities and differences between FIH KO human lung fibroblasts (MRC5) and MEFs. Due to the limited number of upregulated DEGs in FIH KO MEFs, only 8 common GO terms were identified between the two datasets. These included tube morphogenesis, tissue morphogenesis, morphogenesis of an epithelium, extracellular matrix organisation, extracellular structure organisation, external encapsulating structure organisation, skeletal system development, and connective tissue development. The upregulation of these processes suggests an enhanced role in tissue remodeling and structural organisation, particularly in shaping tissues, developing epithelial layers, and organising the ECM, indicating that FIH loss may promote processes related to tissue formation and structural development (Figure.3.22 A).

In FIH KO MRC5 cells, distinct upregulated GO terms are consistent with those discussed previously, highlighting processes related to protein production, autophagy regulation, and membrane organisation (Figure.3.23 A). In contrast, MEFs with FIH knockout showed a significant upregulation in developmental processes, including embryonic limb morphogenesis, appendage morphogenesis, limb development, and skeletal system morphogenesis. These processes are associated with limb patterning, appendage growth, and skeletal structure formation, suggesting that FIH loss in MEFs influences pathways involved in embryonic development and morphogenesis (Figure.3.23 B).

There are 227 common enriched downregulated GO terms between the two datasets (Figure.3.24 A). Among them, tube morphogenesis, positive regulation of cell migration, skeletal system development, tissue morphogenesis, positive regulation of locomotion, and cell motility are linked to cellular movement, tissue organisation, and developmental processes. The downregulation of these terms suggests a reduction in pathways governing cell migration, tissue formation, and skeletal development. This indicates that FIH depletion may impair cellular motility and tissue structuring, potentially disrupting normal tissue remodeling and developmental pathways in both human and mice cells (Figure.3.24 B).

As previously shown, in FIH KO MRC5 cells, the top distinct downregulated GO terms are related to cellular proliferation and genomic integrity maintenance (Figure.3.25 A). In contrast, in MEFs, the loss of FIH leads to the downregulation of processes such as embryonic skeletal system development, anterior/posterior pattern specification, nephron epithelium development, renal tubule development, and regulation of hormone levels. This suggests a decrease in early developmental pathways, organ formation, and hormonal balance. Specifically, these changes may reflect impaired skeletal patterning, disrupted kidney development (including nephron and renal tubule formation), and altered hormone regulation, potentially affecting embryonic development, organ structure, and physiological processes dependent on hormone signaling (Figure.3.25 B).

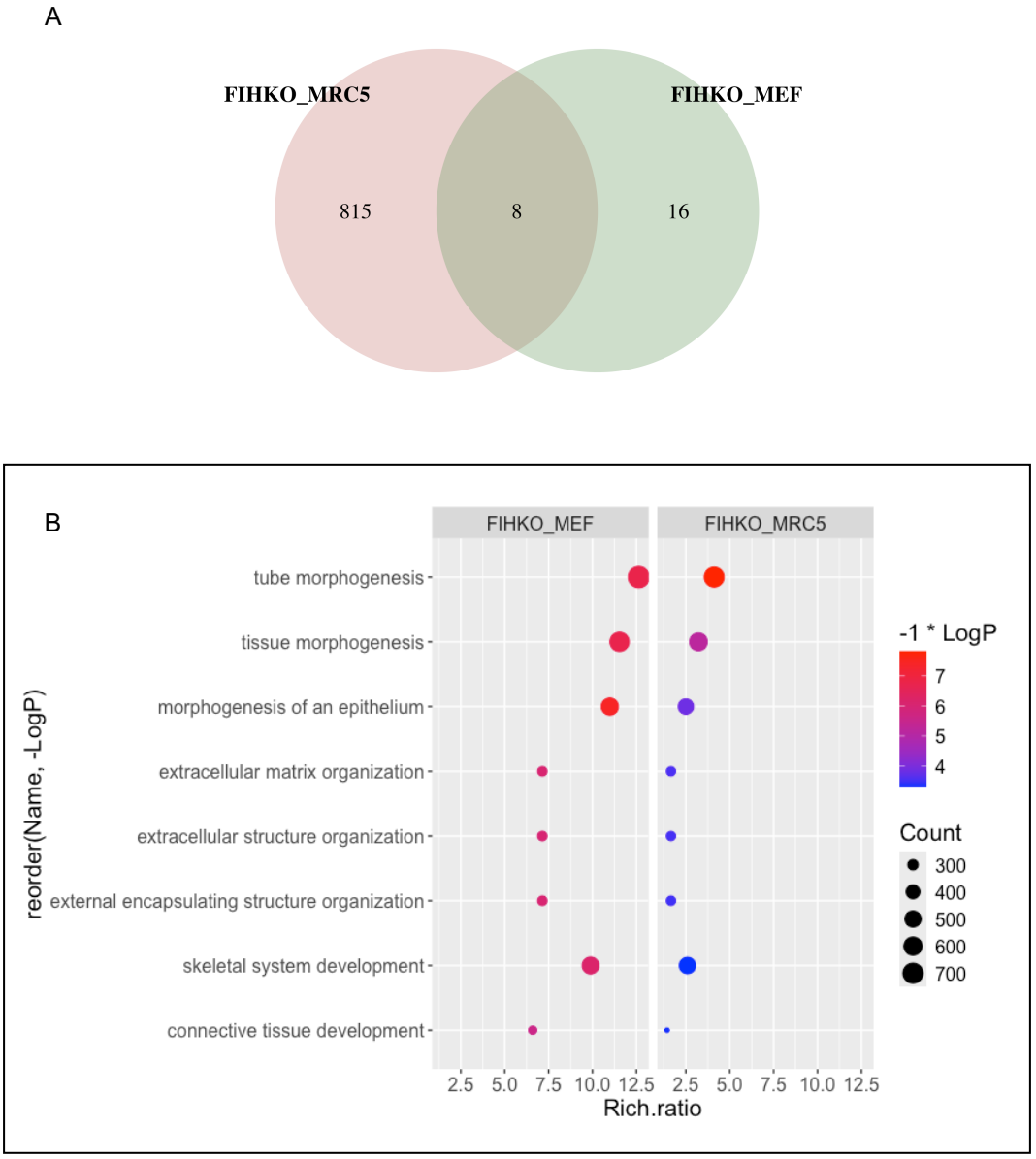

FIGURE 3.22: **Comparison of upregulated biological process GO term between FIH knocked out MRC5 cells and FIH knocked out MEFs**

(A) Venn diagram showing 8 common upregulated BP GO terms enriched in the two datasets; (B) Bubble plot depicting the 8 common BP GO terms in the two datasets. GO BP terms are ranked according to their -Log10 P-value. The sizes of the circles represent gene counts, while the colors of the circles indicate the -Log10 P-value. GO enrichment analysis was performed using Metascape (https://metascape.org/).

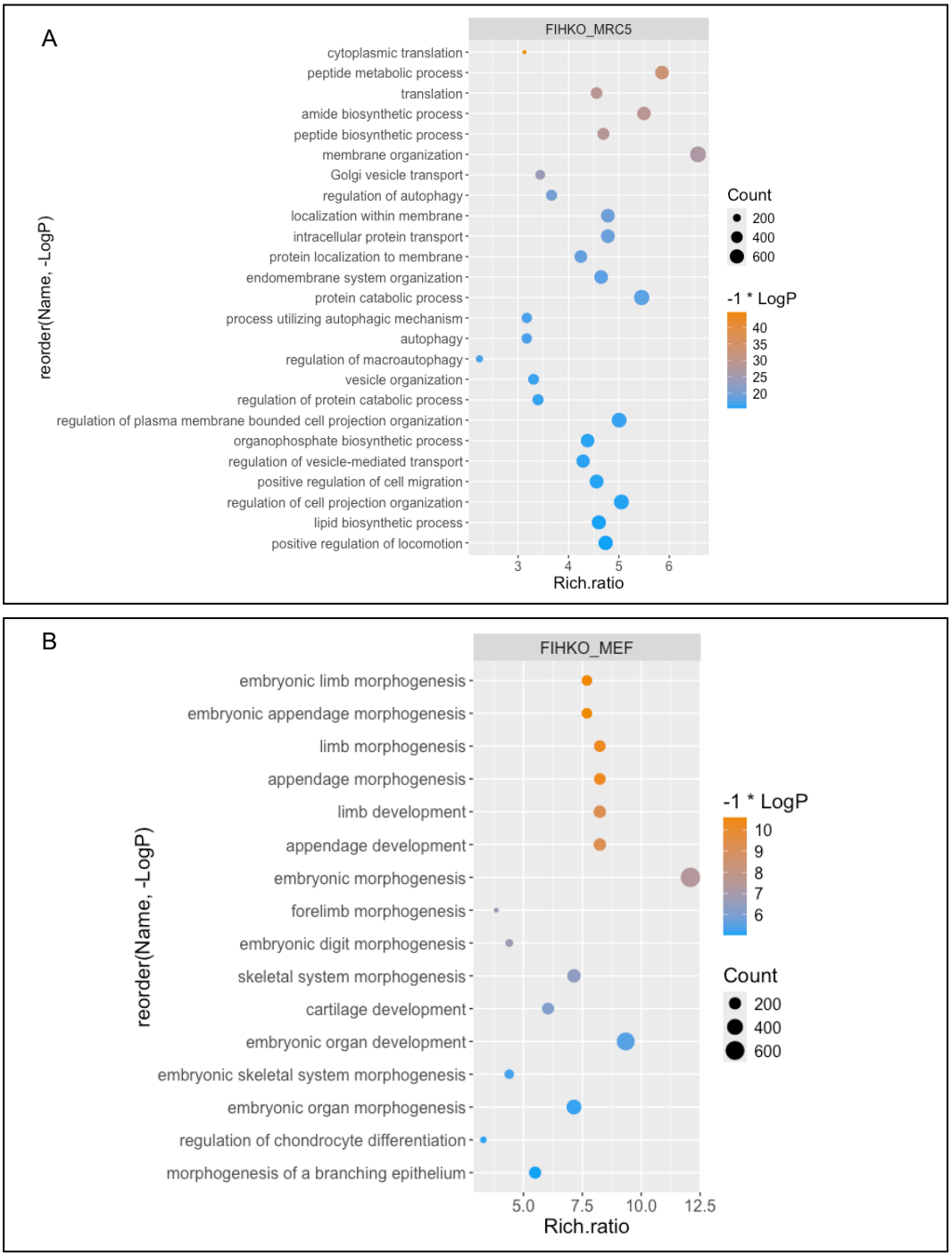

FIGURE 3.23: **Top ranked upregulated biological process GO terms unique to FIH KO MRC5 Cells and FIH KO MEFs**

Bubble plot showing top 25 BP GO terms enriched in upregulated DEGs unique to FIH KO MRC5 cells (A) and top 16 unique to FIH KO MEFs (B). GO BP terms are ranked according to their -Log10 P-value. The sizes of the circles represent gene counts, while the colors of the circles indicate the -Log10 P-value. GO enrichment analysis was performed using Metascape (https://metascape.org/).

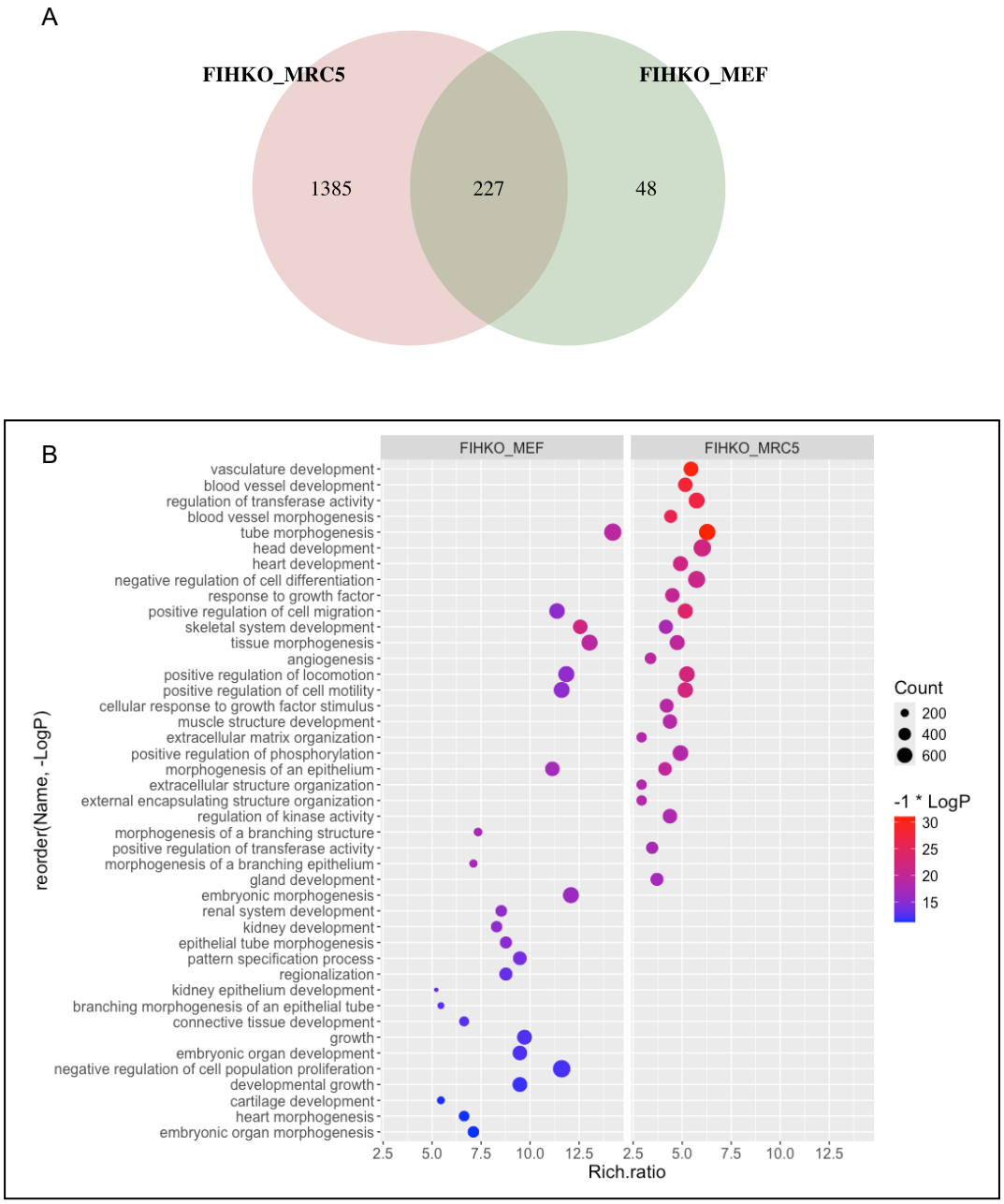

FIGURE 3.24: **Comparison of downregulated biology process GO term between FIH KO MRC5 cells and FIH KO MEFs**

(A) Venn diagram showing 227 common downregulated BP GO terms enriched in the two datasets; (B) Bubble plot depicting the top 25 BP GO terms from the common GO terms in the two datasets. GO BP terms are ranked according to their -Log10 P-value. The sizes of the circles represent gene counts, while the colors of the circles indicate the -Log10 P-value. GO enrichment analysis was performed using Metascape (https://metascape.org/).

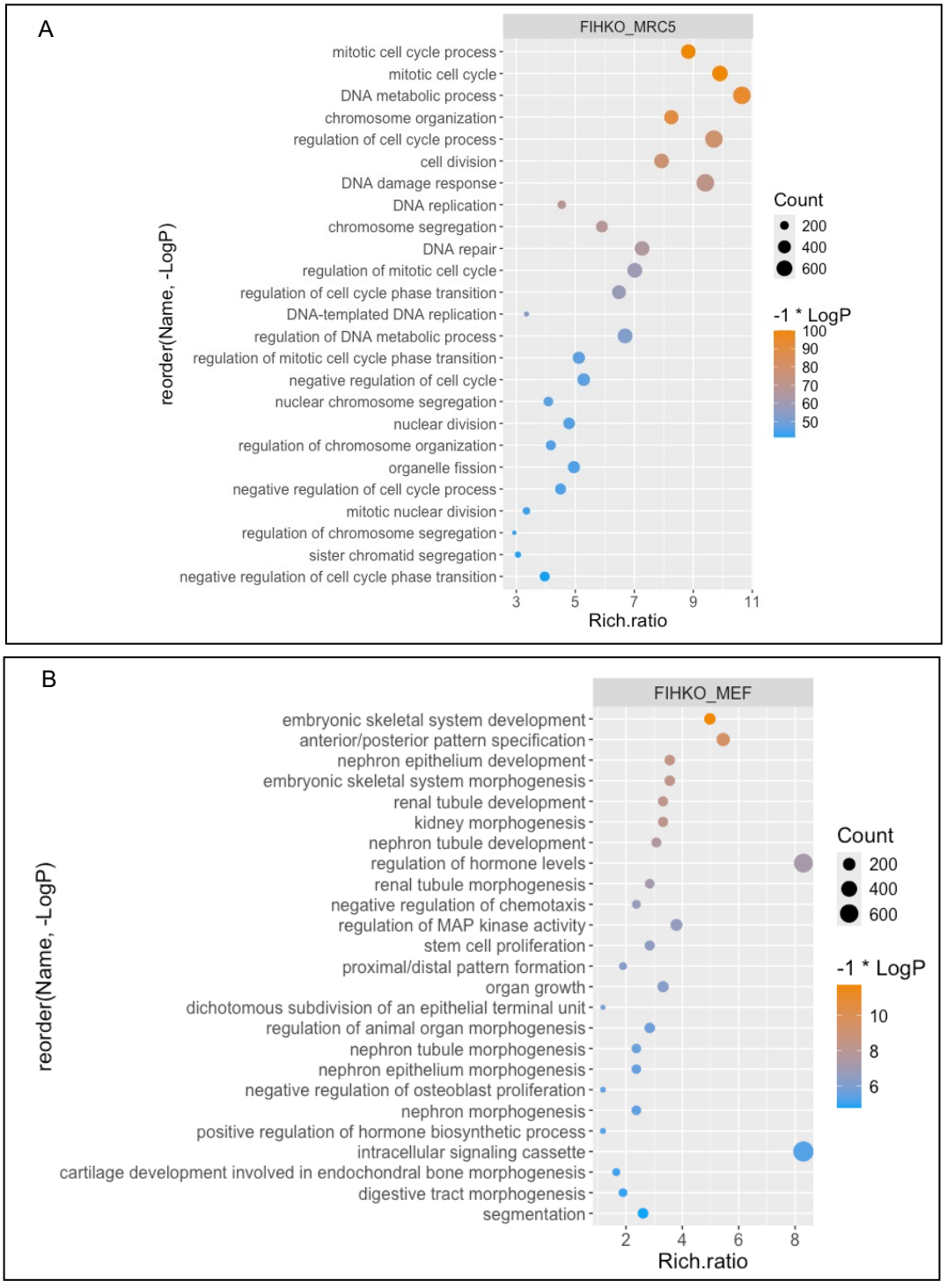

FIGURE 3.25: **Top 25 downregulated biological process GO terms unique to FIH KO MRC5 cells and FIH knocked out MEFs**

Bubble plot showing top 25 BP GO terms unique enriched in downregulated DEGs unique to FIH KO MRC5 cells (A) and FIH KO MEFs (B). GO BP terms are ranked according to their -Log10 P-value. The sizes of the circles represent gene counts, while the colors of the circles indicate the -Log10 P-value. GO enrichment analysis was performed using Metascape (https://metascape.org/).

3.4 Discussion

In this study, we investigated the global transcriptomic changes resulting from the depletion of FIH in MRC5 human lung fibroblasts, NHLFs, and MEFs. By utilizing both CRISPR-Cas9 and siRNA-mediated gene silencing, we aimed to compare the effects of FIH knockout and knockdown on gene expression and biological processes across different fibroblast models. We also included mouse embryonic fibroblasts (MEFs) to provide a complementary model system, enabling us to test whether the observed effects are conserved across species and not restricted to human fibroblasts. In addition to primary human lung fibroblasts, MEFs are widely used as a tractable model system in fibrosis and signalling research. MEFs offer several advantages, including ease of genetic manipulation, availability of well-characterized knockout strains, and reduced variability compared to primary human cells. While they do not fully recapitulate the tissue-specific features of human fibroblasts, MEFs provide complementary insights into conserved signalling pathways and facilitate mechanistic studies that are more difficult to perform in primary cells. Using both MEFs and human fibroblasts therefore allows us to assess species-specific differences while strengthening the generality of our findings.

The CRISPR-Cas9-mediated knockout of FIH in MRC5 cells led to approximately equal numbers of upregulated and downregulated genes. GO enrichment analysis revealed that FIH depletion upregulated processes related to protein synthesis, transport, and localization, particularly within cellular organelle membranes. Downregulated processes predominantly involved cell division and proliferation, with DEGs localized to the chromosome and associated with transcription factor binding and ATP-dependent catalytic activity. GSVA further confirmed that hallmark gene sets related to cell proliferation, such as the G2M checkpoint, E2F targets, and mitotic spindle, were significantly downregulated.

In siFIH-transfected MRC5 cells, upregulated DEGs were associated with cellular responses to oxygen levels and cell locomotion, while downregulated genes were linked to cell cycle regulation and metabolism, consistent with the findings from FIH knockout cells. GSVA analysis highlighted the downregulation of pathways related to cell proliferation and metabolism and upregulation of signaling pathways such as hypoxia, TGF-β, and TNFα signaling via NFκB. Similar results were obtained in NHLFs following FIH knockdown, supporting the role of FIH depletion in modulating cell cycle progression, metabolism, and cellular responses to stimuli. Although FIH depletion reduced TGF-β, ECM, and myofibroblast gene sets in our in-vitro models, this does not exclude a profibrotic role for FIH in disease. FIH has multiple substrates, and its effects are likely to vary with environmental stimuli such as hypoxia, mechanical stress, or chronic TGF-β exposure. In particular, the FIH/HIF axis is known to regulate collagen maturation and

cross-linking in addition to transcriptional programs, which may explain why reduced transcript levels in vitro could still coexist with profibrotic outcomes in vivo.

We observed common changes and differences in the enriched pathways when comparing RNA-seq data from FIH KO and siFIH MRC5 cells. Both CRISPR-Cas9 knockout and siRNA knockdown consistently led to the downregulation of cell cycle-related processes and cellular metabolism and upregulation of pathways associated with hypoxia and cellular migration. Given that FIH acts as a main regulator of HIF-1α, it is expected that hypoxia-related pathways will be activated following FIH depletion. But we didn't see enriched Hallmark hypoxia pathway in FIN KO fibroblast. We assume this is due to a difference between acute vs long-term loss of FIH. In the siRNA setting, acute depletion may transiently derepress HIF transcriptional activity, resulting in a detectable enrichment of hypoxia-related genes. In contrast, long-term CRISPR KO clones are likely to undergo adaptive compensation. Fibroblasts are chemotactic and can migrate to accumulate in response to secreted cytokines, a behavior well characterised in wound healing after tissue injury. During lung fibrosis progression, fibroblast migration is crucial for accumulating cells in fibroblast foci, which contributes to the fibrotic process (Fernandez and Eickelberg, 2012*b*).

The role of HIF-1α and FIH in regulating migration remains complex. Li *et al.* found that HIF-1α promotes cell migration independently of hypoxia; knockout of HIF-1α significantly reduced cell migration by up to 80% in MEFs, which could be partially restored by ectopic expression of HIF-1α, though the detailed mechanism was not identified (Li et al., 2010). In contrast, another study showed that hypoxia (1% oxygen) inhibits mesenchymal stem cell (MSC) migration, primarily through a mechanism involving HIF-1α. Stabilization of HIF-1α under normoxic conditions similarly reduces migration and decreases RhoA activation, akin to the effects seen in hypoxia, and RhoA activation rescues migration in hypoxic cells (Raheja et al., 2011).

In breast cancer cells, FIH indirectly promotes cell migration by hydroxylating HACE1, reducing HACE1's ability to bind and ubiquitinate Rac1, a key regulator of cell migration. Under hypoxic conditions or when FIH is inhibited, hydroxylation is reduced, leading to increased HACE1-Rac1 interaction, decreased Rac1 activity, and impaired cell migration (Kim et al., 2019). These findings suggest that FIH and HIF-1α play complex roles in the regulation of fibroblast migration and the fibrotic process.

Furthermore, the proliferation of fibroblasts contributes to fibrotic progression. Caraci and colleagues demonstrated that TGF-β, via the phosphorylation of ERK1/2, activates the Wnt pathway in lung fibroblasts, inhibiting GSK-3β activity, thus promoting the cytosolic accumulation and subsequent nuclear translocation of β-catenin (Caraci et al., 2008). The transcription of ERK1/2 target genes, induced by TGF-β, could also lead to a secondary activation of other signaling pathways that may regulate cell proliferation and apoptosis (Vancheri, 2012). Currently, there are not many studies discussing

the relationship between FIH and fibroblast proliferation. Whether FIH hydroxylates potential substrates involved in signaling pathways or interacts with unidentified proteins requires further investigation.

Interestingly, notable differences emerged, particularly in the regulation of metabolic processes and signaling pathways like TGF-β and TNFα. GO enrichment analysis showed that loss of FIH via CRISPR-cas9 and RNAi led to downregulation of metabolism process, but in FIH KO MRC5 cells, there were also several biological processes related with metabolism upregulated.

In FIH KO cells, pathways related to genome stability, gene expression, and chromatin organisation are downregulated, indicating impaired DNA repair and transcriptional regulation. Conversely, FIH KD cells exhibit downregulation in lipid metabolism and homeostasis, affecting lipid synthesis, signaling, and membrane structure. Both alterations can result in the mitigation of cell proliferation but via different mechanisms which need further investigation. These variations highlight the different transcriptomic effects that can arise depending on whether gene knockout or knockdown techniques are applied.

There are a lot of discussions about these two different method to manipulate gene expression. RNA interference (RNAi) is currently the most widely used reverse genetics technique for studying gene function in mammalian cells. Its effectiveness is due to its basis in an evolutionarily conserved endogenous pathway that regulates gene expression through small RNAs (Wilson and Doudna, 2013). A key advantage of RNAi is that the silencing machinery is present in almost all mammalian somatic cells. Therefore, no prior genetic modification of the target cell line is necessary, and a straightforward siRNA transfection can effectively produce a loss-of-function phenotype (Boettcher and McManus, 2015) in 48 hours. Due to this efficiency, cells suppose to response to the loss of target gene. So we can see the hypoxia pathway and several pathways realted to cells response to stimulus enriched in upregulated DEGs. The main problem of RNAi is the off-target effect. The off-target effects of RNAi are a significant challenge due to both sequence-specific and non-sequence-specific mechanisms. Sequence-specific effects occur when siRNAs partially match the 3'-UTR of non-target mRNAs, leading to unintended translational repression or degradation of these mRNAs, potentially affecting hundreds of transcripts. These effects are dosage-dependent and can overshadow the intended gene silencing. Additionally, the introduction of exogenous siRNAs or shRNAs can disrupt the natural microRNA regulatory pathway by displacing endogenous microRNAs from RISC, altering gene expression and causing off-target phenotypes unrelated to the siRNA sequence itself. These concerns have driven the search for more precise genetic tools (Sigoillot and King, 2011).

The CRISPR-Cas9 system allows precise genome editing through the use of a guide RNA, which directs the Cas9 nuclease to a target DNA sequence to create double-strand

breaks. These breaks can be repaired either by nonhomologous end joining (NHEJ), leading to insertions or deletions, or by homology-directed repair (HDR) for targeted sequence changes. A double-nicking strategy with a Cas9 mutant enhances specificity, enabling rapid and accurate genome modifications (Ran et al., 2013). Establishing a CRISPR-Cas9 KO cell line typically requires 1-2 weeks to achieve stable gene knockout. There is ongoing discussion about the compensatory effects after CRISPR-Cas9-induced gene KO and comparisons between RNAi and CRISPR-Cas9 approaches. For instance, De and colleagues observed that while both siRNA-mediated knockdown and genetic knockout of Ppara in mice produce phenotypes such as hypoglycemia and hypertriglyceridemia, the timing differs: siRNA-treated mice exhibited these phenotypes in the fed state, whereas in Ppara knockout mice, they emerged primarily after fasting. This suggests that siRNA KD induces a more immediate loss of function without compensatory adaptation, unlike genetic KO, where such mechanisms may develop over time (De Souza et al., 2006). Similarly, Speicher and colleagues compared siRNA-mediated knockdown and CRISPR-Cas9 KO of β1-integrins in liver regeneration, revealing that while both methods impair hepatocyte proliferation and regeneration, the KO leads to more severe effects, including lethality after hepatectomy. In contrast, KD retains residual gene expression, mitigating severity and facilitating mechanistic studies. This indicates that siRNA-mediated KD can closely mimic KO phenotypes with reduced severity, providing a useful model for studying partial gene function loss, akin to certain human diseases (Speicher et al., 2014).

To validate our findings in a different cell type, we analysed transcriptomic changes in MEFs with FIH knockout. While fewer DEGs were identified compared to MRC5 cells, GO term enrichment indicated that FIH depletion upregulated processes related to tissue morphogenesis and ECM organisation, while downregulated processes were associated with cell cycle regulation, metabolism, and developmental processes. GSVA analysis revealed downregulation of pathways such as IL6-JAK-STAT3 signaling, TGF-β signaling, and Notch signaling, whereas pathways like PI3K-AKT-mTOR signaling, apoptosis, and epithelial-mesenchymal transition were upregulated. Tissue remodeling is a multifaceted process involving distinct and sometimes opposing pathways. In our analyses, the upregulated terms (e.g., ECM organisation, connective tissue development) were mainly driven by genes linked to matrix deposition and structural organisation, whereas the downregulated terms (e.g., cell migration, tissue morphogenesis) reflected genes involved in motility and developmental patterning. Taken together, these findings suggest that FIH depletion does not globally activate or suppress tissue remodeling, but rather shifts its balance—enhancing ECM deposition while reducing regenerative or developmental remodeling.

Additionally, comparison between human lung fibroblasts and MEFs highlighted distinct transcriptional responses, with human cells exhibiting consistent downregulation

of proliferation-related pathways, while MEFs displayed upregulation of developmental processes and morphogenesis pathways. Despite these differences, shared downregulated processes across both cell types were related to cell migration, morphogenesis, and skeletal system development, indicating that FIH plays a crucial role in regulating pathways governing cell movement and tissue structuring.

MEFs are cells derived from the connective tissue of developing mouse embryos. They are commonly used in laboratory settings for a variety of purposes, such as gene knockout studies, virus propagation, and as feeder layers to support the growth of stem cells (Conner, 2000). MEFs serve as a model for studying cellular processes like proliferation, differentiation, and response to genetic modifications, making them a versatile tool for both basic and applied biological research. It is rational to hypothesise that development related pathways may be more sensitive in MEFs response to loss of target genes.

The comparison of human and mouse transcriptomes reveals both similarities and differences in gene expression profiles. Although overall gene expression is conserved between the species, the extent of conservation depends on the tissues and genes being analysed. This variation is not directly linked to regulatory sequence conservation, as even shared biological pathways may differ in regulatory mechanisms between humans and mice. For instance, immune and inflammatory responses show transcriptional differences, potentially due to species-specific regulatory elements. Non-coding RNA elements, such as lncRNAs and small RNAs, exhibit less conservation between species compared to protein-coding genes, complicating direct transcriptomic comparisons.

One example is cystic fibrosis (OMIM 219700); while mouse models have been crucial in discovering genetic correction strategies (Egan, 2009), they fail to fully replicate the spontaneous lung disease seen in humans (Fisher et al., 2011). Another example is the study by Obeidat and colleagues, who compared gene expression in smoke-exposed murine lungs to human lungs. They found a significant overlap in smoking-induced gene expression, with nearly half of the human smoking signature shared with murine lung profiles, particularly in genes related to immune response and detoxification pathways. However, only a modest overlap was found between murine models and severe COPD signatures in humans, suggesting that mice more accurately model the effects of smoking rather than COPD-specific changes (Obeidat et al., 2018). Furthermore, approximately 6% of the shared genes were oppositely regulated between the two species, which may be due to inherent biological differences or differences in smoke exposure duration.

Combining above all information, the expression patterns of genes are more species-specific, particularly for non-coding elements, adding to the complexities of translating findings from mouse models to human biology. These complexities emphasize that the

applicability of mouse transcriptomes to human biology depends on the specific genes, tissues, and biological processes in question. For some tissues, such as brain, heart, and liver, there is a higher conservation of gene expression, while other tissues with less specific gene activity exhibit greater interspecies differences.

Overall, our findings demonstrate that FIH depletion leads to significant and diverse transcriptomic changes, affecting key biological processes such as cell proliferation, metabolism, cellular response to stimuli, and ECM organisation across different fibroblast models. These data highlight the critical role of FIH in regulating cellular behavior and underscore the need for further exploration of its function in the context of lung fibrosis and other fibrotic diseases.

Chapter 4

FIH as a metabolic switch in lung fibroblasts

4.1 Introduction and rationale

4.1.1 Cellular metabolism

Core metabolism can be simplified to those pathways involving abundant nutrients like carbohydrates, fatty acids, and amino acids, essential for energy homeostasis and macromolecular synthesis in humans. Pathways of core metabolism can then be separated conveniently into three classes: i) Anabolism: those that synthesize simple molecules or polymerize them into more complex macromolecules; ii) Catabolism: those that degrade molecules to release energy; iii) Waste disposal: those that help to eliminate the toxic waste produced by the other classes (DeBerardinis and Thompson, 2012). Among these three classes, the pathways responsible for energy production in humans and other organisms include core activities such as glycolysis (including the Warburg effect in cancer cells), the tricarboxylic acid (TCA) and urea cycles (Krebs), glycogen catabolism (Cori and Cori), OXPHOS (Mitchell), and the supremacy of ATP in energy transfer reactions (Lipmann). According to our bioinformatic analysis in the previous chapter, we firstly wanted to study the role of FIH in two of the most common biological metabolic process, glycolysis and oxidatice phosphrylation.

4.1.1.1 Glycolysis

Glycolysis is a metabolic process that converts glucose ($C_6H_{12}O_6$) into pyruvate within the cytosol of most cells. This conversion releases free energy, which is utilized to synthesize adenosine triphosphate (ATP) and reduced nicotinamide adenine dinucleotide (NADH), both of which are crucial high-energy molecules.

The entire glycolytic pathway is composed of ten sequential enzymatic reactions, each facilitated by a specific enzyme. It begins with glucose being phosphorylated by hexokinase to form glucose-6-phosphate, which is then rearranged into fructose-6-phosphate by phosphoglucose isomerase. Phosphofructokinase-1 adds a second phosphate group, producing fructose-1,6-bisphosphate, which aldolase cleaves into two three-carbon molecules, glyceraldehyde-3-phosphate (G3P) and dihydroxyacetone phosphate (DHAP). DHAP is quickly converted into G3P by triose phosphate isomerase, allowing both molecules to proceed through the pathway. G3P is oxidized and phosphorylated by glyceraldehyde-3-phosphate dehydrogenase to form 1,3-bisphosphoglycerate and NADH. Phosphoglycerate kinase then transfers a phosphate group from 1,3-bisphosphoglycerate to ADP, creating ATP and 3-phosphoglycerate. This compound is converted into 2-phosphoglycerate by phosphoglycerate mutase, which is then dehydrated by enolase to produce phosphoenolpyruvate (PEP). The final step, catalysed by pyruvate kinase, transfers the phosphate group from PEP to ADP, resulting in the formation of ATP and pyruvate (Xiong et al., 2011; Malaisse et al., 2004) (Figure. 4.1).

Glycolysis occurs in both aerobic and anaerobic conditions. In aerobic glycolysis, glucose is metabolized to pyruvate in the cytosol, generating ATP and NADH. When oxygen is present, pyruvate is transported to the mitochondria, where it is fully oxidized, allowing for more efficient ATP generation through subsequent metabolic pathways. When oxygen is absent, pyruvate is reduced to lactate by lactate dehydrogenase, regenerating NAD+ and allowing glycolysis to continue. This process is called anaerobic glycolysis and and in the context of cancer cells is refered to as the Warburg effect. It provides a quick but limited supply of ATP, which is especially important in muscles during intense exercise (Lunt and Vander Heiden, 2011).

4.1.1.2 TCA cycle and oxidative phosphorylation

The tricarboxylic acid cycle -also known as the Krebs cycle-is a broadly conserved metabolic pathway consisting of a cyclic series of chemical reactions that harness high-energy electrons from fuel sources (Krebs and Johnson, 1937, 1980). The TCA cycle begins with the condensation of acetyl-CoA and oxaloacetate (OAA) to form citrate, catalysed by citrate synthase. Citrate is then isomerized to isocitrate by aconitase. Next, isocitrate undergoes oxidative decarboxylation by isocitrate dehydrogenase to produce α-ketoglutarate and CO_2, with the concomitant reduction of NAD^+ to NADH. α-Ketoglutarate is further oxidatively decarboxylated by the α-ketoglutarate dehydrogenase complex, forming succinyl-CoA, CO_2, and NADH. Succinyl-CoA is then converted to succinate by succinyl-CoA synthetase, generating ATP or GTP through substrate-level phosphorylation. Succinate is oxidized to fumarate by succinate dehydrogenase, coupled with the reduction of FAD to $FADH_2$. Fumarate is subsequently hydrated to malate by fumarase. Finally, malate is oxidized to regenerate oxaloacetate by malate

dehydrogenase, producing NADH and completing the cycle (Arnold and Finley, 2023; Ryan and O'Neill, 2020). The electron transport chain (ETC) is a series of protein complexes located in the inner mitochondrial membrane, crucial for OXPHOS. NADH (generated from glycolysis and the TCA cycle) and $FADH_2$ (generated from the TCA cycle) deposit their electrons onto the ETC. These electrons pass through Complexes I, II, III, and IV, ultimately reducing oxygen to water. As electrons move through the chain, protons are pumped from the mitochondrial matrix into the intermembrane space, creating an electrochemical proton gradient. This gradient drives protons back into the matrix through ATP synthase (Complex V), enabling the synthesis of ATP from ADP and inorganic phosphate (Figure. 4.1). Thus, the ETC is essential for converting the energy stored in electron carriers into ATP, the cell's primary energy currency (Cogliati et al., 2021).

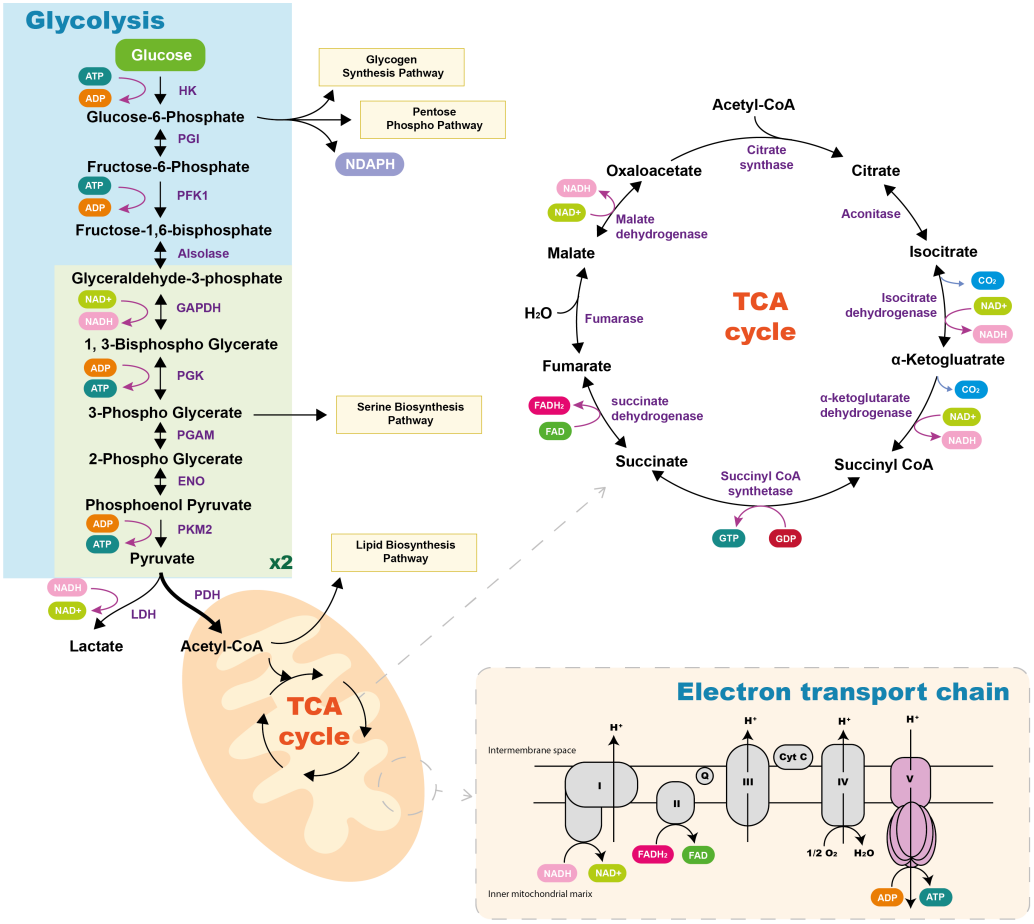

FIGURE 4.1: **Integrated overview of glycolysis, the TCA Cycle, and the electron transport chain**

This diagram provides a detailed overview of the interconnected biochemical pathways involved in cellular energy production: glycolysis, the TCA cycle, and ETC. **Glycolysis**: Shown on the left, this process converts glucose to pyruvate in the cytoplasm, generating ATP and NADH. Key enzymes and alternative fates of glucose intermediates, such as lactate formation and entry into the TCA cycle, are depicted. **TCA Cycle**: Located in the mitochondria, the TCA cycle oxidizes acetyl-CoA to produce NADH, $FADH_2$, and GTP, with labeled intermediates and enzymes. **Electron Transport Chain (ETC)**: Depicted at the bottom right, the ETC uses electrons from NADH and $FADH_2$ to drive ATP production through OXPHOS, with oxygen as the final electron acceptor. HK: Hexokinase; PGI: Phosphoglucose Isomerase; PFK1: Phosphofructokinase-1; GAPDH: Glyceraldehyde-3-Phosphate Dehydrogenase; PGK: Phosphoglycerate Kinase; PGAM: Phosphoglycerate Mutase; ENO: Enolase; PKM2: Pyruvate Kinase M2; LDH: Lactate Dehydrogenase; PDH: Pyruvate Dehydrogenase; TCA: Tricarboxylic Acid (Cycle); FAD^+: Flavin Adenine Dinucleotide (oxidized form); $FADH_2$: Flavin Adenine Dinucleotide (reduced form); NAD^+: Nicotinamide Adenine Dinucleotide (oxidized form); NADH: Nicotinamide Adenine Dinucleotide (reduced form); ADP: Adenosine Diphosphate; ATP: Adenosine Triphosphate.

4.1.1.3 Metabolic reprogramming/Warburg effect

In the presence of oxygen, most differentiated cells mainly metabolize glucose via glycolysis, TCA cycle and OXPHOS to maximaze ATP production, with minimal production of lactate. It is only under anaerobic conditions that differentiated cells prorduce large amounts of lactate. However, in cancer cells and other proliferating or developing cells, the rate of glucose uptake dramatically increases and large amount of lactate is produced regardless of the availablility of oxygen. This process is known as the Warburg Effect (Warburg, 1956). The metabolic reprogramming has several critical functions that can benefit cancer cells. Firstly, it enables rapid ATP production through glycolysis, which, although less efficient per glucose molecule compared to OXPHOS, can occur at a much faster rate (Shestov et al., 2014). This rapid ATP synthesis provides a selective advantage in tumor environments where energy resources are limited, and there is competition for nutrients.

In addition to supporting energy production, the Warburg effect facilitates biosynthesis by diverting glucose metabolites into anabolic pathways. These pathways provide the necessary building blocks for nucleotide, lipid, and protein synthesis, which are crucial for sustaining the accelerated proliferation of cancer cells (Locasale and Cantley, 2011; Vander Heiden et al., 2009). The effect also contributes to the acidification of the tumor microenvironment due to increased lactate production. This acidic environment promotes tumor invasiveness and helps cancer cells evade immune surveillance by impairing the function of immune cells (Chang et al., 2015; Ho et al., 2015; Colegio et al., 2014).

Furthermore, the Warburg effect may play a role in cellular signaling, particularly through the regulation of reactive oxygen species (ROS) (Chang et al., 2013; Locasale and Cantley, 2011) and chromatin modifications (Cluntun et al., 2015; Lu and Thompson, 2012; Liberti and Locasale, 2016). Alterations in ROS levels can affect various signaling pathways, promoting cell survival and proliferation. Meanwhile, the production of acetyl-CoA during glycolysis can influence histone acetylation, thereby impacting gene expression and further driving oncogenic processes (Wellen et al., 2009). Despite these proposed benefits, the full functional implications of the Warburg effect in cancer are complex and continue to be a subject of extensive research, as many aspects of its role in tumor biology remain incompletely understood.

4.1.2 Metabolic alteration in lung disease

Given the well-established occurrence of the Warburg effect in cancer cells, we review the metabolic alterations specific to lung cancer here. Lung cancer is a disease with a high incidence and mortality rate globally. It is mainly divided into small cell lung cancer (SCLC) and non-small cell lung cancer (NSCLC). In lung cancer, the glycolytic

pathway is markedly upregulated, driven by key enzymes and associated oncogenic signaling pathways. Glucose transport into cells is mediated by GLUT1, whose inhibition by WZB117 reduces glucose uptake and suppresses tumor growth, particularly in combination with chemotherapy agents like cisplatin and paclitaxel in A549 cells (Liu, Cao, Zhang, Bergmeier, Qian, Akbar, Colvin, Ding, Tong, Wu et al., 2012). Upon entry into the cell, glucose is phosphorylated by hexokinase 2 (HK2), a reaction crucial for promoting glucose metabolism in tumors. Targeting HK2 with inhibitors such as 2-deoxy-D-glucose (2-DG) enhances the efficacy of conventional chemotherapy and reverses drug resistance in NSCLC. 2-DG combined with Adriamycin or paclitaxel can significantly delay tumor growth and prolong the survival time of mice with NSCLC (Maschek et al., 2004). As glycolysis progresses, phosphofructokinase 1 (PFK1), activated by upstream factors like YAP1 (Lin et al., 2021), drives the conversion of fructose-6-phosphate, furthering glycolytic flux. Pyruvate kinase M2 (PKM2), predominantly expressed in lung cancer, catalyses the final step of glycolysis, generating pyruvate and ATP; its inhibition sensitizes cancer cells to chemotherapy by promoting apoptosis (Guo et al., 2011; Shi et al., 2010). Additionally, lactate dehydrogenase (LDH) upregulation facilitates the conversion of pyruvate to lactate, which not only fuels tumor growth through various metabolic pathways but also promotes immune evasion and drug resistance. Inhibition of LDH activity by small interfering RNA or oxalate can overcome the drug resistance of tumor cells to paclitaxel and trastuzumab (Zhao et al., 2011; Zhou et al., 2010). These metabolic alterations are often regulated by HIF1α and MYC, which regulate the expression of key glycolytic enzymes (Xie et al., 2015), perpetuating the Warburg effect in lung cancer cells.

Moreover, there are a lot of studies reporting the metabolic reprogramming also happens in chronic lung disease such as IPF. According to current studies, one of the most notable changes in pulmonary fibrosis is the upregulation of glycolysis in fibroblasts and myofibroblasts, the key effector cells responsible for ECM production. Researchers have identified an increased expression of GLUT1 in the lungs of patients with IPF and in a bleomycin-induced pulmonary fibrosis mouse model (Andrianifahanana et al., 2016). The induction of TGF-β was found to elevate both mRNA and protein levels of GLUT1 in mouse fibroblast cell lines and primary cells, thereby enhancing glucose uptake (Cho et al., 2017; Inoki et al., 1999; Zhao et al., 2018). After transportation of glucose into cells by GLUTs, there are several key glycolytic enzymes that catalyse the reactions in glycolysis. The abnormal expression of these key glycolytic enzymes in pulmonary fibrosis may regulate the progression of fibrosis. After comprehensive analysis of the gene expression profile and major metabolic programs of alveolar macrophages in bleomycin-induced lung fibrosis mice, researchers found that alveolar macrophages in fibrotic lungs induced by bleomycin and active TGF-β exhibited predominant pro-fibrotic M2-like characteristics. Furthermore, these fibrotic alveolar macrophages were often accompanied by significantly enhanced glycolysis and upregulation of various key glycolytic intermediates (Xie et al., 2017). As a typical pro-fibrotic cytokine, TGF-β

can promote glucose consumption in fibroblasts. It has been shown to induce an increase in lactate levels and enhance the expression levels of glycolytic enzymes, including HK1, PFK, pyruvate kinase M1 (PKM1), and pyruvate dehydrogenase kinase isoform 1 (PDK5) (Selvarajah et al., 2019). Xie *et al.* found that myofibroblasts in IPF exhibit a significant increase in glycolysis which is marked by the upregulation of several key glycolytic enzymes, notably 6-phosphofructo-2-kinase/fructose-2,6-bisphosphatase 3 (PFKFB3). The upregulation of PFKFB3 and the resulting glycolytic shift in myofibroblasts are driven by TGF-β. The application of the inhibitor targeting PFKFB3, 3PO, was shown to attenuate the profibrotic phenotype of myofibroblasts (Xie et al., 2015).

The increased glycolytic activity serves several purposes in fibrotic cells. First, it provides rapid ATP production to meet the high energy demands of fibroblast proliferation and ECM synthesis. Second, glycolysis generates biosynthetic precursors, such as G6P, which can enter the pentose phosphate pathway (PPP) to produce ribose-5-phosphate for nucleotide synthesis and NADPH for reductive biosynthesis and antioxidant defense (Nigdelioglu et al., 2016). Third, the production of pyruvate and its subsequent conversion to lactate by LDH leads to an acidic microenvironment, which can further promote fibrosis by activating latent TGF-β and enhancing the invasive capacity of myofibroblasts (Kottmann et al., 2012).

Mitochondrial dysfunction is another hallmark of metabolic reprogramming in pulmonary fibrosis. In healthy cells, mitochondria efficiently oxidize pyruvate derived from glycolysis via the TCA cycle and OXPHOS to generate ATP. However, in fibrotic fibroblasts, mitochondrial respiration is often impaired due to decreased expression of key enzymes in the TCA cycle and OXPHOS complexes (Álvarez et al., 2017). This impairment leads to reduced ATP production from OXPHOS and an increased reliance on glycolysis for energy.

The dysfunction in mitochondrial respiration is often associated with increased production of ROS, which can further exacerbate fibrosis. Elevated ROS levels promote the activation of profibrotic signaling pathways (Bocchino et al., 2010), including those mediated by TGF-β, and contribute to oxidative damage of cellular components, perpetuating the fibrotic process. Moreover, the reduced efficiency of mitochondrial metabolism limits the ability of cells to utilize fatty acids and glutamine as alternative energy sources, thereby reinforcing the dependence on glycolysis (Bueno et al., 2020).

4.1.3 Cellular senescence in IPF

Cellular senescence is an evolutionarily conserved state of stable replicative arrest induced by pro-ageing stressors also implicated in IPF pathogenesis, including telomere attrition, oxidative stress, DNA damage and proteome instability. Accumulated cellular damage activates cyclin-dependent kinase inhibitors such as $p16^{Ink4a}$ and the

p53-p21$^{Cip1/Waf1}$ pathway, which in turn inhibit cyclin-dependent kinases, leading to a halt in cell cycle progression. Through the secretion of the senescence-associated secretory phenotype (SASP), which includes a wide range of cytokines, chemokines, matrix-remodeling proteases, and growth factors, senescent cells can paracrinely induce the proliferation of nearby cells and exacerbate tissue deterioration(Van Deursen, 2014). On the other hand, cellular senescence serves as an autonomous mechanism to suppress proliferation, playing a pivotal role in cutaneous wound healing (Demaria et al., 2014) and in limiting pathological processes like liver fibrosis (Krizhanovsky et al., 2008).

An increasing evidence suggests that accelerated aging mechanisms, including cellular senescence, play a crucial role in the pathogenesis of IPF (Faner et al., 2012; Schafer et al., 2017; Armanios et al., 2007; Hashimoto et al., 2016). Key senescence biomarkers such as p16, p21, and senescence-associated β-galactosidase activity have been detected in both fibroblasts and epithelial cells within human IPF lung tissue (Chen et al., 2020; Kuwano et al., 1996). Furthermore, cells from IPF patients exhibit a heightened propensity for senescence when studied ex vivo (Yanai et al., 2015). In bleomycin-induced lung fibrosis mouse models, the bleomycin-induced lung injury triggers a senescence-associated molecular signature in alveolar epithelial cells (Aoshiba et al., 2003, 2013), and the age-dependent accumulation of senescent myofibroblasts may hinder the resolution of fibrosis after bleomycin exposure (Hecker et al., 2014). Very interestingly, overexpression of an enzyme involved in the production of the extracellular matrix component hyaluronan worsens bleomycin-induced lung injury (Li et al., 2011), whereas depletion of this enzyme seems to activate senescence (Li et al., 2016), challenging a negative role for senescence in bleomycin-induced lung fibrosis.

These observations highlight the dual role of cellular senescence in IPF, where it can both protect against and contribute to disease progression. The challenge lies in carefully targeting senescence pathways to mitigate fibrosis without disrupting their beneficial effects on tissue repair.

4.1.4 The role of FIH in metabolic reprogramming

Several studies have highlighted the role of FIH in the regulation of cellular metabolism. It has been observed that impairment of FIH often induces the expression of glycolytic genes in a HIF-dependent manner. For instance, Sakamoto *et al.* reported that inhibition of FIH through its interaction with Mint3 led to increased expression of SLC2A1, which encodes GLUT1, in triple-negative breast cancer cell lines under normoxia (Sakamoto et al., 2011). Similarly, Wang *et al.* demonstrated that FIH inhibition elevated GLUT1 mRNA levels in glioblastoma cell lines under hypoxic conditions (Wang et al., 2014). Further, Sim *et al.* found that deletion of HIF1AN, the gene encoding FIH, caused increased glycolysis when oxidative metabolism was compromised in FIH-null MEFs

(Sim et al., 2018). These findings suggest that in many diseases, the loss of FIH typically induces glycolysis via HIF activation.

Interestingly, Zhang *et al.* discovered that deletion of FIH alters cellular metabolism, leading to increased intracellular ATP levels in MEFs and suppression of AMP kinase activation in developing embryos, without the expected acidosis and increased glycolysis typically associated with HIF activation (Zhang et al., 2010). Whole-body energy expenditure analysis in FIH mutants revealed an accelerated metabolic rate, yet no evidence of increased glycolysis, indicating that the altered metabolism in these mutants is not simply a result of increased HIF activity.

Beyond the HIF pathway, FIH has been implicated in the regulation of other metabolic processes. Scholz and colleagues identified the deubiquitinase OTUB1 as a target of FIH-mediated hydroxylation. Mutation of the hydroxylation site N22 of OTUB1 in HEK293 cells altered interactions with several metabolism-related proteins, highlighting the broader metabolic influence of FIH (Scholz et al., 2016). Additionally, Garcia *et al.* reported FIH expression in normal lung tissue as well as in LUAD and LUSC. Depletion of FIH via CRISPR-Cas9 increased glucose uptake and lactate production under both normoxic and hypoxic conditions, though the underlying mechanisms remain unclear (García-del Río et al., 2023).

These researches underscore the multifaceted role of FIH in metabolic regulation, extending beyond its interaction with the HIF pathway to influence broader aspects of cellular metabolism.

4.1.5 The role of FIH in cellular senescence

FIH has been implicated in various cellular processes and cancer pathologies through its interaction with multiple signaling pathways. Kato *et al.* demonstrated that overexpression of FIH in an endometrial cancer cell line (HHUA cells) disrupted HIF1 activity, leading to the induction of senescent cell morphology and a significant increase in β-gal positive cells, markers of cellular senescence. In addition, FIH has been shown to play a crucial role in tumor growth by suppressing the p53-p21 axis in colon carcinoma and melanoma cells (Pelletier et al., 2012).

Furthermore, Kaplan *et al.* identified a multifaceted role for FIH in the regulation of p63α levels in the epidermis and limbal epithelium (Kaplan et al., 2020). This regulation is achieved through several mechanisms: FIH interacts with novel targets such as Plectin1 and STAT1 to upregulate p63α expression, inactivates ASPP2 to further enhance p63α levels, and inhibits HDAC1 to prevent GADD45α expression, which in turn elevates p63α—a process associated with the regulation of keratinocyte senescence (Lena et al., 2012).

These findings underscore the diverse roles of FIH in modulating cellular pathways that influence both tumor progression and cellular senescence, highlighting its potential as a therapeutic target in cancer and other diseases characterised by dysregulated cell growth and aging.

Typically studies on FIH have investigated its role as a HIF-1α regulator. Few studies have investigated the impact of FIH on metabolism or cellular senescence in a HIF-independent manner. Furthermore, the study of the role of FIH in lung fibrosis is lacking. Given our bioinformatic results, we wanted to investigate how the loss of FIH affects cellular metabolism and its role in cellular senescence.

4.2 Aim and Objectives

4.2.1 Aim

This study aims to explore the role of FIH in the regulation of cellular metabolism and its contribution to cellular senescence in human lung fibroblasts. We intend to determine the effects of FIH loss on key metabolic pathways, such as glycolysis and OXPHOS, and to uncover potential HIF-independent mechanisms involved in these processes.

4.2.2 Objectives

1. To investigate the effects of FIH knockdown on mitochondrial respiration and oxidative phosphorylation in lung fibroblasts using Seahorse real-time mitochondrial stress assays.
2. To analyse the impact of FIH depletion on glycolysis by measuring extracellular acidification rates and lactate production.
3. To conduct metabolomic profiling through NMR to identify metabolic shifts resulting from the loss of FIH.
4. To examine the induction of cellular senescence in FIH-deficient fibroblasts and assess whether these effects occur independently of the HIF pathway.

4.3 Results

4.3.1 Mitostress test reveals FIH depletion inhibits mitochondrial function

Following our bioinformatic analysis, we investigated the potential impact of FIH loss on mitochondrial function. We began by conducting a Seahorse real-time mitochondrial stress assay. NHLFs were subjected to FIH knockdown for 72 hours before being tested. The oxygen consumption rate (OCR) was recorded every 5 minutes for a total of 20 minutes after each injection (Figure. 4.2A).

As shown in Figure. 4.2B and C, siRNA-mediated FIH knockdown (siFIH) led to a significant decrease in both basal (control vs siFIH = 5.85 vs 3.01, $P = 0.003$) and maximal respiration OCR (control vs siFIH = 9.85 vs 6.59, $P = 0.004$), indicating that FIH loss impairs both baseline oxidative phosphorylation (OXPHOS) and maximal mitochondrial capacity. To explore potential links with HIF signalling, we separately knocked down FIH, HIF-1β, and both genes simultaneously in NHLFs for 72 hours. HIF-1β depletion alone did not significantly affect basal (control vs siHIF-1β = 5.85 vs 6.57, $P = 0.65$) or maximal respiration OCR (control vs siHIF-1β = 9.85 vs 11.1, $P = 0.39$). Interestingly, co-depletion of HIF-1β reversed the reduction in basal OCR (siFIH vs siFIH+siHIF-1β = 3.01 vs 6.48, $P < 0.001$) and maximal respiration OCR (siFIH vs siFIH+siHIF-1β = 6.59 vs 11.4, $P < 0.001$) observed with FIH knockdown, suggesting that HIF-related pathways may contribute to the mitochondrial changes observed upon FIH loss.

To further assess cellular energy metabolism, ATP production was measured using the Celltiter-Glo kit (Figure. 4.2D). FIH depletion significantly reduced ATP levels compared to controls (siFIH/control = 0.56, $P < 0.001$). Co-depletion of FIH and HIF-1β also resulted in reduced ATP production (siFIH+siHIF-1β/control = 0.54, $P < 0.001$), which did not align with the OCR findings. This discrepancy likely reflects the contribution of other energy-generating pathways, such as glycolysis, which may not be regulated through HIF-related mechanisms.

Given the central role of TGF-β in fibrosis, we next investigated the effect of FIH depletion on mitochondrial function under TGF-β stimulation. MRC5 cells were first transfected with siRNA targeting FIH and then treated with PBS or TGF-β after 24 hours. After an additional 48 hours, cells were subjected to the Seahorse assay (Figure. 4.3A). Compared to the control group, FIH knockdown reduced both basal and maximal OCR (Basal OCR: control vs siFIH = 7.83 vs 5.63, $P < 0.001$; Maximal OCR: control vs siFIH = 16.6 vs 10.2, $P = 0.004$) (Figure. 4.3B, C). Interestingly, after 48-hour TGF-β treatment, both basal and maximal OCR were significantly increased compared to the untreated groups (Basal OCR: siFIH vs siFIH+TGF-β = 5.63 vs 9.62, $P < 0.001$; Maximal OCR: siFIH vs siFIH+TGF-β = 10.2 vs 24.9, $P < 0.001$). In this setting, FIH knockdown no longer reduced OCR, suggesting that TGF-β may override the metabolic effects of FIH depletion.

Building on bioinformatic analysis in Chapter 3 (Figure. 3.17), which indicated differences between FIH KO and siFIH cells, we performed the Seahorse assay in FIH WT and KO MRC5 cells (Figure. B.6D, Appendix B). FIH knockout alone did not significantly affect basal or maximal OCR. However, after 48-hour TGF-β treatment, both parameters were significantly reduced compared to untreated cells. These findings suggest that MRC5 cells may adapt to long-term FIH loss, restoring mitochondrial function, whereas acute knockdown produces more immediate changes. The interplay between FIH and TGF-β signalling in regulating mitochondrial function remains to be clarified.

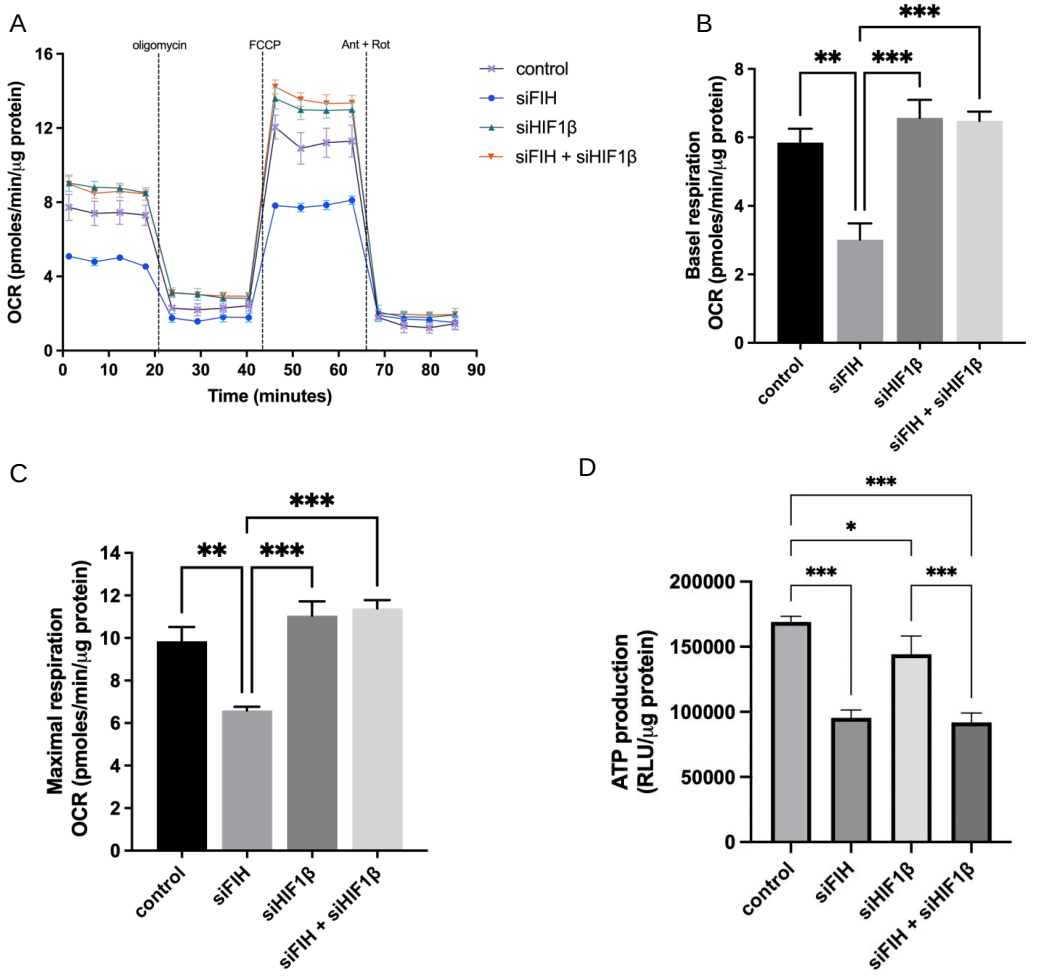

FIGURE 4.2: **FIH depletion impairs mitochondrial function in NHLFs in a HIF-dependent manner**

NHLFs were transfected with siRNA targeting FIH for 72 hours, then subjected to determination of real-time OCR (A). Basal OCR (B) and Maximal respiration OCR. (C) were calculated from data shown in A (mean ± SD, n = 4). *P $<$ 0.05, **P $<$ 0.01, *** P $<$ 0.001 by Tukey's multiplecomparison test. (D) Graph showing the relative ATP production in NHLFs transfected with siRNA oligos indicated for 72 hours using the CellTiter Glo assay. The data was normalized to protein content (μg) in parallel wells (mean ± SD, n = 3). *P $<$ 0.05, **P $<$ 0.01, *** P $<$ 0.001 by Tukey's multiple comparison test. OCR, oxygen consumption rate.

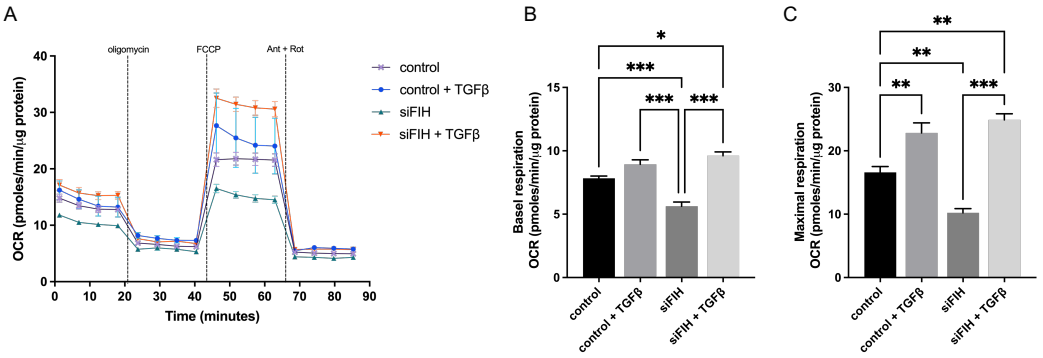

FIGURE 4.3: **FIH depletion inhibits mitochondrial OXPHOS, but can be interfered by TGF-β**

MRC5 cells were transfected with siRNA targeting FIH for 72 hours, followed by real-time measurement of OCR (A). Basal OCR (B) and maximal respiration OCR (C) were calculated from the data shown in (A) (mean ± SD, n = 4). *P $<$ 0.05, **P $<$ 0.01, *** P $<$ 0.001 by Tukey's multiplecomparison test. OCR, oxygen consumption rate.

4.3.2 Glycolytic stress test and Lactate-Glo assay indecated FIH depletion inhibits glycolysis in human lung fibroblasts

Cells often increase their glycolytic activity to ensure energy supply when mitochondrial function is impaired. To further investigate the potential impacts of FIH knockdown on glycolysis in human lung fibroblasts, we measured the extracellular acidification rate (ECAR), an indicator of glycolysis at regular ten-minute intervals before and after each reagent addition (Figure.4.4A).

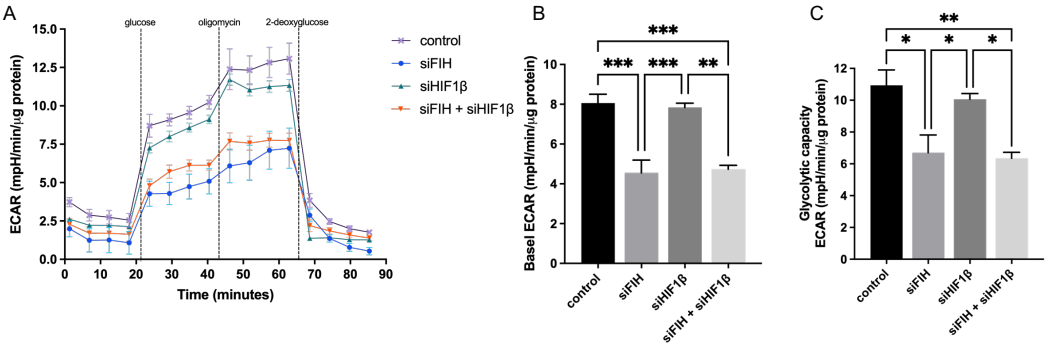

FIGURE 4.4: **FIH depletion inhibits glycolysis independent with the activity of HIF1α pathway in NHLFs**

(A–C) NHLFs were transfected with siRNA targeting FIH for 72 hours, followed by real-time measurement of ECAR (A). Basal ECAR (B) and glycolytic capacity ECAR (C) were calculated from the data shown in (A) (mean ± SD, n = 4). *P $<$ 0.05, **P $<$ 0.01, *** P $<$ 0.001 by Tukey's multiple comparison test. ECAR, extracellular acidification rate.

In addition, NHLFs were used alongside MRC5 cells to validate findings in primary human fibroblasts, as their limited passage capacity makes them unsuitable for CRISPR-based knockout but well-suited for transient siRNA experiments. In NHLFs, we individually knocked down FIH, HIF-1β, and both together. The results (Figure. 4.4B, C) showed that FIH depletion significantly reduced both basal ECAR (control vs siFIH = 8.06 vs 4.55, $P < 0.001$) and glycolytic capacity ECAR (control vs siFIH = 10.94 vs 6.70, $P = 0.0111$). In contrast, HIF-1β knockdown alone had no effect on glycolysis and did not prevent the reductions in ECAR observed with FIH depletion. These data therefore suggest that the effect of FIH on glycolysis in lung fibroblasts is unlikely to be mediated solely through HIF-1β.

To further validate these findings, we performed a Lactate-Glo assay to measure lactate production in fibroblasts. WT and FIH KO MRC5 cells were transfected with siRNA targeting HIF-1β for 72 hours, after which both culture medium and cell lysates were collected following the manufacturer's protocol (Figure. 4.5A, B). FIH knockout led to reduced intracellular and extracellular lactate levels, although the decreases were not statistically significant. In culture medium, HIF-1β depletion increased lactate levels but did not reverse the reduction seen with FIH KO. Conversely, in cell lysates, HIF-1β knockdown decreased lactate levels and further reduced lactate production in FIH KO MRC5 cells.

Together with the Seahorse results, these findings indicate that loss of FIH alters glycolytic metabolism in human lung fibroblasts through mechanisms that appear not to rely exclusively on HIF-1β regulation.

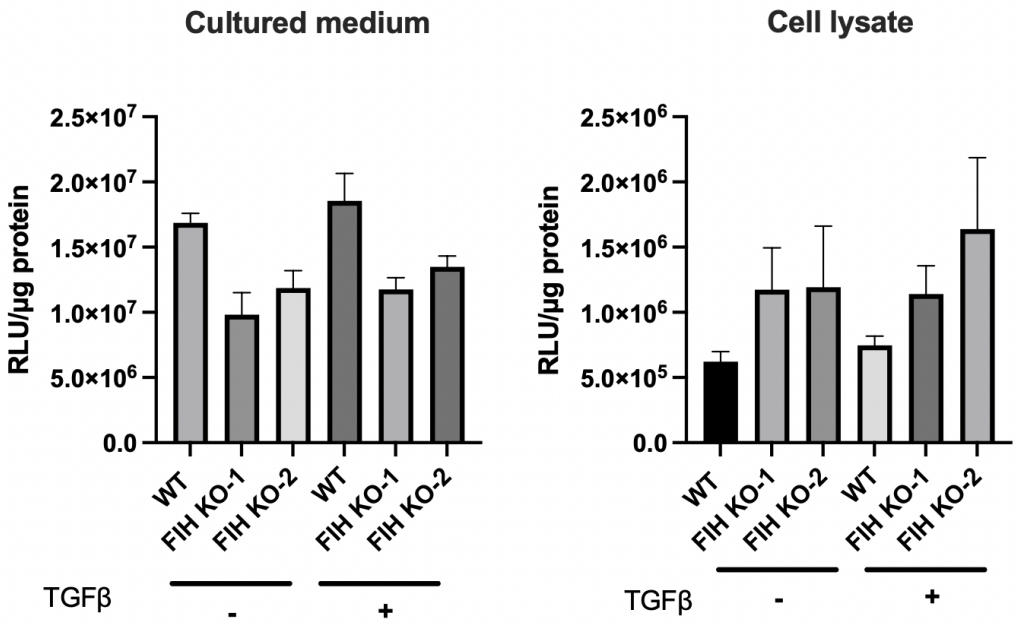

FIGURE 4.5: **FIH depletion reduced the extracellular lactate level which is independent with the activity of HIF1α pathway in MRC5 cells**

MRC5 cells were tranfected with siRNA as indicated for 72 hours. The extracellular (A) and intracellular (B) lactate level was detected using Lactate-Glo kit (Promega, UK). Data from 2 independent biological samples of 3 replicates were plotted which was normalized to the protein level.

We also want to know if TGF-β plays a role in the regulation of glycolysis when FIH is depleted in human lung fibroblasts, so we performed seahorse glycolytic stress test on MRC5 cells transfected with siRNA targeting FIH and treated with TGF-β as indicated (Figure. 4.6 A). The depletion of FIH reduced both basal and glycolytic capacity ECAR (Figure.4.6 B and C) (Basal ECAR: control vs siFIH = 12.6 vs 9.45, P = 0.04; glycolytic capacity ECAR: 18.31 vs 12.73, P = 0.0255), while 48-hour TGF-β treatment didn't reverse both ECAR completely. To further validate the results, we also treated FIH WT and KO MRC5 cells with TGF-β for 48 hours and then send the cells to the seahorse assay (Figure. B.2 A). Consistent with the results using NHLFs in which FIH was knocked down, the basal and glycolytic capacity ECAR decreased in FIH KO MRC5 cells compared to FIH WT MRC5 cells meanwhile TGF-β treatment partially reversed both ECAR in FIH KO MRC5 (Figrue. B.2 B and C).

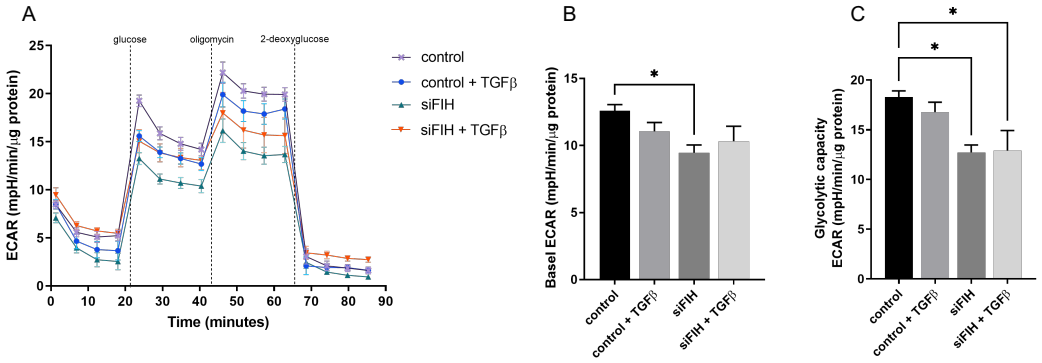

FIGURE 4.6: **FIH depletion inhibits glycolysis in MRC5 cells**
(A–C) MRC5 were transfected with siRNA targeting FIH for 72 hours, with 48-hour TGF-β treatment, then subjected to determination of real-time ECAR (A). Basal ECAR (B) and Glycolytic capacity OCR (C) were calculated from data shown in A (mean ± SD, n = 4). *P $<$ 0.05, **P $<$ 0.01, *** P $<$ 0.001 by Tukey's multiple comparison test. ECAR, Extracellular acidification rate.

The intracellualr and extracellualr lactate level were measured in both FIH WT and KO MRC5 cell lysate and cultured medium with or without TGF-β treatment. In the cultured medium, lactate levels were significantly reduced when FIH was depleted, while TGF-β treatment slightly increased lactate secretion from both WT and FIH KO MRC5 cells. In contrast, intracellular lactate levels showed a slight increase in FIH KO MRC5 cells and were further elevated by TGF-β treatment.

Based on these findings, we conclude that FIH depletion inhibits glycolysis in human lung fibroblasts in a HIF-independent manner, as evidenced by the reduced secretion of lactate. This regulatory effect appears to act upstream of TGF-β-mediated glycolysis. Additionally, there may be an alternative pathway influencing glycolysis that is not directly related to TGF-β, given that TGF-β only partially increased lactate secretion in MRC5 cells. The variability and low reproducibility of intracellular lactate measurements, due to their significantly lower levels compared to secreted lactate, prevent us from drawing firm conclusions about FIH's impact on intracellular lactate.

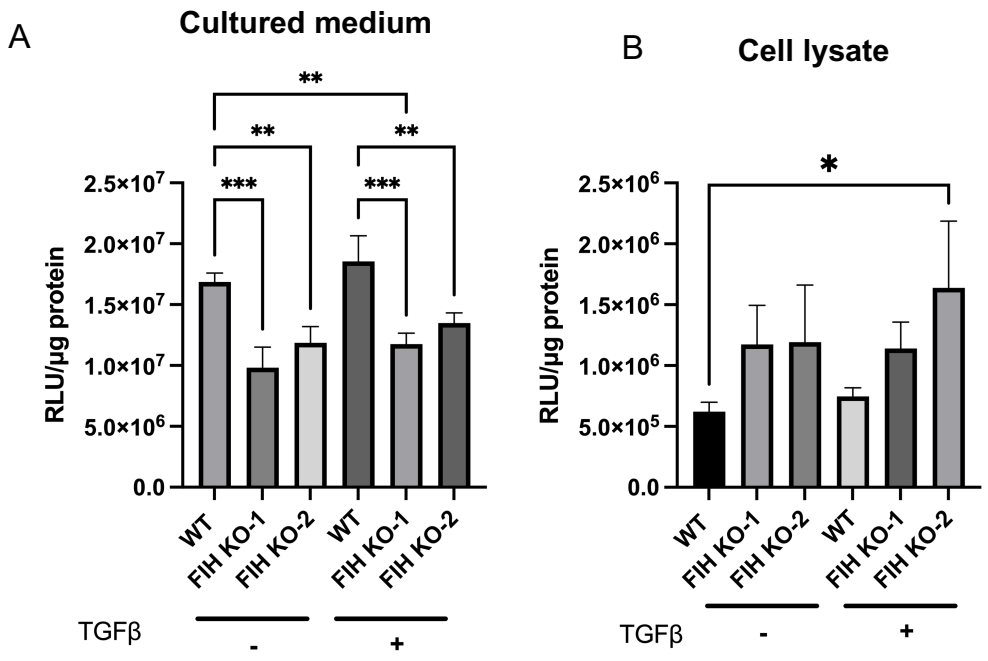

FIGURE 4.7: **FIH depletion reduced extracellular lactate level which was slightly reversed by TGF-β in MRC5 cells**

FIH WT MRC5 cells and two strains of FIH KO MRC5 cells constructed using CRISPR-Cas9 were treat with TGF-β (5ng/mL) for 48 hours. The extracellular (A) and intracellular (B) lactate levels was measured using Lactate-Glo kit (Promega, UK). Data from two independent biological repeats (n =2) with 3 technique repeats in each repeats were plotted.

4.3.3 Metabolic profiling of FIH knockout MRC5 cells reveals distinct lactate alterations following TGF-β treatment

To explore the impact of FIH deletion on cellular metabolism in MRC5 cells, we conducted ^{1}H-NMR-based metabolite screening. FIH WT MRC5 cells and a CRISPR-Cas9-generated FIH KO MRC5 cell line were treated with TGF-β (5 ng/mL) for 48 hours following the workflow as Figure.4.8. Cell lysates were then prepared and analysed by NMR (with the help from Dr. Johnathan Swann and Micheal Harvey). PCA of the ^{1}H-NMR spectral data revealed clear metabolic differences between the four experimental groups, indicating that both FIH status and TGF-β treatment significantly influence the metabolic profile of MRC5 cells (Figure.4.9 A). The distinct clustering observed in the PCA plot suggests that the loss of FIH alters the metabolic response to TGF-β stimulation.

A closer examination of the ^{1}H-NMR spectra allowed for the clear identification of lactate peaks, highlighting its role as a key metabolite affected by FIH deletion (Figure.4.9 B). Quantitative analysis of the spectra showed a significant increasing of intracellular

lactate levels in FIH KO cells compared to WT controls similar with the TGF-β treatment on WT cells. However, to our surprise, the loss of FIH showed a diffrent impact on the cell under TGF-β treatment. It reduced intracellular level under TGF-β treatment. Also, TGF-β treatment decreased lactate production in FIH KO cells (Figure.4.10 A). Additionally, similar result was observed in the ratio of lactate to pyruvate (Figure.4.10 B). We initially intended to analyse the cultured medium via NMR as Figure.4.8 shows; however, upon reviewing the data from the cell lysates, it became apparent that the cell count was significantly lower than expected. This low cell density complicated the assignment of specific metabolites, particularly in the cultured medium, due to the complexity and disruption of its components. Due to time constraints, we were unable to further optimize this aspect of the NMR analysis, and therefore, these results will be treated as supplementary. The current results suggest that FIH deletion significantly disrupts normal metabolic processes in MRC5 cells, particularly by increasing intracellular lactate production under baseline conditions, while decreasing it in the presence of TGF-β.

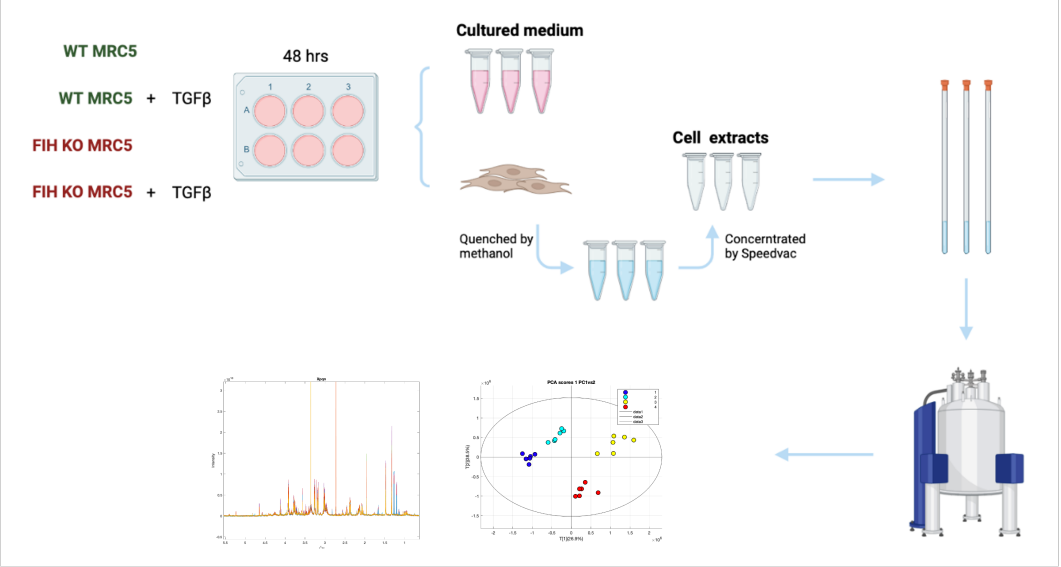

FIGURE 4.8: **Workflow for ^{1}H-NMR-based metabolite screening in FIH KO and WT MRC5 cells under TGF-β treatment**

The workflow illustrates the steps involved in performing ^{1}H-NMR-based metabolite screening. FIH knockout and wild-type MRC5 cells were treated with TGF-β (5 ng/mL) for 48 hours. Following treatment, cell lysates were prepared according to the method described, and samples were subjected to ^{1}H-NMR spectroscopy. The spectral data were then processed for PCA to identify metabolic differences, followed by the identification and quantification of key metabolites.

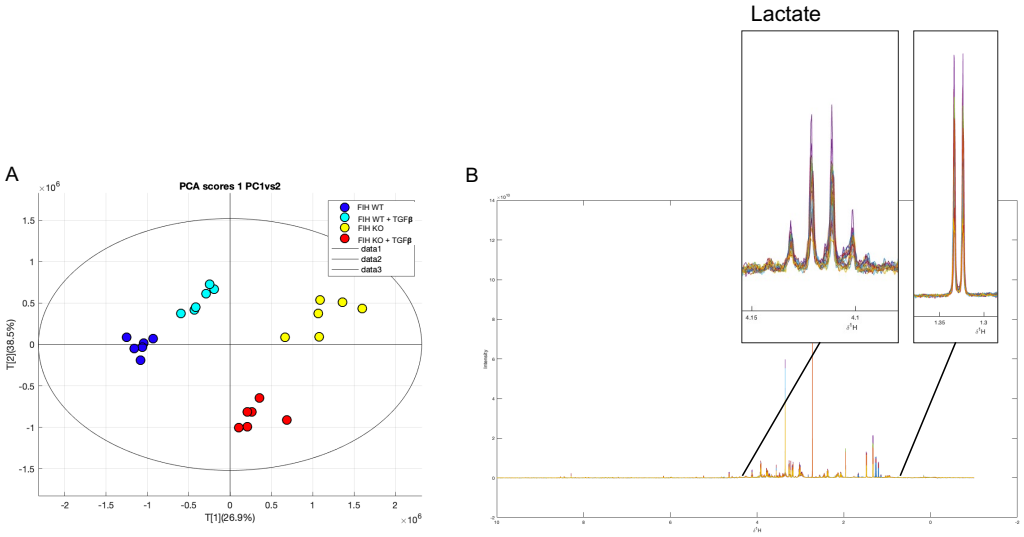

FIGURE 4.9: **^{1}H-NMR based metabolites screening using FIH KO MRC5 cells with or without TGF-β treatment**

FIH WT MRC5 cells and CRISPR-Cas9-generated FIH KO MRC5 cell line were treated with TGF-β (5 ng/mL) for 48 hours. Cell lysates were prepared as described in the Methods section and subsequently analysed by NMR. (A) The PCA score plot from ^{1}H NMR spectral data reveals distinct metabolic differences among the four groups. (B) Representative ^{1}H NMR spectra of the indicated groups, highlighting the assignment of lactate peaks.

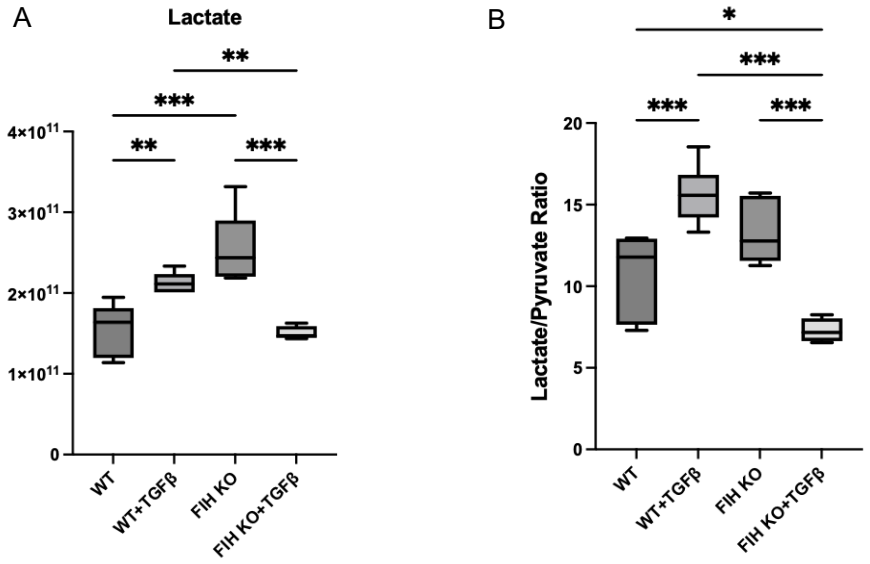

FIGURE 4.10: **^{1}H-NMR based metabolites screening suggests alteration of intracellualr lactate level in FIH KO MRC5 cells**

Box plots showing the expression level of lactate in the cell lysate (A) and the ratio of lactate to pyruvate in the cells treated as indicated (B). *P $<$ 0.05, **P $<$ 0.01, *** P $<$ 0.001 by Tukey's multiple comparison test .

4.3.4 FIH depletion may induce senescence in human lung fibroblasts

Our prior bioinformatics analysis of RNA-seq data suggested that the loss of FIH may influence cell cycle–related pathways (Figure.3.4). Since metabolic alterations are often associated with cellular senescence (Wiley and Campisi, 2016), we conducted a preliminary exploration to assess whether FIH-depleted fibroblasts might display signs of senescence. RNA sequencing data from FIH WT and KO MRC5 cells showed an increase in the GSVA score for the FRIDMAN_SENESCENCE_UP gene set (Fridman and Tainsky, 2008) in FIH KO cells (Figure.4.11 A). Moreover, a heatmap of mRNA expression levels highlighted the genes included in this gene set (Figure.4.11 B).

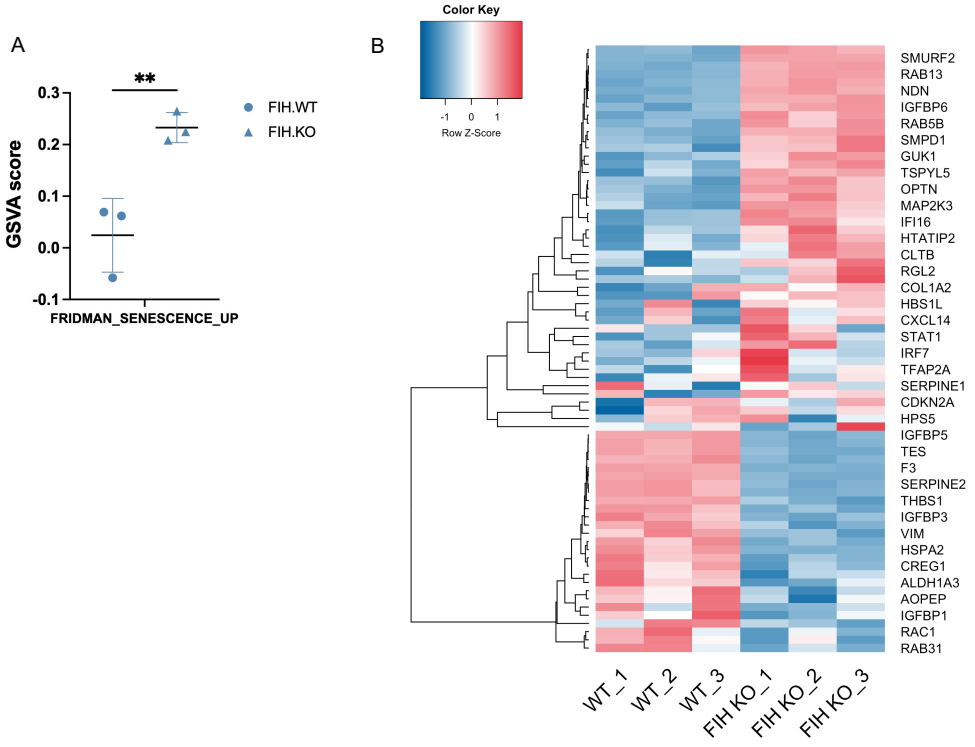

FIGURE 4.11: **RNAseq results reveals the induction of cellular senescence upon FIH depletion**

(A) Scatter plot shows the GSVA score using FRIDMAN_SENESCENCE_UP gene list was induced by deletion of FIH (mean ± SD, n = 4). *P $<$ 0.05, **P $<$ 0.01, *** P $<$ 0.001 by Student's t-test. (B) Heatmap showing the basemean of genes in FRIDMAN_SENESCENCE_UP GO term in RNAseq data.

Encouraged by the RNA-seq analysis results, we performed preliminary β-gal staining in FIH knockdown and knockout MRC5 cells. Representative images of β-gal stained MRC5 cells were captured, and ImageJ was used to quantify the proportion of positive and negative staining cells. After 48 hours of siRNA transfection targeting FIH, the percentage of β-gal positive cells increased significantly (Figure.4.12 A and B) (control

vs siFIH = 1.00 vs 1.94, P $<$ 0.001). A similar trend was observed in FIH KO MRC5 cells (Figure.4.12 C and D) (WT vs FIH KO = 1.00 vs 1.91, P $<$ 0.001).

To further explore this observation, we transfected MRC5 cells with siRNA targeting FIH, HIF-1β, or both for 48 hours. FIH depletion was associated with an increase in β-gal positivity, and HIF-1β knockdown produced a comparable effect. Interestingly, combined depletion of FIH and HIF-1β appeared to further increase the proportion of senescent cells (Figure.4.13 A and B) (control vs siFIH = 1.00 vs 2.82, P = 0.02; control vs siHIF-1β = 1.00 vs 3.54, P = 0.002; control vs siFIH+HIF-1β = 1.00 vs 5.41, P $<$ 0.001).

Taken together, these initial experiments provide preliminary evidence that the loss of FIH may contribute to cellular senescence in lung fibroblasts, potentially through mechanisms not solely dependent on HIF-1β. However, as these data remain exploratory, further validation with additional senescence markers and functional assays will be required to confirm and clarify the role of FIH in regulating fibroblast senescence.

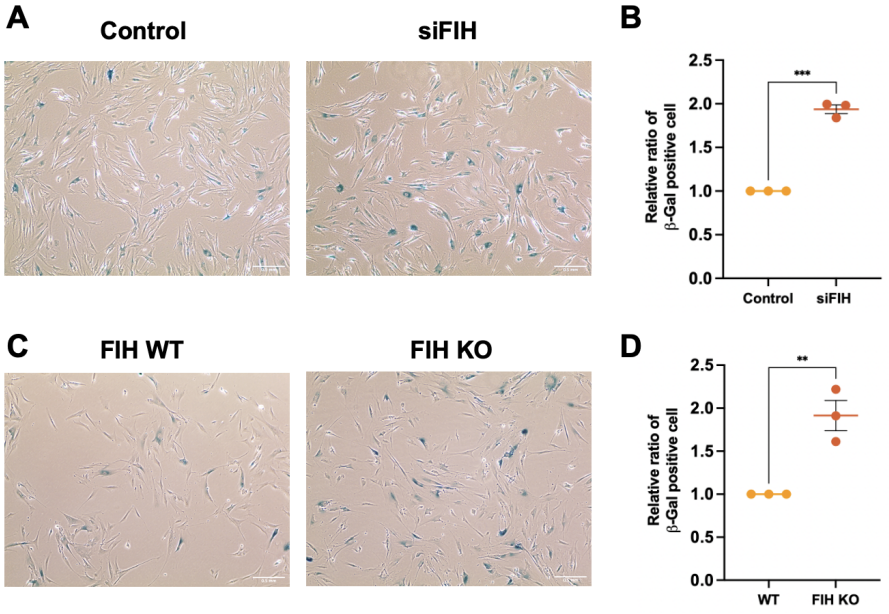

FIGURE 4.12: **β-gal staining showing increasing cellular senescence in both FIH knocked down and knocked out MRC5 cells**

(A) Representative of β-gal staining images of MRC5 cells transfected with siRNA targeting FIH for 48 hours. Micrographs were obtained with phase contrast microscopy. (B) Quantification of β-gal positive cells cultures shown in (A). (C) Representative of β-gal staining images of FIH KO MRC5 cells. Micrographs were obtained with phase contrast microscopy. (D) Quantification of β-gal positive cells cultures shown in (C). β-gal staining positive cells were scored in 5 fields of at least 200 total cells. Results are expressed as the percentage of stained cells (mean ± SE, n = 3). *P $<$ 0.05, **P $<$ 0.01, *** P $<$ 0.001 by Student's t-test.

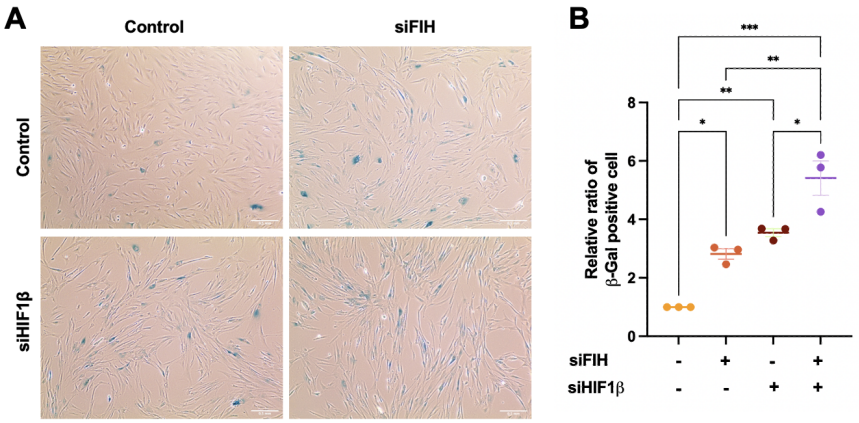

FIGURE 4.13: **FIH depletion is associated with induction of cellular senescence in fibroblasts**

(A) Representative of β-gal staining images of MRC5 cells transfected with siRNA as indicated for 48 hours. Micrographs were obtained with phase contrast microscopy. (B) Quantification of β-gal positive cells cultures shown in (A). β-gal staining positive cells were scored in 5 fields of at least 200 total cells. Results are expressed as the percentage of stained cells (mean ± SE, n = 3). *P $<$ 0.05, **P $<$ 0.01, *** P $<$ 0.001 by Tukey's multiplecomparison test.

4.4 Discussion

In this chapter, we investigated the impact of FIH on mitochondrial function, glycolysis, and cellular senescence in human lung fibroblasts. Our results demonstrate that FIH plays a critical role in maintaining cellular metabolism, with effects that extend beyond its traditional association with the HIF pathway. We found that FIH depletion led to a significant reduction in OXPHOS, as evidenced by decreased basal and maximal OCR. Notably, the mitochondrial dysfunction observed in FIH-deficient cells was partially rescued by TGF-β treatment, suggesting a complex interaction between FIH and TGF-β signaling in the regulation of mitochondrial activity. Our exploration of glycolytic processes revealed that the absence of FIH leads to a marked decrease in glycolysis, as shown by reduced basal ECAR and glycolytic capacity. This was further supported by Lactate-Glo assay data, which indicated lower lactate production in FIH knockout cells. These findings suggest that FIH is essential for sustaining glycolytic flux in lung fibroblasts, in a manner not readily explained by canonical HIF-α pathway activation.

These observations are surprising given that most existing research suggests FIH depletion usually enhances glycolysis, primarily through mechanisms that permit HIF1α-driven metabolic gene expression. For example, Sakamoto *et al.* (Sakamoto et al., 2011) and Wang *et al.* (Wang et al., 2014) reported that FIH inhibition increased GLUT1 and other key glycolytic enzymes in cancer cells under normoxic and hypoxic conditions. The mRNA level of *HKII* was upregulated via HIF1 in NSCLC cells exposed to hypoxia or the iron chelator DFO (Riddle et al., 2000; Iyer et al., 1998). Likewise, Sim *et al.* (Sim et al., 2018) observed that FIH-null cells exhibited increased glycolysis, particularly when oxidative metabolism was compromised. Pyruvate dehydrogenase kinase (PDK), which inactivates PDH, is encoded by four isoforms, and PDK1 is induced by HIF1 in lymphoma cells (Kim, Tchernyshyov, Semenza and Dang, 2006). As a result, pyruvate is shunted away from mitochondria, lowering TCA cycle flux and reducing delivery of NADH and FADH2 to the electron transport chain. Zhang *et al.* (Zhang et al., 2010) found that in MEFs, deletion of FIH increased intracellular ATP levels and suppressed AMP kinase activation, though without the expected increase in glycolysis usually associated with HIF1. In HEK293 cells, Scholz *et al.* (Scholz et al., 2016) identified OTUB1 as an FIH substrate, influencing its interactions with metabolism-related proteins and suggesting that FIH has broader metabolic roles. Garcia *et al.* (García-del Río et al., 2023) similarly showed that in LUAD and LUSC, FIH depletion enhanced glucose uptake and lactate production, though the mechanisms remain unclear. Collectively, these studies indicate that FIH loss often promotes glycolysis in transformed or highly proliferative cells.

By contrast, our findings show that in non-cancerous lung fibroblasts, FIH depletion reduces both glycolysis and mitochondrial function. Notably, although we refer to this

as altered "mitochondrial function," the observed changes may instead reflect a reduction in mitochondrial abundance rather than an intrinsic defect in mitochondrial activity. One explanation for this discrepancy lies in the cellular context. Studies reporting increased glycolysis following FIH inhibition were mostly conducted in cancer cells, which undergo metabolic reprogramming, or in MEFs, which do not represent lung fibroblasts. In these systems, loss of FIH may amplify pre-existing glycolytic activity. In contrast, non-cancerous lung fibroblasts have a different metabolic program, and FIH loss may disrupt the balance between glycolysis and OXPHOS in ways that extend beyond HIF1α regulation. Our data also suggest that FIH interacts with TGF-β signaling, since TGF-β partially restored mitochondrial function in FIH-depleted fibroblasts. This implies that FIH contributes to broader pathways critical for mitochondrial integrity and energy homeostasis.

Furthermore, our results align with the study by Zhang *et al.* (Zhang et al., 2010), which showed that FIH deletion altered cellular metabolism without necessarily increasing glycolysis. Instead, they observed higher ATP levels and reduced AMPK activation. This suggests that the metabolic impact of FIH loss varies substantially by cell type and environmental context. Taken together, our findings emphasize that while FIH inhibition enhances glycolysis in many cancer models, its loss in primary fibroblasts impairs both glycolysis and OXPHOS. These differences highlight the complexity of FIH's role in cellular metabolism and point to the need for further studies in disease-relevant models such as lung fibrosis.

In addition to metabolic effects, our preliminary data suggest that FIH depletion may be associated with cellular senescence. RNA sequencing indicated increased expression of several aging-related genes in FIH knockout cells, which was supported by elevated β-gal staining. Notably, the senescence phenotype appeared stronger when both FIH and HIF-1β were silenced, raising the possibility of interactions between FIH and HIF-associated cofactors. However, these findings should be interpreted cautiously, as they remain exploratory, and further validation with additional senescence markers and functional assays will be required to establish whether FIH plays a direct role in regulating fibroblast senescence.

Our study has several limitations and unanswered questions that need to be addressed. We used complete DMEM (10% FBS) in experiments related to metabolism, such as the Lactate-Glo assay and NMR-based metabolite screening. While this was done to maintain consistency with the conditions used for bulk RNA sequencing, it would have been more accurate to limit FBS, glucose, or pyruvate to better monitor nutrient consumption and metabolite production. In the future, using a modified culture medium that aligns more closely with Seahorse assay conditions, which begin with cell starvation, could improve the relevance of our metabolic investigations. This approach would also allow for the quantification of nutrient consumption, such as glucose or pyruvate. Also, although protein normalization was performed after Seahorse assays to control

for differences in cell number, this approach does not fully account for changes in cell viability or mitochondrial mass that may occur following siRNA transfection. Since altered survival or mitochondrial abundance could contribute to differences in respiration and glycolysis, future experiments should incorporate viability assays (e.g., trypan blue exclusion or propidium iodide staining) alongside measures of mitochondrial mass (e.g., MitoTracker staining or citrate synthase activity). These additional controls would help confirm that the observed metabolic changes reflect genuine alterations in mitochondrial function rather than secondary effects of cell loss or altered organelle content.

Our ^{1}H NMR-based metabolite screening faced challenges, primarily due to the low number of cells used. The analysis of the spectrum data from cell lysate revealed a high background, making it difficult to accurately assign metabolites. This issue likely contributed to the difficulties in interpreting intracellular lactate levels. Due to these limitations, we opted not to analyse the cultured medium from the same experiment to avoid wasting reagents and time. ^{1}H NMR spectroscopy has its constraints, as it tends to be biased toward detecting more abundant metabolites, while less abundant ones may be obscured by larger peaks. This challenge is well-documented in the literature, where the large dynamic range in metabolite concentrations can complicate statistical analysis (Bell et al., 1989; Yamaguchi et al., 1985; Serkova and Niemann, 2006). A potential solution would be to use two-dimensional (2D) NMR spectroscopy, which allows for the detection of both hydrogen and carbon nuclei. The combination of 1D and 2D NMR could provide a more precise metabolite profile and help us identify how FIH knockout impacts specific steps in glycolysis (Van et al., 2008; Pollak et al., 2024).

Moreover, the mechanism by which FIH regulates glycolysis in a HIF-independent manner remains unclear. We hypothesize that FIH may hydroxylate a substrate or interact with a protein that regulates glycolytic enzymes, or that FIH may directly hydroxylate one of these enzymes. In our current studies, we only measured the lactate levels produced by fibroblasts under different treatments. Notably, Zhang *et al.* found that FIH-null cells have a reduced capacity for fatty acid oxidation compared to WT cells. This finding suggests that the increased glycolysis observed in FIH-null cells is more likely directed towards pyruvate production rather than lactate (Zhang et al., 2010). This shift indicates the potential existence of a compensatory metabolic adaptation in response to the loss of FIH. Future studies should focus on identifying the specific reactions and enzymes affected by FIH loss, using data from our NMR-based metabolite screening as a guide. Then we can use the inhibitors targeting specific glycolytic enzymes to perturbate glycolysis to figure out the downstream of FIH regulation.

Lastly, the mechanism by which FIH loss regulates cellular senescence is still unclear. We know that this regulation occurs in a HIF-independent manner. The well-known pathways involved in cellular senescence include the p53/p21$^{WAF1/CIP1}$, p16^{INK4A}/pRB,

p38/MAPK, and PI3K/AKT/mTOR pathways, with HIF1α activation capable of triggering most of these (Gao et al., 2023). Interestingly, Young *et al.* showed that acute VHL inactivation causes a senescent-like phenotype in vitro and in vivo, independent of p53 and HIF, but dependent on the retinoblastoma protein (Rb) and the SWI2/SNF2 chromatin remodeler p400. Rb activation occurred through a decrease in Skp2 mRNA, leading to the upregulation of p27 in a HIF-independent fashion (Young et al., 2008). It is reasonable to hypothesize that FIH may influence cellular senescence through a potential non-HIF substrate, although further evidence is needed to confirm this. Additionally, given the observed metabolic alterations following FIH loss in fibroblasts, we are curious whether the induction of cellular senescence is related to these metabolic changes and, if so, which process occurs first. This will be explored in the final discussion.

There is a growing interest in targeting metabolic pathways as a potential treatment strategy for IPF as introduced in chapter 1. Numerous drugs have been developed to modulate key aspects of metabolism, such as glycolysis and mitochondrial function, which are often altered in IPF. Chen *et al.* demonstrated that Anlotinib reduces glycolysis by lowering PFKFB3, lactate, and glucose consumption, leading to decreased fibrosis markers such as αSMA, Col1, and FN (Chen et al., 2021). Diphenyleneiodonium enhances glycolysis while reducing fibrosis by decreasing lung Col, α-SMA, and TGF-β expression, as well as improving fibrosis severity (Wang, Gao, Wang, Yu, Zhang, Liu, Song, Xu, Wang, Lou et al., 2023). Similarly, Wang *et al.* showed that Fenbendazole inhibits glycolysis and glucose consumption, reducing TGF-β-induced fibrosis markers, including α-SMA and Col1, and mitigating bleomycin-induced lung fibrosis (Wang, Xu, Wang, Ding, Zhao, Wan, Zhao, Guo, Pan, Yang et al., 2022). Fenofibrate decreases OXPHOS while increasing glycolysis, resulting in reduced fibroblast activation and migration in response to TGF-β (Kikuchi et al., 2021). Yin *et al.* found that Lonidamine, an HK2 inhibitor, lowers Col and FN expression while improving lung function in bleomycin-induced fibrosis (Yin et al., 2019). Metformin enhances mitochondrial complex I and increases mtDNA, leading to a reduction in fibrosis markers like α-SMA and Col. While Pirfenidone influences glucose metabolites, its metabolic effects are less clearly defined (Rangarajan et al., 2018). Summer *et al.* reported that Rapamycin reduces OXPHOS and fibrosis markers, such as β-gal and inflammatory cytokines, in bleomycin-treated lungs (Summer et al., 2019). These approaches are being explored to disrupt the pathological processes driving fibrosis and to improve patient outcomes (Details showed in Table.4.1). It is interesting that some drug induced glycolysis while some reduced glycolysis, their final effect is decreasing the expression of profibrotic genes, which means there must be several different impact of metabolic alteration on the progression of lung fibrosis.

Given the critical role of FIH in regulating cellular metabolism, FIH and its substrates present promising targets for future IPF therapies. Our findings suggest that FIH plays

a significant role in maintaining the balance between glycolysis and OXPHOS in lung fibroblasts. Targeting FIH or its downstream effects could offer a novel therapeutic approach to managing IPF, particularly by restoring proper metabolic function in affected cells.

TABLE 4.1: **Metabolic influence of clinical drugs and natural compounds and their therapeutic effects in IPF**

Compound category	Compound name	Metabolic modulatory impact	Therapeutic effects	Reference
Clinical Drug	Anlotinib	↓ glycolysis, PFKFB3, lactate, and glucose consumption	↓ bleomycin-induced lung α-SMA, collagen 1, FN, and hydroxyproline; TGF-β-induced lung fibroblast α-SMA, collagen 1, FN, migration, and proliferation	(Chen et al., 2021)
Clinical Drug	Diphenyleneiodonium	↑ glycolysis	↓ bleomycin-induced lung collagen, mRNA of α-SMA, Col1a1, Fn, and TGF-β, Ashcroft fibrosis score, lung fibrosis microCT, and macrophage CD206 expression and mRNA of CD206 and CD163 ↑ bleomycin-induced lung macrophage mRNA of CD86 and iNOS and mice body weight	(Wang, Gao, Wang, Yu, Zhang, Liu, Song, Xu, Wang, Lou et al., 2023)
Clinical Drug	Fenbendazole	↓ glycolysis and glucose consumption ↔ OXPHOS	↓ TGF-β-induced lung fibroblast α-SMA, collagen 1, FN, N-cadherin, and vimentin; bleomycin-induced lung α-SMA, collagen 1, hydroxyproline, and Ashcroft fibrosis score	(Wang, Xu, Wang, Ding, Zhao, Wan, Zhao, Guo, Pan, Yang et al., 2022)

Continued on next page

Compound category	Compound name	Metabolic modulatory impact	Therapeutic effects	Reference
Clinical Drug	Fenofibrate	↓ OXPHOS ↑ glycolysis	↓ TGF-β-induced lung fibroblast α-SMA, collagen, CTGF, and migration	(Kikuchi et al., 2021)
Clinical Drug	Lonidamine	HK2 inhibitor	↓ bleomycin-induced lung collagen, FN, hydroxyproline, and mRNA of α-SMA, Col1a1, Ctgf, and Pai-1 ↑ bleomycin-induced lung compliance and peripheral blood oxygenation	(Yin et al., 2019)
Clinical Drug	Metformin	↑ complex I and mitochondrial DNA	↓ bleomycin-induced lung α-SMA, collagen, and hydroxyproline	(Rangarajan et al., 2018)
Clinical Drug	Pirfenidone	Glucose metabolites		(Sun et al., 2018)
Clinical Drug	Rapamycin	↓ OXPHOS	↓ bleomycin-induced EC β-galactosidase, p21, phosphorylated p53, and mRNA of Il-1α, Il-6, Mcp-1, Mmp-2, and Tnf-α	(Summer et al., 2019)
Natural Compound	Alamandine	↓ glycolysis, HK2, and PFKFB3 ↑ ATP and OXPHOS	↓ bleomycin-induced lung α-SMA and collagen 1; TGF-β-induced lung fibroblast αSMA and collagen 1	(Wang, Zhang, Huang, Yuan, Hong, Xie, Li, Chen, Li and Meng, 2023)
Natural Compound	Dihydromyricetin	↓ GLUT1 and OXPHOS	↓ TGF-β-induced IPF-derived lung fibroblast αSMA, collagen 1, FN, migration, and proliferation; bleomycin-induced lung αSMA, collagen 1, and FN, Ashcroft fibrosis score, and mice mortality	(Li et al., 2022)

Continued on next page

Compound category	**Compound name**	**Metabolic modulatory impact**	**Therapeutic effects**	**Reference**
Natural Compound	Gossypol	LDHA inhibitor	↓ bleomycin-induced lung collagen, FN, hydroxyproline, and TGF-β, and mRNA of Col1 and Col3; TGF-β-induced lung fibroblast α-SMA, calponin, and mRNA of Col1a1 and Col3a1 No change of bleomycin-induced BALF cell counts	(Kottmann et al., 2015)
Natural Compound	Morin	↓ GLS1, glutamate, and α-KG ↔ GLUD1, GOT1, GPT2	↓ bleomycin-induced lung αSMA, collagen 1, FN, hydroxyproline, and inflammation; TGF-β-induced lung fibroblast αSMA, collagen 1, FN, and migration	(Miao et al., 2022)
Natural Compound	Phloretin	GLUT1 inhibitor	↓ bleomycin-induced lung collagen and fibronectin ↑ body weight ↔ airway cell counts	(Cho et al., 2017)
Natural Compound	Tanshinone IIA	↓ ATP, glutamate, and αKG	↓ bleomycin-induced lung αSMA, collagen, hydroxyproline, and TGF-β, mRNA of Col1, Col3, and Fn, and primary lung fibroblast growth	(An et al., 2019)

Chapter 5

FIH may invlove in ECM regulation and fibroblasts activation

5.1 Introduction and rationale

5.1.1 Fibroblast-to-myofibroblast transition

Lung fibroblasts are a specialized population of mesenchymal cells that play a critical role in maintaining the structural integrity and functional capacity of the lung (Plikus et al., 2021). These cells are responsible for producing ECM proteins and maintaining ECM organisation, which provides the necessary mechanical support for lung tissues to perform essential functions, such as gas exchange and resistance to physical stress.

The transition of fibroblasts to myofibroblasts is a critical event in wound healing, typically marked by increased expression of α-SMA. Myofibroblasts are essential for generating the contractile force necessary for wound closure and are associated with increased collagen deposition. In IPF, the proliferation of myofibroblasts significantly contributes to fibrosis and disease progression. There have been loads of studies reporting the regulation of FMT. Myofibroblast differentiation and their resistance to apoptosis are driven by multiple factors, including TGF-β (Fernandez and Eickelberg, 2012*a*), integrin αVβ6 (Munger et al., 1999), PDGF (Joshi et al., 2020; Adler et al., 2020), CTGF (Pan et al., 2001), VEGF (Murray et al., 2017), overexpression of Wnt (Königshoff et al., 2008, 2009), reduced expression of BMP2 (Fukihara et al., 2022) and decreased AMPK activation (Jiang et al., 2017) as introduced in Chapter 2. Many of these signaling pathways—such as TGF-β, PDGF receptor, EGF, FGF, and Wnt—specifically promote the expression of mesenchymal genes while downregulating epithelial genes, thereby activating fibroblasts. Overall, lung fibroblasts and myofibroblasts are central to both the maintenance of lung function and the pathological processes that lead to fibrosis. Their roles in ECM production, tissue remodeling, and response to injury highlight

their importance in both health and disease, making them key targets for therapeutic intervention in fibrotic lung diseases. However, whether FIH is involved in the regulation of FMT remains unclear.

5.1.2 Extracellualr matrix

The extracellular matrix (ECM) was once considered just a structural framework that supports cells, but it is now recognized as a critical regulator of both health and disease. The ECM is a dynamic and flexible network of interconnected proteins that offers crucial structural support for cells and plays a vital role in regulating nearly all cellular functions (Hynes, 2009). In addition to providing the necessary support for tissues, the ECM sends vital signals to cells that affect their growth, movement, transformation into different cell types, death, and the production of important molecules that are secreted by the cells (Hardie et al., 2009; Mutsaers et al., 1997). The ECM also stores growth factors and cytokines, which are essential during tissue repair, helping to guide and localize the wound healing response. During development, the ECM plays a crucial role in shaping key processes like the branching of the lungs (Sakai et al., 2003) and the development of the heart and nervous systems (Li et al., 1998). Therefore, the ECM is a fundamental part of not only maintaining tissue structure but also ensuring the proper function and development of tissues (Booth et al., 2012)

The ECM of the lung is composed of several major components including fibrillar collagens (type I, II, III, V, XI) (Herrera et al., 2019), elastin, fibronectin, proteoglycans, hyaluronan, and laminin (Kliment and Oury, 2010). Type I collagen is relatively rigid and contributes to tissue stiffness, whereas type III collagen is more flexible and is found in higher proportions in the lungs compared to other tissues (Asgari et al., 2017; Liu et al., 2021). Abrrant deposition of fibrillar collagens is a hallmark of IPF and TGF-β is one of the main modulator of ECM protein deposition. Apart from the ECM proteins deposition, the crosslinking of the ECM proteins is another factor resulting in ECM stiffening. The stiffened ECM is not merely a epiphenomenon of lung fibrosis but can actively drive the progression of fibrotic lung disease. According to the previous work from Brereton and his colleagues, in lung primary fibroblasts derived from IPF patients, the loss of FIH activity induced the expression level of PLOD2 and LOXL2, two enzymes responsible for collagen cross-linking, in a HIF-dependent manner (Brereton et al., 2022).

Interestingly, in our bulk RNAseq data analysis, we found that activity of TGF-β signaling and EMT were downregulated in FIH KO MRC5 cells which leaves us an unclear role of FIH. We are eager to investigate the role of FIH in the regulation of myofibroblast activation and ECM organisation.

5.2 Aim and Objectives

5.2.1 Aim

The aim of this chapter is to investigate the role of FIH in FMT and ECM organisation, particularly in the context of TGF-β signaling This chapter combines bioinformatic analysis with laboratory experiments to explore how FIH affects these processes, which are important in lung fibrosis.

5.2.2 Objectives

1. Analyse RNA sequencing data on FIH WT and KO MRC5 cells treated with PBS or TGF-β to identify key transcriptomic changes, with a focus on pathways related to FMT and ECM organisation.
2. Validate bioinformatic predictions by assessing αSMA and Collagen 1 expression in FIH WT and KO MRC5 cells, as well as in FIH knockdown human primary lung fibroblasts, under TGF-β treatment.
3. Investigate the impact of FIH depletion on the TGF-β signaling pathway, specifically through the analysis of p-Smad2/Smad2 ratios, to determine its role in FMT and ECM regulation.

5.3 Results

5.3.1 Gobal transcriptomic changes identify FIH depletion play an important role in ECM organisation

When investigating the global transcriptomic changes between FIH WT and KO MRC5 cells, we extended our analysis to include two additional groups to evaluate the role of FIH under TGF-β treatment. To provide a comprehensive comparison among the different conditions, we included all four groups in the analysis presented in this chapter. Both FIH WT and KO MRC5 cells were treated with PBS or TGF-β for 24 hours before RNA was extracted for bulk RNA sequencing. PCA revealed that samples within each group clustered closely together, indicating similar gene expression profiles, whereas samples from different groups were clearly separated, suggesting distinct transcriptional responses (Figure.5.1 A).

To better understand the impact of FIH depletion on MRC5 cells, with and without TGF-β, we utilized GSVA on normalized mRNA expression data. The heatmap showed that several pathways activated by TGF-β were attenuated in FIH KO cells (Figure.5.1 B). Notably, pathways related to the cell cycle, such as *E2F targets* and *G2M checkpoint*, were upregulated by TGF-β but downregulated upon FIH loss. Interestingly, the *TGF-β_signaling* pathway (P = 0.001, Difference (FIH KO - WT) = -0.427), as well as the *Epithelial mesenchymal transition* pathway (P = 0.01, Difference = -0.155), were significantly downregulated in FIH KO cells, even under TGF-β treatment (Figure.5.1 C).

TGF-β signaling is crucial for lung fibrosis progression, primarily through the induction of FMT, leading to excessive ECM deposition. EMT, while typically occurring in epithelial cells, involves gene sets that are also crucial for myofibroblast activation and ECM organisation.

In order to further investigate the impact of FIH depletion on FMT ECM organisation, we performed GSVA using several gene lists. The myofibroblast marker gene list was identified using the Seurat `FindMarkers()` function on the Kropski single-cell RNA-seq dataset (Habermann et al., 2020), as provided by Dr. Joseph Bell from the Brookes lab. The scatter plot (Figure.5.2 A) demonstrates that the loss of FIH significantly reduced the myofibroblast score in MRC5 cells without TGF-β treatment compared to FIH WT MRC5 cells (P = 0.004, Difference (FIH KO - WT) = -0.387). Notably, even under TGF-β treatment, FIH depletion still partially decreased the expression of myofibroblast markers (P = 0.004, Difference (FIH KO with TGF$\beta-$ WT with $TGF\beta$) $= -0.39$). This suggests that FIH may regulate the differentiation of fibroblasts into myofibroblasts upstream of TGF-β signaling. Furthermore, the GSVA score calculated using the gene list associated with the GO term "extracellular matrix organisation" revealed that FIH loss downregulated genes involved in ECM organisation, irrespective of TGF-β treatment (Figure.5.2 B) (WT vs FIH KO: P = 0.03, Difference (FIH KO $-$ WT) = -0.20).

Collagens are the most abundant proteins in the human body, primarily found in the ECM of connective tissues such as tendons and skin. They serve as the main structural protein within the ECM, providing tensile strength and playing crucial roles in cellular processes like adhesion and migration. We identified 45 collagen-expressing genes in human lung tissue using MatrisomeDB 2.0 (Shao et al., 2023; Lansky et al., 2019). Additionally, 35 TGF-β-induced collagen genes were identified from preliminary RNA sequencing data of MRC5 cells treated with PBS or TGF-β. Genes were selected based on a Log_2 fold change greater than 0 and an adjusted P-value (padj) less than 0.05. The intersection of these two lists resulted in 17 collagen-expressing genes induced by TGF-β in human fibroblasts. The GSVA score using this gene list revealed that FIH depletion significantly reduced the expression of TGF-β-induced collagens (Figure.5.2 C) (WT with TGF-β vs FIH KO with TGF-β: P = 0.04, Difference (FIH KO with TGF$\beta-$ WT with TGF$\beta) = -0.189$). The accompanying heatmap shows that the overall expression levels of these collagens were downregulated by FIH loss, regardless of TGF-β treatment (Figure.5.2 D).

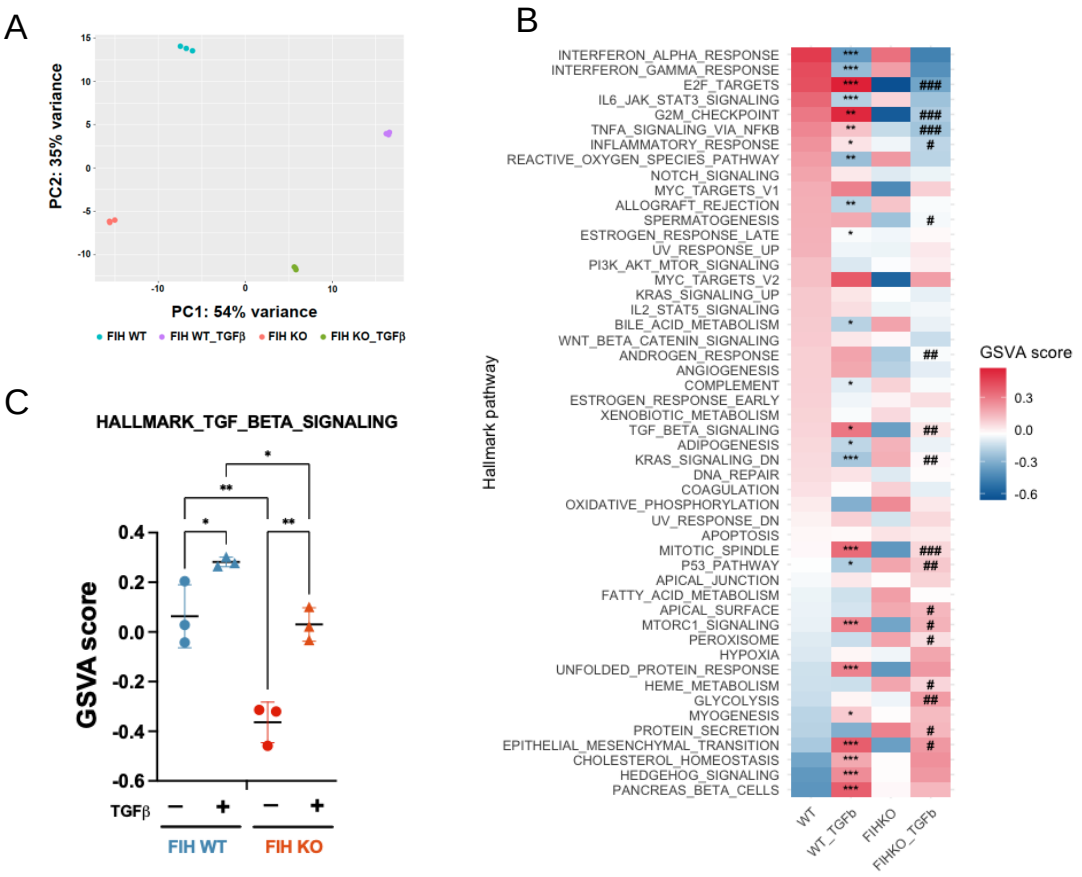

FIGURE 5.1: **Global transcriptomic analysis in FIH KO MRC5 cells with or without TGF-β treatment**

(A) PCA plot of gene expression data from RNA-seq, representing three biological replicates for FIH WT and KO MRC5 cells treated with either PBS or TGF-β (5 ng/mL) for 24 hours. (B) Heatmap displaying GSVA scores for 50 hallmark pathways derived from RNA sequencing data. Statistical significance is indicated as follows: *P $<$ 0.05, **P $<$ 0.01, ***P $<$ 0.001 vs. WT group; # P $<$ 0.05, ## P $<$ 0.01, ### P $<$ 0.001 vs. WT group with TGF-β treatment by Tukey's multiple comparison test. (C) Scatter plot highlighting the GSVA scores for the TGF_BETA_SIGNALING pathway across the four experimental groups. *P $<$ 0.05, **P $<$ 0.01, ***P $<$ 0.001 by Tukey's multiple comparison test.

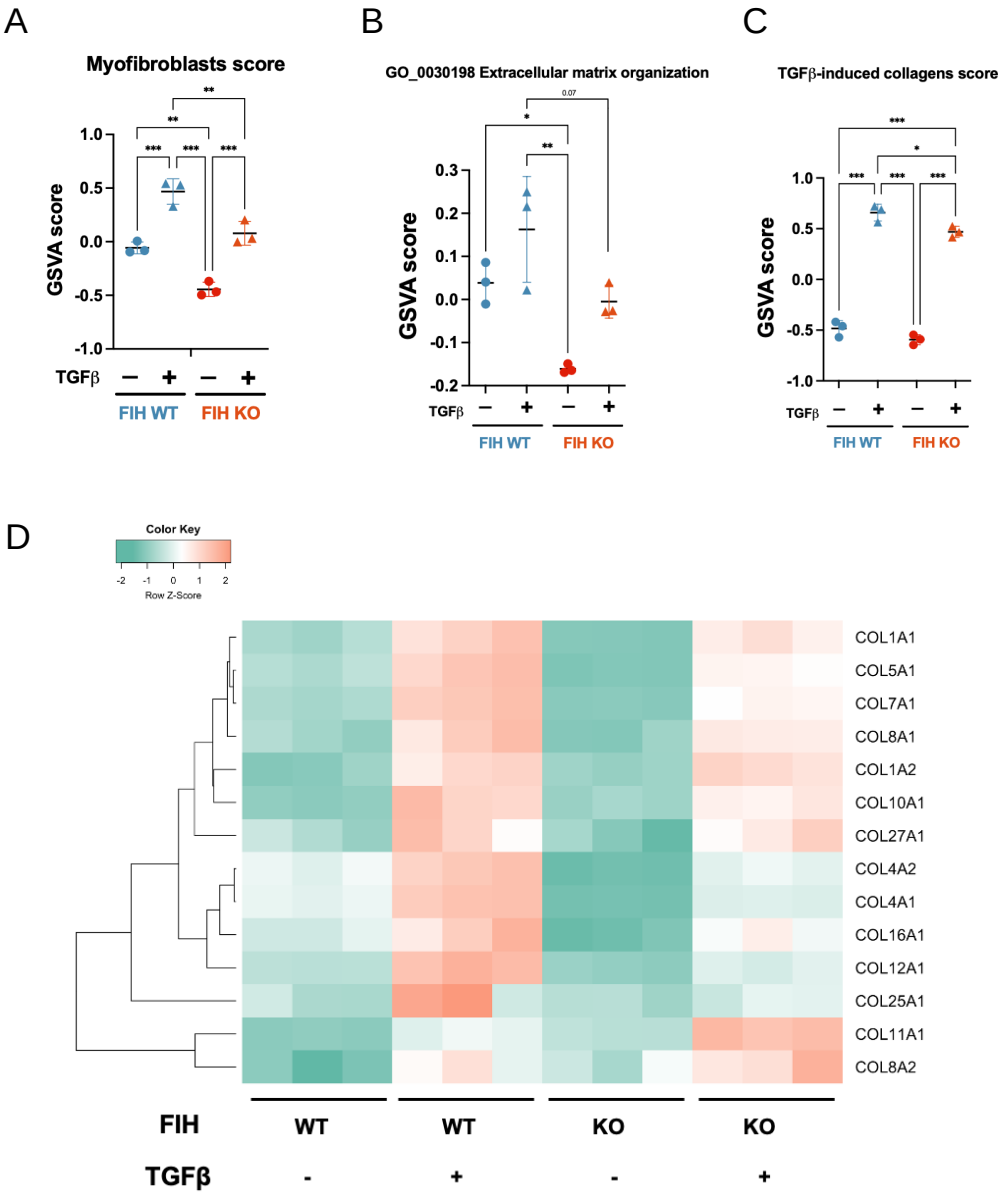

FIGURE 5.2: **Bulk RNA sequencing analysis reveals the loss of FIH mitigates fibroblasts to myofibroblasts transition and collagen production induced by TGF-β treatment**

(A-C) Scatter plots displaying the GSVA scores for the myofibroblast marker gene list (A), the extracellular matrix organisation GO term (B), and the TGF-β-induced collagen gene list (C). (D) Heatmap showing the base mean expression levels of collagen-coding genes that are upregulated by TGF-β treatment. *P $<$ 0.05, **P $<$ 0.01, ***P $<$ 0.001 by Tukey's multiple comparison test.

5.3.2 FIH depletion and the fibroblast to myofibroblasts transition induced by TGF-β

To validate these transcriptomic observations, we performed in vitro experiments in MRC5 cells and primary human lung fibroblasts.

FIH WT and KO MRC5 cells were treated with PBS or TGF-β for 48 hours, followed by the collection of cell lysates and conditioned media for immunoblotting. The results revealed that αSMA, a key marker of myofibroblasts, was upregulated following TGF-β treatment, whereas the loss of FIH inhibited this induction. Similarly, the secretion of Collagen 1 into the culture medium followed the same pattern, with TGF-β treatment enhancing Collagen 1 expression, an effect that was attenuated by FIH depletion (Figure.5.3 A). In human primary lung fibroblasts, FIH knockdown produced comparable results, reducing TGF-β-induced expression of αSMA and Collagen 1 (αSMA: control with TGF-β vs siFIH with TGF-β = 0.848 vs 0.147, $P < 0.001$; Collagen 1: control with TGF-β vs siFIH with TGF-β = 0.559 vs 0.228, $P = 0.02$) (Figure.5.3 B). Triplicate experiments with gray-scale quantification (Figure.5.3 C) confirmed the role of FIH in attenuating FMT. Moreover, the phospho-Smad2 (p-Smad2)/Smad2 ratio suggested that FIH loss disrupts TGF-β signaling, leading to reduced FMT and collagen expression (control with TGF-β vs siFIH with TGF-β = 1.20 vs 0.85, P = 0.14).

5.3.3 FIH and HIF1β in FMT and ECM regulation

We aimed to investigate whether FIH's regulation of FMT and ECM regulation associated with HIF pathway. To do so, we conducted knockdown experiments targeting FIH and HIF1β individually and in combination in human primary lung fibroblasts treated with TGF-β for 48 hours.

Immunoblotting analysis and subsequent quantification indicated that both FIH depletion and HIF1β knockdown were associated with reduced TGF-β-induced αSMA expression (αSMA: control with TGF-β vs. siFIH with TGF-β = 0.777 vs. 0.181, $P = 0.002$) (Figure.5.4 A and C). This observation was consistent in a separate strain of primary lung fibroblasts (Figure.5.4 B). The combined knockdown resulted in a significant reduction of the p-Smad2/Smad2 ratio (P = 0.04), whereas single knockdowns produced inconsistent changes. qRT-PCR analysis further indicated reduced *ACTA2* expression after FIH depletion (P = 0.03) (Figure.5.4 D).

Overall, these findings suggest that FIH may modulate fibroblast activation and ECM regulation, potentially interacting with TGF-β and HIF-related pathways. However, the data remain preliminary and should be interpreted with caution. Additional experiments are needed to clarify the mechanisms, confirm reproducibility across fibroblast strains, and determine the relevance of these pathways in vivo.

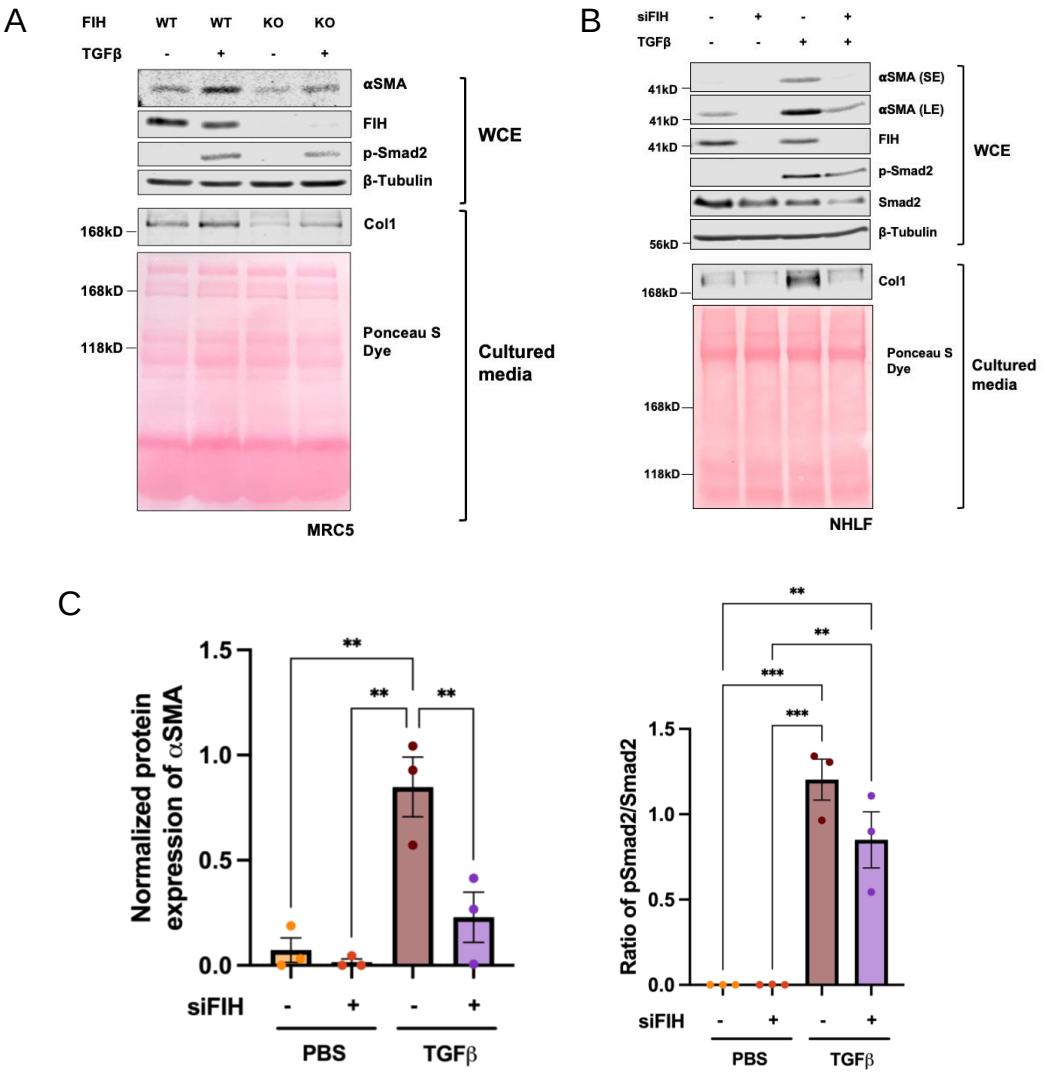

FIGURE 5.3: **TGF-β-induced αSMA and collagen 1 can be partially blocked by FIH depletion**

(A) Protein expression of αSMA, phospho-Smad2 (p-Smad2) and FIH in MRC5 with indicated treatment. β-Tubulin was used as a loading control. Protein expression of Collagen 1 in cultured media from MRC5 with indicated treatment. Ponceau S staining showing total protein levels. (B) Protein expression of αSMA, p-Smad2, total Smad2 and FIH in MRC5 with indicated treatment. β-tubulin was used as a loading control. Protein expression of Collagen 1 in cultured media from NHLFs with indicated treatment. Ponceau S staining showing total protein levels. (C) Quantification of protein expression of αSMA which normalized to the expression of β-Tubulin and the ratio of the expression of p-Smad2 and total Smad2. ImageJ was used to do the quantification. * $P < 0.05$, ** $P < 0.01$, *** $P<0.001$ by Tukey's multiple comparison test.

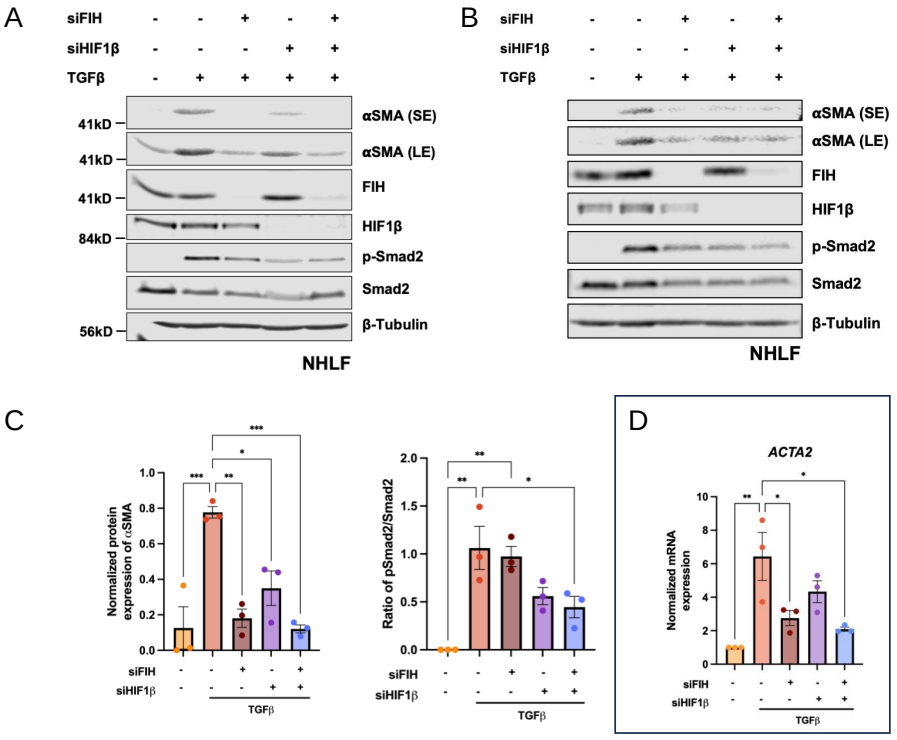

FIGURE 5.4: **Inhibition of FMT by loss of FIH is HIF-independent**
(A-B) Protein expression of αSMA, phospho-Smad2 (p-Smad2), total Smad2, HIF1β and FIH in two strains of NHLFs with indicated treatment. β-Tubulin was used as a loading control. (C) Quantification of protein expression of αSMA which normalized to the expression of β-Tubulin and the ratio of the expression of p-Smad2 and total Smad2. ImageJ was used to do the quantification. (D) The mRNA level of *ACTA2* gene in the NHLFs with indicated treatment. *ACTB* was used as the house-keeping gene. * $P < 0.05$, ** $P < 0.01$, *** $P<0.001$ by Tukey's multiple comparison test.

5.4 Discussion

In this chapter, we investigated the role of FIH in regulating fibroblast-to-myofibroblast transition (FMT) and extracellular matrix (ECM) organisation, particularly in the context of TGF-β signaling. FMT is a critical event in wound healing and fibrosis, characterized by increased α-SMA expression and collagen-rich ECM production. Myofibroblasts are central to the progression of IPF, contributing to excessive ECM deposition and tissue stiffening, which ultimately impairs lung function. While myofibroblast activation involves multiple signaling pathways—including those related to ECM mechanical properties—the contribution of FIH to FMT in human lung disease remains poorly defined.

Transcriptomic analyses revealed that FIH depletion alters pathways related to cell cycle regulation and TGF-β signaling, with a reduction in myofibroblast markers and ECM-related gene sets, including collagens. In line with these findings, immunoblotting showed that under normoxic conditions, loss of FIH was associated with reduced TGF-β-induced α-SMA expression. While these data suggest that FIH may influence fibroblast activation in a manner not fully explained by canonical HIF signaling, the precise mechanism remains uncertain. Although FIH depletion reduced TGF-β, ECM, and myofibroblast gene sets in our in-vitro models, this does not exclude a profibrotic role for FIH in disease. FIH has multiple substrates, and its effects may vary depending on environmental stimuli such as hypoxia, mechanical stress, or chronic TGF-β exposure. In particular, the FIH/HIF axis is known to regulate collagen maturation and cross-linking rather than transcription alone, which may explain why reduced transcript levels in our system could still coexist with profibrotic outcomes in tissue.

Previous work has highlighted important roles for the HIF pathway in fibroblast activation during fibrosis (Haase, 2012; Kim et al., 2022; Strowitzki et al., 2019; Higgins et al., 2007). By contrast, relatively few studies have examined whether FIH regulates fibroblast function independently of HIF. For example, Hu *et al.* demonstrated that FIH acts as a checkpoint in liver fibrosis by suppressing hepatic stellate cell activation, with miR-31-mediated FIH downregulation promoting α-SMA and collagen expression via TGF-β/Smad3 signaling (Hu et al., 2015). Similarly, Manresa *et al.* showed that hydroxylase inhibitors (DMOG and JNJ1935) attenuated TGF-β-mediated fibroblast activation, at least partly through non-HIF mechanisms involving ERK signaling (Manresa et al., 2016). Together, these studies support the possibility that FIH can influence fibroblast activation beyond its role in regulating HIF.

Our results further indicate that FIH depletion reduced secretion of collagen I under TGF-β stimulation. However, interpretation of these data requires caution. Western blotting, while prepared under non-denaturing conditions, has inherent limitations in detecting post-translational modifications of collagen, which are crucial for fibril stability and ECM stiffness (White, 2015; Jones et al., 2018). Indeed, HIF activation in fibrotic

lungs promotes collagen cross-linking through enzymes such as PLOD2 and LOXL2, altering fibril nano-architecture and increasing stiffness (Aquino-Gálvez et al., 2019; Brereton et al., 2022). The extent to which FIH depletion influences these processes directly or indirectly remains unclear.

Single-cell RNA sequencing studies have revealed fibroblast heterogeneity in IPF lungs, including ACTA2$^+$ myofibroblasts, HAS1-high fibroblasts, and PLIN2$^+$ fibroblasts (Habermann et al., 2020). Of note, HAS1-high and PLIN2$^+$ subsets exhibit elevated HIF activity and oxidative stress (Brereton et al., 2022). It is possible that FIH loss influences fibroblast differentiation into distinct mesenchymal subsets with altered ECM output. While our western blot results suggested a trend toward reduced TGF-β-induced collagen I expression in FIH-depleted cells, statistical support was limited, and we cannot conclude whether this effect is HIF-dependent or independent. Given FIH's broad substrate profile—including ankyrin repeat domain (ARD)-containing proteins such as Notch and NF-κB (Cockman et al., 2009)—alternative regulatory mechanisms beyond HIF signaling are also possible.

This study has several limitations. First, our results were obtained under normoxic conditions without hypoxia or hypoxia mimetics, and no direct assessment of HIF1α or HIF2α stability was performed, limiting interpretation of HIF-dependent mechanisms. Second, while collagen I secretion was reduced with FIH depletion, post-translational modifications critical for collagen function (e.g., hydroxylation and cross-linking) were not measured. Third, western blot reproducibility for p-Smad2 was limited, making it difficult to determine whether FIH directly influences TGF-β/Smad signaling. Finally, fibroblast heterogeneity in IPF complicates translation of these findings, and additional experiments—such as transcription factor analysis of *ACTA2* or proteomic pulldown of FIH substrates—will be required to clarify the mechanisms involved.

Future studies are required to clarify how FIH regulates fibroblast-to-myofibroblast transition and ECM remodeling. Single-cell RNA sequencing in FIH-depleted lung fibrosis models would enable identification of mesenchymal subpopulations affected by FIH loss. Candidate markers revealed from these analyses could then be validated by western blotting and qPCR. To broaden our understanding of collagen regulation, it will be important to assess multiple collagen types using immunoblotting, qPCR, immunofluorescence, and immunohistochemistry, thereby providing both quantitative and spatial insights. In addition, the role of FIH in collagen post-translational modifications warrants further study, including measurements of collagen solubility, turnover, and matrix metalloproteinase (MMP)-mediated degradation. ELISA-based quantification of mature trivalent collagen cross-links could offer additional insight into ECM remodeling in fibrotic conditions.

Since 2D cultures cannot fully replicate tissue-level mechanics, 3D culture systems will be critical to investigate the contribution of FIH to ECM regulation. These approaches

capture in vivo-like biochemical and biomechanical interactions, including the impact of stiffness and mechanical stretch on fibroblast behavior. Fibroblasts sense matrix stiffness through integrins, and increased stiffness promotes myofibroblast differentiation via both TGF-β-dependent and -independent pathways. Transcriptional regulators such as YAP1 and TAZ, which are elevated in IPF lungs, act as key mechanotransduction mediators (Chen, Zhao, Sun, Su, Zhang, Li, Liu, Zhang, Lu, Shan et al., 2019; Noguchi et al., 2017). Conversely, prostaglandin E2, which decreases with matrix stiffening, may contribute to the inability of myofibroblasts to resolve after injury (Bozyk and Moore, 2011). Mechanical stretch further amplifies fibrosis by activating latent TGF-β, creating a feed-forward loop.

A promising strategy is the use of fibroblast-derived matrices, generated by culturing pulmonary fibroblasts with or without FIH on substrates, followed by decellularization. These ECM scaffolds can then be used to study how FIH loss alters fibroblast-derived microenvironments. Such systems have been successfully applied to investigate fibroblast TGF-β secretion and activation, differences between fibroblast and myofibroblast ECM, and the contribution of profibrotic genes to ECM remodeling (Klingberg et al., 2014; Liu et al., 2015). Applying this approach to FIH-deficient fibroblasts may provide new mechanistic insights into how FIH influences ECM regulation and fibrotic progression.

Chapter 6

Conclusion and Future Work

6.1 Final conclusion

In the final stages of this thesis, it is important to revisit the central challenge: IPF, a progressive and fatal lung disease with limited treatment options. While the roles of hypoxia and HIF signaling in fibrosis are well established, the contribution of FIH remains much less understood.

In this work, we investigated the consequences of FIH depletion in lung fibroblasts using both CRISPR-Cas9 knockout and siRNA knockdown models. Transcriptomic analysis revealed consistent downregulation of cell cycle–related pathways, alongside upregulation of processes related to hypoxia response and cell migration. These results suggest that FIH influences fibroblast proliferation and stress adaptation, although the precise mechanisms remain to be clarified. Interestingly, we also observed that FIH KO and KD produced distinct transcriptional changes: KO cells showed alterations in genome stability and chromatin regulation, while KD cells displayed changes in lipid metabolism. These observations indicate that FIH may act through multiple mechanisms, some overlapping with HIF signaling and others independent, though further validation is needed.

We next assessed the role of FIH in fibroblast metabolism. Seahorse assays and ATP measurements suggested that FIH loss reduced mitochondrial respiration and energy production. Co-depletion of HIF-1β partially reversed these effects, implying that HIF-related pathways may contribute, although these data should be interpreted cautiously given the absence of hypoxia or hypoxia mimetic conditions in our models.

Transcriptomic and functional assays also indicated that FIH influences fibroblast-to-myofibroblast transition (FMT) and ECM regulation under TGF-β stimulation. In both fibroblast cell lines and primary fibroblasts, FIH depletion was associated with reduced αSMA and collagen I expression. These effects appeared at least partially independent

of HIF-1β, though the underlying mechanisms remain unresolved and require further investigation.

While we have discussed the results at the end of each chapter, there are additional intriguing topics that emerge when we consider insights across multiple chapters.

Links between cellular metabolism and senescence

There is substantial evidence demonstrating metabolic reprogramming in senescent cells, with PF widely recognized as closely linked to aging. Studies have shown that senescent cells exhibit increased PDK4-dependent aerobic glycolysis and elevated lactate production, which stimulates ROS generation through NADPH oxidase 1 (NOX1), promoting the SASP and contributing to disease progression (Dou et al., 2023).

Conversely, metabolic alterations can also induce cellular senescence. Metabolic stress, such as mitochondrial dysfunction, disrupted NAD+ metabolism, and oxidative stress, triggers senescence by increasing ROS production and depleting essential factors like NAD+. Mitochondrial dysfunction is a central contributor, leading to energy imbalances and promoting SASP (Wiley et al., 2016). Velarde and colleagues demonstrated that Sod2 loss results in heightened ROS production, DNA damage, and reduced ATP synthesis, leading to cellular senescence in the epidermis, a hallmark of aging skin (Velarde et al., 2012). Additionally, declining NAD+ levels maintain senescence by impairing DNA repair and autophagy while amplifying inflammation (Nacarelli et al., 2019). Changes in lipid metabolism, especially the accumulation of polyunsaturated fatty acids, further reinforce senescence and the SASP. Venables *et al.* identified ceramide as a key regulator of cellular senescence, distinct from quiescent growth arrest. Elevated ceramide levels and sphingomyelinase activity are specifically observed in senescent cells, where exogenous ceramide induces traits such as inhibited DNA synthesis, growth suppression, and dephosphorylation of the Rb protein in young human diploid fibroblasts, mimicking senescence (Venable et al., 1995). Additionally, Ras-induced senescence (RIS) in IMR-90 fibroblasts is associated with distinct metabolic profiles, including the accumulation of long-chain fatty acids and increased mitochondrial fatty acid oxidation. These metabolic changes drive the production of pro-inflammatory cytokines, particularly IL-1β, contributing to the SASP (Quijano et al., 2012). Senescent cells, in turn, exacerbate metabolic diseases such as diabetes and fatty liver through their pro-inflammatory effects, creating a feedback loop between metabolic dysfunction and aging.

Our results demonstrated that FIH depletion led to a downregulation of both glycolysis and OXPHOS, while simultaneously inducing cellular senescence. This observation contrasts with the widely accepted theory that senescent cells typically exhibit impaired OXPHOS alongside increased glycolysis. Currently, we do not have a clear explanation for this discrepancy, highlighting the need for further validation and investigation. Interestingly, the Hallmark pathway *Fatty Acid Metabolism* was upregulated following

FIH knockout in MRC5 cells, suggesting a potential link between fatty acid metabolism and the induction of cellular senescence caused by FIH loss, which warrants further exploration.

Links between metabolism, ECM remodeling and myofibroblast

The de novo synthesis of serine via the serine biosynthetic pathway diverges from glycolysis at the intermediate 3-phosphoglycerate, which is converted to serine through a three-step enzymatic process involving phosphoglycerate dehydrogenase (PHGDH), phosphoserine aminotransferase 1 (PSAT1), and phosphoserine phosphatase (PSPH). Serine then fuels glycine synthesis through the action of serine hydroxymethyltransferases (SHMT1 in the cytoplasm and SHMT2 in the mitochondria) (Amelio et al., 2014; Pacold et al., 2016; Possemato et al., 2011). Nigdelioglu and colleagues demonstrated that TGF-β induces metabolic reprogramming in lung fibroblasts by upregulating glycolysis and the de novo serine synthesis pathway. This leads to increased expression of PHGDH and SHMT2, essential for glycine production, a key component of collagen. Inhibiting these enzymes or limiting glycine significantly reduces collagen synthesis, underscoring their importance in fibrosis (Nigdelioglu et al., 2016). Another study reinforced this by showing that blocking PHGDH pharmacologically or with siRNA similarly reduces collagen production in vitro and in bleomycin-induced lung fibrosis, suggesting its potential as a therapeutic target for IPF. Notably, myofibroblasts can still produce collagen independently of extracellular serine and glycine by relying on glucose-derived glycine (Hamanaka et al., 2018).

In our study, we observed that FIH depletion downregulated both glycolysis and collagen 1 production. To explore whether FIH affects the de novo serine synthesis pathway, we conducted qPCR to assess the expression of key enzymes (PHGDH, PSAT1, PSPH, SHMT1, and SHMT2). However, the data lacked reproducibility, and no significant changes were observed in their mRNA levels (data not shown). Despite these negative findings, the potential regulation of the de novo serine synthesis pathway by FIH warrants further investigation.

The study reveals that lactic acid levels are elevated in IPF lung tissue and myofibroblasts, driven by increased LDH5 expression, which is upregulated by TGF-β. This elevated lactic acid lowers pH, activating latent TGF-β and promoting myofibroblast differentiation and fibrosis. Inhibiting LDH5 reduces lactic acid production, pH acidification, and myofibroblast differentiation, positioning LDH5 as a potential therapeutic target in IPF. Additionally, the study highlights a feed-forward loop where lactic acid activates TGF-β, which induces HIF1α and further LDH5 expression, perpetuating fibrosis (Kottmann et al., 2012). Extracellular lactate accumulation, as shown by Kottmann and colleagues, is likely due to the balance between lactate production and export via monocarboxylate transporters (MCTs). Hypoxia increases MCT-4 expression to facilitate lactate export in glycolytic cells, while MCT-1 supports lactate uptake

for oxidative phosphorylation. This lactate shuttling between glycolytic and oxidative cells mirrors processes in muscle and brain cells and occurs in cancer-associated fibroblasts, which supply lactate to tumor cells via aerobic glycolysis. In IPF, lactate accumulation in the fibroproliferative environment may affect broader cellular processes beyond TGF-β activation. Investigating MCT isoforms in IPF could elucidate mechanisms behind lactate buildup and reveal novel therapeutic strategies for this fatal disease (Tuder et al., 2012). Xie and colleagues further demonstrated that targeting glycolytic flux via inhibition of a rate-limiting glycolytic enzyme, 6-phosphofructo-2-kinase, effectively reduced myofibroblast differentiation and fibrotic progression (Xie et al., 2015). In contrast, our results showed decreased extracellular lactic acid levels, which may contribute to the attenuation of FMT following FIH depletion. However, whether the reduction in glycolysis directly leads to the inhibition of myofibroblast differentiation remains to be further investigated.

6.2 Future Work

Considering all the results and discussions above, it is clear that FIH plays a crucial role in fibroblasts and may contribute to the progression of lung fibrosis. Based on our findings so far, there are several validations can be done in the future.

1. Defining the subtype of fibroblasts in bioinformatic analysis

It is now widely accepted that several fibroblast subtypes are involved in the progression of IPF (Fries et al., 1994). A recent study highlights that multiple fibroblast subtypes contribute to ECM production in lung fibrosis, with myofibroblasts being the primary contributors. Lipofibroblasts, which typically support alveolar development, also express collagen under fibrotic conditions and can transition into myofibroblasts. EBF1+ fibroblasts and pericytes have been shown to express collagen genes, while intermediate fibroblasts marked by CTHRC1 also play a significant role. Mesothelial cells, though less abundant, may support fibrosis through cell interactions (Liu, Dai, Zhang, Huang, Lynn, Rabata, Liang, Noble and Jiang, 2023). In this project, we focused primarily on myofibroblasts rather than other subtypes. While additional research is needed to validate these various fibroblast subtypes, our study underscores the importance of understanding cellular marker changes following FIH depletion. As part of our future work, we plan to collect genetic markers from different fibroblast subtypes and use CIBERSORT to identify the proportion of each fibroblast subtype present in our samples. This analysis will help clarify the specific roles of fibroblast subtypes in FIH-regulated processes and further elucidate how FIH depletion affects fibroblast composition and function in fibrosis. By exploring the molecular shifts in various fibroblast subtypes, we aim to gain a deeper understanding of FIH's role in lung fibrosis and identify new therapeutic targets.

2. Mechanism underlying metabolic alteration caused by the loss of FIH.

To further investigate the mechanisms behind FIH depletion-induced metabolic changes, a comprehensive metabolite screening is essential. The inconsistencies observed between the transcriptomic alterations in FIH KO and KD MRC5 cells make it challenging to pinpoint the exact metabolic reactions FIH is involved in. Metabolic pathways such as glycolysis and OXPHOS require the coordinated action of numerous enzymes. However, changes in enzyme activity do not always manifest at the mRNA or protein levels, making it difficult to infer functional alterations from transcriptomic data alone. This highlights the limitations of relying solely on gene expression data to understand the metabolic impact of FIH depletion.

A detailed analysis of the metabolite profile in FIH-depleted MRC5 cells could provide crucial insights into the specific metabolic steps regulated by FIH. Identifying alterations in intermediate metabolites could help pinpoint where in the glycolysis or OXPHOS pathways FIH plays a regulatory role. By performing metabolomics studies, we could potentially uncover the direct downstream effects of FIH depletion on cellular metabolism and link them to the observed phenotypic changes.

Among the various metabolomic techniques available, 2D-NMR offers significant potential for achieving this goal. 2D-NMR enables a highly detailed and quantitative assessment of the metabolome, making it an ideal method for identifying changes in metabolic intermediates and pathways. However, before applying NMR techniques, the experimental conditions need optimization. For instance, we must ensure a sufficient number of MRC5 cells are available, and the culture medium should be tailored to avoid interference with the NMR analysis. Optimizing these conditions will be crucial to obtaining high-quality data and ensuring accurate metabolite quantification.

Following the metabolite screening, we can utilize enzyme inhibitors or siRNA to block the function of the identified enzymes, or alternatively, restore enzyme activity using recombinant enzymes from commercial kits. These approaches will allow us to determine whether the enzyme function is directly affected by FIH depletion.

This could not only help us understand the specific metabolic reactions that FIH is involved in, but also uncover novel therapeutic targets for diseases like fibrosis, where altered cellular metabolism plays a significant role.

3. Mechanism underlying induction of cellular senescence by FIH depletion.

To investigate the role of FIH in the regulation of cellular senescence, several key experiments and methodologies can be employed. In my current work, I have already demonstrated that the loss of FIH induces senescence, which was confirmed by β-gal staining, a widely used assay for detecting senescent cells. This method visualizes SA-β-gal activity, a hallmark of senescent cells, and helps identify cells that have entered a growth-arrested state.

Building upon this initial finding, future work will further explore the molecular mechanisms underlying FIH-induced senescence by examining additional markers of senescence, such as p16INK4a, p21, and p53. These are critical regulators of cell cycle arrest during senescence. Immunoblotting and immunofluorescence can be used to detect the expression levels of these proteins, helping to clarify how FIH depletion triggers the senescence pathway.

In addition, the role of oxidative stress in FIH-induced senescence should be explored. As increased ROS levels are commonly associated with senescence, future experiments will measure ROS production in FIH-depleted cells using fluorescent probes like DCFDA. By correlating ROS levels with markers of senescence, this will help determine whether oxidative stress is a driving factor in the senescence phenotype observed with FIH depletion.

Furthermore, it would be essential to assess the DNA damage response (DDR) in FIH-depleted cells, as persistent DNA damage is a known inducer of cellular senescence. Immunofluorescence staining for γH2AX and 53BP1, key markers of DNA damage, will reveal whether the loss of FIH induces DNA damage foci, providing further insights into the relationship between FIH depletion and cellular senescence.

To investigate the relationship between metabolic alterations and increased cellular senescence, we plan to restore lactate levels in the culture environment and subsequently perform the assays mentioned above. This approach will help determine whether normalizing extracellular lactate levels can reverse or mitigate the senescence phenotype induced by FIH depletion. By comparing the results, we aim to assess if restoring lactate can return cellular senescence markers to baseline, providing insight into the role of lactate in regulating senescence.

By integrating these experimental approaches, future studies can provide a more comprehensive understanding of the role of FIH in cellular senescence and reveal potential therapeutic targets for conditions linked to senescence, such as aging and fibrotic diseases.

4. Fibroblast-epithelial cell interactions: metabolism, SASP, and ECM remodeling via conditioned medium or 3D culture systems

While our current models have provided valuable insights, it is important to recognize that they are predominantly 2D systems. Although 2D cultures allow precise control of experimental variables and facilitate mechanistic dissection, they fail to fully capture the structural and cellular complexity of the fibrotic lung. Fibrotic foci in vivo are composed of multiple interacting cell types, including fibroblasts, epithelial cells, immune cells, and endothelial cells, all embedded in a dynamic extracellular matrix (ECM). Within this environment, fibroblasts not only remodel the ECM but also influence epithelial cell fate and function through metabolic reprogramming and secretion

of senescence-associated secretory phenotype (SASP) factors. These interactions are difficult to recapitulate in 2D monolayers, where spatial cues and matrix remodeling are absent.

To address this limitation, our future work emphasizes the use of 3D systems. Embedding fibroblasts within hydrogels or scaffolds and co-culturing them with epithelial cells will provide a more physiologically relevant platform for investigating reciprocal interactions. Such models enable the study of fibroblast-driven changes in epithelial proliferation, migration, and differentiation under conditions that better mimic tissue architecture. Techniques such as 3D bioprinting and organoid co-culture can even recreate aspects of alveolar geometry and ECM heterogeneity, providing insights into how fibroblast-driven metabolic alterations or SASP molecules reshape epithelial behavior in fibrosis.

In parallel, the use of fibroblast-conditioned media offers a complementary approach to isolate the role of secreted factors. By analyzing metabolic outcomes (e.g., lactate production, mitochondrial function) and profiling SASP-associated cytokines, we can delineate fibroblast-to-epithelial signaling pathways. Incorporating epithelial organoids into this workflow provides a valuable intermediate system: these organoids preserve the architecture and differentiation capacity of alveolar epithelium while allowing experimental manipulation of fibroblast inputs.

Finally, direct assessment of ECM remodeling in 3D matrices or decellularized lung scaffolds will allow us to link fibroblast activity to alterations in stiffness, composition, and architecture—critical regulators of epithelial adhesion and plasticity. Combining biophysical readouts (e.g., AFM, rheometry) with imaging of ECM proteins (e.g., collagen, fibronectin) will enable us to connect fibroblast metabolic and secretory programs to tangible structural consequences that drive fibrosis progression.

Taken together, this transition from 2D to 3D approaches will move our studies closer to the in vivo setting, offering a more comprehensive understanding of fibroblast–epithelial crosstalk and revealing therapeutic targets that may be overlooked in reductionist systems.

Appendix A

Supplementary information: Buffers

A.1 Protein Lysis Buffer

TABLE A.1: **Recipe of urea buffer**

Component	Concentration	Manufacturer
Urea	8M	Sigma-Aldrich
Tiourea	1M	Sigma-Aldrich
Dithiothreitol (DTT)	50mM	Sigma-Aldrich
Spermine	24mM	Sigma-Aldrich
CHAPS	0.5%	Sigma-Aldrich

A.2 SDS-PAGE gel preparation

TABLE A.2: **Solutions for preparing separation gel**

Solution component	6% Gel	10% Gel	Manufacturer
dH_2O	5.3ml	4.0ml	
30% acrylamide mix	2.0ml	3.3ml	Severn Biotech Ltd
1.5M Tris (pH8.8)	2.5ml	2.5ml	Severn Biotech Ltd
10% SDS	0.1ml	0.1ml	Severn Biotech Ltd
10 % Ammonium Persulfate (APS)	0.1ml	0.1ml	Sigma-Aldrich
TEMED	0.008ml	0.004ml	ThermoFisher Scientific

TABLE A.3: **Solutions for preparing 5% stacking gel**

Solution Component	Volume	Manufacturer
dH_2O	2.7ml	
30% acrylamide mix	0.67ml	Severn Biotech Ltd
1.0M Tris (pH6.8)	0.5ml	Severn Biotech Ltd
10% SDS	0.04ml	Severn Biotech Ltd
10 % Ammonium Persulfate (APS)	0.04ml	Sigma-Aldrich
TEMED	0.004ml	ThermoFisher Scientific

A.3 Running Buffer for SDS-PAGE

TABLE A.4: **10× Running buffer for SDS-PAGE**

Component	Concentration	Manufacturer
Tris-Base	0.25M	Severn Biotech Ltd
Glycine	1.92M	Fisher Scientific
SDS	1%	Sigma-Aldrich
dH_2O		
Adjust pH to 8.3 using HCl		

Dilute to 1 10 for a 1× working concentration using dH_2O.

A.4 Western Blotting Buffers

TABLE A.5: **10× Transfer buffer**

Component	Concentration	Manufacturer
Tris-Base	0.25M	Severn Biotech Ltd
Glycine	1.92M	Fisher Scientific
dH_2O		

Dilute 1 10 for a 1× working concentration, 700ml dH_2O, 200ml Methanol and 100ml 10× buffer.

TABLE A.6: **0.1% Tween-Tris buffered saline (TBST)**

Component	Concentration	Manufacturer
Sodium Chloride (NaCl)	0.15M	Fisher Scientific
1M Tris-HCl (pH7.5-8.0)	0.1M	Severn Biotech Ltd
Tween 20	0.1%	Sigma-Aldrich

Appendix B

Supplementary information: Figures and tables

B.1 Tables

B.1.1 Tables in chapter 3

TABLE B.1: **Average Hallmark GSVA score and P-value in FIH KO MRC5**

Description	FIH WT	FIH KO	Difference	P value
PROTEIN_SECRETION	-2.56E-01	2.63E-01	5.19E-01	1.65E-02
CHOLESTEROL_HOMEOSTASIS	-2.02E-01	1.51E-01	3.53E-01	2.68E-02
PANCREAS_BETA_CELLS	-2.01E-01	2.05E-01	4.06E-01	1.69E-03
OXIDATIVE_PHOSPHORYLATION	-1.90E-01	1.56E-01	3.46E-01	1.25E-01
PEROXISOME	-1.90E-01	1.67E-01	3.57E-01	2.30E-03
HEME_METABOLISM	-1.86E-01	1.47E-01	3.32E-01	4.69E-04
FATTY_ACID_METABOLISM	-1.79E-01	1.19E-01	2.98E-01	1.42E-02
HEDGEHOG_SIGNALING	-1.52E-01	1.34E-01	2.86E-01	7.16E-02
P53_PATHWAY	-1.21E-01	9.90E-02	2.20E-01	1.32E-01
KRAS_SIGNALING_DN	-1.18E-01	9.21E-02	2.10E-01	5.89E-02
APICAL_SURFACE	-1.15E-01	9.58E-02	2.11E-01	9.20E-02
BILE_ACID_METABOLISM	-7.95E-02	7.96E-02	1.59E-01	1.19E-01
GLYCOLYSIS	-6.13E-02	4.48E-02	1.06E-01	2.37E-01
APOPTOSIS	-4.61E-02	2.28E-02	6.88E-02	1.87E-01
XENOBIOTIC_METABOLISM	-3.67E-02	-6.53E-03	3.02E-02	7.46E-01
ADIPOGENESIS	-3.49E-02	1.50E-02	4.99E-02	4.29E-01
APICAL_JUNCTION	-3.34E-02	-1.27E-03	3.21E-02	7.58E-01
HYPOXIA	-3.08E-02	1.21E-02	4.29E-02	5.44E-01
COAGULATION	-3.07E-02	-4.56E-03	2.61E-02	8.25E-01
MYOGENESIS	-1.61E-02	-3.23E-04	1.58E-02	8.47E-01
REACTIVE_OXYGEN_SPECIES_PATHWAY	-1.57E-02	-5.24E-03	1.05E-02	9.51E-01
COMPLEMENT	-1.07E-02	-1.35E-02	-2.76E-03	9.12E-01
WNT_BETA_CATENIN_SIGNALING	1.59E-02	-6.81E-02	-8.40E-02	7.08E-01
ALLOGRAFT_REJECTION	1.73E-02	-2.32E-03	-1.96E-02	7.68E-01
PI3K_AKT_MTOR_SIGNALING	2.28E-02	-5.63E-02	-7.91E-02	3.47E-01
ESTROGEN_RESPONSE_EARLY	2.46E-02	-3.15E-02	-5.61E-02	5.53E-01
DNA_REPAIR	2.53E-02	-5.66E-02	-8.19E-02	3.42E-01
UV_RESPONSE_UP	3.89E-02	-7.45E-02	-1.13E-01	3.37E-01
UV_RESPONSE_DN	4.74E-02	-6.37E-02	-1.11E-01	5.34E-01
KRAS_SIGNALING_UP	5.82E-02	-9.49E-02	-1.53E-01	4.11E-02
ESTROGEN_RESPONSE_LATE	1.01E-01	-8.82E-02	-1.89E-01	8.79E-02
ANDROGEN_RESPONSE	1.03E-01	-1.32E-01	-2.35E-01	6.53E-02
ANGIOGENESIS	1.04E-01	-1.54E-01	-2.59E-01	1.52E-01
IL2_STAT5_SIGNALING	1.10E-01	-1.05E-01	-2.15E-01	4.31E-03
NOTCH_SIGNALING	1.25E-01	-1.46E-01	-2.72E-01	1.92E-01
INTERFERON_ALPHA_RESPONSE	1.32E-01	-1.16E-01	-2.48E-01	2.72E-01
INFLAMMATORY_RESPONSE	1.37E-01	-1.00E-01	-2.37E-01	5.08E-02
INTERFERON_GAMMA_RESPONSE	1.40E-01	-1.61E-01	-3.01E-01	1.23E-01
MTORC1_SIGNALING	1.43E-01	-1.62E-01	-3.05E-01	9.21E-03
IL6_JAK_STAT3_SIGNALING	1.51E-01	-1.61E-01	-3.12E-01	1.33E-02
EPITHELIAL_MESENCHYMAL_TRANSITION	1.58E-01	-1.68E-01	-3.27E-01	1.01E-03
UNFOLDED_PROTEIN_RESPONSE	1.63E-01	-1.88E-01	-3.51E-01	6.87E-03
SPERMATOGENESIS	1.84E-01	-2.15E-01	-3.99E-01	1.03E-02
TNFA_SIGNALING_VIA_NFKB	2.12E-01	-2.43E-01	-4.55E-01	9.39E-05
TGF_BETA_SIGNALING	2.20E-01	-2.07E-01	-4.27E-01	2.36E-02
MITOTIC_SPINDLE	2.27E-01	-2.35E-01	-4.62E-01	4.18E-03
MYC_TARGETS_V1	2.45E-01	-2.71E-01	-5.16E-01	2.76E-02
MYC_TARGETS_V2	3.39E-01	-3.56E-01	-6.95E-01	4.73E-03
G2M_CHECKPOINT	4.55E-01	-4.69E-01	-9.24E-01	1.34E-05
E2F_TARGETS	5.00E-01	-4.98E-01	-9.98E-01	1.02E-06

TABLE B.2: **Average Hallmark GSVA score and P-value in siFIH MRC5 cells**

Description	Control	siFIH	Difference	P value
ANGIOGENESIS	-3.69E-01	3.03E-01	6.72E-01	3.20E-02
PANCREAS_BETA_CELLS	-2.86E-01	2.52E-01	5.38E-01	2.73E-01
TNFA_SIGNALING_VIA_NFKB	-2.78E-01	2.55E-01	5.32E-01	1.18E-03
WNT_BETA_CATENIN_SIGNALING	-2.08E-01	1.55E-01	3.63E-01	3.29E-02
HEME_METABOLISM	-2.05E-01	2.15E-01	4.19E-01	6.83E-02
TGF_BETA_SIGNALING	-1.76E-01	9.54E-02	2.72E-01	2.16E-01
EPITHELIAL_MESENCHYMAL_TRANSITION	-1.62E-01	1.53E-01	3.14E-01	9.87E-02
ANDROGEN_RESPONSE	-1.47E-01	1.33E-01	2.80E-01	1.48E-01
APOPTOSIS	-1.45E-01	1.21E-01	2.66E-01	1.39E-01
HYPOXIA	-1.42E-01	1.42E-01	2.84E-01	7.96E-02
NOTCH_SIGNALING	-1.40E-01	1.05E-01	2.45E-01	1.07E-01
INFLAMMATORY_RESPONSE	-1.31E-01	1.05E-01	2.36E-01	4.46E-02
GLYCOLYSIS	-1.16E-01	9.01E-02	2.06E-01	1.48E-01
HEDGEHOG_SIGNALING	-7.76E-02	7.88E-02	1.56E-01	5.50E-01
KRAS_SIGNALING_DN	-7.38E-02	5.99E-02	1.34E-01	4.79E-02
P53_PATHWAY	-6.96E-02	5.18E-02	1.21E-01	2.41E-01
IL6_JAK_STAT3_SIGNALING	-6.04E-02	2.38E-02	8.42E-02	6.48E-01
UV_RESPONSE_UP	-5.56E-02	4.44E-02	1.00E-01	5.40E-01
UNFOLDED_PROTEIN_RESPONSE	-5.29E-02	1.46E-02	6.75E-02	6.99E-01
ADIPOGENESIS	-4.62E-02	3.07E-03	4.92E-02	8.21E-01
MYC_TARGETS_V1	-1.80E-02	5.57E-03	2.36E-02	8.96E-01
KRAS_SIGNALING_UP	-1.56E-02	1.89E-02	3.45E-02	6.86E-01
IL2_STAT5_SIGNALING	-1.21E-02	-2.54E-03	9.56E-03	9.23E-01
XENOBIOTIC_METABOLISM	-6.24E-03	1.49E-02	2.11E-02	6.69E-01
PROTEIN_SECRETION	3.40E-03	-3.92E-02	-4.26E-02	7.55E-01
ALLOGRAFT_REJECTION	4.45E-03	-7.07E-02	-7.51E-02	6.03E-01
MYOGENESIS	4.83E-03	9.16E-03	4.33E-03	9.72E-01
DNA_REPAIR	1.01E-02	-6.49E-03	-1.66E-02	9.07E-01
OXIDATIVE_PHOSPHORYLATION	1.07E-02	-5.38E-02	-6.45E-02	7.87E-01
PEROXISOME	1.27E-02	3.19E-03	-9.50E-03	9.07E-01
MITOTIC_SPINDLE	3.06E-02	2.65E-02	-4.17E-03	9.86E-01
ESTROGEN_RESPONSE_EARLY	3.07E-02	-2.90E-02	-5.97E-02	4.66E-01
UV_RESPONSE_DN	3.66E-02	-4.08E-02	-7.74E-02	5.19E-01
MTORC1_SIGNALING	4.59E-02	-1.07E-01	-1.53E-01	4.42E-01
APICAL_JUNCTION	4.93E-02	-4.06E-02	-8.98E-02	3.40E-01
FATTY_ACID_METABOLISM	7.05E-02	-8.24E-03	-7.88E-02	3.86E-01
INTERFERON_GAMMA_RESPONSE	7.32E-02	-1.37E-01	-2.10E-01	4.18E-01
COMPLEMENT	7.39E-02	-5.56E-02	-1.30E-01	2.71E-01
COAGULATION	8.04E-02	-5.41E-02	-1.34E-01	2.07E-01
APICAL_SURFACE	8.57E-02	-1.22E-01	-2.08E-01	1.39E-01
REACTIVE_OXYGEN_SPECIES_PATHWAY	1.11E-01	-1.10E-01	-2.21E-01	4.75E-01
MYC_TARGETS_V2	1.19E-01	-1.31E-01	-2.50E-01	4.60E-02
BILE_ACID_METABOLISM	1.24E-01	-8.97E-02	-2.14E-01	6.64E-02
SPERMATOGENESIS	1.25E-01	-1.23E-01	-2.48E-01	3.79E-02
ESTROGEN_RESPONSE_LATE	1.35E-01	-1.43E-01	-2.78E-01	3.24E-02
E2F_TARGETS	1.44E-01	-1.96E-01	-3.40E-01	1.65E-02
G2M_CHECKPOINT	1.57E-01	-1.75E-01	-3.32E-01	5.37E-02
PI3K_AKT_MTOR_SIGNALING	1.75E-01	-1.76E-01	-3.51E-01	3.30E-02
INTERFERON_ALPHA_RESPONSE	2.06E-01	-2.68E-01	-4.73E-01	1.65E-01
CHOLESTEROL_HOMEOSTASIS	3.21E-01	-3.21E-01	-6.42E-01	1.34E-04

TABLE B.3: **Average Hallmark GSVA score and P-value in siFIH NHLFs**

Description	Control	siFIH	Difference	P value
HYPOXIA	-2.61E-01	2.23E-01	4.84E-01	9.25E-02
TGF_BETA_SIGNALING	-2.50E-01	2.25E-01	4.75E-01	1.61E-02
TNFA_SIGNALING_VIA_NFKB	-2.37E-01	2.30E-01	4.67E-01	4.21E-02
P53_PATHWAY	-2.02E-01	1.50E-01	3.52E-01	1.63E-01
UV_RESPONSE_DN	-1.97E-01	1.77E-01	3.74E-01	7.08E-03
WNT_BETA_CATENIN_SIGNALING	-1.61E-01	1.18E-01	2.79E-01	2.76E-01
KRAS_SIGNALING_UP	-1.55E-01	1.21E-01	2.75E-01	2.96E-01
EPITHELIAL_MESENCHYMAL_TRANSITION	-1.47E-01	1.31E-01	2.78E-01	5.76E-02
MYOGENESIS	-1.33E-01	1.19E-01	2.52E-01	2.97E-02
HEME_METABOLISM	-1.33E-01	8.70E-02	2.19E-01	2.74E-01
ANDROGEN_RESPONSE	-1.13E-01	1.09E-01	2.22E-01	1.87E-01
APOPTOSIS	-8.86E-02	7.85E-02	1.67E-01	3.27E-01
COAGULATION	-8.31E-02	6.63E-02	1.49E-01	1.99E-01
APICAL_JUNCTION	-8.04E-02	8.22E-02	1.63E-01	1.24E-01
UV_RESPONSE_UP	-7.16E-02	4.03E-02	1.12E-01	6.24E-01
ANGIOGENESIS	-5.34E-02	3.45E-02	8.79E-02	7.80E-01
IL2_STAT5_SIGNALING	-3.94E-02	4.52E-02	8.45E-02	3.14E-01
ESTROGEN_RESPONSE_EARLY	-2.09E-02	1.66E-02	3.75E-02	5.34E-01
APICAL_SURFACE	-2.08E-02	5.25E-02	7.33E-02	7.58E-01
COMPLEMENT	-2.01E-02	1.81E-04	2.02E-02	9.26E-01
MYC_TARGETS_V2	-1.77E-02	-3.05E-02	-1.28E-02	7.43E-01
MITOTIC_SPINDLE	-1.19E-02	1.49E-02	2.68E-02	9.01E-01
PROTEIN_SECRETION	3.76E-03	-8.93E-03	-1.27E-02	9.21E-01
GLYCOLYSIS	1.20E-02	1.45E-02	2.51E-03	9.94E-01
DNA_REPAIR	1.47E-02	-5.61E-02	-7.08E-02	7.87E-01
KRAS_SIGNALING_DN	1.67E-02	3.79E-02	2.12E-02	8.90E-01
PI3K_AKT_MTOR_SIGNALING	1.70E-02	-9.52E-03	-2.65E-02	7.78E-01
ESTROGEN_RESPONSE_LATE	2.00E-02	-3.12E-02	-5.12E-02	6.81E-01
PEROXISOME	4.49E-02	-4.29E-02	-8.78E-02	7.59E-01
HEDGEHOG_SIGNALING	4.62E-02	-6.19E-02	-1.08E-01	5.08E-01
ADIPOGENESIS	5.42E-02	-5.88E-02	-1.13E-01	6.32E-01
NOTCH_SIGNALING	5.52E-02	-1.89E-02	-7.42E-02	6.30E-01
ALLOGRAFT_REJECTION	5.87E-02	-3.31E-02	-9.18E-02	4.15E-01
INFLAMMATORY_RESPONSE	6.40E-02	-4.52E-02	-1.09E-01	4.74E-01
FATTY_ACID_METABOLISM	7.35E-02	-6.07E-02	-1.34E-01	6.56E-01
OXIDATIVE_PHOSPHORYLATION	9.12E-02	-5.35E-02	-1.45E-01	7.49E-01
PANCREAS_BETA_CELLS	9.15E-02	1.36E-02	-7.79E-02	6.62E-01
XENOBIOTIC_METABOLISM	9.38E-02	-7.29E-02	-1.67E-01	4.44E-01
REACTIVE_OXYGEN_SPECIES_PATHWAY	1.11E-01	-4.95E-02	-1.60E-01	5.78E-01
BILE_ACID_METABOLISM	1.11E-01	-1.25E-01	-2.37E-01	1.49E-01
CHOLESTEROL_HOMEOSTASIS	1.32E-01	-1.23E-01	-2.55E-01	1.55E-01
UNFOLDED_PROTEIN_RESPONSE	1.44E-01	-1.71E-01	-3.15E-01	7.05E-02
SPERMATOGENESIS	1.75E-01	-1.62E-01	-3.37E-01	2.28E-01
MYC_TARGETS_V1	1.85E-01	-1.28E-01	-3.13E-01	2.61E-01
MTORC1_SIGNALING	1.96E-01	-1.83E-01	-3.78E-01	1.06E-01
IL6_JAK_STAT3_SIGNALING	2.46E-01	-2.46E-01	-4.92E-01	4.23E-02
G2M_CHECKPOINT	3.41E-01	-3.29E-01	-6.71E-01	1.67E-03
INTERFERON_GAMMA_RESPONSE	3.48E-01	-3.42E-01	-6.89E-01	1.14E-02
INTERFERON_ALPHA_RESPONSE	3.93E-01	-3.79E-01	-7.72E-01	1.91E-02
E2F_TARGETS	4.16E-01	-4.03E-01	-8.19E-01	2.19E-03

TABLE B.4: **Average Hallmark GSVA score and P-value in FIH KO MEFs**

Description	FIH WT	FIH KO	Difference	P value
PI3K_AKT_MTOR_SIGNALING	-6.99E-01	6.99E-01	1.40E+00	1.79E-04
SPERMATOGENESIS	-6.97E-01	6.97E-01	1.39E+00	1.29E-02
MTORC1_SIGNALING	-6.46E-01	6.32E-01	1.28E+00	1.39E-02
PANCREAS_BETA_CELLS	-4.00E-01	3.97E-01	7.97E-01	1.43E-02
HEME_METABOLISM	-3.91E-01	5.05E-01	8.96E-01	3.10E-02
ALLOGRAFT_REJECTION	-3.81E-01	2.48E-01	6.29E-01	1.03E-01
HEDGEHOG_SIGNALING	-3.75E-01	6.91E-02	4.44E-01	5.34E-01
REACTIVE_OXYGEN_SPECIES_PATHWAY	-3.65E-01	5.17E-01	8.82E-01	1.03E-01
APICAL_JUNCTION	-3.42E-01	2.89E-01	6.31E-01	1.49E-01
INTERFERON_GAMMA_RESPONSE	-3.20E-01	2.14E-01	5.34E-01	8.00E-02
G2M_CHECKPOINT	-2.75E-01	2.33E-01	5.08E-01	6.52E-02
APOPTOSIS	-2.73E-01	2.48E-01	5.21E-01	4.28E-02
GLYCOLYSIS	-2.55E-01	2.32E-01	4.87E-01	7.36E-02
EPITHELIAL_MESENCHYMAL_TRANSITION	-2.47E-01	2.38E-01	4.85E-01	2.69E-02
UNFOLDED_PROTEIN_RESPONSE	-2.31E-01	1.92E-01	4.22E-01	3.83E-01
ANGIOGENESIS	-2.28E-01	6.33E-02	2.91E-01	3.04E-01
INTERFERON_ALPHA_RESPONSE	-2.13E-01	2.87E-01	4.99E-01	4.61E-01
MITOTIC_SPINDLE	-2.09E-01	3.05E-01	5.14E-01	2.53E-01
E2F_TARGETS	-1.56E-01	2.62E-01	4.18E-01	1.29E-01
P53_PATHWAY	-1.38E-01	3.34E-02	1.72E-01	3.06E-01
ADIPOGENESIS	-1.27E-01	2.50E-01	3.76E-01	4.99E-01
BILE_ACID_METABOLISM	-1.26E-01	-1.77E-02	1.08E-01	7.47E-01
PEROXISOME	-8.78E-02	1.35E-02	1.01E-01	6.11E-01
COMPLEMENT	-8.05E-02	-6.53E-02	1.52E-02	9.71E-01
ANDROGEN_RESPONSE	-7.73E-02	6.24E-02	1.40E-01	5.83E-01
PROTEIN_SECRETION	-6.64E-02	1.35E-01	2.02E-01	7.95E-01
UV_RESPONSE_DN	-3.36E-02	2.19E-02	5.55E-02	8.72E-01
ESTROGEN_RESPONSE_LATE	-2.65E-02	3.64E-02	6.29E-02	8.12E-01
XENOBIOTIC_METABOLISM	-6.62E-03	9.63E-02	1.03E-01	7.06E-01
HYPOXIA	-6.52E-03	-4.91E-02	-4.26E-02	4.68E-01
CHOLESTEROL_HOMEOSTASIS	1.02E-02	5.48E-03	-4.68E-03	9.93E-01
FATTY_ACID_METABOLISM	2.51E-02	-3.34E-02	-5.85E-02	9.05E-01
DNA_REPAIR	6.68E-02	1.28E-01	6.13E-02	9.00E-01
ESTROGEN_RESPONSE_EARLY	6.94E-02	-9.00E-02	-1.59E-01	2.52E-01
UV_RESPONSE_UP	1.09E-01	-1.45E-01	-2.54E-01	5.98E-01
KRAS_SIGNALING_UP	1.34E-01	-1.56E-01	-2.90E-01	4.21E-01
IL2_STAT5_SIGNALING	1.36E-01	-1.18E-01	-2.55E-01	7.42E-02
TNFA_SIGNALING_VIA_NFKB	1.51E-01	-2.69E-01	-4.20E-01	4.10E-02
APICAL_SURFACE	1.52E-01	-3.33E-01	-4.85E-01	3.80E-01
COAGULATION	1.65E-01	4.11E-02	-1.24E-01	6.54E-01
MYOGENESIS	1.99E-01	-2.52E-01	-4.51E-01	2.29E-01
MYC_TARGETS_V2	3.06E-01	-3.06E-01	-6.12E-01	1.02E-01
INFLAMMATORY_RESPONSE	3.11E-01	-3.11E-01	-6.22E-01	1.76E-02
NOTCH_SIGNALING	3.20E-01	-3.08E-01	-6.29E-01	2.75E-01
WNT_BETA_CATENIN_SIGNALING	4.08E-01	-3.94E-01	-8.02E-01	4.17E-02
OXIDATIVE_PHOSPHORYLATION	4.44E-01	-3.48E-01	-7.92E-01	9.66E-02
KRAS_SIGNALING_DN	4.45E-01	-3.46E-01	-7.91E-01	4.08E-02
MYC_TARGETS_V1	4.97E-01	-4.60E-01	-9.57E-01	2.18E-03
TGF_BETA_SIGNALING	5.95E-01	-3.11E-01	-9.06E-01	5.01E-03
IL6_JAK_STAT3_SIGNALING	6.24E-01	-3.46E-01	-9.70E-01	1.04E-01

TABLE B.5: **Average Hallmark GSVA score of 4 datasets**

Description	MRC5_FIHKO	MRC5_siFIH	NHLFs_siFIH	MEF_FIHKO
E2F_TARGETS	-9.98E-01	-5.58E-01	-8.19E-01	4.18E-01
G2M_CHECKPOINT	-9.24E-01	-3.96E-01	-6.71E-01	5.08E-01
MYC_TARGETS_V2	-6.95E-01	1.32E-02	-1.28E-02	-6.12E-01
MYC_TARGETS_V1	-5.16E-01	-3.51E-02	-3.13E-01	-9.57E-01
MITOTIC_SPINDLE	-4.62E-01	-6.12E-02	2.68E-02	5.14E-01
TNFA_SIGNALING_VIA_NFKB	-4.55E-01	5.58E-01	4.67E-01	-4.20E-01
TGF_BETA_SIGNALING	-4.27E-01	2.08E-01	4.75E-01	-9.06E-01
SPERMATOGENESIS	-3.99E-01	-3.02E-01	-3.37E-01	1.39E+00
UNFOLDED_PROTEIN_RESPONSE	-3.51E-01	-1.02E-01	-3.15E-01	4.22E-01
EPITHELIAL_MESENCHYMAL_TRANSITION	-3.27E-01	1.92E-01	2.78E-01	4.85E-01
IL6_JAK_STAT3_SIGNALING	-3.12E-01	5.50E-02	-4.92E-01	-9.70E-01
MTORC1_SIGNALING	-3.05E-01	-2.13E-01	-3.78E-01	1.28E+00
INTERFERON_GAMMA_RESPONSE	-3.01E-01	-1.95E-01	-6.89E-01	5.34E-01
NOTCH_SIGNALING	-2.72E-01	3.48E-01	-7.42E-02	-6.29E-01
ANGIOGENESIS	-2.59E-01	2.06E-03	8.79E-02	2.91E-01
INTERFERON_ALPHA_RESPONSE	-2.48E-01	-4.95E-01	-7.72E-01	5.00E-01
INFLAMMATORY_RESPONSE	-2.37E-01	2.77E-01	-1.09E-01	-6.22E-01
ANDROGEN_RESPONSE	-2.35E-01	6.58E-02	2.22E-01	1.40E-01
IL2_STAT5_SIGNALING	-2.15E-01	8.72E-02	8.45E-02	-2.55E-01
ESTROGEN_RESPONSE_LATE	-1.89E-01	-2.45E-01	-5.12E-02	6.29E-02
KRAS_SIGNALING_UP	-1.53E-01	5.28E-02	2.75E-01	-2.90E-01
UV_RESPONSE_UP	-1.13E-01	1.98E-02	1.12E-01	-2.54E-01
UV_RESPONSE_DN	-1.11E-01	7.08E-02	3.74E-01	5.55E-02
WNT_BETA_CATENIN_SIGNALING	-8.40E-02	-4.37E-02	2.79E-01	-8.02E-01
DNA_REPAIR	-8.19E-02	-1.59E-01	-7.08E-02	6.13E-02
PI3K_AKT_MTOR_SIGNALING	-7.91E-02	-1.96E-01	-2.65E-02	1.40E+00
ESTROGEN_RESPONSE_EARLY	-5.61E-02	2.48E-02	3.75E-02	-1.59E-01
ALLOGRAFT_REJECTION	-1.96E-02	1.35E-01	-9.18E-02	6.29E-01
COMPLEMENT	-2.76E-03	-1.57E-02	2.02E-02	1.52E-02
REACTIVE_OXYGEN_SPECIES_PATHWAY	1.05E-02	-2.87E-01	-1.60E-01	8.82E-01
MYOGENESIS	1.58E-02	2.84E-03	2.52E-01	-4.51E-01
COAGULATION	2.61E-02	6.23E-02	1.49E-01	-1.24E-01
XENOBIOTIC_METABOLISM	3.02E-02	-2.12E-01	-1.67E-01	1.03E-01
APICAL_JUNCTION	3.21E-02	-6.95E-02	1.63E-01	6.31E-01
HYPOXIA	4.29E-02	4.13E-01	4.84E-01	-4.26E-02
ADIPOGENESIS	4.99E-02	-1.01E-01	-1.13E-01	3.76E-01
APOPTOSIS	6.88E-02	2.32E-02	1.67E-01	5.21E-01
GLYCOLYSIS	1.06E-01	1.19E-01	2.51E-03	4.87E-01
BILE_ACID_METABOLISM	1.59E-01	-2.16E-01	-2.37E-01	1.08E-01
KRAS_SIGNALING_DN	2.10E-01	-2.04E-02	2.12E-02	-7.91E-01
APICAL_SURFACE	2.11E-01	-1.60E-01	7.33E-02	-4.85E-01
P53_PATHWAY	2.20E-01	-9.43E-02	3.52E-01	1.72E-01
HEDGEHOG_SIGNALING	2.86E-01	-9.76E-02	-1.08E-01	4.44E-01
FATTY_ACID_METABOLISM	2.98E-01	-3.03E-01	-1.34E-01	-5.85E-02
HEME_METABOLISM	3.32E-01	1.54E-01	2.19E-01	8.96E-01
OXIDATIVE_PHOSPHORYLATION	3.46E-01	-1.17E-01	-1.45E-01	-7.92E-01
CHOLESTEROL_HOMEOSTASIS	3.53E-01	-4.30E-01	-2.55E-01	-4.68E-03
PEROXISOME	3.57E-01	-1.28E-01	-8.78E-02	1.01E-01
PANCREAS_BETA_CELLS	4.06E-01	-3.09E-01	-7.79E-02	7.97E-01
PROTEIN_SECRETION	5.19E-01	2.12E-02	-1.27E-02	2.02E-01

B.1.2 Tables in chapter 5

TABLE B.6: **Average Hallmark GSVA score and P-value in FIH KO MRC5 with/without TGFβ**

	GSVA score				P value	
Hallmark pathway	WT	WT_TGFβ	FIHKO	FIHKO_TGFβ	WT_TGFβ vs FIHKO_TGFβ	WT_TGFβ vs WT
PANCREAS_BETA_CELLS	-3.98E-01	3.78E-01	-2.82E-02	1.32E-01	2.48E-01	8.88E-04
HEDGEHOG_SIGNALING	-3.85E-01	2.49E-01	-3.89E-02	2.13E-01	9.45E-01	5.11E-05
CHOLESTEROL_HOMEOSTASIS	-3.42E-01	1.72E-01	-4.16E-02	2.35E-01	8.14E-01	4.31E-04
EPITHELIAL_MESENCHYMAL_TRANSITION	-2.17E-01	3.79E-01	-3.61E-01	2.14E-01	1.32E-02	1.78E-06
PROTEIN_SECRETION	-1.87E-01	-3.07E-01	2.76E-01	1.33E-01	1.36E-02	6.79E-01
MYOGENESIS	-1.81E-01	7.95E-02	-3.96E-02	1.24E-01	8.75E-01	1.07E-02
GLYCOLYSIS	-1.50E-01	-2.16E-02	-7.71E-02	2.08E-01	5.86E-03	1.03E-01
HEME_METABOLISM	-1.41E-01	-1.46E-01	1.79E-01	5.58E-02	1.20E-02	9.99E-01
UNFOLDED_PROTEIN_RESPONSE	-1.40E-01	2.79E-01	-3.85E-01	2.15E-01	3.36E-01	1.17E-05
HYPOXIA	-1.14E-01	-2.29E-02	-7.34E-02	1.76E-01	5.08E-02	4.97E-01
PEROXISOME	-1.07E-01	-1.48E-01	1.87E-01	3.34E-02	1.13E-02	7.63E-01
MTORC1_SIGNALING	-8.76E-02	2.67E-01	-3.42E-01	1.46E-01	4.22E-02	4.84E-05
APICAL_SURFACE	-8.12E-02	-1.29E-01	1.70E-01	1.33E-01	3.97E-02	9.24E-01
FATTY_ACID_METABOLISM	-8.04E-02	-1.38E-01	1.99E-01	-3.76E-02	5.84E-01	8.73E-01
APICAL_JUNCTION	-6.01E-02	1.18E-02	-3.63E-02	6.37E-02	8.81E-01	7.46E-01
P53_PATHWAY	-4.82E-02	-2.03E-01	1.82E-01	9.14E-02	1.21E-03	4.73E-02
MITOTIC_SPINDLE	-2.81E-02	3.42E-01	-3.89E-01	5.27E-02	1.74E-04	2.86E-05
APOPTOSIS	-2.57E-02	-3.18E-02	2.45E-02	4.32E-03	8.72E-01	9.99E-01
UV_RESPONSE_DN	-1.30E-02	6.74E-02	-1.31E-01	4.83E-02	9.97E-01	8.48E-01
OXIDATIVE_PHOSPHORYLATION	3.23E-03	-3.05E-01	2.53E-01	1.18E-02	8.77E-02	9.75E-02
COAGULATION	2.94E-02	-3.57E-02	6.76E-02	-9.47E-02	6.28E-01	5.57E-01
DNA_REPAIR	4.18E-02	2.22E-02	-1.10E-01	-3.59E-02	8.66E-01	9.93E-01
KRAS_SIGNALING_DN	4.36E-02	-2.27E-01	1.53E-01	-2.90E-02	1.13E-03	1.28E-04
ADIPOGENESIS	5.16E-02	-1.74E-01	1.45E-01	-8.22E-02	4.47E-01	2.08E-02
TGF_BETA_SIGNALING	5.75E-02	3.09E-01	-3.61E-01	1.54E-02	9.24E-03	2.16E-02
XENOBIOTIC_METABOLISM	6.25E-02	-5.48E-02	4.51E-02	-5.68E-02	1.00E+00	4.02E-01
ESTROGEN_RESPONSE_EARLY	6.91E-02	-7.30E-02	-1.58E-02	3.33E-02	1.95E-01	6.84E-02
COMPLEMENT	6.94E-02	-1.03E-01	6.50E-02	-5.67E-02	6.62E-01	1.02E-02
ANGIOGENESIS	7.24E-02	1.75E-01	-1.88E-01	-9.60E-02	1.42E-01	7.90E-01
ANDROGEN_RESPONSE	7.28E-02	1.86E-01	-2.12E-01	-5.55E-02	4.11E-03	1.57E-01
WNT_BETA_CATENIN_SIGNALING	8.17E-02	1.29E-02	-2.88E-02	-1.50E-01	5.89E-01	9.44E-01
BILE_ACID_METABOLISM	8.43E-02	-1.87E-01	1.86E-01	-8.60E-02	5.13E-01	2.01E-02
IL2_STAT5_SIGNALING	8.98E-02	3.34E-02	-8.10E-02	-6.71E-02	3.43E-01	7.51E-01
KRAS_SIGNALING_UP	9.10E-02	1.73E-02	-4.85E-02	-8.91E-02	5.85E-02	2.19E-01
MYC_TARGETS_V2	1.12E-01	3.91E-01	-5.79E-01	1.99E-01	4.17E-01	1.61E-01
PI3K_AKT_MTOR_SIGNALING	1.13E-01	-1.14E-01	-4.93E-02	-6.16E-03	5.95E-01	9.98E-02
UV_RESPONSE_UP	1.44E-01	-7.49E-02	-8.03E-02	7.99E-03	6.67E-01	6.14E-02
ESTROGEN_RESPONSE_LATE	1.49E-01	-5.41E-02	-7.02E-02	-3.02E-02	9.56E-01	1.14E-02
SPERMATOGENESIS	1.51E-01	1.68E-01	-2.43E-01	-6.34E-02	2.32E-02	9.92E-01
ALLOGRAFT_REJECTION	1.55E-01	-1.79E-01	9.94E-02	-5.60E-02	1.79E-01	1.15E-03
MYC_TARGETS_V1	1.56E-01	2.80E-01	-4.37E-01	6.98E-02	1.76E-01	5.59E-01
NOTCH_SIGNALING	1.85E-01	1.19E-02	-1.10E-01	-7.94E-02	8.87E-01	5.54E-01
REACTIVE_OXYGEN_SPECIES_PATHWAY	2.04E-01	-2.53E-01	2.12E-01	-1.82E-01	8.17E-01	2.18E-03
INFLAMMATORY_RESPONSE	2.33E-01	2.09E-02	-7.17E-02	-1.77E-01	2.66E-02	1.85E-02
TNFA_SIGNALING_VIA_NFKB	2.62E-01	1.04E-01	-1.60E-01	-2.35E-01	7.87E-06	1.78E-03
G2M_CHECKPOINT	3.02E-01	5.45E-01	-6.14E-01	-2.09E-01	1.21E-06	4.08E-03
IL6_JAK_STAT3_SIGNALING	3.53E-01	-1.94E-01	5.75E-02	-2.42E-01	2.01E-01	2.93E-08
E2F_TARGETS	4.21E-01	5.71E-01	-6.59E-01	-3.45E-01	1.03E-09	5.75E-04
INTERFERON_GAMMA_RESPONSE	4.33E-01	-2.59E-01	1.98E-01	-4.15E-01	1.46E-01	2.14E-05
INTERFERON_ALPHA_RESPONSE	4.86E-01	-3.79E-01	3.25E-01	-4.66E-01	5.78E-01	5.30E-06

B.2 Figure

B.2.1 Figure for Chapter 4

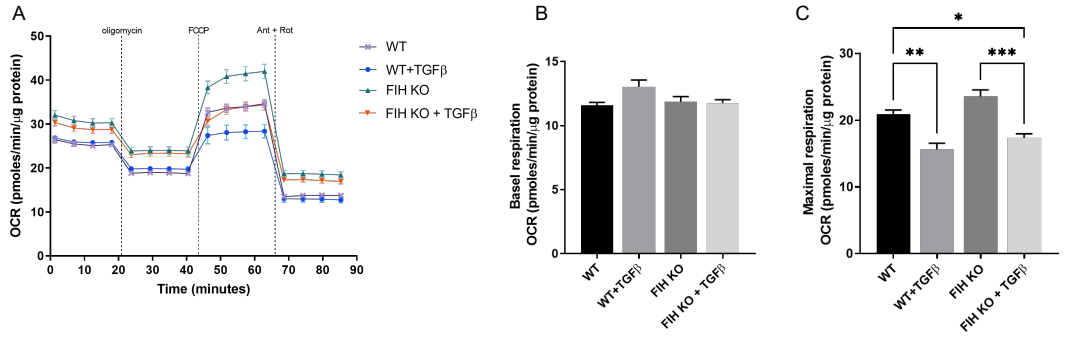

FIGURE B.1: **FIH knockout have no significant effect on mitochondrial oxidative phosphorylation**

FIH WT and KO MRC5 cells were treated with TGFβ for 48 hours, followed by real-time measurement of oxygen consumption rate (OCR) (A). Basal OCR (B) and maximal respiration OCR (C) were calculated from the data shown in (A) (mean ± SD, n = 4). *P $<$ 0.05, **P $<$ 0.01, *** P $<$ 0.001 by Tukey's multiplecomparison test. OCR, Oxygen consumption rate.

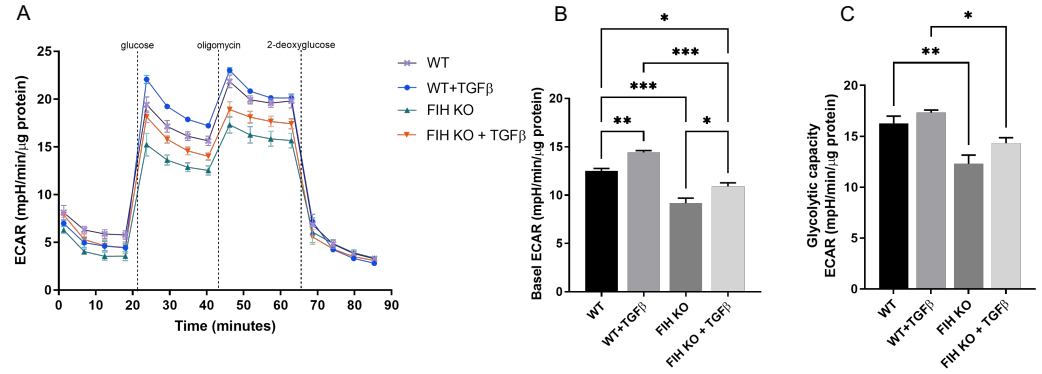

FIGURE B.2: **FIH depletion inhibits glycolysis**

(A–C) FIH WT and FIH KO MRC5 cells were treated with PBS/TGFβ for 48 hours, then subjected to determination of real-time ECAR (A). Basal ECAR (B) and Glycolytic capacity OCR (C) were calculated from data shown in A (mean ± SD, n = 4). *P $<$ 0.05, **P $<$ 0.01, *** P $<$ 0.001 by Tukey's multiple comparison test. ECAR, Extracellular acidification rate.

B.2.2 Figure for Chapter 5

Figure.5.3 A

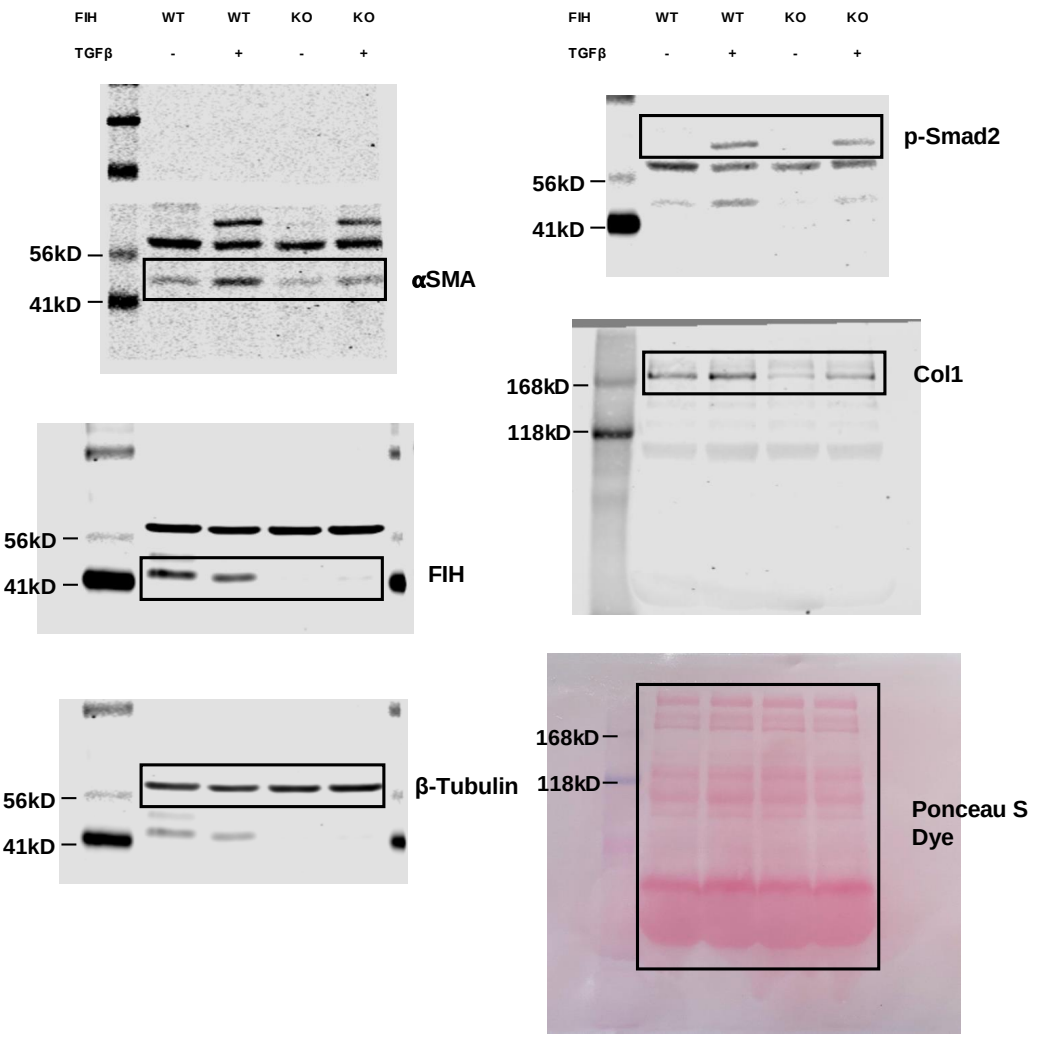

FIGURE B.3: **Raw data of western blotting for Figure.5.3A**

Figure.5.3 B

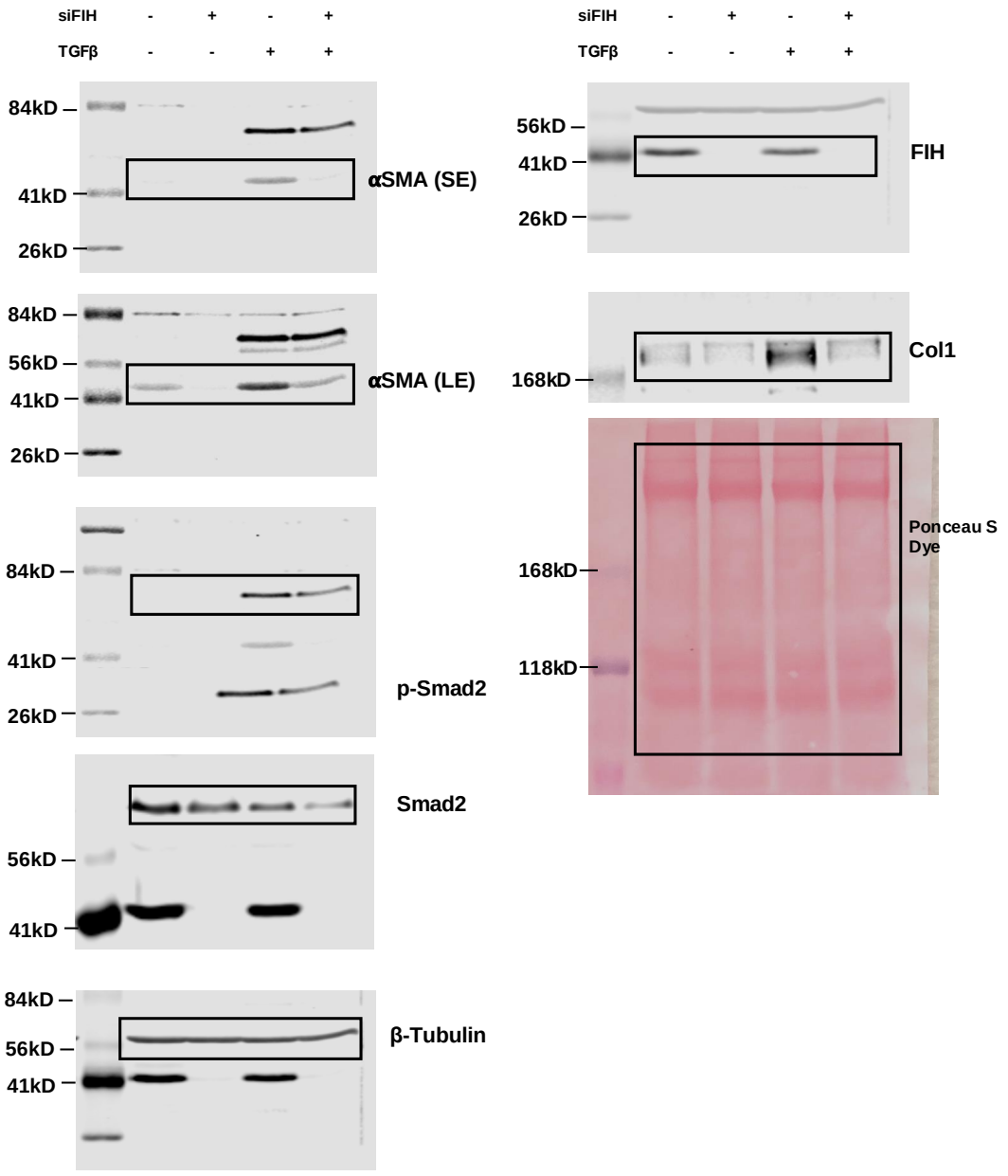

FIGURE B.4: **Raw data of western blotting for Figure.5.3B**

Figure.5.4 A

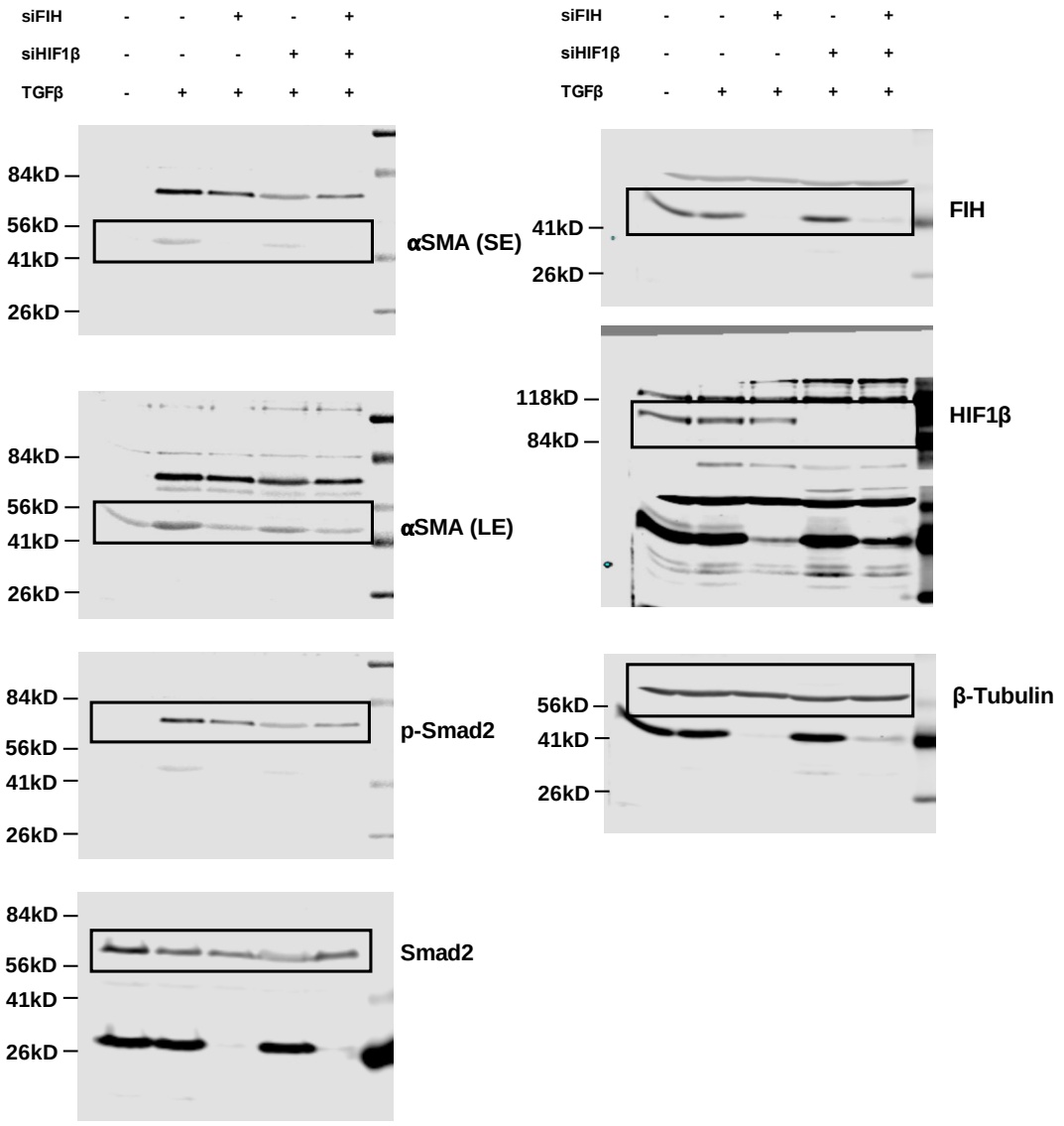

FIGURE B.5: **Raw data of western blotting for Figure.5.4A**

Figure.5.4 B

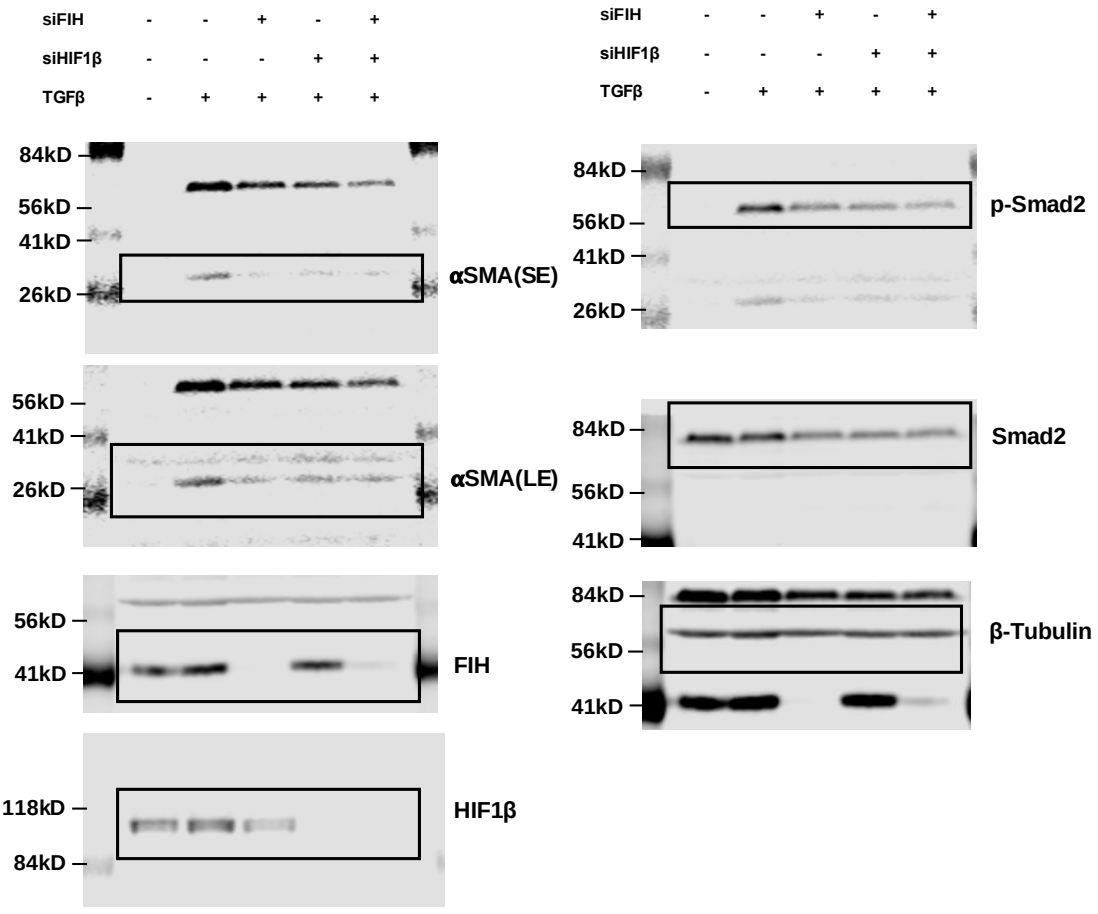

FIGURE B.6: **Raw data of western blotting for Figure.5.4B**

B.3 R script

B.3.1 Raw count processing

```r
## Import raw counts file ##
df <- read.table(file.choose(), header = T, sep = '\t')
df <- df[, c(1,7:12)] # Select the relevant columns

## Remove rows with excessive zero reads ##
zero_count <- c()
to_remove <- c()

# Iterate through each row of the data frame
for (i in 1:nrow(df)) {
  # Count the number of zeros in the current row
  zero_count <- sum(df[i, 2:7] == 0)
  # If the number of zeros is greater than 5, add the index of the
    current row to the vector of rows to be removed
  if (zero_count > 5) {
    to_remove <- c(to_remove, i)
  }
}

# Remove rows that have more than 5 zeros
df_clean <- df[-to_remove, ]

df_clean$Geneid <- as.character(df_clean$Geneid)

## Reset gene symbol ##
# Process the Geneid column to remove the dot and everything after
    it
df_clean$Geneid <- sapply(df_clean$Geneid, function(x) {
  start <- which(strsplit(x, '')[[1]] == '.')
  if (length(start) > 0) {
    return(substr(x, 1, start - 1))
  } else {
    return(x)
  }
})

# Initialize the gene_symbol column
df_clean$gene_symbol <- NA

## Import Ensembl IDs and gene symbols ##
gene_info <- read.table(file.choose(), header = T, sep = '\t')
gene_info <- gene_info[, c(1,6)]
```

```r
colnames(gene_info) <- c("Geneid", "Gene_name")

# Merge the cleaned data with gene_info by Geneid
exprSet <- merge(df_clean, gene_info, by = 'Geneid', all.x = TRUE)
exprSet <- exprSet[, c(1:7, 9)]

# Aggregate duplicate gene entries by calculating the median
exprSet <- aggregate(x = exprSet[, 2:7], by = list(exprSet$Gene_
    name), FUN = median)
rownames(exprSet) <- exprSet$Group.1
exprSet <- exprSet[, -1]

# Save the processed raw counts as a CSV file
write.csv(exprSet, file = 'MRC5_siFIH_RNAseq_rawcount.csv')

#### DESeq Analysis ####
# Replace any NA values with 1
exprSet[is.na(exprSet)] <- 1
exprSet[, c(1:6)] <- sapply(exprSet[, c(1:6)], as.integer)

# Create a factor variable containing sample condition information
condition_rna <- factor(c(rep('siFIH', length(exprSet[1,]) / 2),
    rep('control', length(exprSet[1,]) / 2)))

# Create a data frame containing the sample condition information
coldata <- data.frame(row.names = colnames(exprSet), condition_rna
    )

# Create a DESeq dataset for analysis
dds <- DESeqDataSetFromMatrix(countData = exprSet, colData =
    coldata, design = ~condition_rna)
nrow(dds)
dds <- dds[rowSums(counts(dds)) > 5, ]

# Run the DESeq differential expression analysis
dds <- DESeq(dds)
pdf("qc-dispersions.pdf", pointsize = 2)
plotDispEsts(dds, main = "Dispersion plot")
dev.off()

#### Output expression file & PCA ####
# Log transformation for heatmap plotting
rld <- rlogTransformation(dds)
exprMatrix_rlog = assay(rld)

# Save the expression matrix as a CSV file
write.csv(exprMatrix_rlog, 'exprMatrix.rlog.csv')
```

```
84
85  # Generate colors for heatmap
86  install.packages("RColorBrewer")
87  library('RColorBrewer')
88  hmcol <- colorRampPalette(brewer.pal(9, "GnBu"))(100)
89
90  # Calculate Pearson correlation
91  pearson_cor <- as.matrix(cor(exprMatrix_rlog, method = "pearson"))
92  hc <- hclust(as.dist(1 - pearson_cor), method = "complete")
93  library(stats)
94  library(cluster)  # Contains clustering algorithms
95  library(ggplot2)
96  library(gplots)
97  pdf("ehbio_trans.Count_matrix.xls.DESeq2.normalized.rlog.pearson.
        pdf", pointsize = 10)
98  heatmap.2(pearson_cor, Rowv = as.dendrogram(hc), symm = T, trace =
        "none",
99            col = hmcol, margins = c(11, 11), main = "Pearson
        correlation")
100 dev.off()
```

LISTING B.1: R code for processing raw counts

B.3.2 PCA plot

```
1  library(ggplot2)
2  install.packages('ggfortify')
3  library(ggfortify)
4
5  # Transpose the expression data
6  trans_df <- t(exprSet)
7
8  # Identify columns with constant values or all zeros
9  constant_cols <- apply(trans_df, 2, function(x) length(unique(x))
       == 1)
10 zero_cols <- apply(trans_df, 2, function(x) all(x == 0))
11
12 # Identify columns to remove (either constant or zero)
13 cols_to_remove <- constant_cols | zero_cols
14
15 # Remove the identified columns
16 trans_df_filtered <- trans_df[, !cols_to_remove]
17
18 # Perform PCA on the filtered data
19 PCA_2 <- prcomp(trans_df_filtered, scale = TRUE)
20
```

```r
# Extract standard deviations of principal components
standard_deviations <- PCA_2$sdev

# Calculate variance percentage of each principal component
variance_percent <- round(100 * standard_deviations^2 / sum(
    standard_deviations^2), 2)

# Output variance percentages of principal components
print(variance_percent)

# Define group data (use numbers instead of letters for simplicity
    )
group_data <- c("1", "1", "1", "2", "2", "2")

# Define colors for each group
group_colors <- c("1" = "#35BFC4", "2" = "#F9766D")

# Define labels for the legend
group_labels <- c("Control", "siFIH")

# Plot the PCA data
p <- ggplot() +
  geom_point(data = trans_df_filtered,
             aes(x = PCA_2$x[, 1], y = PCA_2$x[, 2], color =
    factor(group_data)), size = 5) +
  scale_colour_manual(values = group_colors, labels = group_labels
    ) +
  labs(color = "Group",
       x = paste0("PC1 (", variance_percent[1], "% variance)"),
       y = paste0("PC2 (", variance_percent[2], "% variance)")) +
  theme_minimal() +
  theme(
    # Set legend and axis text to bold Arial font with specific
    size
    legend.text = element_text(face = "bold", size = 16),
    legend.title = element_text(face = "bold", size = 20),
    axis.text = element_text(face = "bold", size = 18),
    axis.title = element_text(face = "bold", size = 24)
  )

# Print the plot
print(p)
```

LISTING B.2: R code for generating PCA plot

B.3.3 Volcano plot

```r
library(ggplot2)
library(ggrepel)

# Load data
res <- MRC5i

# Initial labeling of differential expression
res$diffexpressed <- "NO"

# If log2FoldChange > 0.5 and pvalue < 0.05, set as "UP"
res$diffexpressed[res$log2FoldChange > 0.5 & res$pvalue < 0.05] <-
    "UP"

# If log2FoldChange < -0.5 and pvalue < 0.05, set as "DOWN"
res$diffexpressed[res$log2FoldChange < -0.5 & res$pvalue < 0.05]
   <- "DOWN"

# Define colors for different expression states
mycolors <- c("#377EF0", "#F9766D", "grey")
names(mycolors) <- c("DOWN", "UP", "NO")

# Define the gene symbol of interest
Genesymbol <- "HIF1AN"

# Subset data for the gene of interest
gene_data <- subset(res, res$X == 'HIF1AN')

# Define nudge values to adjust the position of the label
nudge_x <- -1  # Adjust horizontally
nudge_y <- -1  # Adjust vertically

# Plot volcano plot
p <- ggplot(data = res, aes(x=log2FoldChange, y=-log10(pvalue),
   col=diffexpressed)) +
  geom_point() +
  scale_colour_manual(values = mycolors) +
  theme(
    # Modify axis title font size and style
    axis.title = element_text(face = "bold", size = 24),
    # Modify axis text font size and style
    axis.text = element_text(face = "bold", size = 18),
    # Modify text font size and style for data points
    text = element_text(face = "bold", size = 16)
  )

```

```r
# Print the plot
print(p)
```

LISTING B.3: R code for generating Volcano plot with annotated gene

B.3.4 Venn plot

```r
# Assign variables to GO_BP descriptions
A <- Mk_decre_GO_BP$Description
C <- Mi_decre_GO_BP$Description
B <- Me_decre_GO_BP$Description
D <- Ni_decre_GO_BP$Description

# Create Venn diagram
venn.plot <- VennDiagram::venn.diagram(
  x = list(
    FIHKO_MRC5 = A,
    FIHKO_MEF = B,
    siFIH_MRC5 = C,
    siFIH_NHLF = D
  ),
  height = 2000, width = 2000, resolution = 500,
  filename = "Venn diagram of decreBP in all datasets.tiff",
  imagetype = "tiff",
  col = "transparent",
  fill = c("#D18C89", "#F5DD9D", "#7CA872", "#ACD2EB"),
  alpha = 0.5,
  cat.col = "black",
  cat.cex = 0.8,
  cat.fontface = "bold",
  margin = 0.07,
  cex = 1,
  na = "none"
)
```

LISTING B.4: R code for generating Venn diagram

B.3.5 Heatmap

```r
# Create data frame for heatmap
heatmap_data <- data.frame(
  Group = rep(c('WT', 'WT_TGFb', 'FIHKO', 'FIHKO_TGFb'), each =
   nrow(KO_GSVA)),
  Value = c(KO_GSVA[,1], KO_GSVA[,2], KO_GSVA[,3], KO_GSVA[,4]),
```

```
  Significance = c(rep(NA, each = nrow(KO_GSVA)), KO_GSVA[,10],
   rep(NA, each = nrow(KO_GSVA)), KO_GSVA[,9]),
  RowName = rownames(KO_GSVA)  # Add row names
)

heatmap_data$Group <- factor(heatmap_data$Group, levels = c('WT',
   'WT_TGFb', 'FIHKO', 'FIHKO_TGFb'))
heatmap_data$RowName <- factor(heatmap_data$RowName, levels =
   rownames(KO_GSVA))

# Add significance symbols based on p-values
heatmap_data$Significance <- ifelse(heatmap_data$Significance <
   0.001 & heatmap_data$Group == "WT_TGFb", "***",
                               ifelse(heatmap_data$Significance <
   0.01 & heatmap_data$Group == "WT_TGFb", "**",
                               ifelse(heatmap_data$Significance <
   0.05 & heatmap_data$Group == "WT_TGFb", "*",
                               ifelse(heatmap_data$Significance <
   0.001 & heatmap_data$Group == "FIHKO_TGFb", "###",
                               ifelse(heatmap_data$Significance <
   0.01 & heatmap_data$Group == "FIHKO_TGFb", "##",
                               ifelse(heatmap_data$Significance <
   0.05 & heatmap_data$Group == "FIHKO_TGFb", "#","")))))))

# Replace empty strings with NA
heatmap_data$Significance[heatmap_data$Significance == ""] <- NA

# Load ggplot2 package and create heatmap
library(ggplot2)
p <- ggplot(heatmap_data, aes(x = Group, y = RowName, fill = Value
   )) +
  geom_tile() +
  geom_text(aes(label = Significance), color = "black", size = 3,
   fontface = "bold", na.rm = TRUE) +  # Show significance markers
  scale_fill_gradientn(colors = colorbar, limits = range(heatmap_
   data$Value),
                       guide = guide_colorbar(title = "GSVA score
   ")) +
  labs(x = NULL, y = "Hallmark pathway", fill = "Value") +
  theme_minimal() +
  theme(axis.text.x = element_text(angle = 45, hjust = 1))  #
   Adjust text angle

# Adjust aspect ratio for heatmap
p = p + theme(
  aspect.ratio = 4.5  # Set aspect ratio for height and width
)
```

```
38
39 # Print heatmap
40 print(p)
```

LISTING B.5: R code for Heatmap of GSVA scores with significance

B.3.6 Bubble plot

```
1  # Create top GO terms data frame for MEF
2  MEF_incre_GO_top10 <- as.data.frame(matrix(data = NA, nrow = 14,
       ncol = 14))
3  colnames(MEF_incre_GO_top10) <- colnames(MEF_incre_GO)
4
5  # Populate data for Biological Processes, Cellular Components, and
       Molecular Functions
6  MEF_incre_GO_top10[c(1:10), ] <- MEF_incre_GO_BP[c(1:10), ]
7  MEF_incre_GO_top10[c(11:13), ] <- MEF_incre_GO_CC[c(1:3), ]
8  MEF_incre_GO_top10[14, ] <- MEF_incre_GO_MF[1, ]
9
10 # Add category column and rename columns for plotting
11 MEF_incre_GO_top10$Category <- c(rep("Biological Processes", 10),
       rep("Cellular Components", 3), rep("Molecular Functions", 1))
12 colnames(MEF_incre_GO_top10)[11] <- "Rich.ratio"
13 colnames(MEF_incre_GO_top10)[10] <- "Count"
14 colnames(MEF_incre_GO_top10)[3] <- "Name"
15
16 # Generate the ggplot
17 ggplot(MEF_incre_GO_top10, aes(
18   x = Rich.ratio,
19   y = reorder(Name, -LogP),
20   color = -1 * LogP,
21   size = Count
22 )) +
23   geom_point() +
24   scale_color_gradient(low = "blue", high = "red") +
25   facet_wrap(~MEF_incre_GO_top10$Category) +
26   theme(text = element_text(size = 15))
```

LISTING B.6: R code for GO Enrichment Analysis Visualization– Bubble plot

B.3.7 Treemap

```
1 # Load treemap package and create treemap visualization
2 treemap::treemap(
3   Mk_incre_BP_50,
```

```
  index = c("PARENT_GO", "Description"),
  vSize = "X.InGO",
  vColor = "LogP",
  type = "index"
)
```

LISTING B.7: R code for Treemap visualization of GO terms

B.3.8 GSVA

```
# Initialize an empty GSVA matrix
GSVA_matrix <- as.data.frame(matrix(data = NA, nrow = 50, ncol =
    4, dimnames = list(c(), colnames(MEF_exp))))

# Read hallmark dataset from .gmt file
hallmark_dataset <- GSA.read.gmt('hallmark_allsymbols.gmt')

# Fill GSVA matrix with calculated GSVA scores
for (i in 1:50) {
  rownames(GSVA_matrix)[i] <- hallmark_dataset$geneset.names[i]
  print(hallmark_dataset$geneset.names[i])
  GSVA_matrix[i, ] <- gsva(as.matrix(MEF_exp), list(hallmark_
    dataset$genesets[i][[1]]), mx.diff = 1)
}
```

LISTING B.8: R code for Calculation of GSVA Scores

B.3.9 One-way ANOVA

```
# Create a vector for the samples and their grouping
samples <- rep(c("WT", "WT_TGFbeta", "FIHKO", "FIHKO_TGFbeta"),
    each = 3)
group_info <- data.frame(Sample = colnames(MRC5k_GSVA), Group =
    samples)

# Create an empty dataframe to store the extracted information
extracted_info <- data.frame(Gene = character(),
                             F_value = numeric(),
                             Pr_gt_F = numeric(),
                             stringsAsFactors = FALSE)

# Create an empty dataframe to store Tukey's HSD results
tukey_summary <- data.frame()

# Loop through each gene's data
```

```r
for (i in 1:50) {
  # Prepare data
  gene_data <- data.frame(Expression = as.numeric(MRC5k_GSVA[i, ]),
                          Group = factor(group_info$Group))

  # Perform one-way ANOVA
  anova_result <- oneway.test(gene_data$Expression ~ gene_data$Group)

  # Extract relevant information
  gene_name <- rownames(MRC5k_GSVA)[i]
  f_value <- anova_result$statistic
  pr_gt_f <- anova_result$p.value

  # Output information for the current gene
  cat("Gene:", gene_name, "\n")
  cat("F value:", f_value, "\n")
  cat("Pr(>F):", pr_gt_f, "\n")

  # Add extracted information to dataframe
  extracted_info <- rbind(extracted_info, data.frame(Gene = gene_name,
                                                     F_value = f_value,
                                                     Pr_gt_F = pr_gt_f))

  # Perform Tukey's HSD multiple comparisons
  posthoc_result <- TukeyHSD(aov(Expression ~ Group, data = gene_data))

  # Check if multiple comparison results exist
  if (!is.null(posthoc_result)) {
    # Get the multiple comparison results
    posthoc_df <- as.data.frame(posthoc_result[[1]])

    # Add gene name column
    posthoc_df$Gene <- gene_name

    # Append results to tukey_summary
    tukey_summary <- rbind(tukey_summary, posthoc_df)
  }
}

# Display extracted ANOVA information
print(extracted_info)
```

```r

# Save results to CSV files
write.csv(tukey_summary, 'FIHKO_GSVA_ANOVA.csv')
write.csv(FIHKO_GSVA_average, 'FIHKO_GSVA_average.csv')
```

LISTING B.9: R code for ANOVA and Tukey's HSD Test for Gene Expression Data

B.3.10 Student's T test

```r
# Load required package
library(dplyr)

# Convert GSVA scores to a data frame
MRC5_KO_GSVA <- as.data.frame(MRC5_KO_GSVA)

# Calculate group averages
FIHKO_average <- MRC5_KO_GSVA %>%
  mutate(
    mean_group1 = rowMeans(select(., c(1:3))),
    mean_group2 = rowMeans(select(., c(4:6)))
  )

# Extract and rename averages
FIHKO_GSVA_average <- FIHKO_average[, c(7, 8)]
colnames(FIHKO_GSVA_average) <- c('WT', 'FIH_KO')

# Initialize vector for storing t-test results
t_test_results <- vector("list", nrow(MRC5_KO_GSVA))

# Perform t-tests on each row for the two groups
for (i in 1:nrow(MRC5_KO_GSVA)) {
  group1 <- MRC5_KO_GSVA[i, 1:3]
  group2 <- MRC5_KO_GSVA[i, 4:6]
  t_test_results[[i]] <- t.test(group1, group2, var.equal = TRUE)
    # Use Student's t-test
}

# Print t-test results
for (i in 1:nrow(MRC5_KO_GSVA)) {
  print(t_test_results[[i]])
}

# Create a data frame to store t-test results
t_test_df <- data.frame(
  row = 1:length(t_test_results),
  statistic = numeric(length(t_test_results)),
```

```r
  p.value = numeric(length(t_test_results)),
  method = character(length(t_test_results)),
  alternative = character(length(t_test_results)),
  mean_group1 = numeric(length(t_test_results)),
  mean_group2 = numeric(length(t_test_results))
)

# Store t-test results in the data frame
for (i in 1:length(t_test_results)) {
  t_test_df[i, "statistic"] <- t_test_results[[i]]$statistic
  t_test_df[i, "p.value"] <- t_test_results[[i]]$p.value
  t_test_df[i, "method"] <- t_test_results[[i]]$method
  t_test_df[i, "alternative"] <- t_test_results[[i]]$alternative
  t_test_df[i, "mean_group1"] <- t_test_results[[i]]$estimate[1]
  t_test_df[i, "mean_group2"] <- t_test_results[[i]]$estimate[2]
}
```

LISTING B.10: R code for Student's T-Test Analysis of GSVA Scores

References

Abramson, M. J., Murambadoro, T., Alif, S. M., Benke, G. P., Dharmage, S. C., Glaspole, I., Hopkins, P., Hoy, R. F., Klebe, S., Moodley, Y. et al. (2020), 'Occupational and environmental risk factors for idiopathic pulmonary fibrosis in australia: case–control study', *Thorax* **75**(10), 864–869.

Adams, T. S., Schupp, J. C., Poli, S., Ayaub, E. A., Neumark, N., Ahangari, F., Chu, S. G., Raby, B. A., DeIuliis, G., Januszyk, M. et al. (2020), 'Single-cell rna-seq reveals ectopic and aberrant lung-resident cell populations in idiopathic pulmonary fibrosis', *Science advances* **6**(28), eaba1983.

Adler, M., Mayo, A., Zhou, X., Franklin, R. A., Meizlish, M. L., Medzhitov, R., Kallenberger, S. M. and Alon, U. (2020), 'Principles of cell circuits for tissue repair and fibrosis', *IScience* **23**(2).

Agabiti, N., Porretta, M., Bauleo, L., Coppola, A., Sergiacomi, G., Fusco, A., Cavalli, F., Zappa, M., Vignarola, R., Carlone, S. et al. (2014), 'Idiopathic pulmonary fibrosis (ipf) incidence and prevalence in italy', *SARCOIDOSIS VASCULITIS AND DIFFUSE LUNG DISEASES* **31**, 191–197.

Alder, J. K., Stanley, S. E., Wagner, C. L., Hamilton, M., Hanumanthu, V. S. and Armanios, M. (2015), 'Exome sequencing identifies mutant tinf2 in a family with pulmonary fibrosis', *Chest* **147**(5), 1361–1368.

Allen, R. J., Guillen-Guio, B., Oldham, J. M., Ma, S.-F., Dressen, A., Paynton, M. L., Kraven, L. M., Obeidat, M., Li, X., Ng, M. et al. (2020), 'Genome-wide association study of susceptibility to idiopathic pulmonary fibrosis', *American journal of respiratory and critical care medicine* **201**(5), 564–574.

Allen, R. J., Porte, J., Braybrooke, R., Flores, C., Fingerlin, T. E., Oldham, J. M., Guillen-Guio, B., Ma, S.-F., Okamoto, T., John, A. E. et al. (2017), 'Genetic variants associated with susceptibility to idiopathic pulmonary fibrosis in people of european ancestry: a genome-wide association study', *The Lancet respiratory medicine* **5**(11), 869–880.

Álvarez, D., Cárdenes, N., Sellarés, J., Bueno, M., Corey, C., Hanumanthu, V. S., Peng, Y., D'Cunha, H., Sembrat, J., Nouraie, M. et al. (2017), 'Ipf lung fibroblasts have a

senescent phenotype', *American Journal of Physiology-Lung Cellular and Molecular Physiology* **313**(6), L1164–L1173.

Amelio, I., Cutruzzolá, F., Antonov, A., Agostini, M. and Melino, G. (2014), 'Serine and glycine metabolism in cancer', *Trends in biochemical sciences* **39**(4), 191–198.

An, L., Peng, L.-Y., Sun, N.-Y., Yang, Y.-L., Zhang, X.-W., Li, B., Liu, B.-L., Li, P. and Chen, J. (2019), 'Tanshinone iia activates nuclear factor-erythroid 2-related factor 2 to restrain pulmonary fibrosis via regulation of redox homeostasis and glutaminolysis', *Antioxidants & Redox Signaling* **30**(15), 1831–1848.

Anderson, S., Dos Santos, P. R., Langlais, B., Campany, M., Donato, B. and D'Cunha, J. (2024), 'Lung transplant outcomes for idiopathic pulmonary fibrosis: are we improving?', *The Annals of Thoracic Surgery* **117**(4), 820–827.

Andersson-Sjöland, A., De Alba, C. G., Nihlberg, K., Becerril, C., Ramírez, R., Pardo, A., Westergren-Thorsson, G. and Selman, M. (2008), 'Fibrocytes are a potential source of lung fibroblasts in idiopathic pulmonary fibrosis', *The international journal of biochemistry & cell biology* **40**(10), 2129–2140.

Andrianifahanana, M., Hernandez, D. M., Yin, X., Kang, J.-H., Jung, M.-Y., Wang, Y., Eunhee, S. Y., Roden, A. C., Limper, A. H. and Leof, E. B. (2016), 'Profibrotic upregulation of glucose transporter 1 by tgf-β involves activation of mek and mammalian target of rapamycin complex 2 pathways', *The FASEB Journal* **30**(11), 3733.

Antoniou, K. M., Tsitoura, E., Vasarmidi, E., Symvoulakis, E. K., Aidinis, V., Tzilas, V., Tzouvelekis, A. and Bouros, D. (2021), 'Precision medicine in idiopathic pulmonary fibrosis therapy: From translational research to patient-centered care', *Current Opinion in Pharmacology* **57**, 71–80.

Aoshiba, K., Tsuji, T., Kameyama, S., Itoh, M., Semba, S., Yamaguchi, K. and Nakamura, H. (2013), 'Senescence-associated secretory phenotype in a mouse model of bleomycin-induced lung injury', *Experimental and Toxicologic Pathology* **65**(7-8), 1053–1062.

Aoshiba, K., Tsuji, T. and Nagai, A. (2003), 'Bleomycin induces cellular senescence in alveolar epithelial cells', *European Respiratory Journal* **22**(3), 436–443.

Appelhoff, R. J., Tian, Y.-M., Raval, R. R., Turley, H., Harris, A. L., Pugh, C. W., Ratcliffe, P. J. and Gleadle, J. M. (2004), 'Differential function of the prolyl hydroxylases phd1, phd2, and phd3 in the regulation of hypoxia-inducible factor', *Journal of Biological Chemistry* **279**(37), 38458–38465.

Aquino-Gálvez, A., González-Ávila, G., Jiménez-Sánchez, L. L., Maldonado-Martínez, H. A., Cisneros, J., Toscano-Marquez, F., Castillejos-López, M., Torres-Espíndola, L. M., Velázquez-Cruz, R., Rodríguez, V. H. O. et al. (2019), 'Dysregulated expression

of hypoxia-inducible factors augments myofibroblasts differentiation in idiopathic pulmonary fibrosis', *Respiratory Research* **20**, 1–10.

Ard, S., Reed, E. B., Smolyaninova, L. V., Orlov, S. N., Mutlu, G. M., Guzy, R. D. and Dulin, N. O. (2019), 'Sustained smad2 phosphorylation is required for myofibroblast transformation in response to tgf-β', *American Journal of Respiratory Cell and Molecular Biology* **60**(3), 367–369.

Armanios, M. Y., Chen, J. J.-L., Cogan, J. D., Alder, J. K., Ingersoll, R. G., Markin, C., Lawson, W. E., Xie, M., Vulto, I., Phillips III, J. A. et al. (2007), 'Telomerase mutations in families with idiopathic pulmonary fibrosis', *New England Journal of Medicine* **356**(13), 1317–1326.

Armulik, A., Genové, G. and Betsholtz, C. (2011), 'Pericytes: developmental, physiological, and pathological perspectives, problems, and promises', *Developmental cell* **21**(2), 193–215.

Arnold, P. K. and Finley, L. W. (2023), 'Regulation and function of the mammalian tricarboxylic acid cycle', *Journal of Biological Chemistry* **299**(2).

Artlett, C. M. (2022), 'The mechanism and regulation of the nlrp3 inflammasome during fibrosis', *Biomolecules* **12**(5), 634.

Asgari, M., Latifi, N., Heris, H. K., Vali, H. and Mongeau, L. (2017), 'In vitro fibrillogenesis of tropocollagen type iii in collagen type i affects its relative fibrillar topology and mechanics', *Scientific reports* **7**(1), 1392.

Aumiller, V., Strobel, B., Romeike, M., Schuler, M., Stierstorfer, B. E. and Kreuz, S. (2017), 'Comparative analysis of lysyl oxidase (like) family members in pulmonary fibrosis', *Scientific reports* **7**(1), 149.

Auyeung, V. C., Downey, M. S., Thamsen, M., Wenger, T. A., Backes, B. J., Sheppard, D. and Papa, F. R. (2022), 'Ire1α drives lung epithelial progenitor dysfunction to establish a niche for pulmonary fibrosis', *American Journal of Physiology-Lung Cellular and Molecular Physiology* .

Baarsma, H. A., Engelbertink, L. H., van Hees, L. J., Menzen, M. H., Meurs, H., Timens, W., Postma, D. S., Kerstjens, H. A. and Gosens, R. (2013), 'Glycogen synthase kinase-3 (gsk-3) regulates tgf-β1-induced differentiation of pulmonary fibroblasts', *British journal of pharmacology* **169**(3), 590–603.

Baarsma, H. A., Spanjer, A. I., Haitsma, G., Engelbertink, L. H., Meurs, H., Jonker, M. R., Timens, W., Postma, D. S., Kerstjens, H. A. and Gosens, R. (2011), 'Activation of wnt/β-catenin signaling in pulmonary fibroblasts by tgf-β1 is increased in chronic obstructive pulmonary disease', *PloS one* **6**(9), e25450.

Barkauskas, C. E., Cronce, M. J., Rackley, C. R., Bowie, E. J., Keene, D. R., Stripp, B. R., Randell, S. H., Noble, P. W., Hogan, B. L. et al. (2013), 'Type 2 alveolar cells are stem cells in adult lung', *The Journal of clinical investigation* **123**(7), 3025–3036.

Barratt, S. L., Blythe, T., Ourradi, K., Jarrett, C., Welsh, G. I., Bates, D. O. and Millar, A. B. (2018), 'Effects of hypoxia and hyperoxia on the differential expression of vegf-a isoforms and receptors in idiopathic pulmonary fibrosis (ipf)', *Respiratory research* **19**, 1–5.

Barry-Hamilton, V., Spangler, R., Marshall, D., McCauley, S., Rodriguez, H. M., Oyasu, M., Mikels, A., Vaysberg, M., Ghermazien, H., Wai, C. et al. (2010), 'Allosteric inhibition of lysyl oxidase–like-2 impedes the development of a pathologic microenvironment', *Nature medicine* **16**(9), 1009–1017.

Barton, D., Foellmer, B., Du, J., Tamm, J., Derynck, R. and Francke, U. (1988), 'Chromosomal mapping of genes for transforming growth factors beta 2 and beta 3 in man and mouse: dispersion of tgf-beta gene family.', *Oncogene research* **3**(4), 323–331.

Baumgartner, K. B., Samet, J. M., Stidley, C. A., Colby, T. V. and Waldron, J. A. (1997), 'Cigarette smoking: a risk factor for idiopathic pulmonary fibrosis.', *American journal of respiratory and critical care medicine* **155**(1), 242–248.

Befani, C. and Liakos, P. (2018), 'The role of hypoxia-inducible factor-2 alpha in angiogenesis', *Journal of cellular physiology* **233**(12), 9087–9098.

Behr, J., Kreuter, M., Hoeper, M. M., Wirtz, H., Klotsche, J., Koschel, D., Andreas, S., Claussen, M., Grohé, C., Wilkens, H. et al. (2015), 'Management of patients with idiopathic pulmonary fibrosis in clinical practice: the insights-ipf registry', *European Respiratory Journal* **46**(1), 186–196.

Behr, J., Prasse, A., Kreuter, M., Johow, J., Rabe, K. F., Bonella, F., Bonnet, R., Grohe, C., Held, M., Wilkens, H. et al. (2021), 'Pirfenidone in patients with progressive fibrotic interstitial lung diseases other than idiopathic pulmonary fibrosis (relief): a double-blind, randomised, placebo-controlled, phase 2b trial', *The Lancet Respiratory Medicine* **9**(5), 476–486.

Behr, J., Prasse, A., Wirtz, H., Koschel, D., Pittrow, D., Held, M., Klotsche, J., Andreas, S., Claussen, M., Grohé, C. et al. (2020), 'Survival and course of lung function in the presence or absence of antifibrotic treatment in patients with idiopathic pulmonary fibrosis: long-term results of the insights-ipf registry', *European Respiratory Journal* **56**(2).

Bell, J. D., Brown, J. C. and Sadler, P. J. (1989), 'Nmr studies of body fluids', *NMR in Biomedicine* **2**(5-6), 246–256.

Berra, E., Benizri, E., Ginouvès, A., Volmat, V., Roux, D. and Pouysségur, J. (2003), 'Hif prolyl-hydroxylase 2 is the key oxygen sensor setting low steady-state levels of hif-1α in normoxia', *The EMBO journal* .

Bialik, J. F., Ding, M., Speight, P., Dan, Q., Miranda, M. Z., Di Ciano-Oliveira, C., Kofler, M. M., Rotstein, O. D., Pedersen, S. F., Szászi, K. et al. (2019), 'Profibrotic epithelial phenotype: a central role for mrtf and taz', *Scientific Reports* **9**(1), 4323.

Bocchino, M., Agnese, S., Fagone, E., Svegliati, S., Grieco, D., Vancheri, C., Gabrielli, A., Sanduzzi, A. and Avvedimento, E. V. (2010), 'Reactive oxygen species are required for maintenance and differentiation of primary lung fibroblasts in idiopathic pulmonary fibrosis', *PLoS One* **5**(11), e14003.

Boettcher, M. and McManus, M. T. (2015), 'Choosing the right tool for the job: Rnai, talen, or crispr', *Molecular cell* **58**(4), 575–585.

Bonella, F., Spagnolo, P. and Ryerson, C. (2023), 'Current and future treatment landscape for idiopathic pulmonary fibrosis', *Drugs* **83**(17), 1581–1593.

Booth, A. J., Hadley, R., Cornett, A. M., Dreffs, A. A., Matthes, S. A., Tsui, J. L., Weiss, K., Horowitz, J. C., Fiore, V. F., Barker, T. H. et al. (2012), 'Acellular normal and fibrotic human lung matrices as a culture system for in vitro investigation', *American journal of respiratory and critical care medicine* **186**(9), 866–876.

Borie, R., Kannengiesser, C., Antoniou, K., Bonella, F., Crestani, B., Fabre, A., Froidure, A., Galvin, L., Griese, M., Grutters, J. C. et al. (2023), 'European respiratory society statement on familial pulmonary fibrosis', *European Respiratory Journal* **61**(3).

Borok, Z., Horie, M., Flodby, P., Wang, H., Liu, Y., Ganesh, S., Firth, A. L., Minoo, P., Li, C., Beers, M. F. et al. (2020), 'Grp78 loss in epithelial progenitors reveals an age-linked role for endoplasmic reticulum stress in pulmonary fibrosis', *American journal of respiratory and critical care medicine* **201**(2), 198–211.

Bozyk, P. D. and Moore, B. B. (2011), 'Prostaglandin e2 and the pathogenesis of pulmonary fibrosis', *American journal of respiratory cell and molecular biology* **45**(3), 445–452.

Branco-Price, C., Zhang, N., Schnelle, M., Evans, C., Katschinski, D. M., Liao, D., Johnson, R. S. and Simon, M. C. (2012), 'Endothelial cell hif-1α and hif-2α differentially regulate metastatic success', *Nature Medicine* **18**(9), 1630–1634.

Brereton, C. J., Yao, L., Davies, E. R., Zhou, Y., Vukmirovic, M., Bell, J. A., Wang, S., Ridley, R. A., Dean, L. S., Andriotis, O. G. et al. (2022), 'Pseudohypoxic hif pathway activation dysregulates collagen structure-function in human lung fibrosis', *Elife* **11**, e69348.

Brinckmann, J., Tronnier, M., Schmeller, W., Notbohm, H., Açil, Y., Fietzek, P. P., Müller, P. K. and Bätge, B. (1999), 'Overhydroxylation of lysyl residues is the initial step for altered collagen cross-links and fibril architecture in fibrotic skin', *Journal of investigative dermatology* **113**(4), 617–621.

Brunetti, G., Malovini, A., Maniscalco, M., Balestrino, A., Carone, M., Visca, D., Capelli, A., Vitacca, M., Bellazzi, R., Piaggi, G. et al. (2021), 'Pulmonary rehabilitation in patients with interstitial lung diseases: Correlates of success', *Respiratory Medicine* **185**, 106473.

Bucala, R., Spiegel, L. A., Chesney, J., Hogan, M. and Cerami, A. (1994), 'Circulating fibrocytes define a new leukocyte subpopulation that mediates tissue repair', *Molecular medicine* **1**, 71–81.

Bueno, M., Calyeca, J., Rojas, M. and Mora, A. L. (2020), 'Mitochondria dysfunction and metabolic reprogramming as drivers of idiopathic pulmonary fibrosis', *Redox biology* **33**, 101509.

Cai, X., Wang, R., Zhu, J., Li, X., Liu, X., Ouyang, G., Wang, J., Li, Z., Zhu, C., Deng, H. et al. (2024), 'Factor inhibiting hif negatively regulates antiviral innate immunity via hydroxylation of ikkϵ', *Cell reports* **43**(1).

Campo, I., Zorzetto, M., Mariani, F., Kadija, Z., Morbini, P., Dore, R., Kaltenborn, E., Frixel, S., Zarbock, R., Liebisch, G. et al. (2014), 'A large kindred of pulmonary fibrosis associated with a novel abca3 gene variant', *Respiratory research* **15**, 1–15.

Caraci, F., Gili, E., Calafiore, M., Failla, M., La Rosa, C., Crimi, N., Sortino, M. A., Nicoletti, F., Copani, A. and Vancheri, C. (2008), 'Tgf-β1 targets the gsk-3β/β-catenin pathway via erk activation in the transition of human lung fibroblasts into myofibroblasts', *Pharmacological research* **57**(4), 274–282.

Chan, M. C., Holt-Martyn, J. P., Schofield, C. J. and Ratcliffe, P. J. (2016), 'Pharmacological targeting of the hif hydroxylases–a new field in medicine development', *Molecular aspects of medicine* **47**, 54–75.

Chan, M. C., Ilott, N. E., Schödel, J., Sims, D., Tumber, A., Lippl, K., Mole, D. R., Pugh, C. W., Ratcliffe, P. J., Ponting, C. P. et al. (2016), 'Tuning the transcriptional response to hypoxia by inhibiting hypoxia-inducible factor (hif) prolyl and asparaginyl hydroxylases', *Journal of Biological Chemistry* **291**(39), 20661–20673.

Chandel, N. and Simon, M. (2008), 'Hypoxia-inducible factor: roles in development, physiology, and disease', *Cell Death & Differentiation* **15**(4), 619–620.

Chang, C.-H., Curtis, J. D., Maggi, L. B., Faubert, B., Villarino, A. V., O'Sullivan, D., Huang, S. C.-C., Van Der Windt, G. J., Blagih, J., Qiu, J. et al. (2013), 'Posttranscriptional control of t cell effector function by aerobic glycolysis', *Cell* **153**(6), 1239–1251.

Chang, C.-H., Qiu, J., O'Sullivan, D., Buck, M. D., Noguchi, T., Curtis, J. D., Chen, Q., Gindin, M., Gubin, M. M., Van Der Windt, G. J. et al. (2015), 'Metabolic competition in the tumor microenvironment is a driver of cancer progression', *Cell* **162**(6), 1229–1241.

Chen, L., Li, S. and Li, W. (2019), 'Lox/loxl in pulmonary fibrosis: potential therapeutic targets', *Journal of drug targeting* **27**(7), 790–796.

Chen, T., Ren, Z., Ye, L.-C., Zhou, P.-H., Xu, J.-M., Shi, Q., Yao, L.-Q. and Zhong, Y.-S. (2015), 'Factor inhibiting hif1α (fih-1) functions as a tumor suppressor in human colorectal cancer by repressing hif1α pathway', *Cancer biology & therapy* **16**(2), 244–252.

Chen, W., Zhang, J., Zhong, W., Liu, Y., Lu, Y., Zeng, Z., Huang, H., Wan, X., Meng, X., Zou, F. et al. (2021), 'Anlotinib inhibits pfkfb3-driven glycolysis in myofibroblasts to reverse pulmonary fibrosis', *Frontiers in pharmacology* **12**, 744826.

Chen, X., Xu, H., Hou, J., Wang, H., Zheng, Y., Li, H., Cai, H., Han, X. and Dai, J. (2020), 'Epithelial cell senescence induces pulmonary fibrosis through nanog-mediated fibroblast activation', *Aging (Albany NY)* **12**(1), 242.

Chen, Y., Zhao, X., Sun, J., Su, W., Zhang, L., Li, Y., Liu, Y., Zhang, L., Lu, Y., Shan, H. et al. (2019), 'Yap1/twist promotes fibroblast activation and lung fibrosis that conferred by mir-15a loss in ipf', *Cell Death & Differentiation* **26**(9), 1832–1844.

Chesney, J., Metz, C., Stavitsky, A. B., Bacher, M. and Bucala, R. (1998), 'Regulated production of type i collagen and inflammatory cytokines by peripheral blood fibrocytes', *The Journal of Immunology* **160**(1), 419–425.

Chilosi, M., Caliò, A., Rossi, A., Gilioli, E., Pedica, F., Montagna, L., Pedron, S., Confalonieri, M., Doglioni, C., Ziesche, R. et al. (2017), 'Epithelial to mesenchymal transition-related proteins zeb1, β-catenin, and β-tubulin-iii in idiopathic pulmonary fibrosis', *Modern Pathology* **30**(1), 26–38.

Cho, S. J., Moon, J.-S., Lee, C.-M., Choi, A. M. and Stout-Delgado, H. W. (2017), 'Glucose transporter 1–dependent glycolysis is increased during aging-related lung fibrosis, and phloretin inhibits lung fibrosis', *American journal of respiratory cell and molecular biology* **56**(4), 521–531.

Choi, H., Hardy, A. P., Leissing, T. M., Chowdhury, R., Nakashima, Y., Ge, W., Markoulides, M., Scotti, J. S., Gerken, P. A., Thorbjornsrud, H. et al. (2020), 'A human protein hydroxylase that accepts d-residues', *Communications Chemistry* **3**(1), 52.

Choi, J., Park, J.-E., Tsagkogeorga, G., Yanagita, M., Koo, B.-K., Han, N. and Lee, J.-H. (2020), 'Inflammatory signals induce at2 cell-derived damage-associated transient progenitors that mediate alveolar regeneration', *Cell stem cell* **27**(3), 366–382.

Chung, M. P., Park, M. S., Oh, I. J., Lee, H. B., Kim, Y. W., Park, J. S., Uh, S. T., Kim, Y. S., Jegal, Y. and Song, J. W. (2020), 'Safety and efficacy of pirfenidone in advanced idiopathic pulmonary fibrosis: a nationwide post-marketing surveillance study in korean patients', *Advances in Therapy* **37**, 2303–2316.

Cluntun, A. A., Huang, H., Dai, L., Liu, X., Zhao, Y. and Locasale, J. W. (2015), 'The rate of glycolysis quantitatively mediates specific histone acetylation sites', *Cancer & metabolism* **3**, 1–12.

Cockman, M. E., Lancaster, D. E., Stolze, I. P., Hewitson, K. S., McDonough, M. A., Coleman, M. L., Coles, C. H., Yu, X., Hay, R. T., Ley, S. C. et al. (2006), 'Posttranslational hydroxylation of ankyrin repeats in iκb proteins by the hypoxia-inducible factor (hif) asparaginyl hydroxylase, factor inhibiting hif (fih)', *Proceedings of the National Academy of Sciences* **103**(40), 14767–14772.

Cockman, M. E., Webb, J. D. and Ratcliffe, P. J. (2009), 'Fih-dependent asparaginyl hydroxylation of ankyrin repeat domain-containing proteins', *Annals of the New York Academy of Sciences* **1177**(1), 9–18.

Cogan, J. D., Kropski, J. A., Zhao, M., Mitchell, D. B., Rives, L., Markin, C., Garnett, E. T., Montgomery, K. H., Mason, W. R., McKean, D. F. et al. (2015), 'Rare variants in rtel1 are associated with familial interstitial pneumonia', *American journal of respiratory and critical care medicine* **191**(6), 646–655.

Cogliati, S., Cabrera-Alarcón, J. L. and Enriquez, J. A. (2021), 'Regulation and functional role of the electron transport chain supercomplexes', *Biochemical Society Transactions* **49**(6), 2655–2668.

Colegio, O. R., Chu, N.-Q., Szabo, A. L., Chu, T., Rhebergen, A. M., Jairam, V., Cyrus, N., Brokowski, C. E., Eisenbarth, S. C., Phillips, G. M. et al. (2014), 'Functional polarization of tumour-associated macrophages by tumour-derived lactic acid', *Nature* **513**(7519), 559–563.

Coleman, M. L., McDonough, M. A., Hewitson, K. S., Coles, C., Mecinovicí, J., Edelmann, M., Cook, K. M., Cockman, M. E., Lancaster, D. E., Kessler, B. M. et al. (2007), 'Asparaginyl hydroxylation of the notch ankyrin repeat domain by factor inhibiting hypoxia-inducible factor', *Journal of Biological Chemistry* **282**(33), 24027–24038.

Conforti, F., Davies, E. R., Calderwood, C. J., Thatcher, T. H., Jones, M. G., Smart, D. E., Mahajan, S., Alzetani, A., Havelock, T., Maher, T. M. et al. (2017), 'The histone deacetylase inhibitor, romidepsin, as a potential treatment for pulmonary fibrosis', *Oncotarget* **8**(30), 48737.

Conner, D. A. (2000), 'Mouse embryo fibroblast (mef) feeder cell preparation', *Current protocols in molecular biology* **51**(1), 23–2.

Consortium, G. O. (2019), 'The gene ontology resource: 20 years and still going strong', *Nucleic acids research* **47**(D1), D330–D338.

Conte, E., Gili, E., Fagone, E., Fruciano, M., Iemmolo, M. and Vancheri, C. (2014), 'Effect of pirfenidone on proliferation, tgf-β-induced myofibroblast differentiation and fibrogenic activity of primary human lung fibroblasts', *European Journal of Pharmaceutical Sciences* **58**, 13–19.

Corte, T., Cottin, V., Glassberg, M., Kreuter, M., Ogura, T., Suda, T., Goldin, J., Berkowitz, E., Elpers, B., Kim, S. et al. (2023), Bms-986278, an oral lysophosphatidic acid receptor 1 (lpa1) antagonist, for patients with idiopathic pulmonary fibrosis: results from a phase 2 randomized trial, *in* 'B17. EMERGING DATA ON DISEASE AND SYMPTOM BASED THERAPEUTICS FOR PATIENTS WITH IPF', American Thoracic Society, pp. A2785–A2785.

Couvelard, A., Deschamps, L., Rebours, V., Sauvanet, A., Gatter, K., Pezzella, F., Ruszniewski, P. and Bedossa, P. (2008), 'Overexpression of the oxygen sensors phd-1, phd-2, phd-3, and fih is associated with tumor aggressiveness in pancreatic endocrine tumors', *Clinical Cancer Research* **14**(20), 6634–6639.

Covello, K. L., Kehler, J., Yu, H., Gordan, J. D., Arsham, A. M., Hu, C.-J., Labosky, P. A., Simon, M. C. and Keith, B. (2006), 'Hif-2α regulates oct-4: effects of hypoxia on stem cell function, embryonic development, and tumor growth', *Genes & Development* **20**(5), 557–570.

Cowburn, A. S., Crosby, A., Macias, D., Branco, C., Colaço, R. D., Southwood, M., Toshner, M., Crotty Alexander, L. E., Morrell, N. W., Chilvers, E. R. et al. (2016), 'Hif2α–arginase axis is essential for the development of pulmonary hypertension', *Proceedings of the National Academy of Sciences* **113**(31), 8801–8806.

Cox, I. A., Otahal, P., de Graaff, B., Corte, T. J., Moodley, Y., Zappala, C., Glaspole, I., Hopkins, P., Macansh, S., Walters, E. H. et al. (2022), 'Incidence, prevalence and mortality of idiopathic pulmonary fibrosis in australia', *Respirology* **27**(3), 209–216.

Cramer-Morales, K. L., Heer, C. D., Mapuskar, K. A. and Domann, F. E. (2020), 'Succinate accumulation links mitochondrial mnsod depletion to aberrant nuclear dna methylation and altered cell fate', *Journal of Experimental Pathology* **1**(2), 60.

Cui, Y., Osorio, J. C., Risquez, C., Wang, H., Shi, Y., Gochuico, B. R., Morse, D., Rosas, I. O. and El-Chemaly, S. (2014), 'Transforming growth factor-β1 downregulates vascular endothelial growth factor-d expression in human lung fibroblasts via the jun nh 2-terminal kinase signaling pathway', *Molecular medicine* **20**, 120–134.

Cutting, C. C., Bowman, W. S., Dao, N., Pugashetti, J. V., Garcia, C. K., Oldham, J. M. and Newton, C. A. (2021), 'Family history of pulmonary fibrosis predicts worse survival in patients with interstitial lung disease', *Chest* **159**(5), 1913–1921.

Dann III, C. E., Bruick, R. K. and Deisenhofer, J. (2002), 'Structure of factor-inhibiting hypoxia-inducible factor 1: An asparaginyl hydroxylase involved in the hypoxic response pathway', *Proceedings of the National Academy of Sciences* **99**(24), 15351–15356.

De Souza, A. T., Dai, X., Spencer, A. G., Reppen, T., Menzie, A., Roesch, P. L., He, Y., Caguyong, M. J., Bloomer, S., Herweijer, H. et al. (2006), 'Transcriptional and phenotypic comparisons of ppara knockout and sirna knockdown mice', *Nucleic acids research* **34**(16), 4486–4494.

DeBerardinis, R. J. and Thompson, C. B. (2012), 'Cellular metabolism and disease: what do metabolic outliers teach us?', *Cell* **148**(6), 1132–1144.

Deeney, B., Orfanos, S., Cao, G., Karmacharya, N. and Panettieri, R. (2024), Treprostinil inhibits human lung fibroblast matrix production via the ip receptor independently of camp, *in* 'A68. UNVEILING NOVEL AVENUES IN IPF THERAPIES', American Thoracic Society, pp. A2465–A2465.

Delbrel, E., Soumare, A., Naguez, A., Label, R., Bernard, O., Bruhat, A., Fafournoux, P., Tremblais, G., Marchant, D., Gille, T. et al. (2018), 'Hif-1α triggers er stress and chop-mediated apoptosis in alveolar epithelial cells, a key event in pulmonary fibrosis', *Scientific reports* **8**(1), 17939.

Demaria, M., Ohtani, N., Youssef, S. A., Rodier, F., Toussaint, W., Mitchell, J. R., Laberge, R.-M., Vijg, J., Van Steeg, H., Dollé, M. E. et al. (2014), 'An essential role for senescent cells in optimal wound healing through secretion of pdgf-aa', *Developmental cell* **31**(6), 722–733.

Deng, X., Jin, K., Li, Y., Gu, W., Liu, M. and Zhou, L. (2015), 'Platelet-derived growth factor and transforming growth factor β1 regulate ards-associated lung fibrosis through distinct signaling pathways', *Cellular Physiology and Biochemistry* **36**(3), 937–946.

Derynck, R. and Budi, E. H. (2019), 'Specificity, versatility, and control of tgf-β family signaling', *Science signaling* **12**(570), eaav5183.

Desai, T. J., Brownfield, D. G. and Krasnow, M. A. (2014), 'Alveolar progenitor and stem cells in lung development, renewal and cancer', *Nature* **507**(7491), 190–194.

Devries, I. L., Hampton-Smith, R. J., Mulvihill, M. M., Alverdi, V., Peet, D. J. and Komives, E. A. (2010), 'Consequences of ikappab alpha hydroxylation by the factor inhibiting hif (fih)', *FEBS letters* **584**(23), 4725–4730.

Dey, A., Varelas, X. and Guan, K.-L. (2020), 'Targeting the hippo pathway in cancer, fibrosis, wound healing and regenerative medicine', *Nature reviews Drug discovery* **19**(7), 480–494.

Dou, X., Fu, Q., Long, Q., Liu, S., Zou, Y., Fu, D., Xu, Q., Jiang, Z., Ren, X., Zhang, G. et al. (2023), 'Pdk4-dependent hypercatabolism and lactate production of senescent cells promotes cancer malignancy', *Nature Metabolism* **5**(11), 1887–1910.

Dove, E. P., Olson, A. L. and Glassberg, M. K. (2019), 'Trends in idiopathic pulmonary fibrosis–related mortality in the united states: 2000–2017', *American Journal of Respiratory and Critical Care Medicine* **200**(7), 929–931.

Dowman, L., Hill, C. J., May, A. and Holland, A. E. (2021), 'Pulmonary rehabilitation for interstitial lung disease', *Cochrane database of systematic reviews* (2).

Dowman, L. M. and Holland, A. E. (2024), 'Pulmonary rehabilitation in idiopathic pulmonary fibrosis', *Current Opinion in Pulmonary Medicine* **30**(5), 516–522.

Duchemann, B., Annesi-Maesano, I., de Naurois, C. J., Sanyal, S., Brillet, P.-Y., Brauner, M., Kambouchner, M., Huynh, S., Naccache, J. M., Borie, R. et al. (2017), 'Prevalence and incidence of interstitial lung diseases in a multi-ethnic county of greater paris', *European Respiratory Journal* **50**(2).

Edwards, G. D., Polgar, O., Patel, S., Barker, R. E., Walsh, J. A., Harvey, J., Man, W. D. and Nolan, C. M. (2023), 'Mood disorder in idiopathic pulmonary fibrosis: response to pulmonary rehabilitation', *ERJ Open Research* **9**(3).

Eekhoff, J. D., Fang, F. and Lake, S. P. (2018), 'Multiscale mechanical effects of native collagen cross-linking in tendon', *Connective tissue research* **59**(5), 410–422.

Egan, M. E. (2009), 'How useful are cystic fibrosis mouse models?', *Drug Discovery Today: Disease Models* **6**(2), 35–41.

Elkins, J. M., Hewitson, K. S., McNeill, L. A., Seibel, J. F., Schlemminger, I., Pugh, C. W., Ratcliffe, P. J. and Schofield, C. J. (2003), 'Structure of factor-inhibiting hypoxia-inducible factor (hif) reveals mechanism of oxidative modification of hif-1α', *Journal of Biological Chemistry* **278**(3), 1802–1806.

Ema, M., Taya, S., Yokotani, N., Sogawa, K., Matsuda, Y. and Fujii-Kuriyama, Y. (1997), 'A novel bhlh-pas factor with close sequence similarity to hypoxia-inducible factor 1α regulates the vegf expression and is potentially involved in lung and vascular development', *Proceedings of the National Academy of Sciences* **94**(9), 4273–4278.

Evans, M. and Hackney, J. (1972), 'Cell proliferation in lungs of mice exposed to elevated concentrations of oxygen', *Aerospace medicine* **43**(6), 620–622.

Faffe, D. S. and Zin, W. A. (2009), 'Lung parenchymal mechanics in health and disease', *Physiological reviews* **89**(3), 759–775.

Faner, R., Rojas, M., MacNee, W. and Agustí, A. (2012), 'Abnormal lung aging in chronic obstructive pulmonary disease and idiopathic pulmonary fibrosis', *American journal of respiratory and critical care medicine* **186**(4), 306–313.

Fang, L., Chen, W.-C., Jaksch, P., Molino, A., Saglia, A., Roth, M. and Lambers, C. (2023), 'Treprostinil reconstitutes mitochondrial organisation and structure in idiopathic pulmonary fibrosis cells', *International Journal of Molecular Sciences* **24**(15), 12148.

Ferguson III, J. E., Wu, Y., Smith, K., Charles, P., Powers, K., Wang, H. and Patterson, C. (2007), 'Asb4 is a hydroxylation substrate of fih and promotes vascular differentiation via an oxygen-dependent mechanism', *Molecular and cellular biology* .

Fernandez, I. E. and Eickelberg, O. (2012*a*), 'The impact of tgf-β on lung fibrosis: from targeting to biomarkers', *Proceedings of the American Thoracic Society* **9**(3), 111–116.

Fernandez, I. E. and Eickelberg, O. (2012*b*), 'New cellular and molecular mechanisms of lung injury and fibrosis in idiopathic pulmonary fibrosis', *The Lancet* **380**(9842), 680–688.

Fierro-Fernandez, M., Busnadiego, O., Sandoval, P., Espinosa-Diez, C., Blanco-Ruiz, E., Rodriguez, M., Pian, H., Ramos, R., Lopez-Cabrera, M., Garcia-Bermejo, M. L. et al. (2015), 'mir-9-5p suppresses pro-fibrogenic transformation of fibroblasts and prevents organ fibrosis by targeting nox 4 and tgfbr 2', *EMBO reports* **16**(10), 1358–1377.

Fingerlin, T. E., Murphy, E., Zhang, W., Peljto, A. L., Brown, K. K., Steele, M. P., Loyd, J. E., Cosgrove, G. P., Lynch, D., Groshong, S. et al. (2013), 'Genome-wide association study identifies multiple susceptibility loci for pulmonary fibrosis', *Nature genetics* **45**(6), 613–620.

Finnson, K. W., Parker, W. L., ten Dijke, P., Thorikay, M. and Philip, A. (2008), 'Alk1 opposes alk5/smad3 signaling and expression of extracellular matrix components in human chondrocytes', *Journal of bone and mineral research* **23**(6), 896–906.

Fisher, J. T., Zhang, Y. and Engelhardt, J. F. (2011), 'Comparative biology of cystic fibrosis animal models', *Cystic Fibrosis: Diagnosis and Protocols, Volume II: Methods and Resources to Understand Cystic Fibrosis* pp. 311–334.

Frangogiannis, N. G. (2022), 'Transforming growth factor-β in myocardial disease', *Nature Reviews Cardiology* **19**(7), 435–455.

Fridman, A. and Tainsky, M. (2008), 'Critical pathways in cellular senescence and immortalization revealed by gene expression profiling', *Oncogene* **27**(46), 5975–5987.

Fries, K. M., Blieden, T., Looney, R. J., Sempowski, G. D., Silvera, M. R., Willis, R. A. and Phipps, R. P. (1994), 'Evidence of fibroblast heterogeneity and the role of fibroblast subpopulations in fibrosis', *Clinical immunology and immunopathology* **72**(3), 283–292.

Frost, J., Galdeano, C., Soares, P., Gadd, M. S., Grzes, K. M., Ellis, L., Epemolu, O., Shimamura, S., Bantscheff, M., Grandi, P. et al. (2016), 'Potent and selective chemical

probe of hypoxic signalling downstream of hif-α hydroxylation via vhl inhibition', *Nature communications* **7**(1), 13312.

Fujii, D., Brissenden, J. E., Derynck, R. and Francke, U. (1986), 'Transforming growth factor β gene maps to human chromosome 19 long arm and to mouse chromosome 7', *Somatic cell and molecular genetics* **12**, 281–288.

Fujino, N., Kubo, H., Suzuki, T., Ota, C., Hegab, A. E., He, M., Suzuki, S., Suzuki, T., Yamada, M., Kondo, T. et al. (2011), 'Isolation of alveolar epithelial type ii progenitor cells from adult human lungs', *Laboratory Investigation* **91**(3), 363–378.

Fukihara, J., Maiolo, S., Kovac, J., Sakamoto, K., Wakahara, K., Hashimoto, N. and Reynolds, P. N. (2022), 'Overexpression of bone morphogenetic protein receptor type 2 suppresses transforming growth factor β-induced profibrotic responses in lung fibroblasts', *Experimental Lung Research* **48**(1), 35–51.

Gao, H., Nepovimova, E., Heger, Z., Valko, M., Wu, Q., Kuca, K. and Adam, V. (2023), 'Role of hypoxia in cellular senescence', *Pharmacological Research* p. 106841.

Garcia-Alvarez, J., Ramirez, R., Checa, M., Nuttall, R. K., Sampieri, C. L., Edwards, D. R., Selman, M. and Pardo, A. (2006), 'Tissue inhibitor of metalloproteinase-3 is up-regulated by transforming growth factor-β 1 in vitro and expressed in fibroblastic foci in vivo in idiopathic pulmonary fibrosis', *Experimental lung research* **32**(5), 201–214.

García de Alba, C., Buendia-Roldán, I., Salgado, A., Becerril, C., Ramírez, R., González, Y., Checa, M., Navarro, C., Ruiz, V., Pardo, A. et al. (2015), 'Fibrocytes contribute to inflammation and fibrosis in chronic hypersensitivity pneumonitis through paracrine effects', *American journal of respiratory and critical care medicine* **191**(4), 427–436.

García-del Río, A., Prieto-Fernández, E., Egia-Mendikute, L., Antoñana-Vildosola, A., Jimenez-Lasheras, B., Lee, S. Y., Barreira-Manrique, A., Zanetti, S. R., de Blas, A., Velasco-Beltrán, P. et al. (2023), 'Factor-inhibiting hif (fih) promotes lung cancer progression', *JCI insight* **8**(20).

Gasse, P., Mary, C., Guenon, I., Noulin, N., Charron, S., Schnyder-Candrian, S., Schnyder, B., Akira, S., Quesniaux, V. F., Lagente, V. et al. (2007), 'Il-1r1/myd88 signaling and the inflammasome are essential in pulmonary inflammation and fibrosis in mice', *The Journal of clinical investigation* **117**(12), 3786–3799.

Gasse, P., Riteau, N., Vacher, R., Michel, M.-L., Fautrel, A., Di Padova, F., Fick, L., Charron, S., Lagente, V., Eberl, G. et al. (2011), 'Il-1 and il-23 mediate early il-17a production in pulmonary inflammation leading to late fibrosis', *PloS one* **6**(8), e23185.

George, P. M., Patterson, C. M., Reed, A. K. and Thillai, M. (2019), 'Lung transplantation for idiopathic pulmonary fibrosis', *The Lancet Respiratory Medicine* **7**(3), 271–282.

George, P. M., Wells, A. U. and Jenkins, R. G. (2020), 'Pulmonary fibrosis and covid-19: the potential role for antifibrotic therapy', *The Lancet Respiratory Medicine* **8**(8), 807–815.

Giannandrea, M. and Parks, W. C. (2014), 'Diverse functions of matrix metalloproteinases during fibrosis', *Disease models & mechanisms* **7**(2), 193–203.

Giatromanolaki, A., Koukourakis, M. I., Pezzella, F., Turley, H., Sivridis, E., Bouros, D., Bougioukas, G., Harris, A. L. and Gatter, K. C. (2008), 'Expression of prolyl-hydroxylases phd-1, 2 and 3 and of the asparagine hydroxylase fih in non-small cell lung cancer relates to an activated hif pathway', *Cancer letters* **262**(1), 87–93.

Gibbons, M. A., MacKinnon, A. C., Ramachandran, P., Dhaliwal, K., Duffin, R., Phythian-Adams, A. T., van Rooijen, N., Haslett, C., Howie, S. E., Simpson, A. J. et al. (2011), 'Ly6chi monocytes direct alternatively activated profibrotic macrophage regulation of lung fibrosis', *American journal of respiratory and critical care medicine* **184**(5), 569–581.

Ginhoux, F. and Jung, S. (2014), 'Monocytes and macrophages: developmental pathways and tissue homeostasis', *Nature Reviews Immunology* **14**(6), 392–404.

Gjonbrataj, J., Choi, W., Bahn, Y., Rho, B., Lee, J. and Lee, C. (2015), 'Incidence of idiopathic pulmonary fibrosis in korea based on the 2011 ats/ers/jrs/alat statement', *The International Journal of Tuberculosis and Lung Disease* **19**(6), 742–746.

Golan-Gerstl, R., Wallach-Dayan, S. B., Zisman, P., Cardoso, W. V., Goldstein, R. H. and Breuer, R. (2012), 'Cellular flice-like inhibitory protein deviates myofibroblast fas-induced apoptosis toward proliferation during lung fibrosis', *American journal of respiratory cell and molecular biology* **47**(3), 271–279.

Goodwin, J., Choi, H., Hsieh, M.-h., Neugent, M. L., Ahn, J.-M., Hayenga, H. N., Singh, P. K., Shackelford, D. B., Lee, I.-K., Shulaev, V. et al. (2018), 'Targeting hypoxia-inducible factor-1α/pyruvate dehydrogenase kinase 1 axis by dichloroacetate suppresses bleomycin-induced pulmonary fibrosis', *American journal of respiratory cell and molecular biology* **58**(2), 216–231.

Gornostaeva, A., Buravkova, L., Lobanova, M. and Andreeva, E. (2024), 'Hifs in hypoxic regulation of the extracellular matrix: focus on little-known player hif-3', *Biocell* .

Gribbin, J., Hubbard, R. B., Le Jeune, I., Smith, C. J., West, J. and Tata, L. J. (2006), 'Incidence and mortality of idiopathic pulmonary fibrosis and sarcoidosis in the uk', *Thorax* **61**(11), 980–985.

Gu, H., Mickler, E. A., Cummings, O. W., Sandusky, G. E., Weber, D. J., Gracon, A., Woodruff, T., Wilkes, D. S. and Vittal, R. (2014), 'Crosstalk between tgf-β1 and complement activation augments epithelial injury in pulmonary fibrosis', *The FASEB Journal* **28**(10), 4223.

Gu, L., ZHU, Y.-j., Yang, X., GUO, Z.-J., XU, W.-b. and TIAN, X.-l. (2007), 'Effect of tgf-β/smad signaling pathway on lung myofibroblast differentiation 4', *Acta pharmacologica sinica* **28**(3), 382–391.

Guan, S. and Zhou, J. (2017), 'Cxcr7 attenuates the tgf-β-induced endothelial-to-mesenchymal transition and pulmonary fibrosis', *Molecular BioSystems* **13**(10), 2116–2124.

Guenther, A., Krauss, E., Tello, S., Wagner, J., Paul, B., Kuhn, S., Maurer, O., Heinemann, S., Costabel, U., Barbero, M. A. N. et al. (2018), 'The european ipf registry (euripfreg): baseline characteristics and survival of patients with idiopathic pulmonary fibrosis', *Respiratory research* **19**, 1–10.

Guo, H., Sun, J., Zhang, S., Nie, Y., Zhou, S. and Zeng, Y. (2023), 'Progress in understanding and treating idiopathic pulmonary fibrosis: Recent insights and emerging therapies', *Frontiers in Pharmacology* **14**, 1205948.

Guo, W., Saito, S., Sanchez, C. G., Zhuang, Y., Gongora Rosero, R. E., Shan, B., Luo, F. and Lasky, J. A. (2017), 'Tgf-β1 stimulates hdac4 nucleus-to-cytoplasm translocation and nadph oxidase 4-derived reactive oxygen species in normal human lung fibroblasts', *American Journal of Physiology-Lung Cellular and Molecular Physiology* **312**(6), L936–L944.

Guo, W., Zhang, Y., Chen, T., Wang, Y., Xue, J., Zhang, Y., Xiao, W., Mo, X. and Lu, Y. (2011), 'Efficacy of rnai targeting of pyruvate kinase m2 combined with cisplatin in a lung cancer model', *Journal of cancer research and clinical oncology* **137**, 65–72.

Gurujeyalakshmi, G., Hollinger, M. and Giri, S. (1999), 'Pirfenidone inhibits pdgf isoforms in bleomycin hamster model of lung fibrosis at the translational level', *American Journal of Physiology-Lung Cellular and Molecular Physiology* **276**(2), L311–L318.

Haase, V. H. (2010), 'Regulation of erythropoiesis by hypoxia-inducible factors', *Blood Reviews* **24**(1), 15–24.

Haase, V. H. (2012), 'Hypoxia-inducible factor signaling in the development of kidney fibrosis', *Fibrogenesis & tissue repair* **5**(Suppl 1), S16.

Habermann, A. C., Gutierrez, A. J., Bui, L. T., Yahn, S. L., Winters, N. I., Calvi, C. L., Peter, L., Chung, M.-I., Taylor, C. J., Jetter, C. et al. (2020), 'Single-cell rna sequencing reveals profibrotic roles of distinct epithelial and mesenchymal lineages in pulmonary fibrosis', *Science advances* **6**(28), eaba1972.

Hackett, T.-L., Shaheen, F., Johnson, A., Wadsworth, S., Pechkovsky, D. V., Jacoby, D. B., Kicic, A., Stick, S. M. and Knight, D. A. (2008), 'Characterization of side population cells from human airway epithelium', *Stem cells* **26**(10), 2576–2585.

Hagood, J. S., Prabhakaran, P., Kumbla, P., Salazar, L., MacEwen, M. W., Barker, T. H., Ortiz, L. A., Schoeb, T., Siegal, G. P., Alexander, C. B. et al. (2005), 'Loss of fibroblast thy-1 expression correlates with lung fibrogenesis', *The American journal of pathology* **167**(2), 365–379.

Halfter, W., Oertle, P., Monnier, C. A., Camenzind, L., Reyes-Lua, M., Hu, H., Candiello, J., Labilloy, A., Balasubramani, M., Henrich, P. B. et al. (2015), 'New concepts in basement membrane biology', *The FEBS journal* **282**(23), 4466–4479.

Hamanaka, R. B., Nigdelioglu, R., Meliton, A. Y., Tian, Y., Witt, L. J., O'Leary, E., Sun, K. A., Woods, P. S., Wu, D., Ansbro, B. et al. (2018), 'Inhibition of phosphoglycerate dehydrogenase attenuates bleomycin-induced pulmonary fibrosis', *American journal of respiratory cell and molecular biology* **58**(5), 585–593.

Hancock, L. A., Hennessy, C. E., Solomon, G. M., Dobrinskikh, E., Estrella, A., Hara, N., Hill, D. B., Kissner, W. J., Markovetz, M. R., Grove Villalon, D. E. et al. (2018), 'Muc5b overexpression causes mucociliary dysfunction and enhances lung fibrosis in mice', *Nature communications* **9**(1), 5363.

Hänzelmann, S., Castelo, R. and Guinney, J. (2013), 'Gsva: gene set variation analysis for microarray and rna-seq data', *BMC bioinformatics* **14**, 1–15.

Harari, S., Madotto, F., Caminati, A., Conti, S. and Cesana, G. (2016), 'Epidemiology of idiopathic pulmonary fibrosis in northern italy', *PloS one* **11**(2), e0147072.

Hardie, W. D., Glasser, S. W. and Hagood, J. S. (2009), 'Emerging concepts in the pathogenesis of lung fibrosis', *The American journal of pathology* **175**(1), 3–16.

Haschek, W. M. and Witschi, H. (1979), 'Pulmonary fibrosis—a possible mechanism', *Toxicology and applied pharmacology* **51**(3), 475–487.

Hashimoto, M., Asai, A., Kawagishi, H., Mikawa, R., Iwashita, Y., Kanayama, K., Sugimoto, K., Sato, T., Maruyama, M. and Sugimoto, M. (2016), 'Elimination of p19arf-expressing cells enhances pulmonary function in mice', *JCI insight* **1**(12).

Hashimoto, N., Phan, S. H., Imaizumi, K., Matsuo, M., Nakashima, H., Kawabe, T., Shimokata, K. and Hasegawa, Y. (2010), 'Endothelial–mesenchymal transition in bleomycin-induced pulmonary fibrosis', *American journal of respiratory cell and molecular biology* **43**(2), 161–172.

Hashimoto, S., GON, Y., Takeshita, I., Matsumoto, K., MARUOKA, S. and HORIE, T. (2001), 'Transforming growth factor-β1 induces phenotypic modulation of human

lung fibroblasts to myofibroblast through a c-jun-nh2-terminal kinase-dependent pathway', *American journal of respiratory and critical care medicine* **163**(1), 152–157.

Hecker, L., Logsdon, N. J., Kurundkar, D., Kurundkar, A., Bernard, K., Hock, T., Meldrum, E., Sanders, Y. Y. and Thannickal, V. J. (2014), 'Reversal of persistent fibrosis in aging by targeting nox4-nrf2 redox imbalance', *Science translational medicine* **6**(231), 231ra47–231ra47.

Heikkilä, M., Pasanen, A., Kivirikko, K. I. and Myllyharju, J. (2011), 'Roles of the human hypoxia-inducible factor (hif)-3α variants in the hypoxia response', *Cellular and Molecular Life Sciences* **68**, 3885–3901.

Henderson, N. C., Arnold, T. D., Katamura, Y., Giacomini, M. M., Rodriguez, J. D., McCarty, J. H., Pellicoro, A., Raschperger, E., Betsholtz, C., Ruminski, P. G. et al. (2013), 'Targeting of αv integrin identifies a core molecular pathway that regulates fibrosis in several organs', *Nature medicine* **19**(12), 1617–1624.

Herrera, J., Forster, C., Pengo, T., Montero, A., Swift, J., Schwartz, M. A., Henke, C. A. and Bitterman, P. B. (2019), 'Registration of the extracellular matrix components constituting the fibroblastic focus in idiopathic pulmonary fibrosis', *JCI insight* **4**(1).

Herzog, E. L., Brody, A. R., Colby, T. V., Mason, R. and Williams, M. C. (2008), 'Knowns and unknowns of the alveolus', *Proceedings of the American Thoracic Society* **5**(7), 778–782.

Heukels, P., Moor, C., Von der Thüsen, J., Wijsenbeek, M. and Kool, M. (2019), 'Inflammation and immunity in ipf pathogenesis and treatment', *Respiratory medicine* **147**, 79–91.

Heukels, P. et al. (2019), 'Enhanced bruton's tyrosine kinase in b-cells and autoreactive iga in patients with idiopathic pulmonary fibrosis', *Respiratory research* **20**(1), 232.

Hewitson, K. S., Lienard, B. M., McDonough, M. A., Clifton, I. J., Butler, D., Soares, A. S., Oldham, N. J., McNeill, L. A. and Schofield, C. J. (2007), 'Structural and mechanistic studies on the inhibition of the hypoxia-inducible transcription factor hydroxylases by tricarboxylic acid cycle intermediates', *Journal of Biological Chemistry* **282**(5), 3293–3301.

Higgins, D. F., Kimura, K., Bernhardt, W. M., Shrimanker, N., Akai, Y., Hohenstein, B., Saito, Y., Johnson, R. S., Kretzler, M., Cohen, C. D. et al. (2007), 'Hypoxia promotes fibrogenesis in vivo via hif-1 stimulation of epithelial-to-mesenchymal transition', *The Journal of clinical investigation* **117**(12), 3810–3820.

Hilberg, F., Roth, G. J., Krssak, M., Kautschitsch, S., Sommergruber, W., Tontsch-Grunt, U., Garin-Chesa, P., Bader, G., Zoephel, A., Quant, J. et al. (2008), 'Bibf 1120: triple angiokinase inhibitor with sustained receptor blockade and good antitumor efficacy', *Cancer research* **68**(12), 4774–4782.

Hirano, A., Kanehiro, A., Ono, K., Ito, W., Yoshida, A., Okada, C., Nakashima, H., Tanimoto, Y., Kataoka, M., Gelfand, E. W. et al. (2006), 'Pirfenidone modulates airway responsiveness, inflammation, and remodeling after repeated challenge', *American journal of respiratory cell and molecular biology* **35**(3), 366–377.

Ho, P.-C., Bihuniak, J. D., Macintyre, A. N., Staron, M., Liu, X., Amezquita, R., Tsui, Y.-C., Cui, G., Micevic, G., Perales, J. C. et al. (2015), 'Phosphoenolpyruvate is a metabolic checkpoint of anti-tumor t cell responses', *Cell* **162**(6), 1217–1228.

Hoffman, E. T., Uhl, F. E., Asarian, L., Deng, B., Becker, C., Uriarte, J. J., Downs, I., Young, B. and Weiss, D. J. (2023), 'Regional and disease specific human lung extracellular matrix composition', *Biomaterials* **293**, 121960.

Hogaboam, C. M., Murray, L. and Martinez, F. J. (2012), 'Epigenetic mechanisms through which toll-like receptor–9 drives idiopathic pulmonary fibrosis progression', *Proceedings of the American Thoracic Society* **9**(3), 172–176.

Holland, A. E., Hill, C. J., Conron, M., Munro, P. and McDonald, C. F. (2008), 'Short term improvement in exercise capacity and symptoms following exercise training in interstitial lung disease', *Thorax* **63**(6), 549–554.

Holland, A. E., Hill, C. J., Conron, M., Munro, P. and McDonald, C. F. (2009), 'Small changes in six-minute walk distance are important in diffuse parenchymal lung disease', *Respiratory medicine* **103**(10), 1430–1435.

Hopkins, R. B., Burke, N., Fell, C., Dion, G. and Kolb, M. (2016), 'Epidemiology and survival of idiopathic pulmonary fibrosis from national data in canada', *European Respiratory Journal* **48**(1), 187–195.

Hostettler, K. E., Zhong, J., Papakonstantinou, E., Karakiulakis, G., Tamm, M., Seidel, P., Sun, Q., Mandal, J., Lardinois, D., Lambers, C. et al. (2014), 'Anti-fibrotic effects of nintedanib in lung fibroblasts derived from patients with idiopathic pulmonary fibrosis', *Respiratory research* **15**, 1–9.

Hu, C.-J., Sataur, A., Wang, L., Chen, H. and Simon, M. C. (2007*a*), 'The n-terminal transactivation domain confers target gene specificity of hypoxia-inducible factors hif-1α and hif-2α', *Molecular biology of the cell* **18**(11), 4528–4542.

Hu, C.-J., Sataur, A., Wang, L.-J., Chen, H. and Simon, M. C. (2007*b*), 'Differential roles of the n-terminal transactivation domain (n-tad) of hypoxia-inducible factors 1α and 2α', *Molecular Biology of the Cell* **18**(1), 452–464.

Hu, J., Chen, C., Liu, Q., Liu, B., Song, C., Zhu, S., Wu, C., Liu, S., Yu, H., Yao, D. et al. (2015), 'The role of the mir-31/fih1 pathway in tgf-β-induced liver fibrosis', *Clinical Science* **129**(4), 305–317.

Huang, C., Liang, Y., Zeng, X., Yang, X., Xu, D., Gou, X., Sathiaseelan, R., Senavirathna, L. K., Wang, P. and Liu, L. (2020), 'Long noncoding rna fendrr exhibits antifibrotic activity in pulmonary fibrosis', *American journal of respiratory cell and molecular biology* **62**(4), 440–453.

Huang, C., Xiao, X., Yang, Y., Mishra, A., Liang, Y., Zeng, X., Yang, X., Xu, D., Blackburn, M. R., Henke, C. A. et al. (2017), 'Microrna-101 attenuates pulmonary fibrosis by inhibiting fibroblast proliferation and activation', *Journal of Biological Chemistry* **292**(40), 16420–16439.

Huang, Y., Xie, Y., Abel, P. W., Wei, P., Plowman, J., Toews, M. L., Strah, H., Siddique, A., Bailey, K. L. and Tu, Y. (2020), 'Tgf-β1-induced mir-424 promotes pulmonary myofibroblast differentiation by targeting slit2 protein expression', *Biochemical pharmacology* **180**, 114172.

Hubbard, R., Cooper, M., Antoniak, M., Venn, A., Khan, S., Johnston, I., Lewis, S. and Britton, J. (2000), 'Risk of cryptogenic fibrosing alveolitis in metal workers', *The Lancet* **355**(9202), 466–467.

Hubbard, R., Lewis, S., Richards, K., Johnston, I. and Britton, J. (1996), 'Occupational exposure to metal or wood dust and aetiology of cryptogenic fibrosing alveolitis', *The Lancet* **347**(8997), 284–289.

Humphreys, B. D., Lin, S.-L., Kobayashi, A., Hudson, T. E., Nowlin, B. T., Bonventre, J. V., Valerius, M. T., McMahon, A. P. and Duffield, J. S. (2010), 'Fate tracing reveals the pericyte and not epithelial origin of myofibroblasts in kidney fibrosis', *The American journal of pathology* **176**(1), 85–97.

Hung, C., Linn, G., Chow, Y.-H., Kobayashi, A., Mittelsteadt, K., Altemeier, W. A., Gharib, S. A., Schnapp, L. M. and Duffield, J. S. (2013), 'Role of lung pericytes and resident fibroblasts in the pathogenesis of pulmonary fibrosis', *American journal of respiratory and critical care medicine* **188**(7), 820–830.

Hutchinson, J. P., McKeever, T. M., Fogarty, A. W., Navaratnam, V. and Hubbard, R. B. (2014), 'Increasing global mortality from idiopathic pulmonary fibrosis in the twenty-first century', *Annals of the American Thoracic Society* **11**(8), 1176–1185.

Hynes, R. O. (2009), 'The extracellular matrix: not just pretty fibrils', *Science* **326**(5957), 1216–1219.

Hyseni, A., Van Der Groep, P., Van Der Wall, E. and Van Diest, P. J. (2011), 'Subcellular fih-1 expression patterns in invasive breast cancer in relation to hif-1α expression', *Cellular oncology* **34**, 565–570.

Hänzelmann, S., Castelo, R. and Guinney, J. (2013), 'Gsva: gene set variation analysis for microarray and rna-seq data', *BMC Bioinformatics* **14**(1), 7.
URL: *https://doi.org/10.1186/1471-2105-14-7*

Inoki, K., Haneda, M., Maeda, S., Koya, D. and Kikkawa, R. (1999), 'Tgf-β1 stimulates glucose uptake by enhancing glut1 expression in mesangial cells', *Kidney international* **55**(5), 1704–1712.

Isaacs, J. S., Xu, W.-C. and Neckers, L. (2002), 'Hsp90 regulates the von hippel-lindau tumor suppressor protein and hif-1α stability', *PNAS* **99**(10), 10423–10428.

Ishiwari, M., Kono, Y., Togashi, Y., Kobayashi, K., Kikuchi, R., Kogami, M. and Abe, S. (2024), 'Prognosis of connective tissue disease related interstitial lung disease after initiation of long-term oxygen therapy: comparison with idiopathic pulmonary fibrosis'.

Issa, R., Zhou, X., Constandinou, C. M., Fallowfield, J., Millward-Sadler, H., Gaca, M. D., Sands, E., Suliman, I., Trim, N., Knorr, A. et al. (2004), 'Spontaneous recovery from micronodular cirrhosis: evidence for incomplete resolution associated with matrix cross-linking', *Gastroenterology* **126**(7), 1795–1808.

Itoh, S., Itoh, F., Goumans, M.-J. and ten Dijke, P. (2000), 'Signaling of transforming growth factor-β family members through smad proteins', *European Journal of Biochemistry* **267**(24), 6954–6967.

Ivan, M., Kondo, K., Yang, H., Kim, W., Valiando, J., Ohh, M., Salic, A., Asara, J. M., Lane, W. S. and Kaelin Jr, W. G. (2001), 'Hifα targeted for vhl-mediated destruction by proline hydroxylation: implications for o2 sensing', *Science* **292**(5516), 464–468.

Iyer, N. V., Kotch, L. E., Agani, F., Leung, S. W., Laughner, E., Wenger, R. H., Gassmann, M., Gearhart, J. D., Lawler, A. M., Aimee, Y. Y. et al. (1998), 'Cellular and developmental control of o2 homeostasis by hypoxia-inducible factor 1α', *Genes & development* **12**(2), 149–162.

Iyer, S., Gurujeyalakshmi, G. and Giri, S. (1999), 'Effects of pirfenidone on transforming growth factor-β gene expression at the transcriptional level in bleomycin hamster model of lung fibrosis', *Journal of Pharmacology and Experimental Therapeutics* **291**(1), 367–373.

Jaakkola, P., Mole, D. R., Tian, Y.-M., Wilson, M. I., Gielbert, J., Gaskell, S. J., von Kriegsheim, A., Hebestreit, H. F., Mukherji, M., Schofield, C. J., Maxwell, P. H., Pugh, C. W. and Ratcliffe, P. J. (2001), 'Targeting of hif-alpha to the von hippel-lindau ubiquitylation complex by o2-regulated prolyl hydroxylation', *Science* **292**(5516), 468–472.

Jablonska, E., Markart, P., Zakrzewicz, D., Preissner, K. T. and Wygrecka, M. (2010), 'Transforming growth factor-β1 induces expression of human coagulation factor xii via smad3 and jnk signaling pathways in human lung fibroblasts', *Journal of Biological Chemistry* **285**(15), 11638–11651.

Janke, K., Brockmeier, U., Kuhlmann, K., Eisenacher, M., Nolde, J., Meyer, H. E., Mairbäurl, H. and Metzen, E. (2013), 'Factor inhibiting hif-1 (fih-1) modulates protein interactions of apoptosis-stimulating p53 binding protein 2 (aspp2)', *Journal of cell science* **126**(12), 2629–2640.

Jarosch, I., Schneeberger, T., Gloeckl, R., Kreuter, M., Neurohr, C., Prasse, A., Behr, J. and Kenn, K. (2016), 'Effects of a 3-week pulmonary rehabilitation program in patients with idiopathic pulmonary fibrosis–a randomized, controlled trial'.

Jewell, U. R., Kvietikova, I., Scheid, A., Bauer, C., Wenger, R. H. and Gassmann, M. (2001), 'Induction of hif–1α in response to hypoxia is instantaneous', *The FASEB Journal* **15**(7), 1312–1314.

Ji, H., Tang, H., Lin, H., Mao, J., Gao, L., Liu, J. and Wu, T. (2014), 'Rho/rock cross-talks with transforming growth factor-β/smad pathway participates in lung fibroblast-myofibroblast differentiation', *Biomedical reports* **2**(6), 787–792.

Jiang, P., Gil de Rubio, R., Hrycaj, S. M., Gurczynski, S. J., Riemondy, K. A., Moore, B. B., Omary, M. B., Ridge, K. M. and Zemans, R. L. (2020), 'Ineffectual type 2–to–type 1 alveolar epithelial cell differentiation in idiopathic pulmonary fibrosis: persistence of the krt8hi transitional state', *American journal of respiratory and critical care medicine* **201**(11), 1443–1447.

Jiang, S., Li, T., Yang, Z., Yi, W., Di, S., Sun, Y., Wang, D. and Yang, Y. (2017), 'Ampk orchestrates an elaborate cascade protecting tissue from fibrosis and aging', *Ageing research reviews* **38**, 18–27.

Jiang, Y., Zhou, X., Hu, R. and Dai, A. (2018), 'Tgf-β1-induced smad2/3/4 activation promotes relm-β transcription to modulate the endothelium-mesenchymal transition in human endothelial cells', *The international journal of biochemistry & cell biology* **105**, 52–60.

Jones, M. G., Andriotis, O. G., Roberts, J. J., Lunn, K., Tear, V. J., Cao, L., Ask, K., Smart, D. E., Bonfanti, A., Johnson, P. et al. (2018), 'Nanoscale dysregulation of collagen structure-function disrupts mechano-homeostasis and mediates pulmonary fibrosis', *Elife* **7**, e36354.

Joshi, N., Watanabe, S., Verma, R., Jablonski, R. P., Chen, C.-I., Cheresh, P., Markov, N. S., Reyfman, P. A., McQuattie-Pimentel, A. C., Sichizya, L. et al. (2020), 'A spatially restricted fibrotic niche in pulmonary fibrosis is sustained by m-csf/m-csfr signalling in monocyte-derived alveolar macrophages', *European Respiratory Journal* **55**(1).

Jung, S.-N., Yang, W. K., Kim, J., Kim, H. S., Kim, E. J., Yun, H., Park, H., Kim, S. S., Choe, W., Kang, I. et al. (2008), 'Reactive oxygen species stabilize hypoxia-inducible factor-1 alpha protein and stimulate transcriptional activity via amp-activated protein kinase in du145 human prostate cancer cells', *Carcinogenesis* **29**(4), 713–721.

Kadoya, K., Togo, S., Tulafu, M., Namba, Y., Iwai, M., Watanabe, J., Okabe, T., Jin, J., Kodama, Y., Kitamura, H. et al. (2019), 'Specific features of fibrotic lung fibroblasts highly sensitive to fibrotic processes mediated via tgf-β-erk5 interaction', *Cell Physiol Biochem* **52**(4), 822–837.

Kaelin, W. G. and Ratcliffe, P. J. (2008), 'Oxygen sensing by metazoans: the central role of the hif hydroxylase pathway', *Molecular cell* **30**(4), 393–402.

Kage, H. and Borok, Z. (2012), 'Emt and interstitial lung disease: a mysterious relationship', *Current opinion in pulmonary medicine* **18**(5), 517–523.

Kakugawa, T., Mukae, H., Hayashi, T., Ishii, H., Abe, K., Fujii, T., Oku, H., Miyazaki, M., Kadota, J. and Kohno, S. (2004), 'Pirfenidone attenuates expression of hsp47 in murine bleomycin-induced pulmonary fibrosis', *European Respiratory Journal* **24**(1), 57–65.

Kalluri, R., Weinberg, R. A. et al. (2009), 'The basics of epithelial-mesenchymal transition', *The Journal of clinical investigation* **119**(6), 1420–1428.

Kang, H.-R., Lee, C. G., Homer, R. J. and Elias, J. A. (2007), 'Semaphorin 7a plays a critical role in tgf-β1–induced pulmonary fibrosis', *The Journal of experimental medicine* **204**(5), 1083–1093.

Kaplan, N., Dong, Y., Wang, S., Yang, W., Park, J. K., Wang, J., Fiolek, E., White, B. P., Chandel, N. S., Peng, H. et al. (2020), 'Fih-1 engages novel binding partners to positively influence epithelial proliferation via p63', *FASEB journal: official publication of the Federation of American Societies for Experimental Biology* **34**(1), 525.

Kapnadak, S. G. and Raghu, G. (2021), 'Lung transplantation for interstitial lung disease', *European Respiratory Review* **30**(161).

Karakatsani, A., Papakosta, D., Rapti, A., Antoniou, K., Dimadi, M., Markopoulou, A., Latsi, P., Polychronopoulos, V., Birba, G., Ch, L. et al. (2009), 'Epidemiology of interstitial lung diseases in greece', *Respiratory medicine* **103**(8), 1122–1129.

Kärkkäinen, M., Nurmi, H., Kettunen, H.-P., Selander, T., Purokivi, M. and Kaarteenaho, R. (2018), 'Underlying and immediate causes of death in patients with idiopathic pulmonary fibrosis', *BMC Pulmonary Medicine* **18**, 1–10.

Karttunen, S., Duffield, M., Scrimgeour, N. R., Squires, L., Lim, W. L., Dallas, M. L., Scragg, J. L., Chicher, J., Dave, K. A., Whitelaw, M. L. et al. (2015), 'Oxygen-dependent hydroxylation by fih regulates the trpv3 ion channel', *Journal of Cell Science* **128**(2), 225–231.

Kasai, H., Allen, J. T., Mason, R. M., Kamimura, T. and Zhang, Z. (2005), 'Tgf-β1 induces human alveolar epithelial to mesenchymal cell transition (emt)', *Respiratory research* **6**, 1–15.

Kataoka, K., Nishiyama, O., Ogura, T., Mori, Y., Kozu, R., Arizono, S., Tsuda, T., Tomioka, H., Tomii, K., Sakamoto, K. et al. (2023), 'Long-term effect of pulmonary rehabilitation in idiopathic pulmonary fibrosis: a randomised controlled trial', *Thorax* **78**(8), 784–791.

Katsuno, Y., Qin, J., Oses-Prieto, J., Wang, H., Jackson-Weaver, O., Zhang, T., Lamouille, S., Wu, J., Burlingame, A., Xu, J. et al. (2018), 'Arginine methylation of smad7 by prmt1 in tgf-β–induced epithelial–mesenchymal transition and epithelial stem-cell generation', *Journal of Biological Chemistry* **293**(34), 13059–13072.

Kaunisto, J., Kelloniemi, K., Sutinen, E., Hodgson, U., Piilonen, A., Kaarteenaho, R., Mäkitaro, R., Purokivi, M., Lappi-Blanco, E., Saarelainen, S. et al. (2015), 'Re-evaluation of diagnostic parameters is crucial for obtaining accurate data on idiopathic pulmonary fibrosis', *BMC pulmonary medicine* **15**, 1–8.

Keith, B., Johnson, R. S. and Simon, M. C. (2012), 'Hypoxia-inducible factors 1 and 2: sibling rivalry in hypoxic tumour growth and progression', *Nature Reviews Cancer* **12**(1), 9–22.

Kelly, B. G., Lok, S. S., Hasleton, P. S., Egan, J. J. and Stewart, J. P. (2002), 'A rearranged form of epstein–barr virus dna is associated with idiopathic pulmonary fibrosis', *American journal of respiratory and critical care medicine* **166**(4), 510–513.

Khalil, N., Bereznay, O., Sporn, M. and Greenberg, A. (1989), 'Macrophage production of transforming growth factor beta and fibroblast collagen synthesis in chronic pulmonary inflammation.', *The Journal of experimental medicine* **170**(3), 727–737.

Khan, M., Bhattacharyya, T., Andrikopoulos, P., Esteban, M., Barod, R., Connor, T., Ashcroft, M., Maxwell, P. and Kiriakidis, S. (2011), 'Factor inhibiting hif (fih-1) promotes renal cancer cell survival by protecting cells from hif-1α-mediated apoptosis', *British journal of cancer* **104**(7), 1151–1159.

Kikuchi, R., Maeda, Y., Tsuji, T., Yamaguchi, K., Abe, S., Nakamura, H. and Aoshiba, K. (2021), 'Fenofibrate inhibits tgf-β-induced myofibroblast differentiation and activation in human lung fibroblasts in vitro', *FEBS Open Bio* **11**(8), 2340–2349.

Kim, H. C., Song, J. S., Park, S., Yoon, H.-Y., Lim, S. Y., Chae, E. J., Jang, S. J. and Song, J. W. (2020), 'Histologic features suggesting connective tissue disease in idiopathic pulmonary fibrosis', *Scientific Reports* **10**(1), 21137.

Kim, I., Choi, S., Yoo, S., Lee, M. and Kim, I.-S. (2022), 'Cancer-associated fibroblasts in the hypoxic tumor microenvironment', *Cancers* **14**(14), 3321.

Kim, I., Shin, S.-H., Lee, J. E. and Park, J.-W. (2019), 'Oxygen sensor fih inhibits hace1-dependent ubiquitination of rac1 to enhance metastatic potential in breast cancer cells', *Oncogene* **38**(19), 3651–3666.

Kim, J.-w., Tchernyshyov, I., Semenza, G. L. and Dang, C. V. (2006), 'Hif-1-mediated expression of pyruvate dehydrogenase kinase: a metabolic switch required for cellular adaptation to hypoxia', *Cell metabolism* **3**(3), 177–185.

Kim, K. K., Kugler, M. C., Wolters, P. J., Robillard, L., Galvez, M. G., Brumwell, A. N., Sheppard, D. and Chapman, H. A. (2006), 'Alveolar epithelial cell mesenchymal transition develops in vivo during pulmonary fibrosis and is regulated by the extracellular matrix', *Proceedings of the National Academy of Sciences* **103**(35), 13180–13185.

King Jr, T. E., Bradford, W. Z., Castro-Bernardini, S., Fagan, E. A., Glaspole, I., Glassberg, M. K., Gorina, E., Hopkins, P. M., Kardatzke, D., Lancaster, L. et al. (2014), 'A phase 3 trial of pirfenidone in patients with idiopathic pulmonary fibrosis', *New England journal of medicine* **370**(22), 2083–2092.

Kitamura, H., Ichinose, S., Hosoya, T., Ando, T., Ikushima, S., Oritsu, M. and Takemura, T. (2007), 'Inhalation of inorganic particles as a risk factor for idiopathic pulmonary fibrosis—elemental microanalysis of pulmonary lymph nodes obtained at autopsy cases', *Pathology-Research and Practice* **203**(8), 575–585.

Kliment, C. R. and Oury, T. D. (2010), 'Oxidative stress, extracellular matrix targets, and idiopathic pulmonary fibrosis', *Free Radical Biology and Medicine* **49**(5), 707–717.

Klingberg, F., Chow, M. L., Koehler, A., Boo, S., Buscemi, L., Quinn, T. M., Costell, M., Alman, B. A., Genot, E. and Hinz, B. (2014), 'Prestress in the extracellular matrix sensitizes latent tgf-β1 for activation', *The Journal of cell biology* **207**(2), 283.

Knowles, H. J., Raval, R. R., Harris, A. L. and Ratcliffe, P. J. (2003), 'Effect of ascorbate on the activity of hypoxia-inducible factor in cancer cells', *Cancer Research* **63**(8), 1764–1768.

Kobayashi, Y., Tata, A., Konkimalla, A., Katsura, H., Lee, R. F., Ou, J., Banovich, N. E., Kropski, J. A. and Tata, P. R. (2020), 'Persistence of a regeneration-associated, transitional alveolar epithelial cell state in pulmonary fibrosis', *Nature cell biology* **22**(8), 934–946.

Koh, M. Y., Lemos Jr, R., Liu, X. and Powis, G. (2011), 'The hypoxia-associated factor switches cells from hif-1α-to hif-2α-dependent signaling promoting stem cell characteristics, aggressive tumor growth and invasion', *Cancer research* **71**(11), 4015–4027.

Koivunen, P., Hirsilä, M., Günzler, V., Kivirikko, K. I. and Myllyharju, J. (2004), 'Catalytic properties of the asparaginyl hydroxylase (fih) in the oxygen sensing pathway are distinct from those of its prolyl 4-hydroxylases', *Journal of Biological Chemistry* **279**(11), 9899–9904.

Kolosionek, E., Savai, R., Ghofrani, H. A., Weissmann, N., Guenther, A., Grimminger, F., Seeger, W., Banat, G. A., Schermuly, R. T. and Pullamsetti, S. S. (2009), 'Expression

and activity of phosphodiesterase isoforms during epithelial mesenchymal transition: the role of phosphodiesterase 4', *Molecular biology of the cell* **20**(22), 4751–4765.

Königshoff, M., Balsara, N., Pfaff, E.-M., Kramer, M., Chrobak, I., Seeger, W. and Eickelberg, O. (2008), 'Functional wnt signaling is increased in idiopathic pulmonary fibrosis', *PloS one* **3**(5), e2142.

Königshoff, M., Kramer, M., Balsara, N., Wilhelm, J., Amarie, O. V., Jahn, A., Rose, F., Fink, L., Seeger, W., Schaefer, L. et al. (2009), 'Wnt1-inducible signaling protein–1 mediates pulmonary fibrosis in mice and is upregulated in humans with idiopathic pulmonary fibrosis', *The Journal of clinical investigation* **119**(4), 772–787.

Korthagen, N. M., van Moorsel, C. H., Barlo, N. P., Kazemier, K. M., Ruven, H. J. and Grutters, J. C. (2012), 'Association between variations in cell cycle genes and idiopathic pulmonary fibrosis', *PloS one* **7**(1), e30442.

Kottmann, R. M., Kulkarni, A. A., Smolnycki, K. A., Lyda, E., Dahanayake, T., Salibi, R., Honnons, S., Jones, C., Isern, N. G., Hu, J. Z. et al. (2012), 'Lactic acid is elevated in idiopathic pulmonary fibrosis and induces myofibroblast differentiation via ph-dependent activation of transforming growth factor-β', *American journal of respiratory and critical care medicine* **186**(8), 740–751.

Kottmann, R. M., Trawick, E., Judge, J. L., Wahl, L. A., Epa, A. P., Owens, K. M., Thatcher, T. H., Phipps, R. P. and Sime, P. J. (2015), 'Pharmacologic inhibition of lactate production prevents myofibroblast differentiation', *American Journal of Physiology-Lung Cellular and Molecular Physiology* **309**(11), L1305–L1312.

Krausgruber, T., Blazek, K., Smallie, T., Alzabin, S., Lockstone, H., Sahgal, N., Hussell, T., Feldmann, M. and Udalova, I. A. (2011), 'Irf5 promotes inflammatory macrophage polarization and th1-th17 responses', *Nature immunology* **12**(3), 231–238.

Krebs, H. A. and Johnson, W. A. (1937), 'Metabolism of ketonic acids in animal tissues', *Biochemical Journal* **31**(4), 645.

Krebs, H. A. and Johnson, W. A. (1980), 'The role of citric acid in intermediate metabolism in animal tissues', *FEBS letters* **117**(S1), K2–K10.

Kreuter, M., Maher, T., Wuyts, W., Valenzuela, C., Hamblin, M., Kim, S., Patel, A., Elpers, B. and Richeldi, L. (2024), Effect of bms-986278, an oral lpa1 antagonist, on time to disease progression in patients with pulmonary fibrosis: A post hoc analysis of data from a phase 2 randomized trial, *in* 'C95. NEW CLINICAL TRIAL RESULTS IN CHRONIC LUNG DISEASE', American Thoracic Society, pp. A6615–A6615.

Krizhanovsky, V., Yon, M., Dickins, R. A., Hearn, S., Simon, J., Miething, C., Yee, H., Zender, L. and Lowe, S. W. (2008), 'Senescence of activated stellate cells limits liver fibrosis', *Cell* **134**(4), 657–667.

Kropski, J. A., Mitchell, D. B., Markin, C., Polosukhin, V. V., Choi, L., Johnson, J. E., Lawson, W. E., Phillips III, J. A., Cogan, J. D., Blackwell, T. S. et al. (2014), 'A novel dyskerin (dkc1) mutation is associated with familial interstitial pneumonia', *Chest* **146**(1), e1–e7.

Kropski, J. A., Pritchett, J. M., Zoz, D. F., Crossno, P. F., Markin, C., Garnett, E. T., Degryse, A. L., Mitchell, D. B., Polosukhin, V. V., Rickman, O. B. et al. (2015), 'Extensive phenotyping of individuals at risk for familial interstitial pneumonia reveals clues to the pathogenesis of interstitial lung disease', *American journal of respiratory and critical care medicine* **191**(4), 417–426.

Kuhn III, C., Boldt, J., King Jr, T. E., Crouch, E., Vartio, T. and McDonald, J. A. (2012), 'An immunohistochemical study of architectural remodeling and connective tissue synthesis in pulmonary fibrosis', *American Review of Respiratory Disease* .

Kulasekaran, P., Scavone, C. A., Rogers, D. S., Arenberg, D. A., Thannickal, V. J. and Horowitz, J. C. (2009), 'Endothelin-1 and transforming growth factor-β1 independently induce fibroblast resistance to apoptosis via akt activation', *American journal of respiratory cell and molecular biology* **41**(4), 484–493.

Kulshrestha, R., Kumar, P., Singh, A., Nair, D. S. et al. (2023), 'Regulation of tgf-β1-smad-1-7 signaling to inhibit epithelial mesenchymal transition by repurposed anti-fibrotic drug pirfenidone can attenuate lung cancer progression', *Journal of Cancer Science and Clinical Therapeutics* **7**(1), 50–64.

Kurita, Y., Araya, J., Minagawa, S., Hara, H., Ichikawa, A., Saito, N., Kadota, T., Tsubouchi, K., Sato, N., Yoshida, M. et al. (2017), 'Pirfenidone inhibits myofibroblast differentiation and lung fibrosis development during insufficient mitophagy', *Respiratory research* **18**, 1–14.

Kuwano, K., Kunitake, R., Kawasaki, M., Nomoto, Y., Hagimoto, N., Nakanishi, Y. and Hara, N. (1996), 'P21waf1/cip1/sdi1 and p53 expression in association with dna strand breaks in idiopathic pulmonary fibrosis.', *American journal of respiratory and critical care medicine* **154**(2), 477–483.

Kuzmanov, A., Wielockx, B., Rezaei, M., Kettelhake, A. and Breier, G. (2012), 'Overexpression of factor inhibiting hif-1 enhances vessel maturation and tumor growth via platelet-derived growth factor-c', *International journal of cancer* **131**(5), E603–E613.

Lai, C.-C., Wang, C.-Y., Lu, H.-M., Chen, L., Teng, N.-C., Yan, Y.-H., Wang, J.-Y., Chang, Y.-T., Chao, T.-T., Lin, H.-I. et al. (2012), 'Idiopathic pulmonary fibrosis in taiwan–a population-based study', *Respiratory medicine* **106**(11), 1566–1574.

Lambrecht, B. N. (2006), 'Alveolar macrophage in the driver's seat', *Immunity* **24**(4), 366–368.

Lancaster, D. E., McNEILL, L. A., McDONOUGH, M. A., Aplin, R. T., Hewitson, K. S., Pugh, C. W., Ratcliffe, P. J. and Schofield, C. J. (2004), 'Disruption of dimerization and substrate phosphorylation inhibit factor inhibiting hypoxia-inducible factor (fih) activity', *Biochemical journal* **383**(3), 429–437.

Landi, C., Bargagli, E., Carleo, A., Bianchi, L., Gagliardi, A., Prasse, A., Perari, M. G., Refini, R. M., Bini, L. and Rottoli, P. (2014), 'A system biology study of balf from patients affected by idiopathic pulmonary fibrosis (ipf) and healthy controls', *PROTEOMICS–Clinical Applications* **8**(11-12), 932–950.

Lando, D., Peet, D. J., Gorman, J. J., Whelan, D. A., Whitelaw, M. L. and Bruick, R. K. (2002), 'Fih-1 is an asparaginyl hydroxylase enzyme that regulates the transcriptional activity of hypoxia-inducible factor', *Genes & development* **16**(12), 1466–1471.

Landsman, L., Varol, C. and Jung, S. (2007), 'Distinct differentiation potential of blood monocyte subsets in the lung', *The Journal of Immunology* **178**(4), 2000–2007.

Lansky, Z., Mutsafi, Y., Houben, L., Ilani, T., Armony, G., Wolf, S. G. and Fass, D. (2019), '3d mapping of native extracellular matrix reveals cellular responses to the microenvironment', *Journal of Structural Biology: X* **1**, 100002.

Lasithiotaki, I., Giannarakis, I., Tsitoura, E., Samara, K. D., Margaritopoulos, G. A., Choulaki, C., Vasarmidi, E., Tzanakis, N., Voloudaki, A., Sidiropoulos, P. et al. (2016), 'Nlrp3 inflammasome expression in idiopathic pulmonary fibrosis and rheumatoid lung', *European Respiratory Journal* **47**(3), 910–918.

Le Pavec, J., Dauriat, G., Gazengel, P., Dolidon, S., Hanna, A., Feuillet, S., Pradere, P., Crutu, A., Florea, V., Boulate, D. et al. (2020), 'Lung transplantation for idiopathic pulmonary fibrosis', *La Presse Médicale* **49**(2), 104026.

LeBleu, V. S., MacDonald, B. and Kalluri, R. (2007), 'Structure and function of basement membranes', *Experimental biology and medicine* **232**(9), 1121–1129.

Lee, H., Myong, J., Kim, H., Rhee, C., Yoon, H. and Koo, J. (2016), 'Incidence and prevalence of idiopathic interstitial pneumonia and idiopathic pulmonary fibrosis in korea', *The International Journal of Tuberculosis and Lung Disease* **20**(7), 978–984.

Lena, A., Nicoloso, M., Rossi, S., Mancini, M., Zhou, H., Saintigny, G., Dellambra, E., Odorisio, T., Mahé, C., Calin, G. et al. (2012), 'p63-microrna feedback in keratinocyte senescence.', *Proceedings of the National Academy of Sciences of the United States of America* **109**(4), 1133–1138.

Li, D. Y., Brooke, B., Davis, E. C., Mecham, R. P., Sorensen, L. K., Boak, B. B., Eichwald, E. and Keating, M. T. (1998), 'Elastin is an essential determinant of arterial morphogenesis', *Nature* **393**(6682), 276–280.

Li, L., Madu, C. O., Lu, A. and Lu, Y. (2010), 'Hif-1α promotes a hypoxia-independent cell migration', *The open biology journal* **3**, 8.

Li, Y., Jiang, D., Liang, J., Meltzer, E. B., Gray, A., Miura, R., Wogensen, L., Yamaguchi, Y. and Noble, P. W. (2011), 'Severe lung fibrosis requires an invasive fibroblast phenotype regulated by hyaluronan and cd44', *The Journal of experimental medicine* **208**(7), 1459.

Li, Y., Li, H., Liu, S., Pan, P., Su, X., Tan, H., Wu, D., Zhang, L., Song, C., Dai, M. et al. (2018), 'Pirfenidone ameliorates lipopolysaccharide-induced pulmonary inflammation and fibrosis by blocking nlrp3 inflammasome activation', *Molecular immunology* **99**, 134–144.

Li, Y., Liang, J., Yang, T., Mena, J. M., Huan, C., Xie, T., Kurkciyan, A., Liu, N., Jiang, D. and Noble, P. W. (2016), 'Hyaluronan synthase 2 regulates fibroblast senescence in pulmonary fibrosis', *Matrix Biology* **55**, 35–48.

Li, Z., Geng, J., Xie, B., He, J., Wang, J., Peng, L., Hu, Y., Dai, H. and Wang, C. (2022), 'Dihydromyricetin alleviates pulmonary fibrosis by regulating abnormal fibroblasts through the stat3/p-stat3/glut1 signaling pathway', *Frontiers in Pharmacology* **13**, 834604.

Liang, J., Zhang, Y., Xie, T., Liu, N., Chen, H., Geng, Y., Kurkciyan, A., Mena, J. M., Stripp, B. R., Jiang, D. et al. (2016), 'Hyaluronan and tlr4 promote surfactant-protein-c-positive alveolar progenitor cell renewal and prevent severe pulmonary fibrosis in mice', *Nature medicine* **22**(11), 1285–1293.

Liberti, M. V. and Locasale, J. W. (2016), 'The warburg effect: how does it benefit cancer cells?', *Trends in biochemical sciences* **41**(3), 211–218.

Liberzon, A., Birger, C., Thorvaldsdóttir, H., Ghandi, M., Mesirov, J. P. and Tamayo, P. (2015), 'The molecular signatures database hallmark gene set collection', *Cell systems* **1**(6), 417–425.

Lim, M. J., Ahn, J., Yi, J. Y., Kim, M.-H., Son, A.-R., Lim, D.-S., Kim, S. S., Kang, M. A., Han, Y., Song, J.-Y. et al. (2014), 'Induction of galectin-1 by tgf-β1 accelerates fibrosis through enhancing nuclear retention of smad2', *Experimental cell research* **326**(1), 125–135.

Lin, S., Li, Y., Wang, D., Huang, C., Marino, D., Bollt, O., Wu, C., Taylor, M. D., Li, W., DeNicola, G. M. et al. (2021), 'Fascin promotes lung cancer growth and metastasis by enhancing glycolysis and pfkfb3 expression', *Cancer letters* **518**, 230–242.

Lipinski, J. H., Moore, B. B. and O'Dwyer, D. N. (2020), 'The evolving role of the lung microbiome in pulmonary fibrosis', *American Journal of Physiology-Lung Cellular and Molecular Physiology* **319**(4), L675–L682.

Liu, F., Lagares, D., Choi, K. M., Stopfer, L., Marinković, A., Vrbanac, V., Probst, C. K., Hiemer, S. E., Sisson, T. H., Horowitz, J. C. et al. (2015), 'Mechanosignaling through yap and taz drives fibroblast activation and fibrosis', *American Journal of Physiology-Lung Cellular and Molecular Physiology* **308**(4), L344–L357.

Liu, G., Philp, A. M., Corte, T., Travis, M. A., Schilter, H., Hansbro, N. G., Burns, C. J., Eapen, M. S., Sohal, S. S., Burgess, J. K. et al. (2021), 'Therapeutic targets in lung tissue remodelling and fibrosis', *Pharmacology & therapeutics* **225**, 107839.

Liu, G. Y., Budinger, G. S. and Dematte, J. E. (2022), 'Advances in the management of idiopathic pulmonary fibrosis and progressive pulmonary fibrosis', *Bmj* **377**.

Liu, H., Drew, P., Gaugler, A. C., Cheng, Y. and Visner, G. A. (2005), 'Pirfenidone inhibits lung allograft fibrosis through l-arginine–arginase pathway', *American Journal of Transplantation* **5**(6), 1256–1263.

Liu, J., Wang, Y., Pan, Q., Su, Y., Zhang, Z., Han, J., Zhu, X., Tang, C. and Hu, D. (2012), 'Wnt/β-catenin pathway forms a negative feedback loop during tgf-β1 induced human normal skin fibroblast-to-myofibroblast transition', *Journal of dermatological science* **65**(1), 38–49.

Liu, S., Liu, C., Wang, Q., Liu, S. and Min, J. (2023), 'Cc chemokines in idiopathic pulmonary fibrosis: pathogenic role and therapeutic potential', *Biomolecules* **13**(2), 333.

Liu, X., Dai, K., Zhang, X., Huang, G., Lynn, H., Rabata, A., Liang, J., Noble, P. W. and Jiang, D. (2023), 'Multiple fibroblast subtypes contribute to matrix deposition in pulmonary fibrosis', *American Journal of Respiratory Cell and Molecular Biology* **69**(1), 45–56.

Liu, Y., Cao, Y., Zhang, W., Bergmeier, S., Qian, Y., Akbar, H., Colvin, R., Ding, J., Tong, L., Wu, S. et al. (2012), 'A small-molecule inhibitor of glucose transporter 1 downregulates glycolysis, induces cell-cycle arrest, and inhibits cancer cell growth in vitro and in vivo', *Molecular cancer therapeutics* **11**(8), 1672–1682.

Locasale, J. W. and Cantley, L. C. (2011), 'Metabolic flux and the regulation of mammalian cell growth', *Cell metabolism* **14**(4), 443–451.

Lodyga, M. and Hinz, B. (2020), Tgf-β1–a truly transforming growth factor in fibrosis and immunity, *in* 'Seminars in cell & developmental biology', Vol. 101, Elsevier, pp. 123–139.

Loyd, J. E. (2003), 'Pulmonary fibrosis in families', *American Journal of Respiratory Cell and Molecular Biology* **29**(3), S47.

Lu, C. and Thompson, C. B. (2012), 'Metabolic regulation of epigenetics', *Cell metabolism* **16**(1), 9–17.

Lu, J., Qian, Y., Jin, W., Tian, R., Zhu, Y., Wang, J., Meng, X. and Wang, R. (2018), 'Hypoxia-inducible factor-1α regulates epithelial-to-mesenchymal transition in paraquat-induced pulmonary fibrosis by activating lysyl oxidase', *Experimental and Therapeutic Medicine* **15**(3), 2287–2294.

Lu, Y., Zhang, T., Shan, S., Wang, S., Bian, W., Ren, T. and Yang, D. (2019), 'Mir-124 regulates transforming growth factor-β1 induced differentiation of lung resident mesenchymal stem cells to myofibroblast by repressing wnt/β-catenin signaling', *Developmental biology* **449**(2), 115–121.

Lunt, S. Y. and Vander Heiden, M. G. (2011), 'Aerobic glycolysis: meeting the metabolic requirements of cell proliferation', *Annual review of cell and developmental biology* **27**(1), 441–464.

Luo, K. (2017), 'Signaling cross talk between tgf-β/smad and other signaling pathways', *Cold Spring Harbor perspectives in biology* **9**(1), a022137.

Ma, H.-Y., Li, Q., Wong, W. R., N'Diaye, E.-N., Caplazi, P., Bender, H., Huang, Z., Arlantico, A., Jeet, S., Wong, A. et al. (2023), 'Loxl4, but not loxl2, is the critical determinant of pathological collagen cross-linking and fibrosis in the lung', *Science Advances* **9**(21), eadf0133.

Ma, M., Hua, S., Li, G., Wang, S., Cheng, X., He, S., Wu, P. and Chen, X. (2017), 'Prolyl hydroxylase domain protein 3 and asparaginyl hydroxylase factor inhibiting hif-1 levels are predictive of tumoral behavior and prognosis in hepatocellular carcinoma', *Oncotarget* **8**(8), 12983.

Ma, Z., Zhao, C., Chen, Q., Yu, C., Zhang, H., Zhang, Z., Huang, W. and Shen, Z. (2018), 'Antifibrotic effects of a novel pirfenidone derivative in vitro and in vivo', *Pulmonary Pharmacology & Therapeutics* **53**, 100–106.

MacKinnon, A. C., Gibbons, M. A., Farnworth, S. L., Leffler, H., Nilsson, U. J., Delaine, T., Simpson, A. J., Forbes, S. J., Hirani, N., Gauldie, J. et al. (2012), 'Regulation of transforming growth factor-β1–driven lung fibrosis by galectin-3', *American journal of respiratory and critical care medicine* **185**(5), 537–546.

Mader, J., Huber, J., Bonn, F., Dötsch, V., Rogov, V. V. and Bremm, A. (2020), 'Oxygen-dependent asparagine hydroxylation of the ubiquitin-associated (uba) domain in cezanne regulates ubiquitin binding', *Journal of biological chemistry* **295**(8), 2160–2174.

Maher, T. M., Bendstrup, E., Dron, L., Langley, J., Smith, G., Khalid, J. M., Patel, H. and Kreuter, M. (2021), 'Global incidence and prevalence of idiopathic pulmonary fibrosis', *Respiratory research* **22**, 1–10.

Maher, T. M., Corte, T. J., Fischer, A., Kreuter, M., Lederer, D. J., Molina-Molina, M., Axmann, J., Kirchgaessler, K.-U., Samara, K., Gilberg, F. et al. (2020), 'Pirfenidone in

patients with unclassifiable progressive fibrosing interstitial lung disease: a double-blind, randomised, placebo-controlled, phase 2 trial', *The lancet Respiratory medicine* **8**(2), 147–157.

Mahon, P. C., Hirota, K. and Semenza, G. L. (2001), 'Fih-1: a novel protein that interacts with hif-1α and vhl to mediate repression of hif-1 transcriptional activity', *Genes & development* **15**(20), 2675–2686.

Makino, Y., Cao, R., Svensson, K., Bertilsson, G., Asman, M., Tanaka, H., Cao, Y., Berkenstam, A. and Poellinger, L. (2001), 'Inhibitory pas domain protein is a negative regulator of hypoxia-inducible gene expression', *Nature* **414**(6863), 550–554.

Malaisse, W. J., Zhang, Y. and Sener, A. (2004), 'Enzyme-to-enzyme channeling in the early steps of glycolysis in rat pancreatic islets', *Endocrine* **24**, 105–109.

Mandl, M. and Depping, R. (2014), 'Hypoxia-inducible aryl hydrocarbon receptor nuclear translocator (arnt)(hif-1β): is it a rare exception?', *Molecular Medicine* **20**, 215–220.

Manresa, M. C., Tambuwala, M. M., Radhakrishnan, P., Harnoss, J. M., Brown, E., Cavadas, M. A., Keogh, C. E., Cheong, A., Barrett, K. E., Cummins, E. P. et al. (2016), 'Hydroxylase inhibition regulates inflammation-induced intestinal fibrosis through the suppression of erk-mediated tgf-β1 signaling', *American Journal of Physiology-Gastrointestinal and Liver Physiology* **311**(6), G1076–G1090.

Mansfield, K. D., Guzy, R. D., Pan, Y., Young, R. M., Cash, T. P., Schumacker, P. T. and Simon, M. C. (2005), 'Mitochondrial dysfunction resulting from loss of cytochrome c impairs cellular oxygen sensing and hypoxic hif-α activation', *Cell metabolism* **1**(6), 393–399.

Margaria, J. P., Moretta, L., Alves-Filho, J. C. and Hirsch, E. (2022), 'Pi3k signaling in mechanisms and treatments of pulmonary fibrosis following sepsis and acute lung injury', *Biomedicines* **10**(4), 756.

Margaritopoulos, G. A., Trachalaki, A., Wells, A. U., Vasarmidi, E., Bibaki, E., Papastratigakis, G., Detorakis, S., Tzanakis, N. and Antoniou, K. M. (2018), 'Pirfenidone improves survival in ipf: results from a real-life study', *BMC pulmonary medicine* **18**, 1–7.

Marquardt, H., Lioubin, M. N. and Ikeda, T. (1987), 'Complete amino acid sequence of human transforming growth factor type beta 2.', *Journal of Biological Chemistry* **262**(25), 12127–12131.

Marshall, D. C., Salciccioli, J. D., Shea, B. S. and Akuthota, P. (2018), 'Trends in mortality from idiopathic pulmonary fibrosis in the european union: an observational study of the who mortality database from 2001–2013', *European Respiratory Journal* **51**(1).

Martin, M. M., Buckenberger, J. A., Jiang, J., Malana, G. E., Knoell, D. L., Feldman, D. S. and Elton, T. S. (2007), 'Tgf-β1 stimulates human at1 receptor expression in lung fibroblasts by cross talk between the smad, p38 mapk, jnk, and pi3k signaling pathways', *American Journal of Physiology-Lung Cellular and Molecular Physiology* **293**(3), L790–L799.

Martinez, F. J., Collard, H. R., Pardo, A., Raghu, G., Richeldi, L., Selman, M., Swigris, J. J., Taniguchi, H. and Wells, A. U. (2017), 'Idiopathic pulmonary fibrosis', *Nature reviews Disease primers* **3**(1), 1–19.

Martinon, F., Burns, K. and Tschopp, J. (2002), 'The inflammasome: a molecular platform triggering activation of inflammatory caspases and processing of proil-β', *Molecular cell* **10**(2), 417–426.

Marxsen, J. H., Stengel, P., Doege, K., Heikkinen, P., Jokilehto, T., Wagner, T., Jelkmann, W., Jaakkola, P. and Metzen, E. (2004), 'Hypoxia-inducible factor-1 (hif-1) promotes its degradation by induction of hif-α-prolyl-4-hydroxylases', *Biochemical Journal* **381**(3), 761–767.

Maschek, G., Savaraj, N., Priebe, W., Braunschweiger, P., Hamilton, K., Tidmarsh, G. F., De Young, L. R. and Lampidis, T. J. (2004), '2-deoxy-d-glucose increases the efficacy of adriamycin and paclitaxel in human osteosarcoma and non-small cell lung cancers in vivo', *Cancer research* **64**(1), 31–34.

Massagué, J. and Sheppard, D. (2023), 'Tgf-β signaling in health and disease', *Cell* **186**(19), 4007–4037.

Masson, N., Singleton, R. S., Sekirnik, R., Trudgian, D. C., Ambrose, L. J., Miranda, M. X., Tian, Y.-M., Kessler, B. M., Schofield, C. J. and Ratcliffe, P. J. (2012), 'The fih hydroxylase is a cellular peroxide sensor that modulates hif transcriptional activity', *EMBO reports* **13**(3), 251–257.

Maxwell, P. H., Wiesener, M. S., Chang, G.-W., Clifford, S. C., Vaux, E. C., Cockman, M. E., Wykoff, C. C., Pugh, C. W., Maher, E. R. and Ratcliffe, P. J. (1999), 'The tumour suppressor protein vhl targets hypoxia-inducible factors for oxygen-dependent proteolysis', *Nature* **399**(6733), 271–275.

McDonough, M. A., McNeill, L. A., Tilliet, M., Papamicaël, C. A., Chen, Q.-Y., Banerji, B., Hewitson, K. S. and Schofield, C. J. (2005), 'Selective inhibition of factor inhibiting hypoxia-inducible factor', *Journal of the American Chemical Society* **127**(21), 7680–7681.

Mendoza, F. A. and Jimenez, S. A. (2022), 'Serine/threonine kinase inhibition as antifibrotic therapy: transforming growth factor-β and rho kinase inhibitors', *Rheumatology* **61**(4), 1354–1365.

Mi, S., Li, Z., Yang, H.-Z., Liu, H., Wang, J.-P., Ma, Y.-G., Wang, X.-X., Liu, H.-Z., Sun, W. and Hu, Z.-W. (2011), 'Blocking il-17a promotes the resolution of pulmonary inflammation and fibrosis via tgf-β1–dependent and–independent mechanisms', *The Journal of Immunology* **187**(6), 3003–3014.

Miao, Y., Geng, Y., Yang, L., Zheng, Y., Dai, Y. and Wei, Z. (2022), 'Morin inhibits the transformation of fibroblasts towards myofibroblasts through regulating "ppar-γ-glutaminolysis-deptor" pathway in pulmonary fibrosis', *The Journal of Nutritional Biochemistry* **101**, 108923.

Miyake, Y., Sasaki, S., Yokoyama, T., Chida, K., Azuma, A., Suda, T., Kudoh, S., Sakamoto, N., Okamoto, K., Kobashi, G. et al. (2005), 'Occupational and environmental factors and idiopathic pulmonary fibrosis in japan', *Annals of occupational hygiene* **49**(3), 259–265.

Molina-Molina, M., Machahua-Huamani, C., Vicens-Zygmunt, V., Llatjós, R., Escobar, I., Sala-Llinas, E., Luburich-Hernaiz, P., Dorca, J. and Montes-Worboys, A. (2018), 'Anti-fibrotic effects of pirfenidone and rapamycin in primary ipf fibroblasts and human alveolar epithelial cells', *BMC pulmonary medicine* **18**, 1–13.

Mondoni, M. et al. (2024), 'Vascular involvement in idiopathic pulmonary fibrosis: mechanisms and therapeutic perspectives', *ERJ Open Research* **10**(1), 00550–2024.

Moon, S. W., Kim, S. Y., Chung, M. P., Yoo, H., Jeong, S. H., Kim, D. S., Song, J. W., Lee, H. L., Choi, S. M., Kim, Y. W. et al. (2021), 'Longitudinal changes in clinical features, management, and outcomes of idiopathic pulmonary fibrosis. a nationwide cohort study', *Annals of the American Thoracic Society* **18**(5), 780–787.

Moore, B. B., Fry, C., Zhou, Y., Murray, S., Han, M. K., Martinez, F. J., Flaherty, K. R. and Investigators, C. (2014), 'Inflammatory leukocyte phenotypes correlate with disease progression in idiopathic pulmonary fibrosis', *Frontiers in Medicine* **1**, 56.

Moore, B. B. and Moore, T. A. (2015), 'Viruses in idiopathic pulmonary fibrosis. etiology and exacerbation', *Annals of the American Thoracic Society* **12**(Supplement 2), S186–S192.

Moss, B. J., Ryter, S. W. and Rosas, I. O. (2022), 'Pathogenic mechanisms underlying idiopathic pulmonary fibrosis', *Annual Review of Pathology: Mechanisms of Disease* **17**(1), 515–546.

Mukherjee, D., Bercz, L. S., Torok, M. A. and Mace, T. A. (2020), 'Regulation of cellular immunity by activating transcription factor 4', *Immunology letters* **228**, 24–34.

Munger, J. S., Huang, X., Kawakatsu, H., Griffiths, M. J., Dalton, S. L., Wu, J., Pittet, J.-F., Kaminski, N., Garat, C., Matthay, M. A. et al. (1999), 'A mechanism for regulating pulmonary inflammation and fibrosis: the integrin $\alpha v\beta 6$ binds and activates latent tgf β1', *Cell* **96**(3), 319–328.

Murray, L. A., Habiel, D. M., Hohmann, M., Camelo, A., Shang, H., Zhou, Y., Coelho, A. L., Peng, X., Gulati, M., Crestani, B. et al. (2017), 'Antifibrotic role of vascular endothelial growth factor in pulmonary fibrosis', *JCI insight* **2**(16).

Mutsaers, S. E., Bishop, J. E., McGrouther, G. and Laurent, G. J. (1997), 'Mechanisms of tissue repair: from wound healing to fibrosis', *The international journal of biochemistry & cell biology* **29**(1), 5–17.

Nacarelli, T., Lau, L., Fukumoto, T., Zundell, J., Fatkhutdinov, N., Wu, S., Aird, K. M., Iwasaki, O., Kossenkov, A. V., Schultz, D. et al. (2019), 'Nad+ metabolism governs the proinflammatory senescence-associated secretome', *Nature cell biology* **21**(3), 397–407.

Nakayama, S., Mukae, H., Sakamoto, N., Kakugawa, T., Yoshioka, S., Soda, H., Oku, H., Urata, Y., Kondo, T., Kubota, H. et al. (2008), 'Pirfenidone inhibits the expression of hsp47 in tgf-β1-stimulated human lung fibroblasts', *Life sciences* **82**(3-4), 210–217.

Nataraj, D., Ernst, A. and Kalluri, R. (2010), 'Idiopathic pulmonary fibrosis is associated with endothelial to mesenchymal transition'.

Natsuizaka, M., Chiba, H., Kuronuma, K., Otsuka, M., Kudo, K., Mori, M., Bando, M., Sugiyama, Y. and Takahashi, H. (2014), 'Epidemiologic survey of japanese patients with idiopathic pulmonary fibrosis and investigation of ethnic differences', *American journal of respiratory and critical care medicine* **190**(7), 773–779.

Navaratnam, V. and Hubbard, R. B. (2019), 'The mortality burden of idiopathic pulmonary fibrosis in the united kingdom', *American journal of respiratory and critical care medicine* **200**(2), 256–258.

Nigdelioglu, R., Hamanaka, R. B., Meliton, A. Y., O'Leary, E., Witt, L. J., Cho, T., Sun, K., Bonham, C., Wu, D., Woods, P. S. et al. (2016), 'Transforming growth factor (tgf)-β promotes de novo serine synthesis for collagen production', *Journal of Biological Chemistry* **291**(53), 27239–27251.

Noble, P. W., Albera, C., Bradford, W. Z., Costabel, U., Glassberg, M. K., Kardatzke, D., King, T. E., Lancaster, L., Sahn, S. A., Szwarcberg, J. et al. (2011), 'Pirfenidone in patients with idiopathic pulmonary fibrosis (capacity): two randomised trials', *The Lancet* **377**(9779), 1760–1769.

Noguchi, S., Saito, A., Mikami, Y., Urushiyama, H., Horie, M., Matsuzaki, H., Takeshima, H., Makita, K., Miyashita, N., Mitani, A. et al. (2017), 'Taz contributes to pulmonary fibrosis by activating profibrotic functions of lung fibroblasts', *Scientific reports* **7**(1), 42595.

Noth, I., Zhang, Y., Ma, S.-F., Flores, C., Barber, M., Huang, Y., Broderick, S. M., Wade, M. S., Hysi, P., Scuirba, J. et al. (2013), 'Genetic variants associated with idiopathic pulmonary fibrosis susceptibility and mortality: a genome-wide association study', *The Lancet respiratory medicine* **1**(4), 309–317.

Obeidat, M., Dvorkin-Gheva, A., Li, X., Bossé, Y., Brandsma, C.-A., Nickle, D. C., Hansbro, P. M., Faner, R., Agusti, A., Paré, P. D. et al. (2018), 'The overlap of lung tissue transcriptome of smoke exposed mice with human smoking and copd', *Scientific reports* **8**(1), 11881.

Ohh, M., Park, C. W., Ivan, M., Hoffman, M. A., Kim, T.-Y., Huang, L. E., Pavletich, N., Chau, V. and Kaelin, W. G. (2000), 'Ubiquitination of hypoxia-inducible factor requires direct binding to the β-domain of the von hippel–lindau protein', *Nature cell biology* **2**(7), 423–427.

Oku, H., Shimizu, T., Kawabata, T., Nagira, M., Hikita, I., Ueyama, A., Matsushima, S., Torii, M. and Arimura, A. (2008), 'Antifibrotic action of pirfenidone and prednisolone: different effects on pulmonary cytokines and growth factors in bleomycin-induced murine pulmonary fibrosis', *European journal of pharmacology* **590**(1-3), 400–408.

Olajuyin, A. M., Zhang, X. and Ji, H.-L. (2019), 'Alveolar type 2 progenitor cells for lung injury repair', *Cell death discovery* **5**(1), 63.

Olson, A. L., Swigris, J. J., Lezotte, D. C., Norris, J. M., Wilson, C. G. and Brown, K. K. (2007), 'Mortality from pulmonary fibrosis increased in the united states from 1992 to 2003', *American journal of respiratory and critical care medicine* **176**(3), 277–284.

O'Dwyer, D. N. and Garantziotis, S. (2021), 'The lung microbiome in health, hypersensitivity pneumonitis, and idiopathic pulmonary fibrosis: a heavy bacterial burden to bear'.

Pacold, M. E., Brimacombe, K. R., Chan, S. H., Rohde, J. M., Lewis, C. A., Swier, L. J., Possemato, R., Chen, W. W., Sullivan, L. B., Fiske, B. P. et al. (2016), 'A phgdh inhibitor reveals coordination of serine synthesis and one-carbon unit fate', *Nature chemical biology* **12**(6), 452–458.

Pan, L., Yamauchi, K., Uzuki, M., Nakanishi, T., Takigawa, M., Inoue, H. and Sawai, T. (2001), 'Type ii alveolar epithelial cells and interstitial fibroblasts express connective tissue growth factor in ipf', *European Respiratory Journal* **17**(6), 1220–1227.

Pannu, J., Nakerakanti, S., Smith, E., ten Dijke, P. and Trojanowska, M. (2007), 'Transforming growth factor-β receptor type i-dependent fibrogenic gene program is mediated via activation of smad1 and erk1/2 pathways', *Journal of Biological Chemistry* **282**(14), 10405–10413.

Parimon, T., Yao, C., Stripp, B. R., Noble, P. W. and Chen, P. (2020), 'Alveolar epithelial type ii cells as drivers of lung fibrosis in idiopathic pulmonary fibrosis', *International journal of molecular sciences* **21**(7), 2269.

Pelletier, J., Dayan, F., Durivault, J., Ilc, K., Pecou, E., Pouyssegur, J. and Mazure, N. (2012), 'The asparaginyl hydroxylase factor-inhibiting hif is essential for tumor growth through suppression of the p53–p21 axis', *Oncogene* **31**(24), 2989–3001.

Pérez, E. R. F., Daniels, C. E., Sauver, J. S., Hartman, T. E., Bartholmai, B. J., Eunhee, S. Y., Ryu, J. H. and Schroeder, D. R. (2010), 'Incidence, prevalence, and clinical course of idiopathic pulmonary fibrosis: a population-based study', *Chest* **137**(1), 129–137.

Phan, S. H. (2002), 'The myofibroblast in pulmonary fibrosis', *Chest* **122**(6), 286S–289S.

Phan, T. H. G., Paliogiannis, P., Nasrallah, G. K., Giordo, R., Eid, A. H., Fois, A. G., Zinellu, A., Mangoni, A. A. and Pintus, G. (2021), 'Emerging cellular and molecular determinants of idiopathic pulmonary fibrosis', *Cellular and Molecular Life Sciences* **78**, 2031–2057.

Philip, K., Mills, T. W., Davies, J., Chen, N.-Y., Karmouty-Quintana, H., Luo, F., Molina, J. G., Amione-Guerra, J., Sinha, N., Guha, A. et al. (2017), 'Hif1a up-regulates the adora2b receptor on alternatively activated macrophages and contributes to pulmonary fibrosis', *The FASEB Journal* **31**(11), 4745.

Pickel, C., Günter, J., Ruiz-Serrano, A., Spielmann, P., Fabrizio, J.-A., Wolski, W., Peet, D. J., Wenger, R. H. and Scholz, C. C. (2019), 'Oxygen-dependent bond formation with fih regulates the activity of the client protein otub1', *Redox biology* **26**, 101265.

Plikus, M. V., Wang, X., Sinha, S., Forte, E., Thompson, S. M., Herzog, E. L., Driskell, R. R., Rosenthal, N., Biernaskie, J. and Horsley, V. (2021), 'Fibroblasts: Origins, definitions, and functions in health and disease', *Cell* **184**(15), 3852–3872.

Podolanczuk, A. J., Thomson, C. C., Remy-Jardin, M., Richeldi, L., Martinez, F. J., Kolb, M. and Raghu, G. (2023), 'Idiopathic pulmonary fibrosis: state of the art for 2023', *European Respiratory Journal* **61**(4).

Pollak, J., Mayonu, M., Jiang, L. and Wang, B. (2024), 'The development of machine learning approaches in two-dimensional nmr data interpretation for metabolomics applications', *Analytical Biochemistry* p. 115654.

Possemato, R., Marks, K. M., Shaul, Y. D., Pacold, M. E., Kim, D., Birsoy, K., Sethumadhavan, S., Woo, H.-K., Jang, H. G., Jha, A. K. et al. (2011), 'Functional genomics reveal that the serine synthesis pathway is essential in breast cancer', *Nature* **476**(7360), 346–350.

Pourgholamhossein, F., Rasooli, R., Pournamdari, M., Pourgholi, L., Samareh-Fekri, M., Ghazi-Khansari, M., Iranpour, M., Poursalehi, H.-R., Heidari, M.-R. and Mandegary, A. (2018), 'Pirfenidone protects against paraquat-induced lung injury and fibrosis in mice by modulation of inflammation, oxidative stress, and gene expression', *Food and chemical toxicology* **112**, 39–46.

Prata, L. O., Rodrigues, C. R., Martins, J. M., Vasconcelos, P. C., Oliveira, F. M. S., Ferreira, A. J., Rodrigues-Machado, M. d. G. and Caliari, M. V. (2017), 'Ace2 activator associated with physical exercise potentiates the reduction of pulmonary fibrosis', *Experimental Biology and Medicine* **242**(1), 8–21.

Qin, W., Liu, B., Yi, M., Li, L., Tang, Y., Wu, B. and Yuan, X. (2018), 'Antifibrotic agent pirfenidone protects against development of radiation-induced pulmonary fibrosis in a murine model', *Radiation research* **190**(4), 396–403.

Quijano, C., Cao, L., Fergusson, M. M., Romero, H., Liu, J., Gutkind, S., Rovira, I. I., Mohney, R. P., Karoly, E. D. and Finkel, T. (2012), 'Oncogene-induced senescence results in marked metabolic and bioenergetic alterations', *Cell Cycle* **11**(7), 1383–1392.

R Lapthorn, A., L Harding, S., M Feltham, K., Sathyananth, D., C Salisbury, D. and Cellek, S. (2024), 'A review of the current landscape of anti-fibrotic medicines'.

Rabinowitz, M. H. (2013), 'Inhibition of hypoxia-inducible factor prolyl hydroxylase domain oxygen sensors: tricking the body into mounting orchestrated survival and repair responses', *Journal of medicinal chemistry* **56**(23), 9369–9402.

Raghu, G., Chen, S.-Y., Yeh, W.-S., Maroni, B., Li, Q., Lee, Y.-C. and Collard, H. R. (2014), 'Idiopathic pulmonary fibrosis in us medicare beneficiaries aged 65 years and older: incidence, prevalence, and survival, 2001–11', *The lancet Respiratory medicine* **2**(7), 566–572.

Raghu, G., Collard, H. R., Egan, J. J., Martinez, F. J., Behr, J., Brown, K. K., Colby, T. V., Cordier, J.-F., Flaherty, K. R., Lasky, J. A. et al. (2011), 'An official ats/ers/jrs/alat statement: idiopathic pulmonary fibrosis: evidence-based guidelines for diagnosis and management', *American journal of respiratory and critical care medicine* **183**(6), 788–824.

Raghu, G., Remy-Jardin, M., Myers, J. L., Richeldi, L., Ryerson, C. J., Lederer, D. J., Behr, J., Cottin, V., Danoff, S. K., Morell, F. et al. (2018), 'Diagnosis of idiopathic pulmonary fibrosis. an official ats/ers/jrs/alat clinical practice guideline', *American journal of respiratory and critical care medicine* **198**(5), e44–e68.

Raghu, G., Remy-Jardin, M., Richeldi, L., Thomson, C. C., Inoue, Y., Johkoh, T., Kreuter, M., Lynch, D. A., Maher, T. M., Martinez, F. J. et al. (2022), 'Idiopathic pulmonary fibrosis (an update) and progressive pulmonary fibrosis in adults: an official ats/ers/jrs/alat clinical practice guideline', *American Journal of Respiratory and Critical Care Medicine* **205**(9), e18–e47.

Raghu, G., Weycker, D., Edelsberg, J., Bradford, W. Z. and Oster, G. (2006), 'Incidence and prevalence of idiopathic pulmonary fibrosis', *American journal of respiratory and critical care medicine* **174**(7), 810–816.

Raheja, L. F., Genetos, D. C., Wong, A. and Yellowley, C. E. (2011), 'Hypoxic regulation of mesenchymal stem cell migration: the role of rhoa and hif-1α', *Cell biology international* **35**(10), 981–989.

Raimundo, K., Chang, E., Broder, M. S., Alexander, K., Zazzali, J. and Swigris, J. J. (2016), 'Clinical and economic burden of idiopathic pulmonary fibrosis: a retrospective cohort study', *BMC pulmonary medicine* **16**, 1–8.

Ramirez, A., Ballard, E. N. and Roman, J. (2012), 'Tgfβ1 controls pparγ expression, transcriptional potential, and activity, in part, through smad3 signaling in murine lung fibroblasts', *PPAR research* **2012**(1), 375876.

Ran, F., Hsu, P. D., Wright, J., Agarwala, V., Scott, D. A. and Zhang, F. (2013), 'Genome engineering using the crispr-cas9 system', *Nature protocols* **8**(11), 2281–2308.

Rangarajan, S., Bone, N. B., Zmijewska, A. A., Jiang, S., Park, D. W., Bernard, K., Locy, M. L., Ravi, S., Deshane, J., Mannon, R. B. et al. (2018), 'Metformin reverses established lung fibrosis in a bleomycin model', *Nature medicine* **24**(8), 1121–1127.

Rangarajan, S., Kurundkar, A., Kurundkar, D., Bernard, K., Sanders, Y. Y., Ding, Q., Antony, V. B., Zhang, J., Zmijewski, J. and Thannickal, V. J. (2016), 'Novel mechanisms for the antifibrotic action of nintedanib', *American journal of respiratory cell and molecular biology* **54**(1), 51–59.

Rangel-Moreno, J., Hartson, L., Navarro, C., Gaxiola, M., Selman, M., Randall, T. D. et al. (2006), 'Inducible bronchus-associated lymphoid tissue (ibalt) in patients with pulmonary complications of rheumatoid arthritis', *The Journal of clinical investigation* **116**(12), 3183–3194.

Rankin, E. á. and Giaccia, A. (2008), 'The role of hypoxia-inducible factors in tumorigenesis', *Cell Death & Differentiation* **15**(4), 678–685.

Richeldi, L., Azuma, A., Cottin, V., Hesslinger, C., Stowasser, S., Valenzuela, C., Wijsenbeek, M. S., Zoz, D. F., Voss, F. and Maher, T. M. (2022), 'Trial of a preferential phosphodiesterase 4b inhibitor for idiopathic pulmonary fibrosis', *New England Journal of Medicine* **386**(23), 2178–2187.

Richeldi, L., Collard, H. R. and Jones, M. G. (2017), 'Idiopathic pulmonary fibrosis', *The Lancet* **389**(10082), 1941–1952.

Richeldi, L., Du Bois, R. M., Raghu, G., Azuma, A., Brown, K. K., Costabel, U., Cottin, V., Flaherty, K. R., Hansell, D. M., Inoue, Y. et al. (2014), 'Efficacy and safety of nintedanib in idiopathic pulmonary fibrosis', *New England Journal of Medicine* **370**(22), 2071–2082.

Riddle, S. R., Ahmad, A., Ahmad, S., Deeb, S. S., Malkki, M., Schneider, B. K., Allen, C. B. and White, C. W. (2000), 'Hypoxia induces hexokinase ii gene expression in

human lung cell line a549', *American Journal of Physiology-Lung Cellular and Molecular Physiology* **278**(2), L407–L416.

Rifkin, D. B., Rifkin, W. J. and Zilberberg, L. (2018), 'Ltbps in biology and medicine: Ltbp diseases', *Matrix Biology* **71**, 90–99.

Roberts, A. B., Anzano, M. A., Lamb, L. C., Smith, J. M. and Sporn, M. B. (1981), 'New class of transforming growth factors potentiated by epidermal growth factor: isolation from non-neoplastic tissues.', *Proceedings of the National Academy of Sciences* **78**(9), 5339–5343.

Rock, J. R., Barkauskas, C. E., Cronce, M. J., Xue, Y., Harris, J. R., Liang, J., Noble, P. W. and Hogan, B. L. (2011), 'Multiple stromal populations contribute to pulmonary fibrosis without evidence for epithelial to mesenchymal transition', *Proceedings of the National Academy of Sciences* **108**(52), E1475–E1483.

Rouhani, F. N., Brantly, M. L., Markello, T. C., Helip-Wooley, A., O'Brien, K., Hess, R., Huizing, M., Gahl, W. A. and Gochuico, B. R. (2009), 'Alveolar macrophage dysregulation in hermansky-pudlak syndrome type 1', *American journal of respiratory and critical care medicine* **180**(11), 1114–1121.

Rout-Pitt, N., Farrow, N., Parsons, D. and Donnelley, M. (2018), 'Epithelial mesenchymal transition (emt): a universal process in lung diseases with implications for cystic fibrosis pathophysiology', *Respiratory research* **19**, 1–10.

Ruterbusch, M., Pruner, K. B., Shehata, L. and Pepper, M. (2020), 'In vivo cd4+ t cell differentiation and function: revisiting the th1/th2 paradigm', *Annual review of immunology* **38**(1), 705–725.

Ruwanpura, S. M., Thomas, B. J. and Bardin, P. G. (2020), 'Pirfenidone: molecular mechanisms and potential clinical applications in lung disease', *American journal of respiratory cell and molecular biology* **62**(4), 413–422.

Ryan, D. G. and O'Neill, L. A. (2020), 'Krebs cycle reborn in macrophage immunometabolism', *Annual review of immunology* **38**(1), 289–313.

Sack, C. and Raghu, G. (2019), 'Idiopathic pulmonary fibrosis: unmasking cryptogenic environmental factors', *European Respiratory Journal* **53**(2).

Sadeghi, F., Kardar, G. A., Bolouri, M. R., Nasri, F., Sadri, M. and Falak, R. (2020), 'Overexpression of bhlh domain of hif-1 failed to inhibit the hif-1 transcriptional activity in hypoxia', *Biological Research* **53**, 1–11.

Saito, M. and Marumo, K. (2010), 'Collagen cross-links as a determinant of bone quality: a possible explanation for bone fragility in aging, osteoporosis, and diabetes mellitus', *Osteoporosis international* **21**, 195–214.

Sakai, N., Chun, J., Duffield, J. S., Lagares, D., Wada, T., Luster, A. D. and Tager, A. M. (2017), 'Lysophosphatidic acid signaling through its receptor initiates profibrotic epithelial cell fibroblast communication mediated by epithelial cell derived connective tissue growth factor', *Kidney international* **91**(3), 628–641.

Sakai, T., Larsen, M. and Yamada, K. M. (2003), 'Fibronectin requirement in branching morphogenesis', *Nature* **423**(6942), 876–881.

Sakamoto, T., Niiya, D. and Seiki, M. (2011), 'Targeting the warburg effect that arises in tumor cells expressing membrane type-1 matrix metalloproteinase', *Journal of Biological Chemistry* **286**(16), 14691–14704.

Sakamoto, T. and Seiki, M. (2009), 'Mint3 enhances the activity of hypoxia-inducible factor-1 (hif-1) in macrophages by suppressing the activity of factor inhibiting hif-1', *Journal of Biological Chemistry* **284**(44), 30350–30359.

Salton, F., Volpe, M. C. and Confalonieri, M. (2019), 'Epithelial–mesenchymal transition in the pathogenesis of idiopathic pulmonary fibrosis', *Medicina* **55**(4), 83.

Sang, N., Stiehl, D. P., Bohensky, J., Leshchinsky, I., Srinivas, V. and Caro, J. (2003), 'Mapk signaling up-regulates the activity of hypoxia-inducible factors by its effects on p300', *Journal of Biological chemistry* **278**(16), 14013–14019.

Saward, B. G., Leissing, T. M., Clifton, I. J., Tumber, A., Timperley, C. M., Hopkinson, R. J. and Schofield, C. J. (2023), 'Biochemical and structural insights into fih-catalysed hydroxylation of transient receptor potential ankyrin repeat domains', *ChemBioChem* **24**(4), e202200576.

Schafer, M. J., White, T. A., Iijima, K., Haak, A. J., Ligresti, G., Atkinson, E. J., Oberg, A. L., Birch, J., Salmonowicz, H., Zhu, Y. et al. (2017), 'Cellular senescence mediates fibrotic pulmonary disease', *Nature communications* **8**(1), 14532.

Scheuermann, T. H., Yang, J., Zhang, L., Gardner, K. H. and Bruick, R. K. (2007), 'Hypoxia-inducible factors per/arnt/sim domains: structure and function', *Methods in enzymology* **435**, 1–24.

Schofield, C. J. and Ratcliffe, P. J. (2004), 'Oxygen sensing by hif hydroxylases', *Nature reviews Molecular cell biology* **5**(5), 343–354.

Scholz, C. C., Cavadas, M. A., Tambuwala, M. M., Hams, E., Rodríguez, J., Kriegsheim, A. v., Cotter, P., Bruning, U., Fallon, P. G., Cheong, A. et al. (2013), 'Regulation of il-1β–induced nf-κb by hydroxylases links key hypoxic and inflammatory signaling pathways', *Proceedings of the National Academy of Sciences* **110**(46), 18490–18495.

Scholz, C. C., Rodriguez, J., Pickel, C., Burr, S., Fabrizio, J.-a., Nolan, K. A., Spielmann, P., Cavadas, M. A., Crifo, B., Halligan, D. N. et al. (2016), 'Fih regulates cellular metabolism through hydroxylation of the deubiquitinase otub1', *PLoS biology* **14**(1), e1002347.

Seibold, M. A., Wise, A. L., Speer, M. C., Steele, M. P., Brown, K. K., Loyd, J. E., Fingerlin, T. E., Zhang, W., Gudmundsson, G., Groshong, S. D. et al. (2011), 'A common muc5b promoter polymorphism and pulmonary fibrosis', *New England Journal of Medicine* **364**(16), 1503–1512.

Selak, M. A., Armour, S. M., MacKenzie, E. D., Boulahbel, H., Watson, D. G., Mansfield, K. D., Pan, Y., Simon, M. C., Thompson, C. B. and Gottlieb, E. (2005), 'Succinate links tca cycle dysfunction to oncogenesis by inhibiting hif-α prolyl hydroxylase', *Cancer Cell* **7**(1), 77–85.

Selvarajah, B., Azuelos, I., Platé, M., Guillotin, D., Forty, E. J., Contento, G., Woodcock, H. V., Redding, M., Taylor, A., Brunori, G. et al. (2019), 'mtorc1 amplifies the atf4-dependent de novo serine-glycine pathway to supply glycine during tgf-β1–induced collagen biosynthesis', *Science signaling* **12**(582), eaav3048.

Semenza, G. L. (2000), 'Hif-1 and human disease: one highly involved factor', *Genes & development* **14**(16), 1983–1991.

Semenza, G. L. (2012), 'Hypoxia-inducible factors in physiology and medicine', *Cell* **148**(3), 399–408.

Semenza, G. L. (2013), 'Hif-1 mediates metabolic responses to intratumoral hypoxia and oncogenic mutations', *The Journal of Clinical Investigation* **123**(9), 3664–3671.

Serkova, N. J. and Niemann, C. U. (2006), 'Pattern recognition and biomarker validation using quantitative 1h-nmr-based metabolomics', *Expert review of molecular diagnostics* **6**(5), 717–731.

Shao, X., Gomez, C. D., Kapoor, N., Considine, J. M., Grams, C., Gao, Y. and Naba, A. (2023), 'Matrisomedb 2.0: 2023 updates to the ecm-protein knowledge database', *Nucleic acids research* **51**(D1), D1519–D1530.

Sharif, R. (2017), 'Overview of idiopathic pulmonary fibrosis (ipf) and evidence-based guidelines', *Am J Manag Care* **23**(11 Suppl), S176–82.

Sheng, G., Chen, P., Wei, Y., Yue, H., Chu, J., Zhao, J., Wang, Y., Zhang, W. and Zhang, H.-L. (2020), 'Viral infection increases the risk of idiopathic pulmonary fibrosis: a meta-analysis', *Chest* **157**(5), 1175–1187.

Shestov, A. A., Liu, X., Ser, Z., Cluntun, A. A., Hung, Y. P., Huang, L., Kim, D., Le, A., Yellen, G., Albeck, J. G. et al. (2014), 'Quantitative determinants of aerobic glycolysis identify flux through the enzyme gapdh as a limiting step', *elife* **3**, e03342.

Shi, H.-s., Li, D., Zhang, J., Wang, Y.-s., Yang, L., Zhang, H.-l., Wang, X.-h., Mu, B., Wang, W., Ma, Y. et al. (2010), 'Silencing of pkm2 increases the efficacy of docetaxel in human lung cancer xenografts in mice', *Cancer science* **101**(6), 1447–1453.

Shi, L., Dong, N., Fang, X. and Wang, X. (2016), 'Regulatory mechanisms of tgf-β1-induced fibrogenesis of human alveolar epithelial cells', *Journal of cellular and molecular medicine* **20**(11), 2183–2193.

Shi-Wen, X., Rodriguez-Pascual, F., Lamas, S., Holmes, A., Howat, S., Pearson, J. D., Dashwood, M. R., du Bois, R. M., Denton, C. P., Black, C. M. et al. (2006), 'Constitutive alk5-independent c-jun n-terminal kinase activation contributes to endothelin-1 overexpression in pulmonary fibrosis: evidence of an autocrine endothelin loop operating through the endothelin a and b receptors', *Molecular and cellular biology* **26**(14), 5518–5527.

Sigoillot, F. D. and King, R. W. (2011), 'Vigilance and validation: Keys to success in rnai screening', *ACS chemical biology* **6**(1), 47–60.

Sim, J., Cowburn, A. S., Palazon, A., Madhu, B., Tyrakis, P. A., Macías, D., Bargiela, D. M., Pietsch, S., Gralla, M., Evans, C. E. et al. (2018), 'The factor inhibiting hif asparaginyl hydroxylase regulates oxidative metabolism and accelerates metabolic adaptation to hypoxia', *Cell metabolism* **27**(4), 898–913.

Song, M. J., Kim, S. Y., Park, M. S., Kang, M. J., Lee, S. H. and Park, S. C. (2021), 'A nationwide population-based study of incidence and mortality of lung cancer in idiopathic pulmonary fibrosis', *Scientific Reports* **11**(1), 2596.

Speicher, T., Siegenthaler, B., Bogorad, R. L., Ruppert, R., Petzold, T., Padrissa-Altes, S., Bachofner, M., Anderson, D. G., Koteliansky, V., Fässler, R. et al. (2014), 'Knockdown and knockout of β1-integrin in hepatocytes impairs liver regeneration through inhibition of growth factor signalling', *Nature communications* **5**(1), 3862.

Spruit, M. A., Singh, S. J., Garvey, C., ZuWallack, R., Nici, L., Rochester, C., Hill, K., Holland, A. E., Lareau, S. C., Man, W. D.-C. et al. (2013), 'An official american thoracic society/european respiratory society statement: key concepts and advances in pulmonary rehabilitation', *American journal of respiratory and critical care medicine* **188**(8), e13–e64.

Stiehl, D. P., Wirthner, R., Koditz, J., Spielmann, P., Camenisch, G. and Wenger, R. H. (2006), 'Increased prolyl 4-hydroxylase domain proteins compensate for decreased oxygen levels: evidence for an autoregulatory oxygen-sensing system', *Journal of Biological Chemistry* **281**(33), 23482–23491.

Strongman, H., Kausar, I. and Maher, T. M. (2018), 'Incidence, prevalence, and survival of patients with idiopathic pulmonary fibrosis in the uk', *Advances in therapy* **35**, 724–736.

Strowitzki, M. J., Ritter, A. S., Kimmer, G. and Schneider, M. (2019), 'Hypoxia-adaptive pathways: A pharmacological target in fibrotic disease?', *Pharmacological Research* **147**, 104364.

Strunz, M., Simon, L. M., Ansari, M., Kathiriya, J. J., Angelidis, I., Mayr, C. H., Tsidiridis, G., Lange, M., Mattner, L. F., Yee, M. et al. (2020), 'Alveolar regeneration through a krt8+ transitional stem cell state that persists in human lung fibrosis', *Nature communications* **11**(1), 3559.

Stuart, B. D., Choi, J., Zaidi, S., Xing, C., Holohan, B., Chen, R., Choi, M., Dharwadkar, P., Torres, F., Girod, C. E. et al. (2015), 'Exome sequencing links mutations in parn and rtel1 with familial pulmonary fibrosis and telomere shortening', *Nature genetics* **47**(5), 512–517.

Summer, R., Shaghaghi, H., Schriner, D., Roque, W., Sales, D., Cuevas-Mora, K., Desai, V., Bhushan, A., Ramirez, M. I. and Romero, F. (2019), 'Activation of the mtorc1/pgc-1 axis promotes mitochondrial biogenesis and induces cellular senescence in the lung epithelium', *American Journal of Physiology-Lung Cellular and Molecular Physiology* **316**(6), L1049–L1060.

Sun, N., Fernandez, I. E., Wei, M., Witting, M., Aichler, M., Feuchtinger, A., Burgstaller, G., Verleden, S. E., Schmitt-Kopplin, P., Eickelberg, O. et al. (2018), 'Pharmacometabolic response to pirfenidone in pulmonary fibrosis detected by maldi-fticr-msi', *European Respiratory Journal* **52**(3).

Sun, Z., Costell, M. and Fässler, R. (2019), 'Integrin activation by talin, kindlin and mechanical forces', *Nature cell biology* **21**(1), 25–31.

Takezaki, A., Tsukumo, S.-i., Setoguchi, Y., Ledford, J. G., Goto, H., Hosomichi, K., Uehara, H., Nishioka, Y. and Yasutomo, K. (2019), 'A homozygous sftpa1 mutation drives necroptosis of type ii alveolar epithelial cells in patients with idiopathic pulmonary fibrosis', *The Journal of experimental medicine* **216**(12), 2724.

Talks, K. L., Turley, H., Gatter, K. C., Maxwell, P. H., Pugh, C. W., Ratcliffe, P. J. and Harris, A. L. (2000), 'The expression and distribution of the hypoxia-inducible factors hif-1α and hif-2α in normal human tissues, cancers, and tumor-associated macrophages', *The American Journal of Pathology* **157**(2), 411–421.

Tang, Y.-W., Johnson, J. E., Browning, P. J., Cruz-Gervis, R. A., Davis, A., Graham, B. S., Brigham, K. L., Oates Jr, J. A., Loyd, J. E. and Stecenko, A. A. (2003), 'Herpesvirus dna is consistently detected in lungs of patients with idiopathic pulmonary fibrosis', *Journal of clinical microbiology* **41**(6), 2633–2640.

Tanjore, H., Xu, X. C., Polosukhin, V. V., Degryse, A. L., Li, B., Han, W., Sherrill, T. P., Plieth, D., Neilson, E. G., Blackwell, T. S. et al. (2009), 'Contribution of epithelial-derived fibroblasts to bleomycin-induced lung fibrosis', *American journal of respiratory and critical care medicine* **180**(7), 657–665.

Tarride, J.-E., Hopkins, R. B., Burke, N., Guertin, J. R., O'Reilly, D., Fell, C. D., Dion, G. and Kolb, M. (2018), 'Clinical and economic burden of idiopathic pulmonary fibrosis in quebec, canada', *ClinicoEconomics and Outcomes Research* pp. 127–137.

Thabut, G., Christie, J. D., Ravaud, P., Castier, Y., Dauriat, G., Jebrak, G., Fournier, M., Lesèche, G., Porcher, R. and Mal, H. (2009), 'Survival after bilateral versus single-lung transplantation for idiopathic pulmonary fibrosis', *Annals of internal medicine* **151**(11), 767–774.

Thannickal, V. J., Lee, D. Y., White, E. S., Cui, Z., Larios, J. M., Chacon, R., Horowitz, J. C., Day, R. M. and Thomas, P. E. (2003), 'Myofibroblast differentiation by transforming growth factor-β1 is dependent on cell adhesion and integrin signaling via focal adhesion kinase', *Journal of Biological Chemistry* **278**(14), 12384–12389.

Thomas, A. Q., Lane, K., Phillips III, J., Prince, M., Markin, C., Speer, M., Schwartz, D. A., Gaddipati, R., Marney, A., Johnson, J. et al. (2002), 'Heterozygosity for a surfactant protein c gene mutation associated with usual interstitial pneumonitis and cellular nonspecific interstitial pneumonitis in one kindred', *American journal of respiratory and critical care medicine* **165**(9), 1322–1328.

Tian, X., Yao, W., Guo, Z., Gu, L. and Zhu, Y. (2006), 'Low dose pirfenidone suppresses transforming growth factor beta-1 and tissue inhibitor of metalloproteinase-1, and protects rats from lung fibrosis induced by bleomycina.', *Chinese medical sciences journal= Chung-kuo i hsueh k'o hsueh tsa chih* **21**(3), 145–151.

Tjin, G., White, E. S., Faiz, A., Sicard, D., Tschumperlin, D. J., Mahar, A., Kable, E. P. and Burgess, J. K. (2017), 'Lysyl oxidases regulate fibrillar collagen remodelling in idiopathic pulmonary fibrosis', *Disease models & mechanisms* **10**(11), 1301–1312.

Toda, M., Mizuguchi, S., Minamiyama, Y., Yamamoto-Oka, H., Aota, T., Kubo, S., Nishiyama, N., Shibata, T. and Takemura, S. (2018), 'Pirfenidone suppresses polarization to m2 phenotype macrophages and the fibrogenic activity of rat lung fibroblasts', *Journal of clinical biochemistry and nutrition* **63**(1), 58–65.

Tomos, I., Roussis, I., Matthaiou, A. M. and Dimakou, K. (2023), 'Molecular and genetic biomarkers in idiopathic pulmonary fibrosis: where are we now?', *Biomedicines* **11**(10), 2796.

Torre, A., Martínez-Sánchez, F. D., Narvaez-Chávez, S. M., Herrera-Islas, M. A., Aguilar-Salinas, C. A. and Córdova-Gallardo, J. (2024), 'Pirfenidone use in fibrotic diseases: What do we know so far?', *Immunity, Inflammation and Disease* **12**(7), e1335.

Trivedi, R., Redente, E. F., Thakur, A., Riches, D. W. and Kompella, U. B. (2012), 'Local delivery of biodegradable pirfenidone nanoparticles ameliorates bleomycin-induced pulmonary fibrosis in mice', *Nanotechnology* **23**(50), 505101.

Tsukui, T., Sun, K.-H., Wetter, J. B., Wilson-Kanamori, J. R., Hazelwood, L. A., Henderson, N. C., Adams, T. S., Schupp, J. C., Poli, S. D., Rosas, I. O. et al. (2020), 'Collagen-producing lung cell atlas identifies multiple subsets with distinct localization and relevance to fibrosis', *Nature communications* **11**(1), 1920.

Tuder, R. M., Lara, A. R. and Thannickal, V. J. (2012), 'Lactate, a novel trigger of transforming growth factor-β activation in idiopathic pulmonary fibrosis'.

Tweedell, R. E. and Kanneganti, T.-D. (2024), 'Inflammasomes at the foundation of inflammatory cell death complexes', *The Journal of Immunology* **213**(3), 247–249.

Tzouvelekis, A., Harokopos, V., Paparountas, T., Oikonomou, N., Chatziioannou, A., Vilaras, G., Tsiambas, E., Karameris, A., Bouros, D. and Aidinis, V. (2007), 'Comparative expression profiling in pulmonary fibrosis suggests a role of hypoxia-inducible factor-1α in disease pathogenesis', *American journal of respiratory and critical care medicine* **176**(11), 1108–1119.

Upadhya, P., Chary, R., Chawla, G., Vadala, R. and Mohanty, M. (2021), 'New twist to an old problem: Covid-19 and idiopathic pulmonary fibrosis', *Advances in Respiratory Medicine* **89**(1), 84–85.

Vakil, L., Najafipour, R., Rakhshani, N., Zamani, F., Morakabati, A. and Javadi, A. (2016), 'Investigation of fih-1 and socs3 expression in kras mutant and wild-type patients with colorectal cancer', *Tumor Biology* **37**, 8841–8848.

Valapour, M., Lehr, C., Skeans, M., Smith, J., Miller, E., Goff, R., Foutz, J., Israni, A., Snyder, J. and Kasiske, B. (2021), 'Optn/srtr 2019 annual data report: lung', *American Journal of Transplantation* **21**, 441–520.

van der Vliet, A., Janssen-Heininger, Y. M. and Anathy, V. (2018), 'Oxidative stress in chronic lung disease: From mitochondrial dysfunction to dysregulated redox signaling', *Molecular aspects of medicine* **63**, 59–69.

Van Deursen, J. M. (2014), 'The role of senescent cells in ageing', *Nature* **509**(7501), 439–446.

Van, Q. N., Issaq, H. J., Jiang, Q., Li, Q., Muschik, G. M., Waybright, T. J., Lou, H., Dean, M., Uitto, J. and Veenstra, T. D. (2008), 'Comparison of 1d and 2d nmr spectroscopy for metabolic profiling', *Journal of Proteome Research* **7**(2), 630–639.

Vancheri, C. (2012), 'Idiopathic pulmonary fibrosis: an altered fibroblast proliferation linked to cancer biology', *Proceedings of the American Thoracic Society* **9**(3), 153–157.

Vander Heiden, M. G., Cantley, L. C. and Thompson, C. B. (2009), 'Understanding the warburg effect: the metabolic requirements of cell proliferation', *science* **324**(5930), 1029–1033.

Vaz, M., Hwang, S. Y., Kagiampakis, I., Phallen, J., Patil, A., O'Hagan, H. M., Murphy, L., Zahnow, C. A., Gabrielson, E., Velculescu, V. E. et al. (2017), 'Chronic cigarette smoke-induced epigenomic changes precede sensitization of bronchial epithelial cells to single-step transformation by kras mutations', *Cancer cell* **32**(3), 360–376.

Velarde, M. C., Flynn, J. M., Day, N. U., Melov, S. and Campisi, J. (2012), 'Mitochondrial oxidative stress caused by sod2 deficiency promotes cellular senescence and aging phenotypes in the skin', *Aging (Albany NY)* **4**(1), 3.

Venable, M. E., Lee, J. Y., Smyth, M. J., Bielawska, A. and Obeid, L. M. (1995), 'Role of ceramide in cellular senescence ()', *Journal of Biological Chemistry* **270**(51), 30701–30708.

Vicens-Zygmunt, V., Estany, S., Colom, A., Montes-Worboys, A., Machahua, C., Sanabria, A. J., Llatjos, R., Escobar, I., Manresa, F., Dorca, J. et al. (2015), 'Fibroblast viability and phenotypic changes within glycated stiffened three-dimensional collagen matrices', *Respiratory research* **16**, 1–15.

Virk, H. S., Biddle, M. S., Smallwood, D. T., Weston, C. A., Castells, E., Bowman, V. W., McCarthy, J., Amrani, Y., Duffy, S. M., Bradding, P. et al. (2021), 'Tgfβ1 induces resistance of human lung myofibroblasts to cell death via down-regulation of trpa1 channels', *British journal of pharmacology* **178**(15), 2948–2962.

Volkova, Y. L., Jucht, A. E., Oechsler, N., Krishnankutty, R., von Kriegsheim, A., Wenger, R. H. and Scholz, C. C. (2024), 'Selective hypoxia-sensitive oxomer formation by fih prevents binding of the nf-κb inhibitor iκbβ to nf-κb subunits', *Molecular and Cellular Biology* **44**(4), 138–148.

Wang, E., Zhang, C., Polavaram, N., Liu, F., Wu, G., Schroeder, M. A., Lau, J. S., Mukhopadhyay, D., Jiang, S.-W., O'Neill, B. P. et al. (2014), 'The role of factor inhibiting hif (fih-1) in inhibiting hif-1 transcriptional activity in glioblastoma multiforme', *PLoS One* **9**(1), e86102.

Wang, G. L., Jiang, B.-h., Rue, E. A. and Semenza, G. L. (1995), 'Hypoxia-inducible factor 1 is a basic-helix-loop-helix-pas heterodimer regulated by cellular o2 tension.', *Proceedings of the national academy of sciences* **92**(12), 5510–5514.

Wang, H., Gao, Y., Wang, L., Yu, Y., Zhang, J., Liu, C., Song, Y., Xu, H., Wang, J., Lou, H. et al. (2023), 'Lung specific homing of diphenyleneiodonium chloride improves pulmonary fibrosis by inhibiting macrophage m2 metabolic program', *Journal of Advanced Research* **44**, 213–225.

Wang, J., Hu, K., Cai, X., Yang, B., He, Q., Wang, J. and Weng, Q. (2022), 'Targeting pi3k/akt signaling for treatment of idiopathic pulmonary fibrosis', *Acta Pharmaceutica Sinica B* **12**(1), 18–32.

Wang, L., Xu, K., Wang, N., Ding, L., Zhao, W., Wan, R., Zhao, W., Guo, X., Pan, X., Yang, J. et al. (2022), 'Fenbendazole attenuates bleomycin-induced pulmonary fibrosis in mice via suppression of fibroblast-to-myofibroblast differentiation', *International journal of molecular sciences* **23**(22), 14088.

Wang, W., Zhang, Y., Huang, W., Yuan, Y., Hong, Q., Xie, Z., Li, L., Chen, Y., Li, X. and Meng, Y. (2023), 'Alamandine/mrgd axis prevents tgf-β1-mediated fibroblast activation via regulation of aerobic glycolysis and mitophagy', *Journal of Translational Medicine* **21**(1), 24.

Wang, Y., Kuan, P. J., Xing, C., Cronkhite, J. T., Torres, F., Rosenblatt, R. L., DiMaio, J. M., Kinch, L. N., Grishin, N. V. and Garcia, C. K. (2009), 'Genetic defects in surfactant protein a2 are associated with pulmonary fibrosis and lung cancer', *The American Journal of Human Genetics* **84**(1), 52–59.

Warburg, O. (1956), 'On the origin of cancer cells', *Science* **123**(3191), 309–314.

Waxman, A., Restrepo, R., Thenappan, T., Ravichandran, A., Smith, P., Borg, E., Edwards, L., Tapson, V. and Nathan, S. (2020), 'The impact of inhaled treprostinil on patient lung function: results from the increase study', *Chest* **158**(4), A2179–A2180.

Webb, J. D., Murányi, A., Pugh, C. W., Ratcliffe, P. J. and Coleman, M. L. (2009), 'Mypt1, the targeting subunit of smooth-muscle myosin phosphatase, is a substrate for the asparaginyl hydroxylase factor inhibiting hypoxia-inducible factor (fih)', *Biochemical journal* **420**(2), 327–336.

Weidemann, A. and Johnson, R. (2008), 'Biology of hif-1α', *Cell Death & Differentiation* **15**(4), 621–627.

Wellen, K. E., Hatzivassiliou, G., Sachdeva, U. M., Bui, T. V., Cross, J. R. and Thompson, C. B. (2009), 'Atp-citrate lyase links cellular metabolism to histone acetylation', *Science* **324**(5930), 1076–1080.

Werner, F., Jain, M. K., Feinberg, M. W., Sibinga, N. E., Pellacani, A., Wiesel, P., Chin, M. T., Topper, J. N., Perrella, M. A. and Lee, M.-E. (2000), 'Transforming growth factor-β1 inhibition of macrophage activation is mediated via smad3', *Journal of Biological Chemistry* **275**(47), 36653–36658.

White, E. S. (2015), 'Lung extracellular matrix and fibroblast function', *Annals of the American Thoracic Society* **12**(Supplement 1), S30–S33.

Wiley, C. D. and Campisi, J. (2016), 'From ancient pathways to aging cells—connecting metabolism and cellular senescence', *Cell metabolism* **23**(6), 1013–1021.

Wiley, C. D., Velarde, M. C., Lecot, P., Liu, S., Sarnoski, E. A., Freund, A., Shirakawa, K., Lim, H. W., Davis, S. S., Ramanathan, A. et al. (2016), 'Mitochondrial dysfunction induces senescence with a distinct secretory phenotype', *Cell metabolism* **23**(2), 303–314.

Wilkins, S. E., Hyvärinen, J., Chicher, J., Gorman, J. J., Peet, D. J., Bilton, R. L. and Koivunen, P. (2009), 'Differences in hydroxylation and binding of notch and hif-1α

demonstrate substrate selectivity for factor inhibiting hif-1 (fih-1)', *The international journal of biochemistry & cell biology* **41**(7), 1563–1571.

Willis, B. C. and Borok, Z. (2007), 'Tgf-β-induced emt: mechanisms and implications for fibrotic lung disease', *American Journal of Physiology-Lung Cellular and Molecular Physiology* **293**(3), L525–L534.

Wilson, M. S., Madala, S. K., Ramalingam, T. R., Gochuico, B. R., Rosas, I. O., Cheever, A. W. and Wynn, T. A. (2010), 'Bleomycin and il-1β–mediated pulmonary fibrosis is il-17a dependent', *Journal of Experimental Medicine* **207**(3), 535–552.

Wilson, R. C. and Doudna, J. A. (2013), 'Molecular mechanisms of rna interference', *Annual review of biophysics* **42**(1), 217–239.

Wipff, P.-J., Rifkin, D. B., Meister, J.-J. and Hinz, B. (2007), 'Myofibroblast contraction activates latent tgf-β1 from the extracellular matrix', *The Journal of cell biology* **179**(6), 1311–1323.

Wollin, L., Maillet, I., Quesniaux, V., Holweg, A. and Ryffel, B. (2014), 'Antifibrotic and anti-inflammatory activity of the tyrosine kinase inhibitor nintedanib in experimental models of lung fibrosis', *Journal of Pharmacology and Experimental Therapeutics* **349**(2), 209–220.

Wollin, L., Wex, E., Pautsch, A., Schnapp, G., Hostettler, K. E., Stowasser, S. and Kolb, M. (2015), 'Mode of action of nintedanib in the treatment of idiopathic pulmonary fibrosis', *European Respiratory Journal* **45**(5), 1434–1445.

Wygrecka, M., Zakrzewicz, D., Taborski, B., Didiasova, M., Kwapiszewska, G., Preissner, K. T. and Markart, P. (2012), 'Tgf-β1 induces tissue factor expression in human lung fibroblasts in a pi3k/jnk/akt-dependent and ap-1–dependent manner', *American journal of respiratory cell and molecular biology* **47**(5), 614–627.

Wynn, T. A. (2011), 'Integrating mechanisms of pulmonary fibrosis', *Journal of Experimental Medicine* **208**(7), 1339–1350.

Xie, N., Cui, H., Ge, J., Banerjee, S., Guo, S., Dubey, S., Abraham, E., Liu, R.-M. and Liu, G. (2017), 'Metabolic characterization and rna profiling reveal glycolytic dependence of profibrotic phenotype of alveolar macrophages in lung fibrosis', *American Journal of Physiology-Lung Cellular and Molecular Physiology* **313**(5), L834–L844.

Xie, N., Tan, Z., Banerjee, S., Cui, H., Ge, J., Liu, R.-M., Bernard, K., Thannickal, V. J. and Liu, G. (2015), 'Glycolytic reprogramming in myofibroblast differentiation and lung fibrosis', *American journal of respiratory and critical care medicine* **192**(12), 1462–1474.

Xie, Y., Shi, S., Lv, W., Wang, X., Yue, L., Deng, C., Wang, D., Han, J., Ye, T. and Lin, Y. (2024), 'Tetrahedral framework nucleic acids delivery of pirfenidone for anti-inflammatory and antioxidative effects to treat idiopathic pulmonary fibrosis', *ACS nano* .

Xiong, Y., Lei, Q., Zhao, S. and Guan, K. (2011), Regulation of glycolysis and gluconeogenesis by acetylation of pkm and pepck, *in* 'Cold Spring Harbor symposia on quantitative biology', Vol. 76, Cold Spring Harbor Laboratory Press, pp. 285–289.

Xu, L., Cui, W.-H., Zhou, W.-C., Li, D.-L., Li, L.-C., Zhao, P., Mo, X.-T., Zhang, Z. and Gao, J. (2017), 'Activation of wnt/β-catenin signalling is required for tgf-β/smad2/3 signalling during myofibroblast proliferation', *Journal of Cellular and Molecular Medicine* **21**(8), 1545–1554.

Xu, Y., Mizuno, T., Sridharan, A., Du, Y., Guo, M., Tang, J., Wikenheiser-Brokamp, K. A., Perl, A.-K. T., Funari, V. A., Gokey, J. J. et al. (2016), 'Single-cell rna sequencing identifies diverse roles of epithelial cells in idiopathic pulmonary fibrosis', *JCI insight* **1**(20).

Xue, J., Kass, D. J., Bon, J., Vuga, L., Tan, J., Csizmadia, E., Otterbein, L., Soejima, M., Levesque, M. C., Gibson, K. F. et al. (2013), 'Plasma b lymphocyte stimulator and b cell differentiation in idiopathic pulmonary fibrosis patients', *The Journal of Immunology* **191**(5), 2089–2095.

Yamaguchi, S., Koda, N., Eto, Y. and Aoki, K. (1985), 'Quick screening and diagnosis of organic acidemia by nmr urinalysis', *The Journal of pediatrics* **106**(4), 620–622.

Yamamura, Y., Sakai, N., Iwata, Y., Lagares, D., Hara, A., Kitajima, S., Toyama, T., Miyagawa, T., Ogura, H., Sato, K. et al. (2023), 'Myocardin-related transcription factor contributes to renal fibrosis through the regulation of extracellular microenvironment surrounding fibroblasts', *The FASEB Journal* **37**(7), e23005.

Yan, P., Liu, J., Li, Z., Wang, J., Zhu, Z., Wang, L. and Yu, G. (2023), 'Glycolysis reprogramming in idiopathic pulmonary fibrosis: Unveiling the mystery of lactate in the lung', *International Journal of Molecular Sciences* **25**(1), 315.

Yanagihara, T., Tsubouchi, K., Gholiof, M., Chong, S. G., Lipson, K. E., Zhou, Q., Scallan, C., Upagupta, C., Tikkanen, J., Keshavjee, S. et al. (2022), 'Connective-tissue growth factor contributes to tgf-β1–induced lung fibrosis', *American journal of respiratory cell and molecular biology* **66**(3), 260–270.

Yanai, H., Shteinberg, A., Porat, Z., Budovsky, A., Braiman, A., Zeische, R. and Fraifeld, V. E. (2015), 'Cellular senescence-like features of lung fibroblasts derived from idiopathic pulmonary fibrosis patients', *Aging (Albany NY)* **7**(9), 664.

Yang, L., Gilbertsen, A., Xia, H., Benyumov, A., Smith, K., Herrera, J., Racila, E., Bitterman, P. B. and Henke, C. A. (2023), 'Hypoxia enhances ipf mesenchymal progenitor cell fibrogenicity via the lactate/gpr81/hif1α pathway', *JCI insight* **8**(4).

Yang, M., Chowdhury, R., Ge, W., Hamed, R. B., McDonough, M. A., Claridge, T. D., Kessler, B. M., Cockman, M. E., Ratcliffe, P. J. and Schofield, C. J. (2011),

'Factor-inhibiting hypoxia-inducible factor (fih) catalyses the post-translational hydroxylation of histidinyl residues within ankyrin repeat domains', *The FEBS journal* **278**(7), 1086–1097.

Yang, M., Hardy, A. P., Chowdhury, R., Loik, N. D., Scotti, J. S., McCullagh, J. S., Claridge, T. D., McDonough, M. A., Ge, W. and Schofield, C. J. (2013), 'Substrate selectivity analyses of factor inhibiting hypoxia-inducible factor.', *Angewandte Chemie International Edition* **52**(6).

Yang, S.-N., Perng, D.-W., Ko, H.-K., Chang, Y.-L., Hsu, C.-C., Huang, H.-Y. and Chung, M.-I. (2020), Epidemiologic analysis of taiwanese patients with idiopathic pulmonary fibrosis, *in* 'Healthcare', Vol. 8, MDPI, p. 580.

Yao, C., Guan, X., Carraro, G., Parimon, T., Liu, X., Huang, G., Mulay, A., Soukiasian, H. J., David, G., Weigt, S. S. et al. (2021), 'Senescence of alveolar type 2 cells drives progressive pulmonary fibrosis', *American journal of respiratory and critical care medicine* **203**(6), 707–717.

Ye, Z. and Hu, Y. (2021), 'Tgf-β1: Gentlemanly orchestrator in idiopathic pulmonary fibrosis', *International journal of molecular medicine* **48**(1), 1–14.

Yin, X., Choudhury, M., Kang, J.-H., Schaefbauer, K. J., Jung, M.-Y., Andrianifahanana, M., Hernandez, D. M. and Leof, E. B. (2019), 'Hexokinase 2 couples glycolysis with the profibrotic actions of tgf-β', *Science signaling* **12**(612), eaax4067.

Young, A. P., Schlisio, S., Minamishima, Y. A., Zhang, Q., Li, L., Grisanzio, C., Signoretti, S. and Kaelin Jr, W. G. (2008), 'Vhl loss actuates a hif-independent senescence programme mediated by rb and p400', *Nature cell biology* **10**(3), 361–369.

Yu, W., Guo, F. and Song, X. (2017), 'Effects and mechanisms of pirfenidone, prednisone and acetylcysteine on pulmonary fibrosis in rat idiopathic pulmonary fibrosis models', *Pharmaceutical biology* **55**(1), 450–455.

Zhang, H., Du, L., Zhong, Y., Flanders, K. C. and Roberts Jr, J. D. (2017), 'Transforming growth factor-β stimulates smad1/5 signaling in pulmonary artery smooth muscle cells and fibroblasts of the newborn mouse through alk1', *American Journal of Physiology-Lung Cellular and Molecular Physiology* **313**(3), L615–L627.

Zhang, H., Ren, L. and Shivnaraine, R. V. (2022), 'Targeting gpcrs to treat cardiac fibrosis', *Frontiers in Cardiovascular Medicine* **9**, 1011176.

Zhang, H.-Y. and Phan, S. H. (1999), 'Inhibition of myofibroblast apoptosis by transforming growth factor β1', *American journal of respiratory cell and molecular biology* **21**(6), 658–665.

Zhang, J. et al. (2019), 'Profibrotic effect of il-17a and elevated il-17ra in idiopathic pulmonary fibrosis and rheumatoid arthritis-associated lung disease support a direct

role for il-17a/il-17ra in human fibrotic interstitial lung disease', *American Journal of Physiology-Lung Cellular and Molecular Physiology* **316**(3), L487–L497.

Zhang, N., Fu, Z., Linke, S., Chicher, J., Gorman, J. J., Visk, D., Haddad, G. G., Poellinger, L., Peet, D. J., Powell, F. et al. (2010), 'The asparaginyl hydroxylase factor inhibiting hif-1α is an essential regulator of metabolism', *Cell metabolism* **11**(5), 364–378.

Zhang, Q., Tu, W., Tian, K., Han, L., Wang, Q., Chen, P. and Zhou, X. (2019), 'Sirtuin 6 inhibits myofibroblast differentiation via inactivating transforming growth factor-β1/smad2 and nuclear factor-κb signaling pathways in human fetal lung fibroblasts', *Journal of cellular biochemistry* **120**(1), 93–104.

Zhang, X., Wang, F., Shen, Y., Zhang, X., Cen, Y., Wang, B., Zhao, S., Zhou, Y., Hu, B., Wang, M. et al. (2021), 'Symptoms and health outcomes among survivors of covid-19 infection 1 year after discharge from hospitals in wuhan, china', *JAMA Network open* **4**(9), e2127403–e2127403.

Zhang, Y. (2017), 'Non-smad signaling pathways of the tgf-beta family. cold spring harb perspect biol 9: a022129'.

Zhao, H., Dennery, P. A. and Yao, H. (2018), 'Metabolic reprogramming in the pathogenesis of chronic lung diseases, including bpd, copd, and pulmonary fibrosis', *American Journal of Physiology-Lung Cellular and Molecular Physiology* **314**(4), L544–L554.

Zhao, Y., Liu, H., Liu, Z., Ding, Y., LeDoux, S. P., Wilson, G. L., Voellmy, R., Lin, Y., Lin, W., Nahta, R. et al. (2011), 'Overcoming trastuzumab resistance in breast cancer by targeting dysregulated glucose metabolism', *Cancer research* **71**(13), 4585–4597.

Zheng, X., Linke, S., Dias, J. M., Zheng, X., Gradin, K., Wallis, T. P., Hamilton, B. R., Gustafsson, M., Ruas, J. L., Wilkins, S. et al. (2008), 'Interaction with factor inhibiting hif-1 defines an additional mode of cross-coupling between the notch and hypoxia signaling pathways', *Proceedings of the National Academy of Sciences* **105**(9), 3368–3373.

Zheng, X., Qi, C., Zhang, S., Fang, Y. and Ning, W. (2017), 'Tgf-β1 induces fstl1 via the smad3-c-jun pathway in lung fibroblasts', *American Journal of Physiology-Lung Cellular and Molecular Physiology* **313**(2), L240–L251.

Zhou, B., Liu, Y., Kahn, M., Ann, D. K., Han, A., Wang, H., Nguyen, C., Flodby, P., Zhong, Q., Krishnaveni, M. S. et al. (2012), 'Interactions between β-catenin and transforming growth factor-β signaling pathways mediate epithelial-mesenchymal transition and are dependent on the transcriptional co-activator camp-response element-binding protein (creb)-binding protein (cbp)', *Journal of Biological Chemistry* **287**(10), 7026–7038.

Zhou, M., Zhao, Y., Ding, Y., Liu, H., Liu, Z., Fodstad, O., Riker, A. I., Kamarajugadda, S., Lu, J., Owen, L. B. et al. (2010), 'Warburg effect in chemosensitivity: targeting lactate dehydrogenase-a re-sensitizes taxol-resistant cancer cells to taxol', *Molecular cancer* **9**, 1–12.

Zhou, Y., Ling, T. and Shi, W. (2024), 'Current state of signaling pathways associated with the pathogenesis of idiopathic pulmonary fibrosis', *Respiratory Research* **25**(1), 245.

Zhou, Y., Zhou, B., Pache, L., Chang, M., Khodabakhshi, A. H., Tanaseichuk, O., Benner, C. and Chanda, S. K. (2019), 'Metascape provides a biologist-oriented resource for the analysis of systems-level datasets', *Nature communications* **10**(1), 1523.

Zhu, W., Tan, C. and Zhang, J. (2022), 'Alveolar epithelial type 2 cell dysfunction in idiopathic pulmonary fibrosis', *Lung* **200**(5), 539–547.

Zhu, Y., Tan, J., Xie, H., Wang, J., Meng, X. and Wang, R. (2016), 'Hif-1α regulates emt via the snail and β-catenin pathways in paraquat poisoning-induced early pulmonary fibrosis', *Journal of cellular and molecular medicine* **20**(4), 688–697.